

Optimisation of Tidal Range Schemes



Jingjing Xue
School of Engineering
Cardiff University, Wales, UK

Supervised by
Dr Reza Ahmadian and Prof Roger A Falconer

This thesis is submitted in partial fulfilment of the requirements
for degree of
Doctor of Philosophy (Ph.D.)
January 2021

Acknowledgements

I would like to thank my supervisors, Dr Reza Ahmadian and Professor Roger A Falconer for their guidance, patience and support throughout my PhD. I could not have completed this thesis without their technical expertise and experience. Also, I would like to thank Prof Owen Jones (School of Mathematics, Cardiff University, UK), who continuously share the knowledge of mathematics and optimisation with me. Besides, I greatly appreciate Prof Chris Bennie (Exeter University Water Centre, Exeter, UK), David Kerr (Vice-chairman ICE Energy Board), and Henry Dixon (the chairman in North Wales Tidal Energy), et al., for contributing to very smooth and efficient collaborations.

This research project was funded by Cardiff University and China Scholarship Council (CSC), and would not have been possible without the use of ARCCA supercomputing facilities. I give my thanks to the staff at Cardiff University and CSC, including Andrew Williams from ARCCA who provided great support in running my models on ARCCA.

To my friends in the department (Giovanni, Nejc, Joe, Bin, Qing, Ben, Catherine, Bikash and Shahla) and out of it (Wen, Likun), I am always grateful, you have been there for keeping me sane at stressful moments.

Finally, I would like to express my gratitude to my family, especially my mother (Mrs Chen), father (Mr Xue), grandfather (Mr Xue) and my husband (Dr Wang) for their continuous support and encouragement over the course of the PhD.

Jingjing Xue

Cardiff, 2021

Abstract

Marine renewable energy, including tidal renewable energy, is one of the less exploited renewable energy sources that could contribute to energy demand while reducing greenhouse gas emissions. Several proposals to build tidal range structures, e.g. Swansea Bay Lagoon (SBL), have not received support from the UK government due to the high electricity costs or uncertainty about the environmental impacts. This makes the optimisation of such schemes particularly important for the future.

The aim of this research was to optimise the design and operational characteristics of Tidal Range Schemes (TRSs) to make them more economically attractive by maximising the energy generation, or a flexible energy output to achieve multi-objectives. The study has focused on two key issues of TRSs optimisation. Firstly, the majority of studies before adopted the traditional non-flexible operation scenarios for electricity generation. In this approach, the operation heads were fixed throughout the operation simulations. It ignores the variability of tidal range over time and the fact that the operation of each generation phase affects the water levels inside the basin which in turn impact the electricity generation of the next phase. Secondly, the flexibility of energy output provided by renewable energies including tidal energy was underexploited, but it is regarded as one of the most important parts of the UK's energy mix.

Hence, the first objective was to propose and optimise flexible operation schemes to maximise energy generation. To achieve this, optimisation approaches were considered by breaking the operation into small components to optimise the operation of TRSs using a widely used 0-D modelling methodology. The optimisation outcomes were verified by a 2-D unstructured model under the same conditions. The flexibility of operation could at least increase generated electricity by 10% compared to the traditional non-flexible head operation. This increase was further improved by at least 10% when pumping was included. Meanwhile, a Genetic Algorithm (GA) method used for flexible operation optimisation was able to achieve the same amount of electricity generation compared to using a Grid Search (GS) method. However, the GA model could save approximately 50% of the computational cost, and it could be 95% in the optimisation of multiple variables, e.g. design parameter combining with flexible operation. Additionally, the optimisation using GA was used in designing of the two of the biggest lagoons proposed in the UK, namely West Somerset Lagoon and North Wales Tidal Lagoon, with the energy generation of 5.57 TWh/Year and 4.81 TWh/Year, respectively. The second objective in this study was to achieve the flexible energy output optimisation, including utilising generation flexibility from multi-lagoons to help match the continuous trends of energy output. The flexible operation optimisation was proved to facilitate better utilisation of renewable energy through the development of TRSs for multi-objective decision making.

Contents

Acknowledgements	iii
Abstract	iv
Related Publication	ix
Nomenclature	x
List of Figures	xiv
List of Table	xxi
1. Introduction	1
1.1 Background	1
1.2 Research objective	4
1.3 Outline of the thesis	5
2. Literature review	6
2.1 Introduction.....	6
2.2 Renewable energy	7
2.2.1 Tidal energy	7
2.2.2 Tidal Range Schemes.....	9
2.2.3 Tidal Range Schemes optimisation.....	13
2.3 Predictive tools for electricity generation	16
2.3.1 0-D modelling	16
2.3.2 multi-dimensional modelling.....	18
2.4 Hyperparameter optimisation.....	20
2.4.1 Grid Search Methods	20

2.4.2 Genetic Algorithm	21
2.5 Chapter Summary	23
3. Numerical modelling	24
3.1 Introduction.....	24
3.2 0-D modelling.....	25
3.3 2-D modelling.....	26
3.3.1 Governing equations.....	26
3.3.2 Domain decomposition	27
3.4. Power and discharge calculation.....	29
3.4.1 Turbines	29
3.4.2 Sluices	32
3.4.3 implementation into the numerical model	32
3.5 Use of High Performance Computer.....	34
3.6 Chapter summary	35
4. Case studies.....	36
4.1 Introduction.....	36
4.2 Swansea Bay Lagoon.....	37
4.2.1 Swansea Bay Lagoon modelling.....	39
4.2.2 2-D modelling	46
4.2.3 0-D and 2-D comparison.....	54
4.3 West Somerset Lagoon	57
4.3.1 WSL modelling.....	57
4.3.2 2-D Modelling.....	60
4.3.3 0-D and 2-D comparison.....	64
4.4 North Wales Tidal Lagoon	67
4.4.1 NWTL modelling.....	68
4.5 Chapter summary	74
5. Tidal Range Schemes’ Operational and Design Optimisation	77

5.1 Introduction.....	77
5.2 Flexible operation heads	79
5.2.1 Methodology.....	79
5.2.2 Optimisation without pumping	81
5.2.3 With pumping operation	84
5.2.4 0-D and 2-D comparison.....	85
5.3 Flexible turbine numbers	87
5.3.1 Non-flexible operation schemes	88
5.3.2 Flexible operation schemes.....	94
5.4 Chapter summary	98
6. Tidal Range Schemes optimisation using a Genetic Algorithm.....	99
6.1 Introduction.....	99
6.2 Operational heads optimisation.....	101
6.2.1 Model Setup.....	101
6.2.2 Performance of GA model.....	106
6.2.3 Validation of the GA model by comparing with EHN method	108
6.2.4 Inclusion of Pumping in the GA model	110
6.3 Design parameters optimisation.....	112
6.3.1 The Improved Model	112
6.3.2 Case study of West Somerset Lagoon	114
6.3.3 Case Study of North Wales Tidal Lagoon	129
6.4 Chapter summary	132
7. Flexible operation optimisation	133
7.1 Introduction.....	133
7.2 Methodology.....	135
7.3 Model development	136
7.3.1 Input tidal levels.....	136
7.3.2 Improved Genetic Algorithm model.....	137

7.4 Optimisation.....	139
7.4.1 No pumping utilised.....	139
7.4.2 pumping utilised	141
7.5 Chapter summary	143
8. Conclusion and future work.....	144
8.1 Conclusions and limitations.....	144
8.2 Recommendations for future work	149
Reference	150

Related Publication

Journal Articles

J. Xue, R. Ahmadian, and R. A. Falconer, "Optimising the operation of tidal range schemes," *Energies* 2019;12(15);2870.

J. Xue, R. Ahmadian, and O. Jones, "Genetic algorithm in tidal range schemes' optimisation", *Energy* 2020;200.

J. Xue, R. Ahmadian, O. Jones, and R. A. Falconer, "Design of tidal range energy generation schemes using a Genetic Algorithm model", *Applied Energy* 2021;286.

Conference

J. Xue, R. Ahmadian, and O. Jones, " Optimisation of tidal lagoon using genetic algorithm", *Proceeding of 13th European Wave and Tidal Energy Conference* 2019.

J. Xue, R. Ahmadian and R. A. Falconer, "Operational characteristics optimisation of tidal range schemes, " Presented at: 5th IAHR Europe Congress, Trento, Italy, 13-15 June 2018.

R. Ahmadian, **J. Xue**, R. A. Falconer, and N. Hanousek, "Optimisation of tidal range schemes", *Proceeding of 12th European Wave and Tidal Energy Conference* 2017.

Nomenclature

Abbreviations

0-D	Zero-dimensional
2-D	Two-dimensional
3-D	Three-dimensional
ADCPs	Acoustic Doppler Current Profilers
ARCCA	Advanced Research Computing at Cardiff
BO	Bayesian Optimisation
BODC	British Oceanographic Data Centre
CO ₂	Carbon Dioxide
CFD	Computational Fluid Dynamics
DCO	Development Consent Order
DECC	Department of Energy and Climate Change
DIVAST 2-DU	Depth Integrated Velocities And Solute Transport 2-D Unstructured
EAs	Evolutionary Algorithms
EFDC	Environmental Fluid Dynamics Code
EH	Every Half tidal cycle model
EHN	Every Half tidal cycle and Next model
EHNP	Every Half tidal cycle and Next Pump model
EHP	Every Half tidal cycle and Pump model
ET	Every Tidal cycle model
ETN	Every Tidal cycle and Next model
ETNP	Every Tidal cycle and Next Pump model
ETP	Every Tidal cycle and Pump model
GA	Genetic Algorithm
GAs	Genetic Algorithms
GHGs	Green House Gasses
GS	Grid Search
HAT	High Astronomical Tide
HPC	High Performance Computer
HRC	Hydro-environmental Research Centre
HW	High water level
L2	Observed location at western of bay
L3	Observed location at central of bay
L5	Observed location at eastern of bay
LAT	Lowest Astronomical Tide
LCICG	Low Carbon Innovation Co-ordination Group
LRM	Linear Recombination Method
LW	Low water level
MRE	Marine Renewable Energy
NWTL	North Wales Tidal Lagoon
NWTE	North Wales Tidal Energy & Coastal Protection
OpenMP	Open Multi-Processing
ORE	Offshore Renewable Energy
RMSE	Root Mean Square Error

RRM	Ring Recombination Method
SBL	Swansea Bay Lagoon
SMM	Sequential Mutation Method
SWE	Shallow Water Equation
SLA	Sea Level Anomaly
TRSs	Tidal Range Schemes
TLP	Tidal Lagoon Power
WSL	West Somerset Lagoon

Dimensionless parameters

C_d	Coefficient of discharge
CoefQ_GT	Coefficient of generator efficiency
CoefQ_sluice	Coefficient for sluice
CoefQ_Turb	Coefficient for turbines
C_p	Coefficient of turbine power
Op_Turb_Ratio	Coefficient of turbine ratio
η_p	Pump Efficiency
η_t	Turbine Efficiency
C	Chezy bed roughness coefficient
mn	Manning roughness coefficient
C_s	Air-water resistance coefficient
α	Interpolation factor

Greek Symbols

η	Efficiency	-
β	Momentum correction factor	-
ρ	Fluid density	Kg/m ³
K	Karman's constant	-
ρ_a	Air density	Kg/m ³
ξ	Water surface elevation above datum	m

Roman Symbols

A	Cross-section area of turbine	m ²
Av	Averaged electricity generation	MW
DNE	accumulated Duration that with No Energy output	hr
St	Standard deviation	-
co_av	Weight to the Av	-
co_dne	Weight to the DNE	-
co_st	Weight to the St	-
DI_hillchart	Diameter of Turbine used in the hill chart	m
DI_TB	Diameter of Turbine used in TRS	m
E	Electricity generation	GWh
f	Coriolis parameter	rad/s
g	Acceleration due to gravity	m ² /s
IC	Installed Capacity	MW

H	Water head difference	m
Max_Elect	The maximum electricity generation	GWh
P_hillchart	Power output from hill chart	MW
Q(H)	Total discharge through turbines and sluices at H	m ³ /s
Q_hillchart	Discharge through turbine from hill chart	m ³ /s
V	Fluid stream velocity	m/s
NumTB	Turbine Number	-
STPC	Sluices To Power Capacity	m ² /MW
t	Time	s
Δt	Time step	s

Superscripts

R ²	R-squared
\bar{x}	Mean value of the specific term

Subscripts

A _p	Plan area impounded	m ²
A _s	Sluice gate area	m ²
H _e	Ending generating head	m
H _{e,i}	Ending generating head at i th half-tide	m
H _{ee}	Ending generating head during ebb tide	m
H _{ef}	Ending generating head during flood tide	m
H _p	Starting pumping head	m
H _{p,i}	Pumping generating head at i th half-tide	m
H _{p_limited}	Pumping head limitation	m
H _{pe}	Starting pumping head during ebb tide	m
H _{pf}	Starting pumping head during flood tide	m
H _s	Starting generating head	m
H _{s,i}	Starting generating head at i th half-tide	m
H _{se}	Starting generating head during ebb tide	m
H _{sf}	Starting generating head during flood tide	m
O _i	Observed terms at timestep i	-
P _i	Predicted terms at timestep i	-
P _{input}	Power input during pumping phase	MW
P _m	Probability for mutation	%
P _{output}	Power output during pumping phase	MW
P _{potential}	Potential power output of turbine or used as pumping	MW
P _r	Probability for recombination	%
P _s	Probability for selection	%
P _{tb}	Power output for TRSs	MW
P _{max}	Maximum rate per turbine	MW
Q _{in}	Inflow/outflow to the lagoon through sources other than through TRSs	m ³ /s
Q _{tb}	Discharge through turbine for TRSs	m ³ /s
q _x	Discharge per unit width in x-axis direction	m ³ /s
q _y	Discharge per unit width in y-axis direction	m ³ /s

q_z	Discharge per unit width in z-axis direction	m^3/s
U_{av}	Averaged velocity	m/s
Z_{dn}	Downstream water level	m
Z_{up}	Upstream water level	m
η_{min}	Minimum generating head	m
τ_{xb}	Bed shear stress in x-axis direction	m^2/s
τ_{xw}	Surface wind stress in x-axis direction	N/m^2
τ_{yb}	Bed shear stress in y-axis direction	m^2/s
τ_{yw}	Surface wind stress in y-axis direction	N/m^2
W_x	Wind velocity component in the x-direction	m/s
W_s	Wind speed	m/s
V_s	Depth average fluid speed	m^3/s
N_p	Number of points in the Q-H table	-

List of Figures

Fig 2. 1 Cross-section of a typical bulb turbine [43].....	7
Fig 2. 2. An example of (a) a water passageway [47] and (b) a sliding gate [48] typically used in TRSs designs.	8
Fig 2. 3. Cross-section of a sluice caisson proposed for the Swansea Bay Lagoon [48].	8
Fig 2. 4. Schematic representation of the operational schemes: (a) one-way ebb-generation; (b) a two-way tidal power plant.....	11
Fig 2. 5. Schematic representation of the operational mode (including pumping) of (a) one-way ebb-generation; (b) a two-way tidal power plant.	12
Fig 2. 6. Grid Search of nine trials for optimising a function $f(x, y) = g(x) + h(x) \approx g(x)$ with low effective dimensionality. Above square $g(x)$ is shown in green, left square $h(x)$ is shown in yellow. Nine trials only test $g(x)$ in three distinct places [94].....	21
Fig 3. 1. Andritz Hydro three-Blade low head bulb turbine unit [36].....	30
Fig 3. 2. Turbine Q-H and P-H comparison for the diameters of 7.2 m and 9 m, respectively.	30
Fig 3. 3. Turbine efficiency: (a) calculated from Fig. 3.1; (b) measured turbine and pump efficiency [23].....	32
Fig 4. 1. Swansea Bay Lagoon layout overlaid on the Admiralty Chart background [124].	37
Fig 4. 2. Illustrative cross-section of a bi-directional bulb fixed speed turbine [125].	38
Fig 4. 3. Swansea Bay Lagoon bathymetry [126].....	39
Fig 4. 4. Wetted area versus water level of Swansea Bay Lagoon.	39
Fig 4. 5. Power output: (a) with a constant impounded area; (b) with impounded area varying with the water level.....	42
Fig 4. 6. Operation scheduling of the impoundment and water head difference for four neap tides in the 0-D model without pumping included, in which ‘h’, ‘g’ and ‘f’ denotes holding, generating and filling phases, respectively.....	43
Fig 4. 7. Water levels inside the impoundment and power output for four neap tides in the 0-D model without pumping included.	43
Fig 4. 8. Discharge through sluice gates and turbines comparisons for four neap tides in the 0-D model without pumping included.	44

Fig 4. 9. Operation scheduling of the impoundment and water head difference for four neap tides in the 0-D model with pumping included, ‘h’, ‘g’, ‘f’ and ‘p’ denote holding, generating, filling, and pumping phases, respectively.....	44
Fig 4. 10. Water levels inside the impoundment and power output for four neap tides in the 0-D model with pumping included.	45
Fig 4. 11. Discharge through sluice gates and turbines comparisons for four neap tides in the 0-D model without pumping included.	45
Fig 4. 12. Swansea Bay Lagoon region and bathymetry as included in the DIVAST 2-DU model.....	46
Fig 4. 13. Typical comparison of observed and predicted water levels at L2 (a), L3 (b) and L5 (c)....	48
Fig 4. 14. Typical comparison of observed and predicted current speed at L2 (a), L3 (b) and L5 (c).	49
Fig 4. 15. Typical comparison of observed and predicted current direction from North at L2 (a), L3 (b) and L5 (c).....	50
Fig 4. 16. Water Level of L2 for model independency in (a) spring and (b) neap tides.	51
Fig 4. 17. Average velocity of L2 for model independency in (a) spring and (b) neap tides.	51
Fig 4. 18. Current direction of L2 for model independence in (a) spring and (b) neap tides.....	52
Fig 4. 19. Water level (a) and Current (b) streamlines during the flood generating mode in the 2-D model.	53
Fig 4. 20. Water level (a) and Current (b) streamlines during the ebb generating mode in the 2-D model.	54
Fig 4. 21. 2-D and 0-D model comparisons between water level and power output.	55
Fig 4. 22. 2-D and 0-D model comparisons between water head difference and energy generated.	55
Fig 4. 23. 2-D and 0-D model comparisons between discharge through the sluice gates and turbines.....	55
Fig 4. 24. 2-D and 0-D model comparisons with pumping between water level and power output.	55
Fig 4. 25. 2-D and 0-D model comparisons with pumping between water head difference and energy generated.....	56
Fig 4. 26. 2-D and 0-D model comparisons with pumping between discharge through the sluice gates and turbines.....	56
Fig 4. 27. Map of the West Somerset Lagoon.	57
Fig 4. 28. Map of the Bristol Channel, known as the black line, showing the location of the West Somerset Lagoon along the south-west coast of England from Google Map [132]. The validation points of Hinkley and Ilfracombe in the 2-D model were marked as red dots.	58

Fig 4. 29. Wetted area versus water level of West Somerset Lagoon.....	58
Fig 4. 30. Electricity generation with preliminary design parameters under non-flexible operation schemes.....	59
Fig 4. 31. Electricity generation per cycle for the 0-D model.....	60
Fig 4. 32. A typical comparison of observed and predicted water levels at (a) Hinkley and (b) Ilfracombe.....	61
Fig 4. 33. Sketch of grid refinement and deployment of turbines and sluice gates (Brown line is the wall boundary in the mesh, with the Orange line showing the turbines and the Red line shows the sluice gates).....	61
Fig 4. 34. Water level and Current streamlines in the 2-D model for (a) ebb and (b) flood filling mode, respectively.	63
Fig 4. 35. Water level and Current streamlines in the 2-D model for (a) ebb and (b) flood generating mode, respectively.	64
Fig 4. 36. 2-D and 0-D model comparisons between water level and power output during 5 neap tides, in which the ‘Zup’ and ‘Zlw’ represent the upstream and downstream water levels, respectively, ‘Power output’ denotes the power output.....	65
Fig 4. 37. 2-D and 0-D model comparisons between discharge through the sluice gates and turbines during 5 neap tides, in which the ‘QTB’ and ‘QSL’ denote the discharge through turbines and sluice gates, respectively.....	65
Fig 4. 38. 2-D and 0-D model comparisons between electricity generation throughout the typical Spring Neap cycle, in which the ‘Elect’ denotes the electricity generation.	66
Fig 4. 39. Location of North Wales Tidal Lagoon [135].	67
Fig 4. 40. North Wales Tidal Lagoon bathymetry.	68
Fig 4. 41. Wetted area versus water level of North Wales Tidal Lagoon.	68
Fig 4. 42. Layout of the North Wales Tidal Lagoon constitutes including the blocks of turbines and sluice gates, in which the left 10 red rectangular represent the blocks of turbines and the rest 8 for sluice gates.	69
Fig 4. 43. High Water at the outside of each block of the North Wales Tidal Lagoon marked as blue dot with the averaged value shown as orange line.	69
Fig 4. 44. Low Water at the outside of each block of the North Wales Tidal Lagoon marked as blue dot with the averaged value shown as orange line.	70

Fig 4. 45. Water levels in typical Spring Neap cycle for West Somerset Lagoon and North Wales Tidal Lagoon.	70
Fig 4. 46. Water levels and scheduling in the 2-D model with ‘time control’ method for operation. ..	71
Fig 4. 47. Water levels inside the impoundment and power output for West Somerset Lagoon during 5 neap tides in the 0-D model.	72
Fig 4. 48. Discharge through sluice gates and turbines for West Somerset Lagoon during 5 neap tides in the 0-D model.	72
Fig 4. 49. Water head difference for West Somerset Lagoon during 5 neap tides in the 0-D model. ..	72
Fig 4. 50. Electricity generation for West Somerset Lagoon during the typical cycle in the 0-D model.	73
Fig 5. 1. 3 Schematic illustration of different optimisation methodologies: a) full tide optimisation illustrations: ET and ETN methods; and b) half-tide optimisation illustrations: EH and EHN methods.	80
Fig 5. 2. ET model for 10 tides, with the maximum energy point, i.e. most optimised operation, is shown with a red cross.	82
Fig 5. 3. Optimised operation schemes from the ET model during the typical Spring Neap tides.....	82
Fig 5. 4. Operation scheduling of the impoundment, in which ‘h’, ‘g’ and ‘f’ denotes holding, generating and filling phases, respectively, for 4 neap tidal cycles from the 15 th hour during the Spring Neap cycle, equals to 13/08/2012 00:42 and based on ET, ETN, EH, EHN and fixed head models.	83
Fig 5. 5. water levels inside the impoundment for 4 neap tidal cycles from the 15 th hour during the Spring Neap cycle, equals to 13/08/2012 00:42. and based on ET, ETN, EH, EHN and fixed head models.....	84
Fig 5. 6. Power output comparisons for four neap tides from the 15 th hour during the Spring Neap cycle, equals to 13/08/2012 00:42. and based on ET, ETN, EH, EHN and fixed head models.	84
Fig 5. 7. Electricity generation with different turbine numbers within the typical Spring Neap cycle if the non-flexible operation adopted.	87
Fig 5. 8. Selected downstream water level during neap tides denotes as grey line.....	88
Fig 5. 9. Comparison of basin water levels with different turbine numbers (10-16) under constant head schemes during the neap tides from the typical Sprint Neap tidal cycle. ‘Zlw’ represents the downstream water levels.	89
Fig 5. 10. Comparison of water head difference with different turbine numbers (10-16) under constant head schemes during the neap tides from the typical Sprint Neap tidal cycle.	89

Fig 5. 11. Comparison of discharges through turbines with different turbine numbers (10-16) under constant head schemes during the neap tides from the typical Sprint Neap tidal cycle.....	90
Fig 5. 12. Comparison of power output with different turbine numbers (10-16) under constant head schemes during the neap tides from the typical Sprint Neap tidal cycle.....	90
Fig 5. 13. Comparison of electricity generation with different turbine numbers (10-16) under constant head schemes during the neap tides from the typical Sprint Neap tidal cycle.	91
Fig 5. 14. Comparison of discharges through sluice gates with different turbine numbers (10-16) under constant head schemes during the neap tides from the typical Sprint Neap tidal cycle.....	91
Fig 5. 15. Comparison of the basin water level with different turbine numbers (10-16) under constant head schemes plus-pumping during neap tides of the typical Spring Neap cycle. ‘Zlw’ represents the downstream water levels.....	92
Fig 5. 16. Comparison of the water head difference with different turbine numbers (10-16) under constant head schemes plus-pumping during neap tides of the typical Spring Neap cycle.	93
Fig 5. 17. Comparison of the discharges through turbines with different turbine numbers (10-16) under constant head schemes plus-pumping during neap tides of the typical Spring Neap cycle.	93
Fig 5. 18. Comparison of the power output with different turbine numbers (10-16) under constant head schemes plus-pumping during neap tides of the typical Spring Neap cycle.	93
Fig 5. 19. Comparison of the electricity generation with different turbine numbers (10-16) under constant head schemes plus-pumping during neap tides of the typical Spring Neap cycle.	94
Fig 5. 20. Comparison of the discharges through sluice gates with different turbine numbers (10-16) under constant head schemes plus-pumping during neap tides of the typical Spring Neap cycle.	94
Fig 5. 21. Optimised operation head moving trend under different turbine numbers during selected 1 st neap tide.	95
Fig 5. 22. Optimised electricity output under different turbine numbers during selected 1 st neap tide.	96
Fig 6. 1. Flow-chart of the GA model.....	102
Fig 6. 2. Sequential Mutation Methods (SMM) illustration (the highlighted cell represents the place of applying the mutation in each generation).....	104
Fig 6. 3. Linear Recombination Methods (LRM) illustration: a) before LRM; and b) after LRM.....	105
Fig 6. 4. Ring Recombination Methods (RRM) illustration: a) before RRM; and b) after RRM.....	105
Fig 6. 5. Convergence speed comparison.	106
Fig 6. 6. Box plots of convergence speed using (a) RRM or (b) LRM.....	107

Fig 6. 7. Optimised operation heads comparison from GA and EHN models for 4 neap tides. Triangular and cycler represent the starting head (Hs) and ending head (He) using GA (Green) and EHN (Orange), respectively. Solid blue line denotes the water levels outside the basin.	109
Fig 6. 8. Comparison of the lagoon operation optimised by GA and EHN models for a tidal cycle. Solid lines show water levels. Dashed lines show electricity generated. Green: GA model. Orange: EHN model. Blue: Water levels outside the basin. ‘P’ denotes the power output.	109
Fig 6. 9. Operation scheduling of the impoundment and water head difference (a), in which ‘f’, ‘g’, ‘h’, and ‘p’ denotes filling, generating, holding and pumping phases, respectively, for four neap tides in the 0-D model without pumping included.	110
Fig 6. 10. water levels inside the impoundment and power output comparisons for four neap tides in the 0-D model without pumping included.	111
Fig 6. 11. Discharge through sluice gates and turbines, respectively, for four neap tides in the 0-D model without pumping included.	111
Fig 6. 12. Schematic illustration of the updated EHN optimisation methodology.	113
Fig 6. 13. Map of the updated West Somerset Lagoon.	115
Fig 6. 14. Electricity generation with a range of turbines numbers and STPC, under the non-flexible schedules.	116
Fig 6. 15. Electricity generation under flexible operation schemes with no pumping optimised by the GA model.	117
Fig 6. 16. Electricity generation under flexible operation schemes with pumping optimised by the GA model.	117
Fig 6. 17. Water levels and scheduling in 2-D model with traditional ‘head control’ method, in which the Mode denotes the operation phase with ‘1’ to ‘3’ represent filling, holding and generating, respectively; Zup denotes the basin water level; Zlw denotes the downstream water level.	119
Fig 6. 18. Hydrodynamics at the beginning of: (a) ebb generating; (b) ebb sluicing.	121
Fig 6. 19. Water levels and scheduling in 2-D model with ‘time control’ method for operation.	122
Fig 6. 20. Water levels in the modified 0-D model with 5 blocks of turbines under the single-block operation schemes, in which ‘Zup’ represents the basin water level; ‘Zlw’ denote the downstream water levels and ‘1’-‘5’ indicate the corresponding terms at 5 blocks of turbines.	123
Fig 6. 21. Operation scheduling in the modified 0-D model with 5 blocks of turbines under the single-block operation schemes, in which ‘Mode’ stands for the operation scheduling and ‘1’-‘5’ indicate the corresponding terms at 5 blocks of turbines.	124

Fig 6. 22. Power output in the modified 0-D model with 5 blocks of turbines under the single-block operation schemes, in which ‘Power output’ represents the power output and ‘1’-‘5’ indicate the corresponding terms at 5 blocks of turbines.	124
Fig 6. 23. Water levels comparisons for four neap tides in the modified 0-D model for multi-blocks optimisation, in which ‘Zup’, ‘Zlw’ represent the basin water level and downstream water level, respectively; ‘1’-‘5’ denote the number of turbines block, respectively.....	126
Fig 6. 24. water head difference comparisons for four neap tides in the modified 0-D model for multi-blocks optimisation, in which ‘DH’ represents the basin water level. ‘1’-‘5’ denote the number of turbines block, respectively.	127
Fig 6. 25. Discharge through turbines, in which ‘QTB’ represents the discharge through turbines. ‘1’-‘5’ denote the number of turbines block, respectively.....	127
Fig 6. 26. Power output comparisons for four neap tides in the modified 0-D model for multi-blocks optimisation, in which ‘Power output’ represents the power output. ‘1’-‘5’ denote the number of turbines block, respectively.	128
Fig 6. 27. Discharge through sluice gates comparisons for four neap tides in the modified 0-D model for multi-blocks optimisation, in which ‘QSL’ represents discharge through sluice gates. ‘1’-‘5’ denote the number of turbines block, respectively.	128
Fig 6. 28. Flexible operation schemes without pumping optimised by the GA model.....	129
Fig 6. 29. Water levels inside the impoundment and energy for 5 neap tides for North Wales Tidal Lagoon.	130
Fig 6. 30. Discharge through sluice gates and turbines for 5 neap tides for North Wales Tidal Lagoon.	130
Fig 6. 31. Water head difference for 5 neap tides for North Wales Tidal Lagoon.....	130
Fig 6. 32. Electricity generation during the typical cycle for North Wales Tidal Lagoon.....	131
Fig 7. 1. Tidal level comparison between TELEMAC, DIVAST and BODC at Hinkley.	137
Fig 7. 2. Water level and power output with optimisation of revenue under scenario 2, during (a): neap tides and (b): spring tides, in which ‘Zup’, ‘Zlw’ and ‘Power output’ denoted the basin water levels, downstream water levels and power output at each time step for West Somerset Lagoon and North Wales Tidal Lagoon, respectively.....	141

List of Table

Table 3. 1 Pseudocode of the interpolation method of the discharge and power output from the hill chart.	33
Table 3. 2. Pseudocode of the OpenMP utilisation in the GA model.	34
Table 4. 1. Energy generation per cycle for the 0-D model.	41
Table 4. 2. Analysis of measured and predicted data at L2, L3 and L5.	50
Table 4. 3. Energy generation comparison between 0-D and 2-D models.	56
Table 5. 1. Optimisation scenarios for 2 nd tidal cycle.	82
Table 5. 2. Plus pumping optimisation scenarios for 2 nd tidal cycle.	85
Table 5. 3. Comparison of optimisation scenarios without pumping.	85
Table 5. 4. Comparison of optimisation scenarios with pumping.	86
Table 5. 5. Optimised operation heads under different turbine numbers during selected 1 st neap tide.	96
Table 5. 6. Optimised electricity output under different turbine numbers during selected neap tides.	96
Table 5. 7. Optimised electricity output under different turbine numbers during selected neap tide with pumping.	97
Table 5. 8. Summary of the flexible turbine numbers operated during selected neap tides.	97
Table 6. 1. Pseudocode of the Genetic Algorithm.	101
Table 6. 2. Comparison of different approaches used to optimise the operation of TRSs.	108
Table 6. 3. Optimisation under fixed operation schemes using GA and GS.	115
Table 6. 4. Comparison of optimisation scenarios using GA.	118
Table 6. 5. Optimum operation heads during the 1 st tide in multi-blocks optimisation.	125
Table 6. 6. Comparison of optimisation scenarios with updated West Somerset Lagoon (NumTB =125 and STPC=8).	126
Table 6. 7. Comparison of optimisation scenarios with North Wales Tidal Lagoon (NumTB =150 and STPC=10)	129
Table 7. 1. Pseudocode of the Genetic Algorithm with developed part highlighted based on Table 6.1.	138
Table 7. 2. Parameters setting in scenarios for flexible operation optimisation.	139
Table 7. 3. Summary of scenarios of flexible operation optimisation.	140

Table 7. 4. Parameters setting in scenarios for flexible operation optimisation with pumping. 142

Table 7. 5. Summary of scenarios of flexible operation optimisation with pumping. 142

1. Introduction

1.1 Background

There is a much better understanding of the impact of the Green House Gasses (GHGs) on climate change, and there are further social and political pressures to reduce GHGs [1]. The utilising of traditional energy, e.g. burning of coal, oil and natural gas could lead to a certain number of serious issues. Firstly, it is the main reason of the cause of global warming, which does harm to the planet and the living beings. Secondly, the exploitation of fossil fuel could cause unfortunate mishaps. Last but not least, traditional energy sources are finite and will be exhausted one day in the future. Hence, it is crucial for researchers to pay more attention to the development of renewable energy efficiency and so make it as the leading sources for electricity generation. Since clean and sustainable nature of renewable energy causes less harm to the environment comparing to the conventional energy including fossil energy technologies, enthusiasm for developing renewable energy has been continuously growing in recent years in the UK and globally. Scientists and engineers globally are continuously working in this area, especially in finding ways to develop these resources of energy in a more efficient way.

As mentioned above, it has caused a change in mindset at the demand level. At the same time, government schemes such as the Low Carbon Innovation Co-ordination Group (LCICG) aim to tackle supply issues [2]. The UK government wants to making sure that UK has a secure supply, reducing GHGs to slow down Climate Change and to stimulate investment in new jobs and businesses. Alongside this, the UK has set targets to deliver 50% of its energy consumption from renewable sources by 2025 [3], and an 80% decrease in carbon emissions [4], and finally achieve Net-Zero target by 2050 [5].

Marine Renewable Energy (MRE) is one of the emerging renewable energies being explored further. Currently, around 0.5 GW of commercial marine energy generation capacity is in operation globally and another 1.7 GW is under construction, with most of this accounted for the tidal range [6]. However, hydro and wave/tidal electricity generation only accounts for less than 5% of the total renewable energy in 2019 [7]. Tidal energy has the vital advantage of predictability over other renewable energy sources including wind and solar energy which largely depend on the weather condition. It is estimated that the tidal range resource in the UK will be between 25 and 30 GW [8]. However, the cost-efficiency of tidal range structures has been questioned and may not represent a good value for money. For instance, the UK Government has not supported the proposed Swansea Bay Lagoon (SBL) due to the high cost of electricity [9]. However, infrastructure projects are deemed to be a crucial way of creating thousands of jobs and this can help to speed up Britain's recovery from the COVID-19 pandemic [10]. This emphasizes the importance of fully exploiting these predictable tides to generate maximum possible electricity and revenue while keeping the cost down. Apart from the maximisation of the energy

generation, it is also possible to operate the schemes more flexibly to respond to the grid requirements. For example, generate and store more electricity into a 'battery' and then feed more into the grid at high demand times. As another example is, to generate a continuous power output distribution, known as one scenario of the flexible operation optimisation. This is also significant to the supply and demand balance. It is fundamental to the scheduling management of supply and demand for customers, especially when other forms of renewable energy such as wind or solar energy shut down in some extreme weather conditions including storm.

There are two major types of tidal renewable energy schemes: tidal stream and Tidal Range Schemes (TRSs), in which the tidal stream is designed to extract kinetic energy from tidal currents and TRSs are designed to harness the potential energy from rising and falling tides [11]. It will be a key scientific advancement to bring TRSs to a technological level that they can be a viable component in the renewable energy mix through engineering design, operation, reliability and cost reduction [12]. With the discount of the surges and other meteorological effects, tide times and levels can often be predicted long into the future, and therefore the potential energy generation can also be accurately assessed.

Tidal lagoons and barrages share the same theory for energy generation, which is to create an artificial head difference across the structure by impounding water at certain times and then using this hydraulic head difference to generate electricity [13]. However, rather than spanning the whole rivers or estuaries like barrages, tidal lagoons are designed to be offshore or onshore impoundments which encompass only part of the river. This is considered to be more environmental friendly comparing to barrages, particularly due to the lesser impact on fish migration [14].

In the absence of any operating tidal lagoon and the limited number of barrages, numerical models have an important role in the development of TRSs. Not only do they play a key part in the design and optimisation, but also facilitate the environmental impact assessment [15, 16]. These numerical models extend from 0-D models [17-20] to more sophisticated multi-dimensional modelling [13, 15, 17, 21-30] with High Performance Computing (HPC) capabilities. 0-D models, which are based on a range of simplifications and therefore have significantly reduced computational time, have been widely used in the optimisation of the TRSs which require an extremely large number of iterations [31-33]. Subsequently, the 2-D or 3-D models can be applied to validate the performance of the optimisation from 0-D model and assessment of environmental impacts [17, 34].

In the preliminary TRSs design stage, one of the key aspects is the optimisation of operational characteristics. This mainly involves the calculations of the head difference during the course when the scheme starts generating electricity and when generation stops, and also the active number of turbines, etc. Therefore, this operation will influence discharge transferred between the impoundment and open water, the basin water level, and therefore affect the amount of energy to be generated [31, 35]. Conventionally, the TRSs operate under the assumption that the generating head differences are set to be a constant value, which means the large difference in tidal ranges over time has been ignored, i.e. similar operation heads for all spring and neap and flood and ebb tides. However, it was found that this

scheme may not generate any electricity during some neap tides under fixed operation due to insufficient head difference across the scheme [35]. This high variability in the generation as well as maximising potential generation emphasise the significance to operate the schemes flexibly. To achieve this, this study will facilitate the flexible operation by splitting the operation for each tidal cycle up into smaller components, e.g. every tide or every half tide, and optimising the operation of TRSs using two typical optimisation approaches, namely Grid Search method and Genetic Algorithm. This can help to either generate the maximum energy and reduce the cost of the energy generation, or facilitate better utilisation of renewable energy by making multi-objective decisions to the needs of different researches.

Another key step of the preliminary design of TRSs is to identify the most suitable and optimised characteristics of the scheme, including the number of turbines and sluice gates. This could lead to a very large number of possibilities due to various combinations in the number of turbines, sluice gates and the tides over time which could affect the operation of the schemes and hence its electricity generation [36, 37]. However, this optimisation is crucial as it is directly linked to the economic feasibility of the scheme and its cost-benefit analysis. All these variables present a complex multi-objective task, e.g. a continuous or flat power output, that requires an efficient decision-making tool using advanced optimisation methods for optimisation.

The sheer scale of the tidal range plants requires a significant initial investment and the nascent status of the technology relative to other electricity generation methods which make the researches in TRSs to be essential for further development [31]. Hence, the operational characteristics and deployment of such hydraulic structures play a decisive role in not only the aspect of electricity generation but also the economical aspect of the scheme including investment and earnings. This in turn directly impact the approval of the scheme and therefore needs to be conducted to a high level of accuracy.

1.2 Research objective

In this thesis, 0-D model coupling with two optimisation methods has been developed to deliver the complete design of the most optimised TRSs, through identifying the number of turbines, sluice gates and most optimised operation schemes including pumping, for particular sites. The aim of this research was to optimise the design and operational characteristics of Tidal Range Schemes (TRSs) to make them more economically attractive by maximising the energy generation, or a flexible energy output to achieve multi-objectives. The objectives were to propose and optimise flexible operation schemes to maximise energy generation and to achieve the flexible energy output optimisation, including utilising generation flexibility from multi-lagoons to help match the continuous trends of energy output. The aim has been attained by achieving the following key objectives:

- Assessing the modelling approaches for the TRSs simulations, especially for the electricity generations and the state-of-the-art hyperparameter optimisation approaches.
- Implementing traditional and two different optimisation approaches, e.g. Grid Search and Genetic Algorithm methods, to maximise the electricity generation under flexible operation scenarios, by breaking the operation into small components, e.g. Every tide or Every half tide, to optimise the operation of TRS and coupling with a widely used 0-D modelling as the evaluation tool.
- Developing the optimisation approaches to optimise the design and deployment of TRSs coupled with flexible operation and even with pumping utilised.
- Achieving optimisation to contribute to flexible power output by utilising the flexibility of multi-schemes using multi-objective decision making, including continuous power output.

Achieving these research objectives will help to promote the TRSs proposals being more economically attractive and help the electricity system. It will provide a better understanding of the operation flexibly and assist with more reasonable designs of TRSs proposals.

1.3 Outline of the thesis

The thesis is divided into eight chapters, including:

Chapter 1: Introduction, which introduces the research background and identifies the research objectives for this study.

Chapter 2: Literature review, which provides an introduction of the Tidal Range Schemes and relevant optimisation methods, as well as an overview of the published articles in the relevant fields while highlighting the gaps in knowledge which this thesis aims to fill.

Chapter 3: Numerical modelling, which presents the relevant governing equations and background of a traditional 0-D and 2-D models, including the DIVAST 2-DU model used in this thesis.

Chapter 4: Case studies, which illustrates the details of different case studies selected for this research, including Swansea Bay Lagoon, West Somerset Lagoon and North Wales Tidal Lagoon. In particular, the baseline scenario with the traditional non-flexible operation was implemented with both the 0-D and 2-D model, which constitutes the baseline scenario for the development of more advanced optimisation schemes.

Chapter 5: Tidal Range Schemes' Operational and Design Optimisation, which addresses the optimisation of flexible operations using various Grid Search methods with a case study of Swansea Bay Lagoon, and then the performance will be verified by developing the 2-D modelling under the same scenarios.

Chapter 6: Tidal Range Schemes Optimisation using a Genetic Algorithm, which proposes a developed Genetic Algorithm model to further optimise the design parameters combining the flexible operations simultaneously. A comparison between the Genetic Algorithms herein and Grid Search methods in Chapter 5 was carried out in terms of the amount of electricity generation and computational efficiency. In addition, designing the optimal layout of West Somerset Lagoon and North Wales Tidal Lagoon were carried out in this chapter included optimisation of the schemes based on a single block or multiple blocks of turbines, e.g. all turbines located in one housing unit or located in different housing units along the structure.

Chapter 7: Flexible operation optimisation, which discusses the application of the Genetic Algorithm model in the flexible operation optimisation for multi-objective decision making by considering multi-scheme collaboration.

Chapter 8: Conclusion, which summarises the main outcomes of this research and provides recommendations for future works.

2. Literature review

2.1 Introduction

This chapter presents an overview of the currently available literature relevant to this study. It covers various aspects of the research. The emphasis has also been put on the introduction of two hyperparameter optimisation methods, namely Grid Search methods (GS) and Genetic Algorithms (GAs) which will be utilised in this thesis for optimisation of the TRSs.

In section 2.2, a general insight into renewable energy, describing the development of tidal power, is given. Then the operation approaches for energy generation (electricity) in TRSs are described, known as flood-only, ebb-only and dual-way generation methods. On the one hand, the optimisation of operational parameters introduced in the generation method is one of the targets in this research; on the other hand, the design parameters are another fundamental field for TRSs optimisation. This highlights the potential of the multi-parameter optimisation in TRSs, such as optimising the flexible operation schemes and even with design parameters simultaneously. In section 2.3, the existing numerical models are illustrated, including a widely used 0-D model and more sophisticated multi-dimensional models and software. The 2-D Unstructured model, known as Depth Integrated Velocities And Solute Transport (DIVAST 2-DU) model, is presented. The 2-D model is utilised as an input tool for the 0-D modelling setup and the validation tool to evaluate the 0-D optimisation performance in this research. And finally, a quick review is given to the assessment of using GS and GAs for predictions and optimisations mainly in the field of marine energy in section 2.4.

2.2 Renewable energy

2.2.1 Tidal energy

Energy can be extracted from the marine environment from either the tides or waves. Tidal energy, in particular, has the important advantage of predictability over other renewable energy sources and it is estimated that the tidal range resource in the UK will be between 25 and 30 GW [8]. However, as illustrated in the introduction, the key scientific advances are required to bring tidal energy generation to a technological level, allowing it to be fully exploited with higher efficiency. This is a complex issue that requires consideration of many factors including the engineering design, operation, reliability and cost reduction [12]. With the discount of the effects of surges and other meteorological impacts, tidal cycles times and levels can be predicted long into the future, and hence the energy-generating potential can also be accurately assessed. Generating energy from the tides requires harnessing either the potential energy of rising and falling tides, or kinetic energy from tidal currents [11].

As two of the key elements of tidal energy, the turbine and sluice play essential roles in the energy generation. A turbine (from the Greek word "τύρβη" for "whirling" or a "vortex") is a rotary machine that converts kinetic energy and potential energy of water into mechanical work [38]. It has two types in general, namely the reaction turbine and the impulse turbine, in which the reaction turbine operates by changing pressure as it moves through the turbine and it is commonly used in low and medium head applications, e.g. in TRSs [39] due to the variable and even low head of water levels especially during the neap tides [40]; The impulse turbine operates by changing the velocity of a water jet which often used in very high head applications. Take the La Rance tidal plant as an example, it employed a series of small reaction turbines (known as bulb turbines) running along with the structure [41, 42]. That is, as one of the most efficient reaction turbines, bulb turbine is designed with the generator attached to the turbine shaft in a watertight pod, or bulb, directly behind the turbine runner [43, 44], as shown in Figure 2.1. To fully exploited the available energy more effectively, this type of turbine has been utilised in the design of other TRSs including the SBL by Tidal Lagoon Power (TLP) [45].

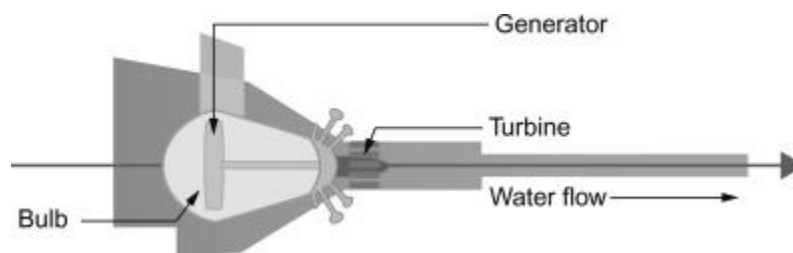


Fig 2. 1 Cross-section of a typical bulb turbine [43].

A sluice (from the Dutch "sluis") is originally a hydraulic structure to control the water channel at its head by a gate. The terms sluice, sluice gate, knife gate, and slide gate are used interchangeably in the water-related field including hydropower and wastewater control [46]. It can be used to control

water levels and flow rates by regulating the water flow through an impermeable structure, such as an impoundment wall in TRSs. An extended concept of sluice gate simply consists of an entire sluice caisson including the gate which is made of wood or metal barrier, sliding in grooves as shown Figure 2.2, although technically speaking, the sluice gate refers to only the gate structure.

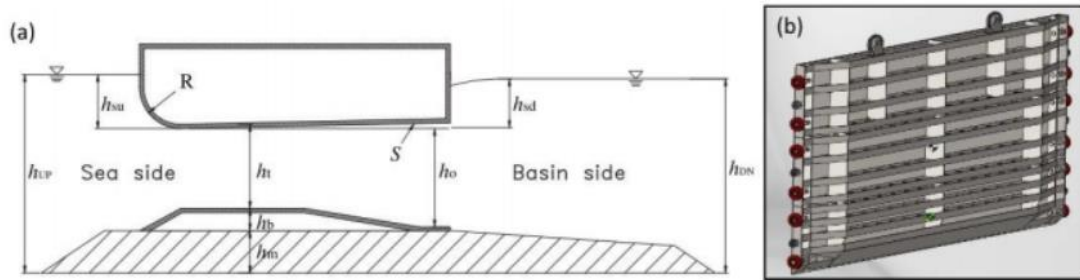


Fig 2. 2. An example of (a) a water passageway [47] and (b) a sliding gate [48] typically used in TRSs designs.

Sluice gates are one of the critical parts of the tidal range structures which allow more water flows in/out of the impounded basin. The main functionality of the sluice gates is to increase the efficiency of the scheme as well as ensuring managing the hydro-environmental and ecological impacts of the scheme. A typical design of a sluice caisson used in SBL is represented as follows:

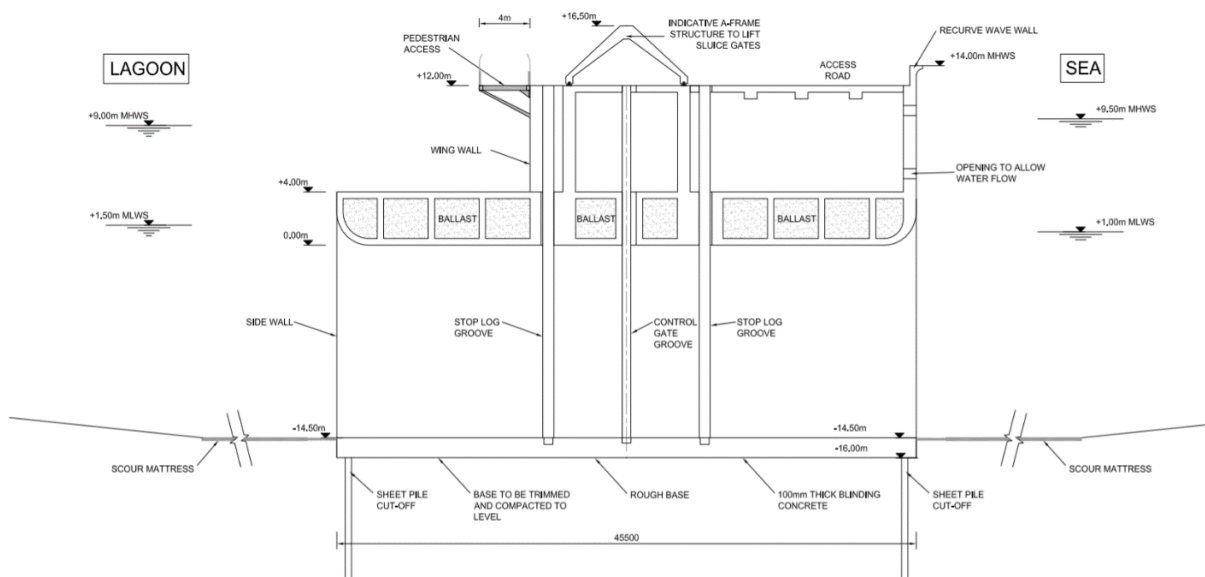


Fig 2. 3. Cross-section of a sluice caisson proposed for the Swansea Bay Lagoon [48].

They are two major types of tidal renewable energy schemes: tidal stream and TRSs. The power output of tidal stream turbines is calculated as follows [49]:

$$P = \frac{1}{2} C_p \rho A V^3 \tag{2.1}$$

where P is the extracted power; C_p is the turbine power coefficient; ρ is the fluid density; A is the cross-sectional area of the turbine and V is the fluid stream velocity. Potential power extracted by TRSs is calculated as follows:

$$P = \rho g H Q \quad (2.2)$$

where g is the gravitational acceleration; H is the head difference across the impoundment and Q is the discharge through the turbines. Integrating power to time is given as follows:

$$E \propto A_p H^2 \quad (2.3)$$

where A_p is the plan surface area of the impoundment and E is the power output. The equation demonstrates that for high energy yield, a large surface area with a high tidal range must be enclosed. Similar to tidal stream resources, sites identified as having high potential for tidal range generation can be hydrodynamically modelled to investigate yield, explore optimisation options and assess potential environmental impacts [50-52].

2.2.2 Tidal Range Schemes

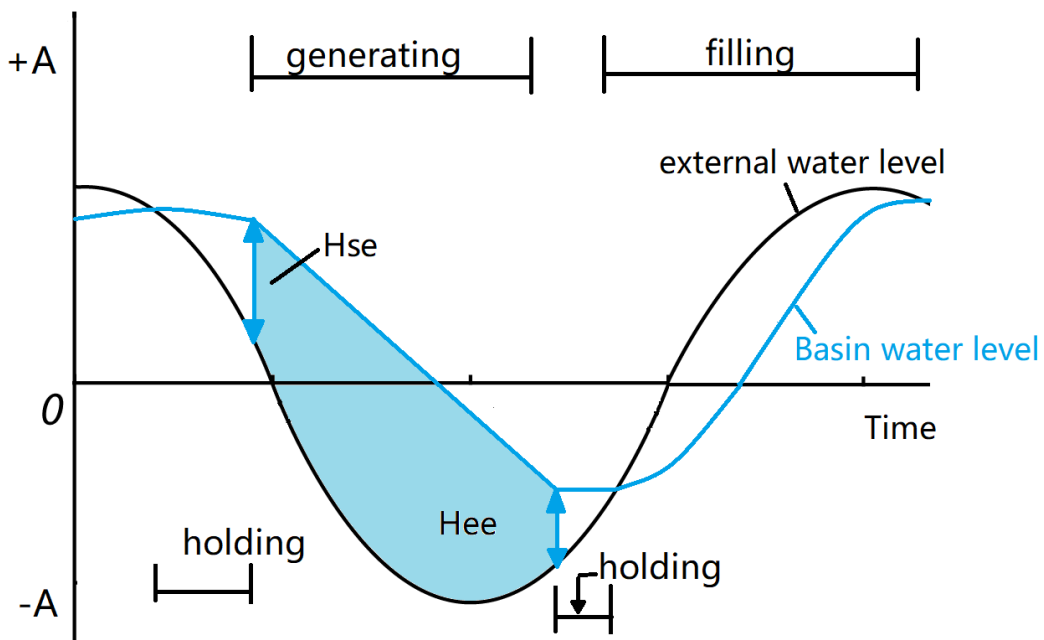
2.2.2.1 No pumping operation

Xia et al. [26] showed that the two most effective operational schemes are ebb-only and 2-way generation. Therefore, this study mainly focuses on these operational schemes and schematic illustrations of them are shown in Figures 2.4(a) and (b), respectively.

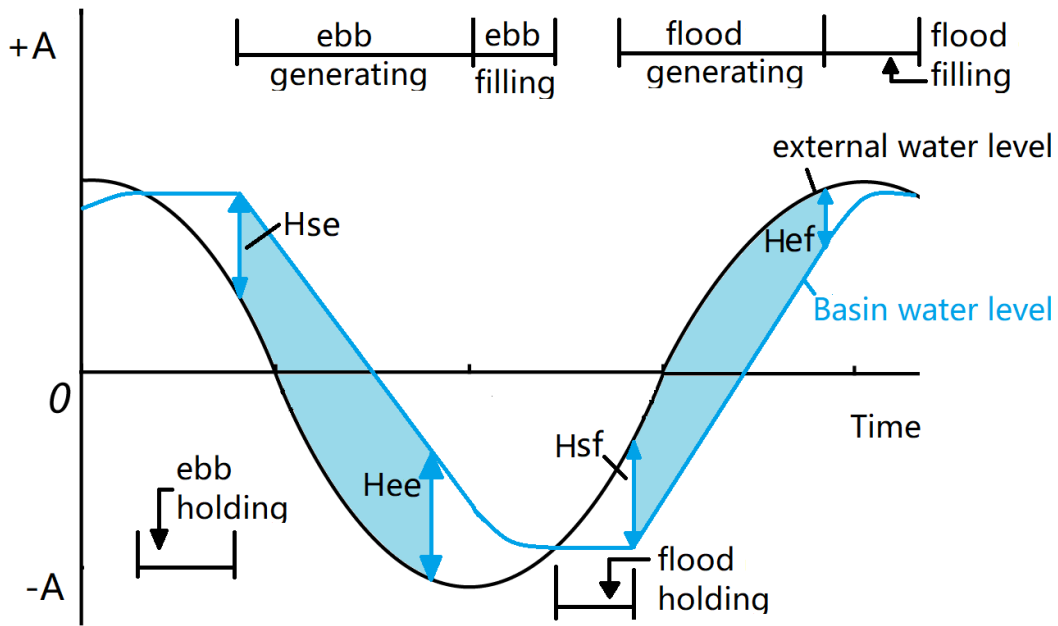
Ebb-only generation starts with a holding stage at a high tide by closing both the turbines and sluice gates. This means that there is no flow between the outside sea and the impounded water body and hence the impounded basin water level stays at around high tide, while the seaward water level recedes with the tide. Ebb generation phase commences when the head difference between the water level inside and outside the basin, referred to as H_{se} herein, is large enough to generate energy efficiently by turbines' rotating. This ebb generation phase keeps continuing until the head difference across the impoundment embankment is not sufficient to generate energy efficiently anymore, referred to as H_{ee} herein. At this time, the second holding phase commences, with both the turbines and sluice gates being closed again. The downstream water levels are then raised again with the flooding tide and the filling phase starts by opening both sluice gates and turbines which allowing the seaward water entering the basin. This filling stage is followed by a holding phase for the next cycle when the water levels at both sides reach almost the same level. A schematic of the ebb generation scheme is illustrated in Figure 2.4(a).

Starting from the ebb holding phase, for two-way generation, both the sluice gates and turbines are closed until the head difference across the impoundment embankment is large enough for an efficient generation, in other words, reaching a starting head for ebb tides of H_{se} . This stage of the ebb generating phase works by operating the turbines in order to generate energy from water head difference and continues until the head difference across the impoundment is no longer adequate for efficient energy

generation, i.e. reaching the ending head H_{ee} towards the end of the ebb tide. Following that, the sluice gates and turbines are opened to empty the basin, until the water levels across the impoundment embankment are almost the same. After that, the flood holding phase begins by closing the turbines and sluice gates until the head difference is higher than the starting head during flooding, i.e. H_{sf} . This is followed by the flood generation phase, where the turbines are operated again to generate energy from water head difference. When the head difference is smaller than ending head, namely H_{ef} , the sluice gates are opened as well to raise the water levels inside the impoundment. The next ebb holding phase commences when the water levels across the impoundment embankment reach the same levels and the water level outside the impoundment starts falling again with the ebb tide. This can be seen as a periodic process, which repeats itself throughout each cycle. A schematic of the two-way generation scheme is illustrated in Figure 2.4(b).



(a)



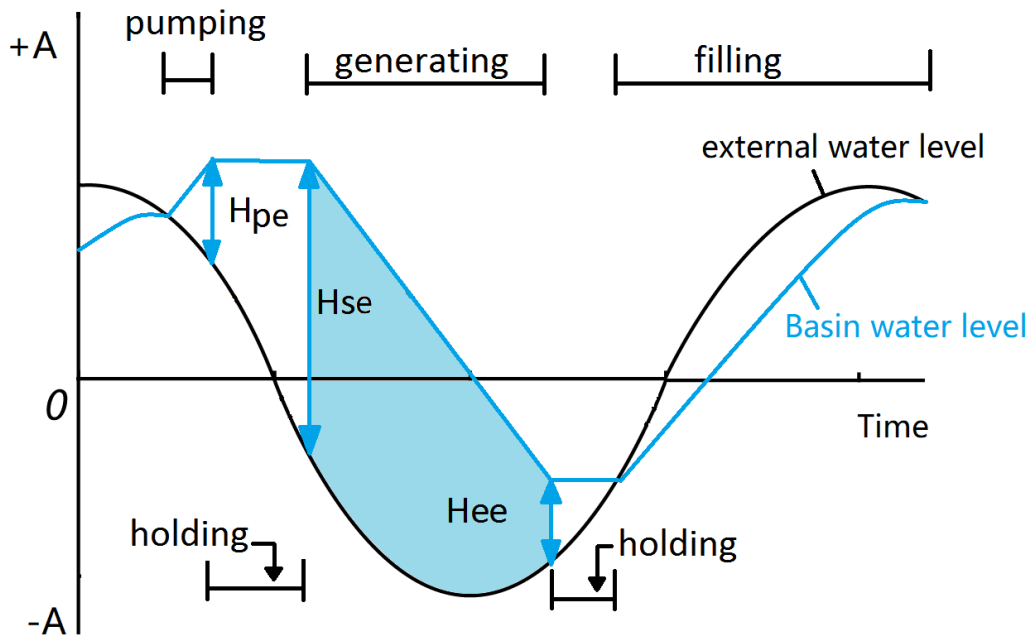
(b)

Fig 2. 4. Schematic representation of the operational schemes: (a) one-way ebb-generation; (b) a two-way tidal power plant.

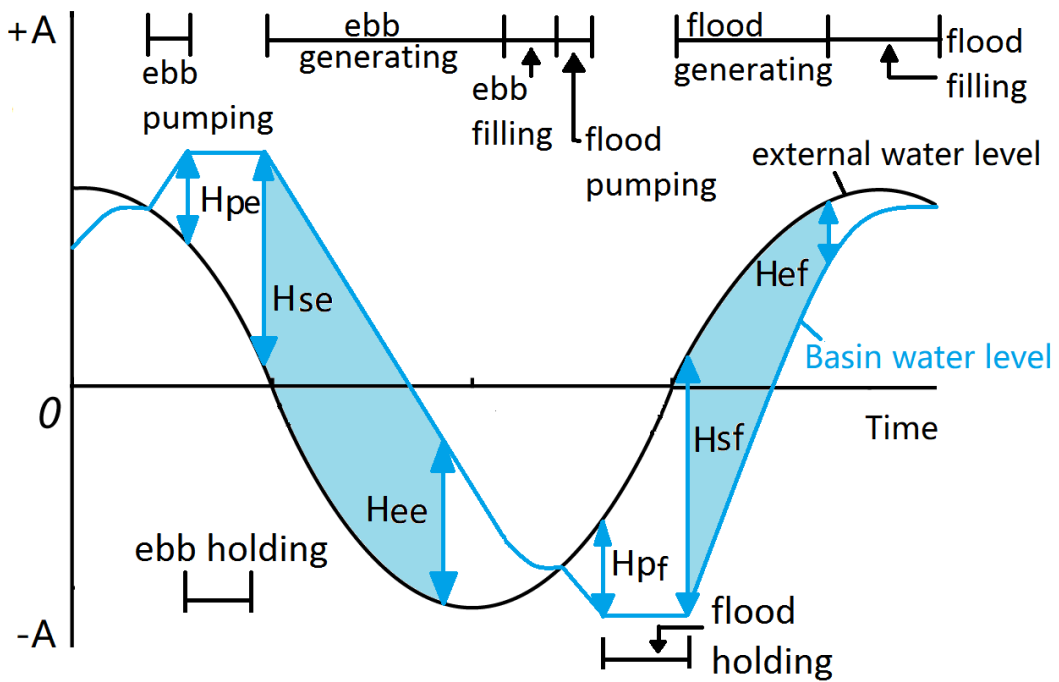
2.2.2.2 with pumping operation

The total energy generated by a tidal range scheme can be potentially increased by taking advantage of pumping, at high and low water [53]. It should be noted that if the turbines are also designed for pumping there will not have any significant increase in the cost of the scheme. Furthermore, pumping could also bring additional environmental benefits [53] not only generating more energy.

In practise pumping is introduced during the holding phases if the bi-direction turbines utilised in a TRS. In the ebb-only generation mode, the objective is to raise the water level inside the basin to a maximum by pumping when the water level difference across the impoundment embankment is small. This generates a bigger head difference H_{pe} , and in turn more energy when the seaward water level falls with the ebbing tide. For the two-way generation scheme, pumping during ebb generation will be similar to pumping for the ebb-only scheme. Pumping will be used to lower the water levels H_{pf} inside the basing during the flood holding phase. This will generate a higher head difference during the flood generation phase. After pumping, the extra energy output due to the larger head difference with lifted or lowered basin water elevations could offset the energy consumption during pumping. Hence, pumping is economically feasible when the combined efficiency losses of pumping and generation are partially offset by the gained power output as a result of an increased head difference in the TRSs revenue optimisation. Schematic illustrations for the ebb-only and two-way generation with pumping are illustrated in Figures 2.5(a) and (b), respectively.



(a)



(b)

Fig 2. 5. Schematic representation of the operational mode (including pumping) of (a) one-way ebb-generation; (b) a two-way tidal power plant.

Hence, one of the key aspects of the operation of such schemes is the head difference at the time when the scheme would be programmed to start generating energy and when generation stops, and even pumping during ebbing or flooding tides. Therefore, TRSs can be operated in various ways for each type of operation scheme, i.e. for flood, ebb or two-way generation, and this operation will influence

the basin water level and discharge transferred between the impoundment and open waters, and therefore affecting the energy generated [31, 35].

2.2.3 Tidal Range Schemes optimisation

Key aspects of design, in the preliminary stage of TRSs, is the characteristics of the scheme, such as the number of turbines and area of sluice gates, and optimisation of operational characteristics as introduced above. This optimisation could be carried out in different ways based on the requirement and the purpose of the scheme. For instance, optimisation could be carried out for multi-objective decision making, such as to maximise electricity generation or revenue or use multiple schemes to work in a synchronised way to generate a continuous power output.

Flexibility in TRSs is the ability to generate flexible electricity through an unrestricted, free range of motion [54], refer to a flexible operation scheme and hence flexible electricity output. It is crucial to achieve flexible operation of the scheme and its cost-benefit analysis during the optimisation in order to ensure that the scheme is practical and the number of turbines and sluice gates are providing the maximum benefit. Hence, the optimal design and operational characteristics at the preliminary stage can benefit an informed quantification of investment risk and return for investors and decision-makers.

2.2.3.1 Operational Parameters Optimisation

2.2.3.1.1 Maximization of electricity generation

In fact, tidal power technologies have advanced considerably over the past few years and one of its key purposes is to provide electricity for local needs. A variety of numerical modelling tools have been developed to optimise the TRSs parameters and to maximise the electricity generation which has a significant influence on the feasibility of any proposed scheme [55]. The researches in terms of the maximisation of annual electricity generation were mainly achieved using 0-D modelling, which can be seen in section 2.3.1.

2.2.3.1.2 Flexible operation optimisation

Flexible operation is the capture of energy produced flexibly. TRS can be used as one of gravitational potential energy to convert potential tidal energy into electricity at a specific time. However, as known that the tidal energy is intermittent from the semi-diurnal flood and ebb of the tides for twice a day, through to Spring-Neap variability for approximately 14 days [56], which makes it to be a big challenge to produce flat or continuous power output from a TRS especially during neap tides, known as one of the scenarios in the flexible operation optimisation. Hence, it is promising to optimise the overall energy generated from multi-scheme [57] and to the supply for predictable changes in demand, such as the daily patterns of human activity, as well as unexpected changes from equipment overloads and storms. Flexible operation optimisation plays an essential role in this balancing act. Additionally, it can facilitate

better utilisation of renewable energy through the development of TRSs by making multi-objective decisions to the needs of different researches, including the revenue optimisation [58].

To compensate the duration without power output for flat or continuous power output, future studies could consider other renewable energy sources including wave, solar and wind acting on other timescales and apply appropriate optimisation approaches to determine optimum renewable energy roadmap scenarios [56]. One of the concepts was the use of a land fault between lakes in a large park preserve for generating and storing clean renewable energy [59], known as the pumped hydro storage facility. This stored electric energy for peak demand is valuable on the wholesale electricity industry, especially when it is created in a zero-carbon renewable form. It is useful among worldwide to harness hydroelectricity from water as it is inputted and outputted to the grid during peak times and then developed again during low usage to restore the water back up to the reservoir.

However, based on the author's review, there is no research qualify this optimisation. As put forward by Neill et al. [57] and Schaffer et al. [60], the gap without power output could be potentially makeup by treating multiple lagoons as a system and taking advantage of operational flexibility to generate electricity during high national demand for electricity and thus the value of power output was seen to be increased with electricity price variance. Benefit from this method, tidal power will be fed to the grid at several locations and it will contribute to a more efficient electricity distribution [22]. It has been partially supported by limited studies [31, 32]. For example, a combined operation of two tidal lagoons was simulated by taking a gradient-based technique for flexible operation schemes optimisation [31]. It revealed a flexible distribution of power output if considering operation flexibly although only the maximisation of electricity generation was targeted in this study. More recently, Harcourt et al. [32] improved the gradient approach for operation flexibly over the precise timing of power generation with a single case study, aiming to generate greater power output during peak demand for electricity and hence results in an increase of more income. Besides, a continuous operation was delivered by introducing financial incentives associated with reliable, baseload supply, making the economic assessment of the tidal power plant system being achieved [61]. However, a comprehensive flexible operation optimisation with more scenarios is waiting to be achieved and evidenced through simulation by developing an appropriate optimisation algorithm and taking multiple case studies [62] into consideration.

2.2.3.2 Design Parameters Optimisation

The design parameters of the scheme influence the cost and annual electricity generation, i.e. revenue, and has a direct impact on the feasibility of the scheme and therefore it needs to be conducted to a high level of accuracy. Hence, it is significant to optimise various scenarios with different basin sizes, number of sluice gates and turbines during the design phase of the scheme. However, the researches in the optimisation of designed parameters to Marine Renewable Energy (MRE) are limited. Leite Neto et al. optimised the dispatch of turbines during the generation process to maximise the electricity generation [63]. Results showed that it was possible to increase the electricity generated

significantly by optimising the dispatch of turbines with the non-flexible operation schemes [63]. Aggidis and Benzon used a 0-D model to evaluate the electricity generation in relation to varying trends in energy demand [18]. They optimised non-flexible driving heads based on the size and number of turbines, which varies with the barrage and/or lagoon dimensions and characteristics.

However, as described above, there is limited research on the researches of traditional non-flexible operational and design parameters, and no study on the optimisation of operation flexibly with various design factors simultaneously, which are closely relevant to the electricity generation and hence impact the feasibility of the TRSs. Furthermore, some TRSs could have multiple blocks of turbines located in sperate turbine housing units and the most optimised operation schemes for a single unit is expected not be the most optimum one for all the other blocks.

2.3 Predictive tools for electricity generation

2.3.1 0-D modelling

A variety of numerical modelling tools have been developed for optimising the TRSs parameters and to predict and maximise the electricity generation, from 0-D models [17-20] to more sophisticated multi-dimensional models [13, 15, 17, 21-30] with HPC capabilities.

On the one hand, the accuracy of multi-dimensional models is higher than the 0-D model because it underpins the inherent basic fluid mechanics, with the preliminary assumptions in 0-D model refined and developed more accurately. On the other hand, the 2-D or 3-D models are more expensive than 0-D models, especially during the optimisation of TRSs which requires a large number of runs [55] even with the utilisation of the HPC [17].

0-D modelling has been used for the preliminary assessment of hydraulic structure representation, in comparison with multi-dimensional modelling [17, 52]. For example, a particular focus was on the comparison of the water levels adjacent to the impoundment, the discharge through the hydraulic structure and the power generation between the 0-D and 2-D modelling, which highlighted that the 0-D methodology could be utilised for the optimisation of the processes [17]. However, it was argued that the 0-D model overestimated the potential energy for large intertidal regions as well as the upstream surface area, in comparison with 2-D modelling [21]. For example, Angeloudis et al. showed that 0-D models could overestimate the energy predictions by up to 40% when compared to the prediction based on more sophisticated and accurate 2-D numerical models [17, 52, 64]. They concluded that the 0-D approach overestimation is relative to the size of the scheme. They suggested that 0-D predictions are reliable for design optimisation at the preliminary stage and need to be complemented by more sophisticated 2-D or 3-D models [64].

In 0-D modelling, a typical 0-D backward difference model based on the continuity equation was proved to be able to minimise the overestimated results in some extension [18, 29, 65], ensuring it to be a reliable tool for the prediction of the electricity generation and hence contributes to the optimisation of TRSs. However, in practice, the development of 0-D model refinement has considerable potential with more accurate expressions and estimations. For example, Burrows et al. [29] took advantage of the previous turbine hill-chart given by Baker [66], developing a Turgency program to calculate the outflow and power output relationship accurately; Also, Aggidis et al. refined its characteristics in the hill-chart with a non-dimensional formula known as affinity laws [36] and the volume of water enclosed the combination of depth-volume curve and tidal curve [18]; Petley et al. implemented the cutting-edge turbine data and high-resolution bathymetric data into 0-D modelling for more accurate prediction [65].

It should be noted that all of these studies have used constant driving and minimum generation heads throughout the operation, i.e. for all spring and neap and flood and ebb tides. However, with this fixed operation schemes, there might not have any power output during some neap tides due to insufficient

tidal range. This emphasized the significance of using flexible operation schemes, which uses variable operation heads in each unit of operation to maximise the electricity generation.

Following that, various parameters including the starting water head, turbine numbers and turbine diameters have been optimised to explore the maximum annual power output utilising the 0-D model [65]. Based on the authors' extensive literature review, Ahmadian et al. [35] and Yates et al. [67] have separately discussed the concept of variable driving and minimum generation heads for each operation period, namely half a tide, and highlighted the potential improvements achievable by implementing variable driving and minimum generation heads. More recently, Angeloudis et al. [31] and Xue et al. [33] took advantage of a gradient-based and grid-search methods, respectively, for the optimisation of flexible operation heads with an overall increase in electricity generation of around 10% delivered with pumping, compared to conventional non-flexible operation. Moreover, Merlin et al. [40] have explored the optimisation of TRSs in terms of the maximisation of revenue income. By improving the gradient-based method [31], it could increase the income for the case study of SBL to at least 20% compared to a non-adaptive operation [32].

Research on using pumping to increase electricity generation has been limited and was mainly carried out using a constant driving and minimum generation head throughout. Yates et al. used an unlimited pumping head and constant generating head to study the influence of turbines (including pumping) efficiencies in a 0-D model [23]. They found that the overall energy could be improved by about 17% if pumping was included in a two-way generation scheme which uses constant values for turbine and pump efficiencies. Furthermore, Douglas et al. [68] showed that pumping could increase energy generation by approximately 10%. Their results were consistent with the findings of Aggidis and Benzoni [18]. However, it should be noted that they used the same hill-chart for both the energy generation and pumping phases, with scaled-down maximum power output. With a lack of detailed information, they also assumed a combined efficiency during the pumping phase. In the literature there is a very limited number of studies for the case of pumping, with the majority of studies using fixed operation heads for the schemes. Additionally, in these studies, unified operation schemes was adopted at different blocks of turbines in large TRSs, ignoring that the tidal range varying at each block which may not yield to the most optimised energy output. Multi-blocks operation refers to different blocks of turbines operates using different optimal operation schemes, taking the most use of tidal ranges at different sites. Consequently, developing the flexible operation scheme/schemes for a single block or multi-blocks of turbines, during the whole tidal cycle and including pumping, is another novel aspect being investigated in this study.

Optimisation of the entire scheme with some degree of confidence is particularly crucial in the early stages of operational design, due to its significant influence to the cost and annual electricity generated and has a direct impact on the feasibility of any proposed scheme [55]. However, one of the key challenges is the various design variables of the scheme, including basin size, number of turbines and sluice gates and the operation schedule. The optimal design of a scheme requires a large number of

simulations to be undertaken due to the multi-parameter nature of such schemes for optimisation which can be computationally expensive. This simplified approach of 0-D modelling is cheaper than any other multi-dimensional models, although it provides a higher level of uncertainty in the early stage of design which can be verified further using either 2-D or 3-D modelling tools.

2.3.2 multi-dimensional modelling

The simulation of hydrodynamics of coastal waters is expected to provide significant insight into tidal energy assessment. A number of different hydro-environmental models, including the Depth Integrated Velocities And Solute Transport (DIVAST), Environmental Fluid Dynamics Code (EFDC) and TELEMAC-2D, and more computationally expensive 3-D models have been used in hydro-environmental modelling of TRSs [47, 69, 70].

Depth-average 2-D models, including DIVAST model, enjoy the greatly simplifies in the analyses by assuming the solute can be well-mixed vertically over the water column. This model is constructed using a “cell-centred” and “mesh vertex” layout [71], in which the “cell-centred” is achieved by assuming each grid as a controlled volume and the variables are placed at the centre of the volume, and the “mesh vertex” denotes that the variables are positioned at the centre of the vertexes of a cell. It has been proved to be able to simulate the mass and momentum transfer between the basins separated by the structure [71]. These simulations can be a powerful tool for the calculation and optimisation of energy extracted from tides, as well as the potential impacts of coastal constructions.

DIVAST model was developed at the Cardiff University Hydro-environmental Research Centre (HRC) for modelling the hydrodynamic, sediment transport and bacterial processes which has been widely used in various projects. For example, Brammer et al. simulated the hydro-environmental impacts at Severn Estuary by using DIVAST and physical models [72]. The numerical results showed good agreement with the corresponding laboratory data. Ahmadian et al. developed DIVAST to investigate both the potential far-field and near-field hydro-environmental impacts of the North Wales Coast [73]. DIVAST showed a satisfying performance in terms of the prediction of the water elevations, tidal currents and consequently flood risk, sediment concentrations and background bacterial levels in a large domain in the Severn Estuary and Bristol Channel.

On the other hand, DIVAST model can be used to predict the electricity generation. Xia et al. [50] used a numerical estimation based on the solution gained from DIVAST model. After predicting the potential annual power output from Severn Barrage, it has been demonstrated that the electricity generation calculated from DIVAST model could be similar to the officially reported value by the Department of Energy and Climate Change (DECC), in the UK. Furthermore, DIVAST model can be developed with many improved terms, especially for turbines. For example, Ahmadian and Falconer refined and applied this model with significant interactions of turbine arrays and flows successfully [38]. Results proved that this DIVAST model is a vital tool for the assessment of power output. Besides, the

potential tidal stream energy was assessed by Xia et al. [74] under with or without the Severn Barrage, mean power distribution and different candidate tidal stream energy sites, which could also be the evidence that the DIVAST model was reliable for the prediction of electricity generation. All of these make DIVAST to be a useful tool to verify the electricity prediction using 0-D modelling in this study. Its full development and application will be presented in more details in Chapter 3, 5 and 6, respectively.

EFDC is a hydrodynamic modelling suite which is an open-source code developed and supported by the engineering company Dynamic Solutions-International. The code was first adapted for the simulation of TRSs in a study by Zhou et al. [28], including the numerical implementation of hydraulic structures to represent turbines and sluice gates, the use of hill chart to calculate turbine flow rate and implementation of operational sequence algorithm for different operating modes. The EFDC model was further developed under a certain number of configurations of the turbines and sluice gates [75].

TELEMAC-2D is another hydrodynamic modelling suite in the field of free-surface flow by solving the Shallow Water Equation (SWE) in a studied domain discretized by finite element mesh. It is able to simulate the hydrodynamics [76] with a wide range of applications, such as dam breaks, harbour structures design and river floods [77-80]. Apart from that, it can be developed for the evaluation of tidal energies including the tidal stream energy [81] and TRSs [13], with the velocities over the simulation period could be utilised for the optimisation of tidal structures at a wide range of sites. It could be developed and applied to analyse, predict, and quantify the potential changes in tidal hydrodynamics (water levels, tidal range, circulation patterns and tidal currents) due to a certain number of scenarios with several numbers, size and location of TRSs.

3-D model is normally developed from the 2-D grid with the vertical direction extended by a certain number of vertical layers, as employed in the popular 3-D software like TELEMAC-3D [82] and Delft 3D [83, 84]. Results showed that 3-D models could simulate the magnitude of velocity more accurately which may be overestimated in the 2-D models [82]. One of the significant concerns of the 3-D model is that the computational cost is much expensive than lower-dimensional models which are proportional to the number of layers, but with higher accuracy of prediction [83, 84].

The long list of the collected literature above indicated the gradual progression from a simple conceptual model to a flexible and stable numerical multidimensional model. The simple 0-D model is cheap under a large number of scenarios for the tidal energy analysis but with relatively lower accuracy due to the absence of hydrodynamics simulation, compared with multi-dimensional models. Multi-dimensional models can support the investigation of hydrodynamics processes related to the TRSs but only under very limited scenarios due to its costly running time. Consequently, it has been shown that the 0-D model and 2-D models can complement one another, particularly in enabling the number of computationally expensive 2-D model simulations to be reduced and improve the accuracy of the 0-D model. In other words, multi-dimensional numerical models without barrages or lagoons can provide the input water level as boundary conditions for 0-D models. In return, 0-D models can support multi-dimensional models with optimised parameters for more accurate predictions [33].

2.4 Hyperparameter optimisation

The problem of flexible operational and design parameters in TRSs described corresponds to the hyperparameter optimisation [85, 86]. In detail, hyperparameter optimisation or tuning is the problem of choosing a set of optimal hyperparameters for a learning algorithm [87]. A hyperparameter is a parameter whose value could be used to control the evaluation process. The approaches to hyperparameter optimisation cover a wide range of methods [88], ranging from the traditional local optimisation approaches such as Grid Search (GS) [33] and Gradient-based methods [31] to a global optimisation approaches such as Evolutionary Algorithms (EAs) [87, 89] and Bayesian Optimisation (BO) [90]. Global optimisation finds the optimal value of a given function among all possible solution whereas local optimisation refers to find the optimal value within the neighbouring set of candidate solutions [91]. In this study, the global optimisation refers to a most optimised results during the typical Spring Neap tidal cycle while the local optimisation refers to the optimisation during a small component, e.g. Every Tide or Every Half-tide. Normally we consider the local optimisation as the baseline, providing the prior belief of global optimisation to jump out of the most local optimal solutions [88]. Thus, this research developed the GS methods as the representative of the local optimisation methods and the GA as the global optimisation methods which will be developed further mainly in Chapter 5, 6 and 7, respectively.

2.4.1 Grid Search Methods

A traditional way of performing multi-objective optimisation has been GS method, which is simply an exhaustive searching through a manually specified subset of the hyperparameter space [92, 93]. Figure 2.6 illustrates the GS of nine trials for optimisation a function of $f(x, y) = g(x) + h(x) \approx g(x)$. Each dot represents one trial with a set of hyperparameters. The distributions shown on each axis represent the model's score. We're searching over a hyperparameter space where the one hyperparameter has significantly more influence on optimising the model score while holding all other unimportant hyperparameters constant. All possible combinations of hyperparameter values defined by the grid are evaluated to select the best set. The advantage of the GS is that it is capable of finding the most optimised parameters after exploring throughout the whole searching space and it is simple to implement with no technical overhead or barrier. However, the GS method may suffer from the coarse of the grid. For example, in Figure 2.6, the nine trials blatantly missed the optimal score, that is, the peak of $g(x)$ (marked as green area) was not obtained via the grid with nine trials. However, if a finer grid adopted, it will spend redundant time exploring the unimportant parameter and hence to be computational expensive [94].

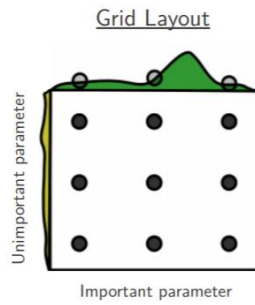


Fig 2. 6. Grid Search of nine trials for optimising a function $f(x,y) = g(x) + h(x) \approx g(x)$ with low effective dimensionality. Above square $g(x)$ is shown in green, left square $h(x)$ is shown in yellow. Nine trials only test $g(x)$ in three distinct places [94].

There are a large number of studies applying the GS into engineering and computational science [95-97]. Dinh and Baan developed the GS to study the discrimination between changes of pore pressure and water saturation by predicting the grids of time-lapse attributes within a range of pressure and saturation. Results showed that the GS model performed very well and the model was able to contribute to the quality control and uncertainty analysis [95]. Ensor and Glynn implemented the GS in the parameter estimation of stochastic optimisation. The objective function was managed to be optimised by GS in the mathematical aspect [96].

However, very limited studies can be found in the optimisation of TRSs using GS in the seeking of optimal local parameters [33]. Importantly, there is no research on the optimisation of operational and design parameters which needs to be conducted to a high level of accuracy.

2.4.2 Genetic Algorithm

Genetic Algorithm (GA) is one of the most popular types of Evolutionary Algorithms (EAs) in optimisation problems [98]. GA approach considers each parameter being optimised as a gene and each solution which includes all the genes is called an individual or a chromosome. Genes can be reproduced in each iteration or generation for some of the individuals in the population through evolutionary processes. For each generation, all individuals are evaluated for fitness using a fitness function. The iterating process or reproduction of new generations is stopped if an individual in that generation satisfies the predefined termination criterion.

EAs have been widely used as an efficient and time effective optimisation tool which allows cutting-edge modelling especially in the fields of engineering and science [99]. EAs and particularly GAs have demonstrated to be competitive methods in several fields including Engineering [100-102]. Besides, GA has been used for the prediction of hydrodynamics such as tidal currents [103], wave height [104] and sea levels [105]. For instance, a GA model has been used and found to be quite satisfactory in conjunction with empirical orthogonal function analysis for the forecast of the basin-scale tidal current

[103]; Also, prediction of satellite altimeter derived fields of Sea Level Anomaly (SLA) has been carried out using GA by Ratheesh et al. [105]. It has been found that GA was able to improve upon persistence forecast in all the cases and the improvement varies from 6% to 23%. However, the exploitation of GAs to MRE has been limited [106-108]. Sullivan and McCombie investigated the potential of using GAs for optimisation of tidal power arrays as a multi-objective problem [106]. Their work demonstrated the ability of GAs to find a successful arrangement of tidal stream turbines, with minimum cost and appropriate performance of tidal stream turbines. Furthermore, Child and Venugopal showed that superior results could be obtained using GAs for the optimisation of wave energy converters layout [107]. Their results were consistent with the findings by Kontoleon et al. [108] which proved that it was possible to predict tidal stream energy or TRSs using EAs particular GAs with a satisfactory result. Leite Neto et al. discussed the maximum energy gains obtained with the dispatchable turbines by using GA for the optimisation. They investigated the potential of using GA to address the simple-effect operation [63]. Two major advantages of GA coupled with 0-D models are its relative computational simplicity and the fact that it requires much less input information for optimisation, in comparison with multi-dimensional models. As a result, it can be concluded that although the GA may not provide insight into the physical connection between TRSs, it can quickly provide us with reliable information on operational purposes at a low computational cost.

It should be noted that there were very few studies using GAs or similar EAs to optimise the TRSs with various variables, e.g. different numbers of turbines and sluice gates when TRSs operate flexibly, in terms of the maximisation of electricity generation or the flexible operation optimisation. But once achieved, it will have significant value at the TRSs design stage.

2.5 Chapter Summary

In this chapter, a literature review of using 0-D or multi-dimensional modelling in the optimisation of TRSs has been presented. It emphasizes the significance of the optimisation of TRSs using 0-D or other multi-dimensional modelling for the purpose of maximisation of electricity generation and the flexible operation optimisation. Furthermore, GS and GA as the representatives of local and global optimisation methods in hyperparameter optimisation were illustrated which provides significant confidence of using both approaches in the optimisation of TRSs in this study.

The previous studies on renewable energy and particularly TRSs have been investigated In section 2.2. Although there are a number of studies on the optimisation of TRSs in the literature, the studies on the design and operational parameters optimisation were found to be very limited. Moreover, there was no study on the optimisation of multi-blocks operation in which each block of turbines has its own operation scheme. This could significantly influence the cost and annual electricity generation, and has a direct impact on the feasibility of the scheme. To fill these gaps, the flexible operational parameters will be studied in this thesis using the GS and GA approaches, under single blocks and multi-blocks scenarios, respectively. Besides, the flexible operation optimisation by two schemes simulations proved to be another aspect and required to be further studied. It helps the TRSs to facilitate better utilisation of renewable energy through the development of TRSs by making multi-objective decisions to the needs of different researches. This will be addressed in this thesis by considering more schemes, including the West Somerset Lagoon (WSL) and North Wales Tidal Lagoon (NWTL) in Chapter 7.

In section 2.3, a variety of numerical modelling researches have been reviewed for predicting and optimising the TRSs, from 0-D models to more sophisticate multi-dimensional models. It highlighted that the 0-D model as a simple and cheap method could be considered an ideal tool for the optimisation of TRSs which may require a large number of runs and cannot be achieved by other multi-dimensional models. In section 2.4, as the representatives of the local or global hyperparameter optimisation methods, the GS methods and the GA have been introduced, respectively, and proved to be capable for the optimisation of TRSs in this study.

3. Numerical modelling

3.1 Introduction

This chapter mainly introduces the relevant governing equations and background of a traditional 0-D and 2-D models, respectively. In the 0-D modelling, the basin water levels are calculated from the previous upstream and downstream water levels according to the continuity principle. The model assumes that the water is distributed uniformly and instantaneously in the impoundment when the inflow or outflow goes through turbines and/or sluice gates, instead of using a more complex but realistic 2-D modelling approach. Comparing to multi-dimensional modelling, 0-D modelling is able to save the computational cost significantly and hence can be considered to be an efficient tool for the TRSs optimisation with a large number of scenarios in this study. However, the 2-D numerical models present to be a more sophisticated and accurate alternative to 0-D model because that they can underpin the inherent basic fluid mechanics and hence are more accurately but computationally expensive. Consequently, 2-D modelling plays an important role in this study, to be used to predict the input water levels in 0-D models and to validate the performance of a series of optimisation using 0-D modelling but with the simulation of hydrodynamics.

In section 3.2, the simplified continuity equation in the 0-D model is explained. In section 3.3, the methodology and governing equations that define the hydrodynamics properties in the 2-D model are introduced. Following the calculation of the water level from the 0-D or 2-D models, the energy and discharge through turbines can then be calculated based on the hill chart, as illustrated in section 3.4. Finally, section 3.5 describes the HPC utilised in this study.

3.2 0-D modelling

As one of the most important factors in the energy generation prediction, the water level is calculated based on the mass conservation equation, also known as the continuity equation, which reflects the fact that mass is conserved in any non-nuclear continuum mechanics analysis [109]. The equation is developed by adding up the rate at which mass is flowing in and out of a control volume, and setting the net in-flow equal to the rate of change of mass within it [110].

$$\frac{\partial H}{\partial t} + \frac{\partial q_x}{\partial x} + \frac{\partial q_y}{\partial y} + \frac{\partial q_z}{\partial z} = 0 \quad (3.1)$$

where q_x , q_y and q_z represent discharges per unit width in the x-, y- and z-axis directions, respectively ($m^2 s^{-1}$); H denotes the water surface elevation above datum (m) and t represents time (second).

In the approach outlined by Baker [66], the key assumptions in 0-D models include that the discharge through turbines (Q) is a constant and the wetted plan surface area (A) is a constant. So that the changes of the basin water level (dH) at a time duration (dt) can be expressed as:

$$\frac{dH}{dt} + \frac{Q}{A} = 0 \quad (3.2)$$

Based on the assumption that the water is distributed uniformly and instantaneously in the impoundment when discharging, a typical 0-D backward difference model was developed from the Eq. 3.2 to solve the continuity equation for the water level calculation. The new upstream water levels inside the impoundment ($Z_{up, i+1}$) at any point in time can be calculated according to both the upstream water levels at the previous time step ($Z_{up, i}$) and the downstream water levels ($Z_{dn, i}$), as follows:

$$Z_{up, i+1} = Z_{up, i} - \frac{Q(H) + Q_{in}}{A(H)} \Delta t \quad (3.3)$$

where Δt denotes the time step (second); Q_{in} is the inflow/outflow to the lagoon through sources other than through the TRS (m^3/s), e.g. a river or outflows; $A(H)$ is the wetted plan surface area (m^2) of the lagoon at the water surface H; $Q(H)$ is the total discharge through the turbines and sluices (m^3/s) which is +ve when flows into the impoundment, which will be discussed further in section 3.4 [17].

3.3 2-D modelling

3.3.1 Governing equations

DIVAST 2-DU has been widely used in simulating marine renewable energy schemes in the past [25, 51, 111]. It has been modified in this study to simulate lagoons, with flexible operation schemes being generated from 0-D models. The governing equations used in the DIVAST 2-DU model are developed based on the mass and momentum conservation equations.

3.3.1.1 Mass conservation equation

Developed from the mass conservation equation in Eq. 3.1 and based on the assumption in DIVAST 2-DU model that the flow is well-mixed in z-direction [112], the mass conservation equation can be written as:

$$\frac{\partial H}{\partial t} + \frac{\partial q_x}{\partial x} + \frac{\partial q_y}{\partial y} = 0 \quad (3.4)$$

3.3.1.2 Momentum conservation equation

The momentum conservation equations were utilised to describe the motion with viscous fluids and developed based on Newton's second law of motion to an infinitesimal fluid element [70]. The 2-D depth-integrated momentum conservation equations in x and y directions, respectively, are given in Eqs. 3.5-3.6 which are derived by integrating the 3-D Reynolds average equations [71, 112].

$$\frac{\partial q_x}{\partial t} + \beta \left[\frac{\partial u q_x}{\partial x} + \frac{\partial v q_x}{\partial y} \right] = \underbrace{f q_y}_3 - \underbrace{g H \frac{\partial \xi}{\partial x}}_4 + \underbrace{\frac{\tau_{xw}}{\rho}}_5 - \underbrace{\frac{\tau_{xb}}{\rho}}_6 + \underbrace{\varepsilon \left[2 \frac{\partial^2 q_x}{\partial x^2} + \frac{\partial^2 q_x}{\partial y^2} + \frac{\partial^2 q_y}{\partial x \partial y} \right]}_7 \quad (3.5)$$

$$\frac{\partial q_y}{\partial t} + \beta \left[\frac{\partial u q_y}{\partial x} + \frac{\partial v q_y}{\partial y} \right] = \underbrace{f q_x}_3 - \underbrace{g H \frac{\partial \xi}{\partial x}}_4 + \underbrace{\frac{\tau_{yw}}{\rho}}_5 - \underbrace{\frac{\tau_{yb}}{\rho}}_6 + \underbrace{\varepsilon \left[2 \frac{\partial^2 q_y}{\partial x^2} + \frac{\partial^2 q_y}{\partial y^2} + \frac{\partial^2 q_x}{\partial x \partial y} \right]}_7 \quad (3.6)$$

where H is the total water depth (m) and ξ is the water surface elevation above datum (m); β represents the momentum correction factor; f denotes the Coriolis parameter, which is caused by earth rotation (rad s^{-1}); g is the gravitational acceleration (m s^{-2}); τ_{xw} and τ_{yw} are the surface wind stress components in the x- and y-axis directions, respectively (N m^{-2}); τ_{xb} and τ_{yb} represent bed shear stress, also in both directions; and ε is depth-averaged eddy viscosity ($\text{m}^2 \text{s}^{-1}$).

Based on the finding that it is expected to have very limited impact on the predicted energy generation as shown by Coz et al. [70], the momentum terms can improve the accuracy of the wake characteristics. However, since this study mainly focused on the optimisation of TRSs, rather than investigating the hydro-environmental performance of the scheme, no extra momentum source terms have been included across the impoundment wall. In briefly, term 1-3 in the momentum conservation equation refer to the local acceleration, advective (or convective) acceleration and the external body forces, respectively. For an accurate simulate the hydrodynamics, the momentum correction factor β in term 2 is a dimensionless value accounting for the non-uniform distribution of velocity across the flow

section. This parameter can be estimated either from field data, which is preferable, or alternatively by assuming a logarithmic velocity profile to give [112]:

$$\beta = \left[1 + \frac{g}{C^2 \kappa^2}\right] \quad (3.7)$$

where κ is von Karman's constant of 0.41 and C is de Chezy bed roughness coefficient which can be determined using the Manning formula, which expresses C in terms of the local depth H as follows:

$$C = \frac{H^{1/6}}{mn} \quad (3.8)$$

where mn = Manning roughness coefficient, with typical values of n being in the range from 0.015 for smooth lined basins rivers to 0.04 or more for complex bed topographies or where vegetation effects are significant.

The effects of the earth's rotation, wind shear, bed friction, and turbulent shear stresses are denoted as term 4 to 7, respectively. Take the x -direction as an example, a quadratic friction law for surface wind stress expression is generally assumed, giving:

$$\tau_{xw} = C_s \rho_a W_x W_s \quad (3.9)$$

where ρ_a is the air density (kg/m^3); W_x is the wind velocity component in the x -direction (m/s) and W_s is the wind speed (m/s)[112]; C_s represents the air-water resistance coefficient which is normally specified using a piecewise formulation, such as [113], whereby:

$$\left\{ \begin{array}{l} C_s = 1.25 \times 10^{-3} W_s^{-0.2} \text{ for } W_s \leq 1 \text{ m/s} \\ C_s = 0.5 \times 10^{-3} W_s^{-0.5} \text{ for } 1 < W_s \leq 15 \text{ m/s} \\ C_s = 2.6 \times 10^{-3} \text{ for } W_s > 15 \text{ m/s} \end{array} \right\} \quad (3.10)$$

For the bed friction, this term is also generally represented in the form of a quadratic friction law, as given by:

$$\tau_{xb} = \rho g Q_x \frac{V_s}{C^2 H} \quad (3.11)$$

where V_s denotes depth average fluid speed (m^3/s).

A structured or unstructured mesh with grids is generated to make the master equation suitable for the numerical simulation [114]. In this study, an unstructured triangular mesh has been deployed to cover the studied domain which enables the arbitrary and geometry at a finite set of points to be replicated at each time step [71].

3.3.2 Domain decomposition

In numerical modelling, discretization is the process of transferring continuous functions, models, variables, and equations into discrete counterparts [115]. This process is usually carried out as a first step toward making them suitable for numerical evaluation and implementation on digital computers. As one of the discretization methods, finite volume method has been widely used in a variety of

researches [24-27, 50, 70, 114, 116], based on the integral form of the conservation laws rather than pure continuum mathematical concept [115]. This enables two sub-domains to be generated and which are fully detachable to simulate the complex flow going through hydraulic structures.

Domain decomposition is used in this study to simulate the lagoon. In particular, the upstream sub-domain represents the lagoon impoundment, whereas the downstream sub-domain represents the rest of the Bristol Chanel and the Severn Estuary. It should be noted that both of the sub-domains are non-overlapping, and each is covered by its own triangular unstructured mesh. Both sub-domains are linked dynamically, according to interior open boundary conditions defined through a water level and discharge relationship, as introduced in next section and operated over time according to the sequences without and with pumping implemented, respectively.

3.4. Power and discharge calculation

3.4.1 Turbines

A hill chart is commonly used in TRSs researches to represent the discharges through the turbines and subsequently the energy generated [66]. That is, at a specific water head calculated from the 0-D or 2-D models, the corresponding discharge and power output are interpolated through the explicit relationship in the hill chart which is normally not available to obtain due to the commercially sensitive nature. Alternatively, like in the continental shelf scale model, the discharge through turbines was calculated by applying the Eq. 3.17 [66, 75].

The hill chart for the Andritz Hydro double-regulated bulb turbine with the diameter of 9 m is shown in Figure 3.1 and this relationship was used in the calculation of discharges and power output via turbines [66]. This hill chart has been widely applied to a wide range of researches in terms of electricity estimation and hydrodynamic assessment in 0-D or multi-dimensional models [17, 24, 26]. Notably, the minimum operation head in the hill chart is from 1 m which indicates an operation head of equal or greater to 1m should be considered when using the hill chart for the interpolation calculation.

The hill chart from turbines with different sizes have been derived by scaling the existing hill chart based on the area. For this purpose, a coefficient of turbine ratio (Op_Turb_Ratio) in Eq. 3.12 was implemented in this study to adjust the hill chart for a specific size, with the results can be seen in Figure 3.2 with an example of a 7.2m diameter of the turbine.

$$Op_tb_ratio = \left(\frac{DI_TB}{DI_hillchart}\right)^2 \quad (3.12)$$

$$P_{tb} = P_hillchart \times Op_tb_ratio \quad (3.13)$$

$$Q_{tb} = Q_hillchart \times Op_tb_ratio \quad (3.14)$$

where Op_tb_ratio represents the squat of the ratio of the diameter of the designed turbines in a specific study (DI_TB) over the diameter of the turbines utilised in the hill chart ($DI_hillchart$); the $P_hillchart$ and $Q_hillchart$ denote the power output and discharge in the hill chart, respectively; the P_{tb} and Q_{tb} are the calculated power output and discharge for the designed turbines, respectively.

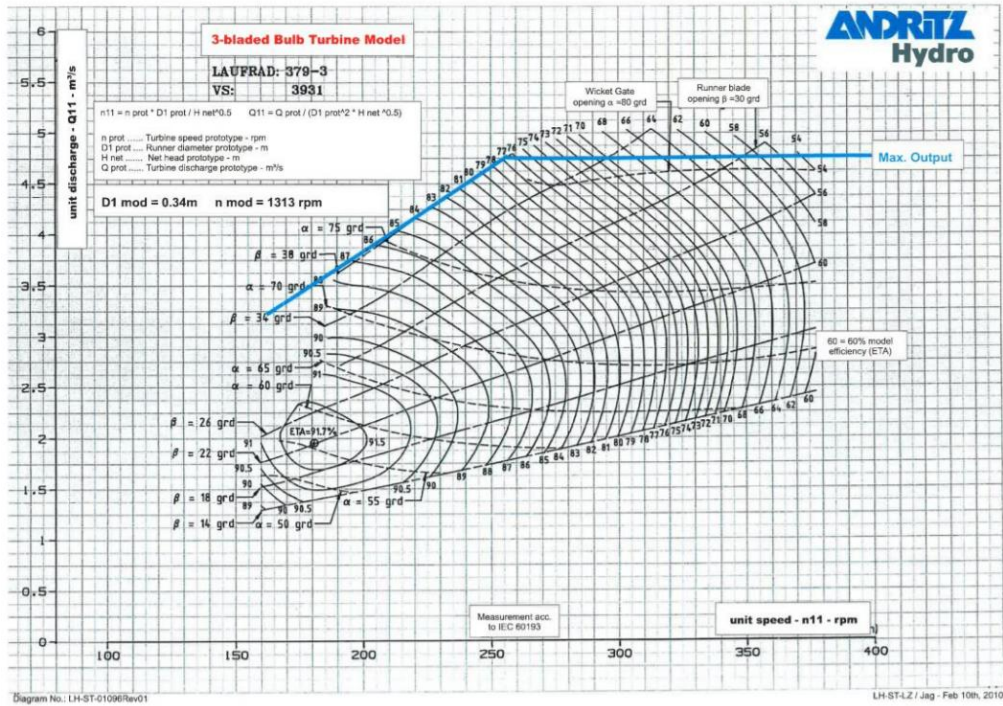


Fig 3. 1. Andritz Hydro three-Blade low head bulb turbine unit [36].

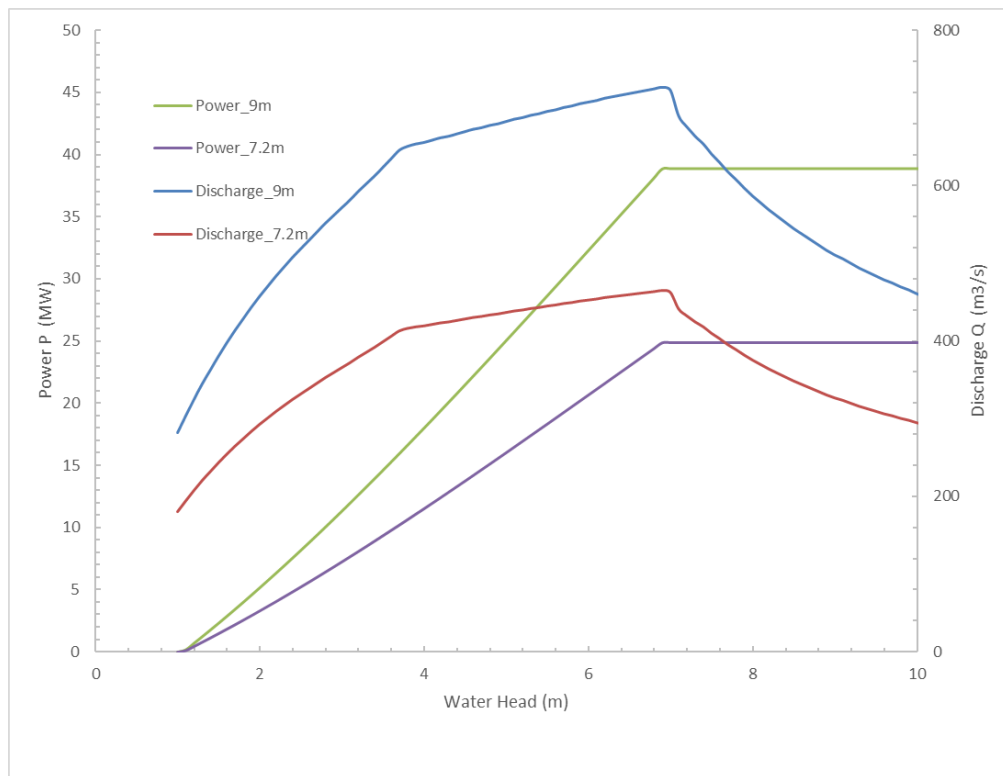


Fig 3. 2. Turbine Q-H and P-H comparison for the diameters of 7.2 m and 9 m, respectively.

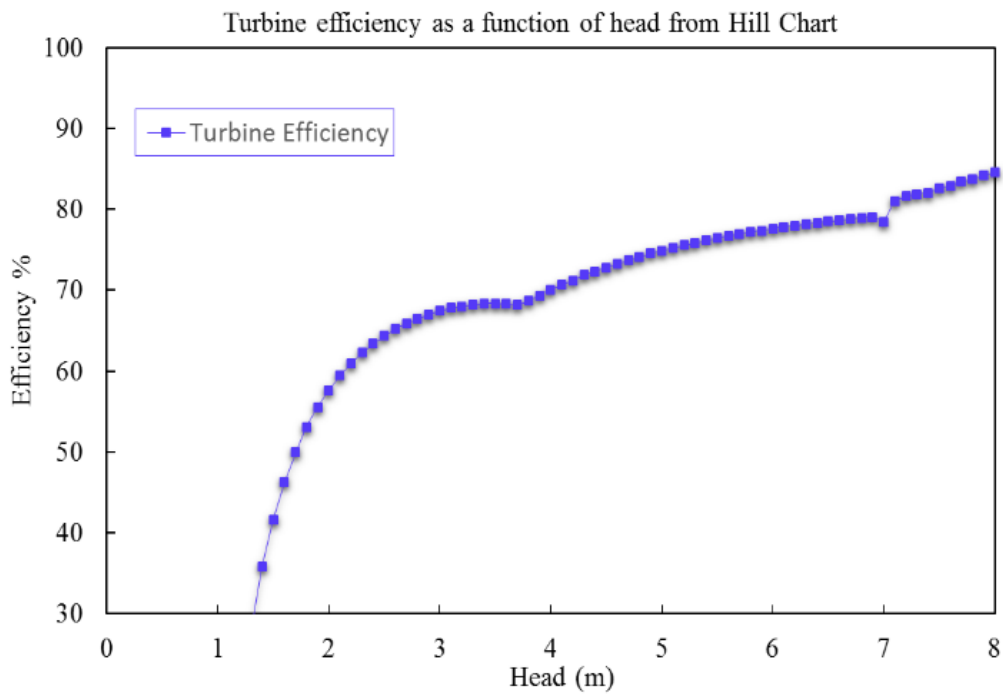
As introduced in Chapter 2, pumping can be implemented to increase electricity generation by creating a higher water level difference for energy generation through turbines' rotating. The turbine and pump efficiency can be calculated as:

$$\eta_t = \frac{P_{\text{output}}}{P_{\text{potential}}} \quad (3.15)$$

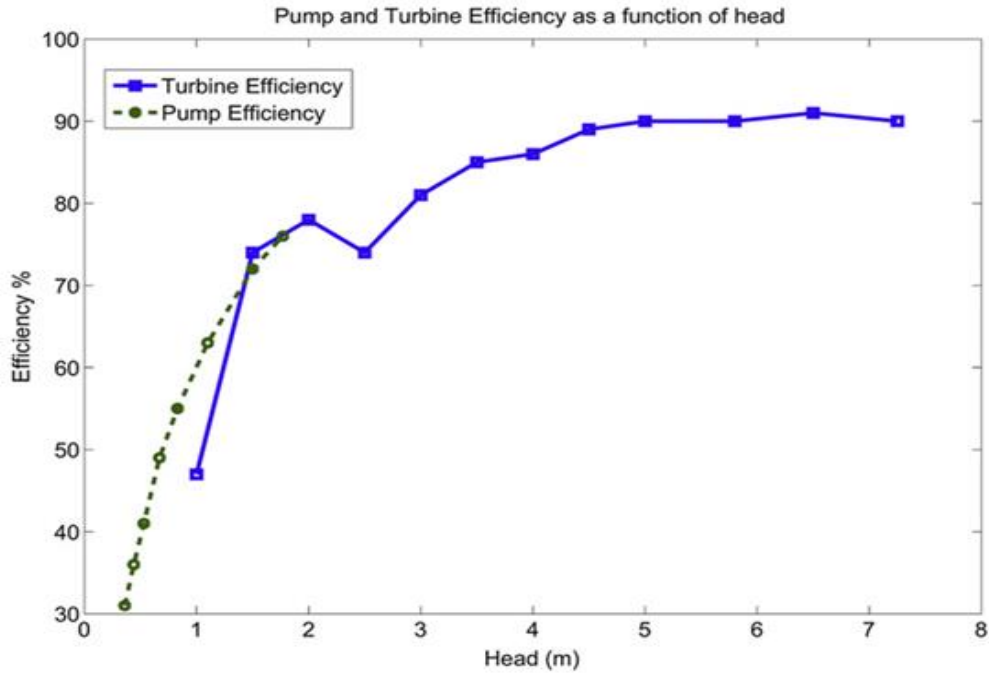
$$\eta_p = \frac{P_{\text{potential}}}{P_{\text{input}}} \quad (3.16)$$

where η_t and η_p are the turbine and pump efficiencies, respectively; P_{output} and P_{input} denote the power output for the turbines and the power used during the pumping phase, respectively; $P_{\text{potential}}$ represents the potential power output of the turbines or as used in pumping.

The resulting turbine efficiency obtained from the hill chart is shown in Figure 3.3(a). Figure 3.3(b) illustrates the measured turbine and efficiency for the bulb turbines with $DI_{\text{hillchart}}=7.2$ m [23]. Clearly, the turbine efficiency utilised in this study matches very well with the measured efficiency, mirroring the reliability of the hill chart used in this study.



(a)



(b)

Fig 3. 3. Turbine efficiency: (a) calculated from Fig. 3.1; (b) measured turbine and pump efficiency [23].

3.4.2 Sluices

The sluice gates have been incorporated in the numerical model in a similar way to turbines [116, 117] or were regarded as the ‘gap’ in a wall, using adjustable cells that could be switched between open and close, or changed between wet and dry. However, more recently, they have been represented as orifices [75]. The discharge through a sluice gate is calculated only during the sluicing phase using the following equation [36, 114]:

$$Q_{in} = C_d A_s \sqrt{2gH} \quad (3.17)$$

where g is the gravitational acceleration (m/s^2); A_s is the sluice gate area (m^2) and H is the head difference across the impoundment wall, calculated as $Z_{up,i} - Z_{dn,i}$; C_d is the dimensionless coefficient to characterise the flow behaviour from an orifice or valve.

Backer suggested a value of 1 for the C_d [66]. The studies of the choice of C_d have been very limited [27] with the majority of researches also applied a C_d of 1 as the suggested value [38, 116]. Although a certain number of uncertainties existing regarding this coefficient, Bray has shown that the impacts are limited and minor changes in C_d can be adjusted during the later stage of the design [114].

3.4.3 implementation into the numerical model

Following the holding phase, the discharge and power output through turbines are interpolated from the hill chart based on the pseudo-code in the table below. The discharge through turbines is calculated during the generating and sluicing phase. The power output is only interpolated during the generating phase.

Table 3. 1 Pseudocode of the interpolation method of the discharge and power output from the hill chart.

Algorithm The pseudocode of the interpolation method

Given

- Number of points in the Q-H table: N_p
- Q, P and H values in the table: $(Q_{t,i})$, $(P_{t,i})$ and $(H_{t,i})$
- Water level at upstream and downstream: $(Z_{up,i})$ and $(Z_{lw,i})$

Calculation

- 1: Calculate the head difference; $H = |(Z_{up,i}) - (Z_{lw,i})|$
 - 2: **If** it is during generating phase:
 - 3: **If** $H \leq H_{t,1}$, then $Q_{tb} = 0, P_{tb} = 0$
 - 4: **Elseif** $H \geq H_{t,N_p}$, then $Q_{tb} = Q_{t,N_p}, P_{tb} = P_{t,N_p}$
 - 5: **Else:**
 - 6: **For** $i=2, N_p$
 - 7: **If** $(H_{t,i-1} \leq H \leq H_{t,i})$
 - 8: Calculate the interpolation factor: $\alpha = \frac{(H-H_{t,i-1})}{(H_{t,i}-H_{t,i-1})}$
 - 9: Interpolate: $Q_{tb} = (1 - \alpha)Q_{t,i-1} + \alpha \times Q_{t,i}$
 - 10: $P_{tb} = (1 - \alpha)P_{t,i-1} + \alpha \times P_{t,i}$
-

3.5 Use of High Performance Computer

High Performance Computing (HPC) is a rapidly evolving area which helps research in different fields by increasing the computing power significantly.

The utilisation of HPC and running the models parallelly has a major impact on the speed and the efficiency of the 0-D and multi-dimensional modelling. Open Multi-Processing (OpenMP), as an efficient method in shared-memory machines, can distribute the do-loop over the different threads: each thread computes part of the iterations. It is a valuable tool that enhances the performance of the numerical model and reduces the computational time proportionally to the number of cores utilised [118].

In this study, an OpenMP version of the 0-D model was developed which gave a significant reduction on simulation time comparing to the original serial code, particularly when the models were executed on the HPC. The pseudo-code of achieving OpenMP can be seen in Table 3.2.

Table 3. 2. Pseudocode of the OpenMP utilisation in the GA model.

Algorithm The pseudocode of the OpenMP in the GA model

```
1:  proc Set_up          //Set up algorithm's parameters
2:  proc the mutation and recombination in the GA process
3:  !$OMP DO           //Calculate the electricity generation parallelly in the process of selection
4:    Do i = 1, solution_size
5:      Evaluation of the electricity generation of each solution
6:    End do
7:  !$OMP END DO
```

3.6 Chapter summary

This chapter outlined various methodologies of numerical modelling in TRSs that will be utilised in this study, including the 0-D and DIVAST 2-DU models. Furthermore, the HPC along with parallel programming using OpenMP has been illustrated in this chapter. Its technique will be used in this study to speed up the simulations which require millions of runs with significantly reduced computational time.

In section 3.2, the simplified continuity equation in the 0-D modelling has been introduced to simulate the water levels based on a series of assumptions. After that, the mass conservation equation and the 2-D depth-integrated momentum conservation equations in x and y directions in the DIVAST 2-DU model were described in section 3.3, respectively. It followed by a domain decomposition approach that is used to link the upstream and downstream of sub-domains dynamically via a hill chart. Then in section 3.4, the hill chart has been introduced which will be implemented and interpolated at every time step within the simulation duration in the numerical models. In section 3.5, the technique of HPC with a parallel programming method of OpenMP has been introduced.

4. Case studies

4.1 Introduction

There are many possible locations in the UK that could be potentially feasible for the development of Tidal Range Schemes (TRSs). Three notable sites currently being considered are Swansea Bay Lagoon (SBL) and West Somerset Lagoon (WSL) located in Bristol Channel in the South West of the UK, and North Wales Tidal Lagoon (NWTL) located along the North Wales coast. The development of the 0-D model is achieved under the traditional fixed operation heads schemes and will be further developed as part of the key contributions in this study. Next, the 2-D model is set up with the optimised operation schemes from the 0-D model to evaluate the feasibility of the schemes and identify the differences between 0-D and 2-D models.

In section 4.2, the details of SBL proposed by TLP is introduced. The 0-D model is set up with a case study of SBL and a typical Spring Neap cycle was selected in the year of 2012 as the representative of the capacity of annual electricity generation. Following that, a range of fixed operation schemes have been optimised without/with pumping included, respectively, to achieve the maximum electricity generation and this result is verified by the 2-D model.

In section 4.3 and 4.4, the proposals of WSL and NWTL promoted by Long Bay Sea Power and North Wales Tidal Energy & Coastal Protection (NWTE) are introduced, respectively. Currently, both projects are at the feasibility study stage and the finding of this thesis have contributed to these studies. The operation of each scheme for the maximisation of energy generation is optimised and reported in Chapter 6 while the combined generation of the schemes for flexible energy output optimisation was optimised and reported in Chapter 7, respectively.

4.2 Swansea Bay Lagoon

Swansea Bay is located in the South West of the UK and constitutes part of the South Wales coastline. As a part of the Bristol Channel, the tidal range in the bay often exceeds 10 m [65], which makes it a suitable location for a tidal range scheme. SBL was proposed by TLP in 2004 [119]. SBL was granted planning permission by the UK DECC in June 2015 [120] and was positively supported by the independent Hendry Review, commissioned by the UK government and published in January 2017 [121]. However, the cost of electricity has been found to be an issue [122] and the UK government Business and Energy Secretary Greg Clark said that the £1.3bn project was not good value for money. This was despite claims to the contrary by the developers TLP [123]. The UK Government has been decided not to support the scheme due to the high cost of electricity [9], although more recently, UK's Prime Minister Boris Johnson was urged to give the go-ahead for SBL, a pioneering green energy project that will especially power Britain's recovery from COVID-19 pandemic [10]. This further re-emphasizes the importance of optimising TRSs to generate maximum possible electricity and revenue while keeping the cost down.

The proposed lagoon wall would be about 9.5 km long, creating a lagoon area of about 11.5 km², as shown in Figure 4.1. The scheme would have an energy-generating life of 120 years and would consist of 16 bulb turbines, each of diameter 7.2 m, and with the installed capacity of 320 MW [120]. The lagoon-specific type of bi-directional bulb turbine is shown in Figure 4.2. The area of the sluice gates would be approximately 800 m² and the lagoon is designed to be operated under the two-way generation scheme [65, 119]. Based on the most recent report published by TLP [120], the annual energy generation is expected to be about 530 GWh per year.

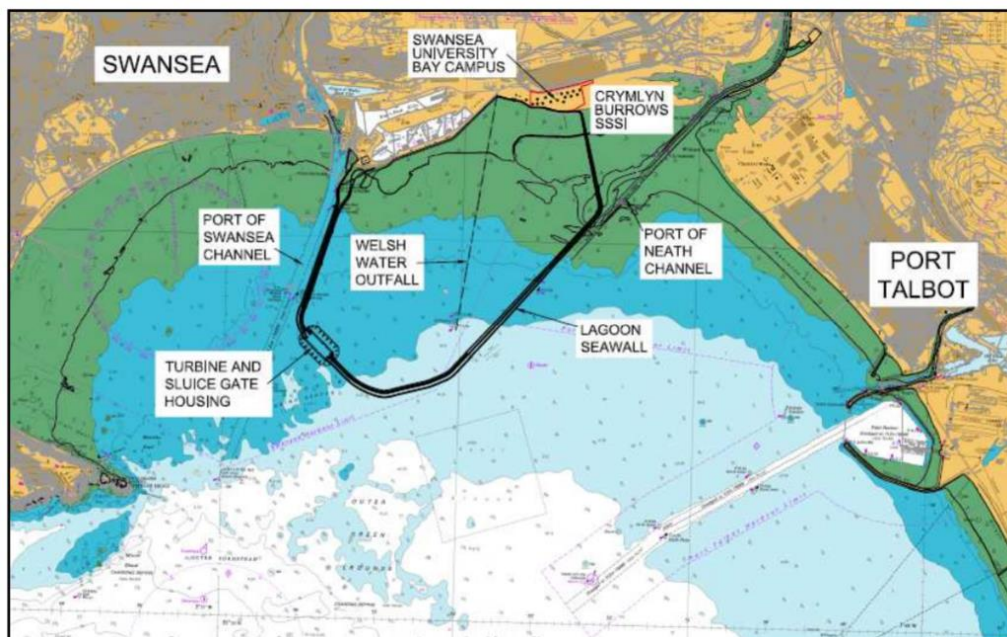


Fig 4. 1. Swansea Bay Lagoon layout overlaid on the Admiralty Chart background [124].

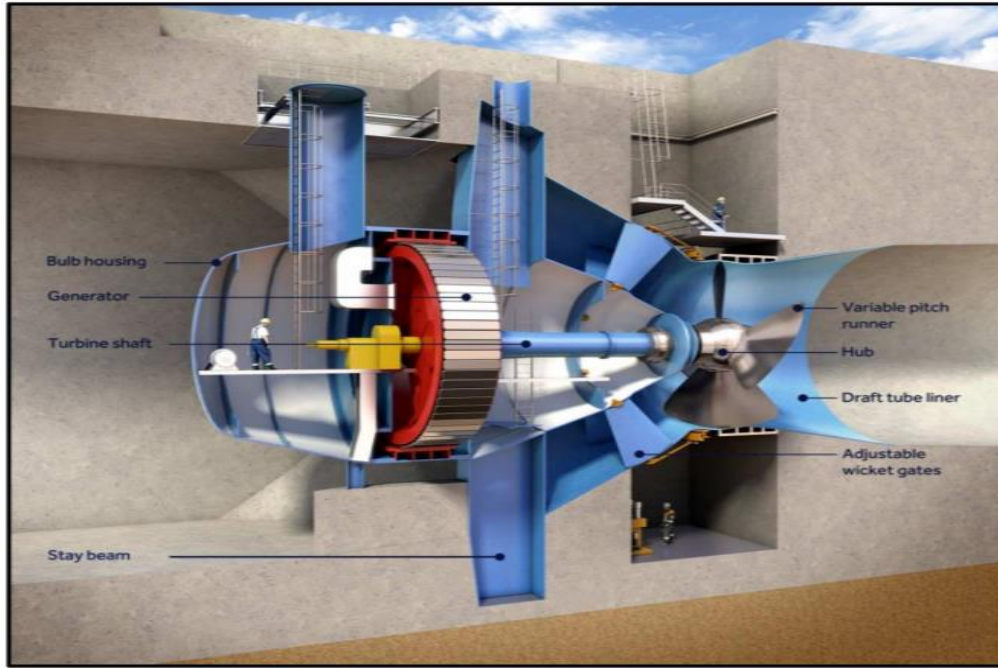


Fig 4. 2. Illustrative cross-section of a bi-directional bulb fixed speed turbine [125].

In the absence of substantial wetting and drying, the plan surface area of a lagoon (A in Eq.3.3) could be assumed to be a constant value in 0-D models [19, 32]. However, due to extensive flooding and drying in some regions of Swansea Bay, the plan surface area of the impoundment could change significantly through the tidal cycle. Figure 4.3 illustrates the bathymetry of the area inside the lagoon and Figure 4.4 shows the plan surface area of the lagoon for different impounded water levels (relatively to Ordnance Datum) calculated based on the bathymetry. The variable wetted plan surface area as a function of the impounded water level, is used in this study.

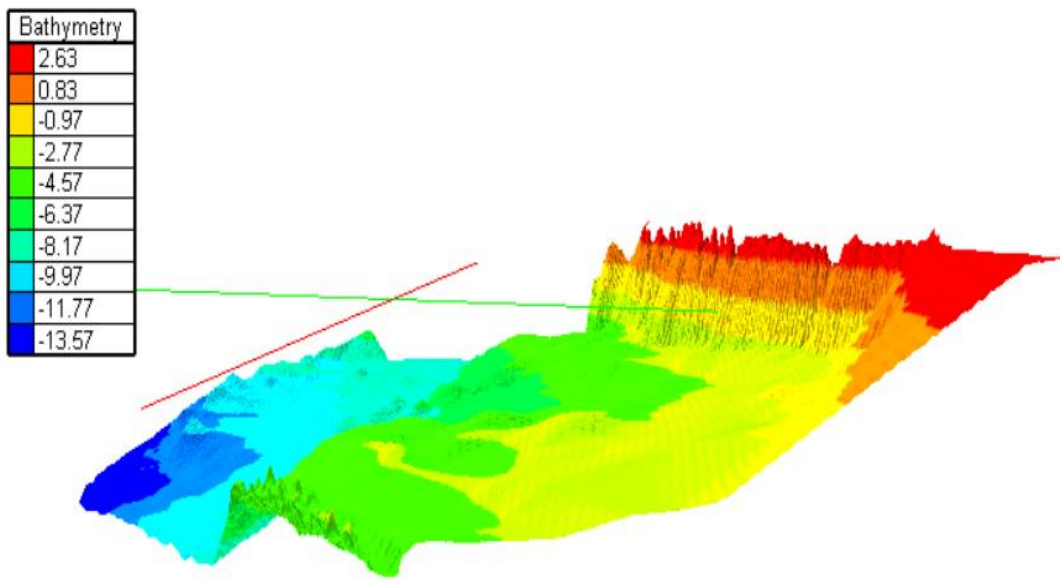


Fig 4. 3. Swansea Bay Lagoon bathymetry [126].

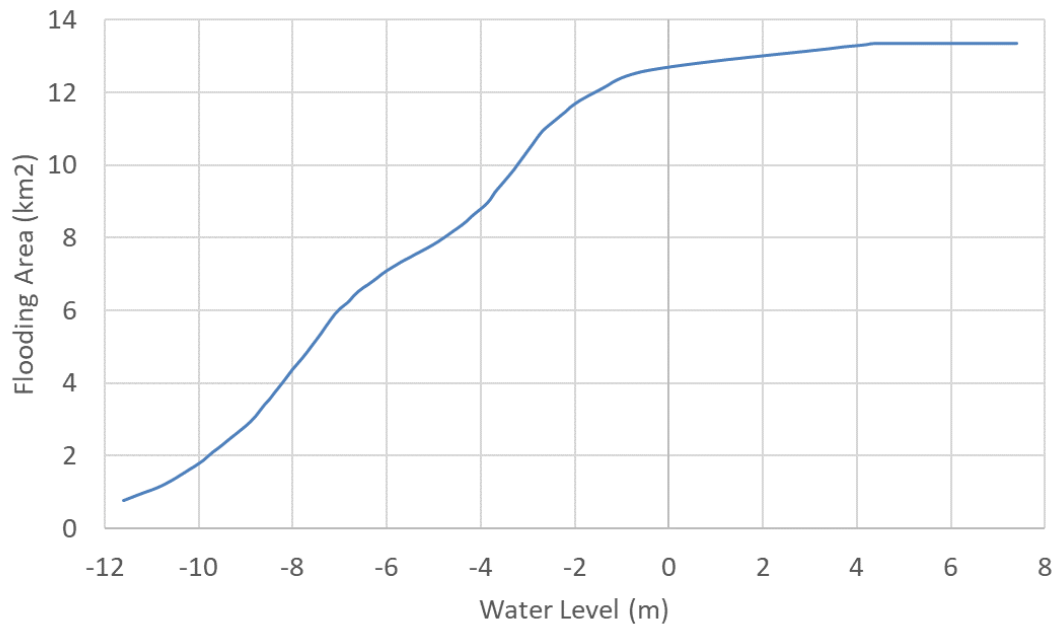


Fig 4. 4. Wetted area versus water level of Swansea Bay Lagoon.

4.2.1 Swansea Bay Lagoon modelling

4.2.1.1 Model Setup

In this study, sensitivity tests of the time step were implemented, covering the time steps of 1 second, 1 minute and 2 minutes. Results indicated an approximately 0.8% increase of energy calculation was

obtained with a time step of 1 minute, in comparison to the 1 second time step scenario. the difference was about 1.6% if a time step of 2 minutes was adopted. Hence, the electricity generation from the 0-D model can be considered as insensitivity to the time step and it can be set to 1 minute, ensuring an accurate prediction of simulation within the affordable computational cost. In the absence of precise measurements, the coefficients for sluices (CoefQ_sluice) and turbines (CoefQ_Turb) were set to 1 [127]. The coefficients of generator efficiency (CoefGT) was approximately 0.768 used in this study according to the equation below:

$$\text{CoefGT} = \frac{P_{\max}}{\rho g H Q} \quad (4. 1)$$

where P_{\max} is the maximum rate per turbine, e.g. 20 MW in this study; H and Q are the water head and discharges when Pmax reaches, e.g. 5.856 m and 453.12 m³/s according to the hill-chart.

4.2.1.2 Optimisation

The model simulations were compared to the 0-D results published for verification [65]. The model was set up with constant operation heads, namely H_{se} and H_{sf} of 3.0 m and H_{ee} and H_{ef} of 1.0 m. The annual energy-generated was predicted to be 472.89 GWh which is within 2% of the value reported by Petley and Aggidis [65]. This is considered to be acceptable and the very limited difference could be due to differences in the downstream water levels or details in the operation of the lagoon.

Tidal data generated from a more sophisticated 2-D model, namely the Depth Integrated Velocities And Solute Transport (DIVAST 2-DU) model introduced in Chapter 3. The 2-D model without SBL was set up to provide the downstream water levels in the 0-D model. However, it is common to use nearby tidal gauges in the absence of such data. To identify potential errors introduced by such assumptions, comparison of the model predicted power output using the simulated downstream water levels at the location of the lagoon and the Mumbles tidal gauge was carried out. This gauge is part of the UK Tide Gauge Network of the British Oceanographic Data Centre (BODC) [128]. It was noted that using the fixed operation and water levels from the Mumbles Gauging station underestimated the annual power output by about 10%, compared to the predicted energy using water levels generated from a 2-D model.

The year of 2012 was chosen for this study due to the availability of a complete set of boundary conditions provided by the National Oceanographic Centre [35]. Optimising the operation of the schemes for different scenarios over the entire year and analysis of the results could be time-consuming. Therefore, a typical Spring Neap tidal cycle which represents an average electricity output throughout the year was selected for simulation. Details of the power output and variation per tidal cycle are listed in Table 4.1. For the accuracy of energy prediction, the date of the first cycle started from 60.6 hr, which coincides with the first neap tide for that year. The average power output per Spring Neap cycle of about 360 hours was approximately 20.85 GWh, with the difference between the maximum and minimum outputs being over 25%. Therefore, the representative tidal cycle was chosen to exemplify an average tidal cycle and to compare with the annual results. The 2nd cycle in the year which deviates by less than

2% from the average was chosen as the representative tidal cycle for optimisation in this study. A coefficient of 24.377, which is the proportional time of the year for one complete tidal cycle, was used to convert the predicted energy over one cycle to the annual energy generated.

Table 4. 1. Energy generation per cycle for the 0-D model.

Cycle No	Starting time (hr)	Ending time (hr)	Energy (GWh)	Relative deviation (%)	Cycle No	Starting time (hr)	Ending time (hr)	Energy (GWh)	Relative deviation (%)
1	60.60	421.50	19.69	-5.57	13	4284.40	4619.60	22.62	8.46
2	421.50	781.80	20.44	-1.96	14	4619.60	4991.40	19.03	-8.75
3	781.80	1130.10	21.36	2.42	15	4991.40	5341.20	22.31	6.99
4	1130.10	1489.50	19.86	-4.77	16	5341.20	5699.40	19.72	-5.42
5	1489.50	1824.90	21.81	4.60	17	5699.40	6061.40	21.43	2.76
6	1824.90	2197.50	19.06	-8.59	18	6061.40	6445.60	21.84	4.75
7	2197.50	2534.10	22.57	8.24	19	6445.60	6804.80	19.20	-7.92
8	2534.10	2892.90	19.15	-8.14	20	6804.80	7165.80	23.58	13.09
9	2892.90	3241.80	23.30	11.76	21	7165.80	7512.20	18.29	-12.29
10	3241.80	3612.30	18.55	-11.04	22	7512.20	7873.20	23.83	14.29
11	3612.30	3924.60	22.17	6.32	23	7873.20	8221.20	19.26	-7.63
12	3924.60	4284.40	17.98	-13.77	24	8221.20	8568.60	23.39	12.16

Due to the large variability in the tidal range through a Spring Neap cycle, optimisation process in this study involves finding the most efficient operational conditions for the smallest component that generation could occur independently, i.e. each ebb and flood tide. In order to achieve this, a range of starting generation water elevations H_s , including H_{se} and H_{sf} , was considered, varying from 2 m to 8 m and in 1 cm increments, and for a range of ending generation water levels H_e , including H_{ee} and H_{ef} , from 0.5 m to 4.5 m and also with 1 cm increments. Figures 4.5 (a) and (b) illustrate the contour map of power output excluding and including the impact of flooding and drying, respectively. Although both H_s and H_e covered the whole range in the 0-D models, it was found that the generated energy was insignificant when H_s was between 6.5 m and 8 m and H_e between 3.5 m and 4.5 m. Hence, the contour results shown in Figures 4.5(a) and (b), and for the rest of this study, only cover from 2 m to 6.5 m for H_s and from 0.5 m to 3.5 m for H_e .

It can be seen that the highest energy appears in the middle region areas in these figures, which represents the operation head of H_s and H_e . It should be mentioned that the red cross in Figures 4.5(b) represented the most optimised operation heads of $H_s = 4.6$ m and $H_e = 1.9$ m with the maximum electricity generation of 21.30 GWh during the selected cycle. This shows an improvement of approximately 4% in comparison with the original 20.44 GWh as mentioned in Table 4.1. It can also be seen that the impact of excluding flooding and drying within the impoundment is less than 5% compared to including it.

It should be noted that the optimum conditions are different for with and without flooding drying as shown in Figures 4.5 (a) and (b). These changes in operation are caused by feedback within the system when the head difference across the structure is reduced, and is similar to that found by Bray et al. [114] when the discharge was reduced in the 2-D modelling. However, these changes are often ignored when comparing the simulations with and without flooding and drying [35].

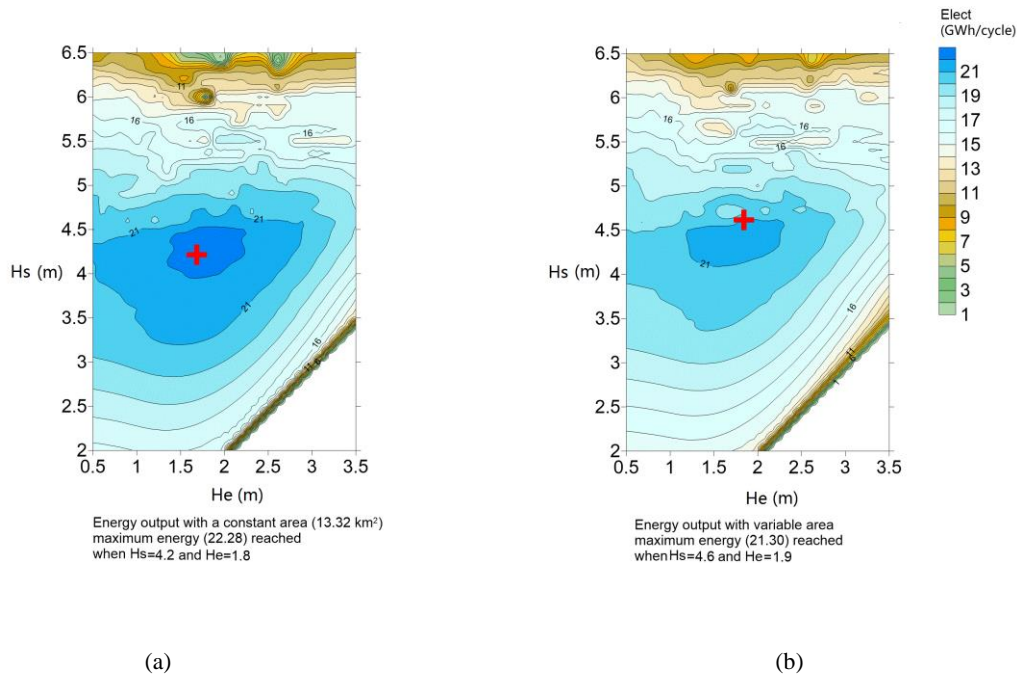


Fig 4. 5. Power output: (a) with a constant impounded area; (b) with impounded area varying with the water level.

The details of operation scheduling of the impoundment and water head difference, water levels inside the impoundment and power output and discharge through sluice gates and turbines for 4 neap tides during the typical cycle under the $H_s = 4.6$ m and $H_e = 1.9$ m are shown in Figures 4.6-4.8, respectively. For the simulation of power output during the selected cycle, it can be concluded that although the optimised pair of operation heads were implemented in the 0-D model, the power output during each neap or spring tides could not reach the maximum power output of 320 MW by turbines rating. Importantly, it was founded that under fixed operation schemes, there might not have any power output during some neap tides due to insufficient tidal range, this emphasized the significance of using flexible operation schemes, which divided the tides into small components e.g. every tide or half-tide and applied variable operation heads in each unit, to maximise the electricity generation in Chapter 5.

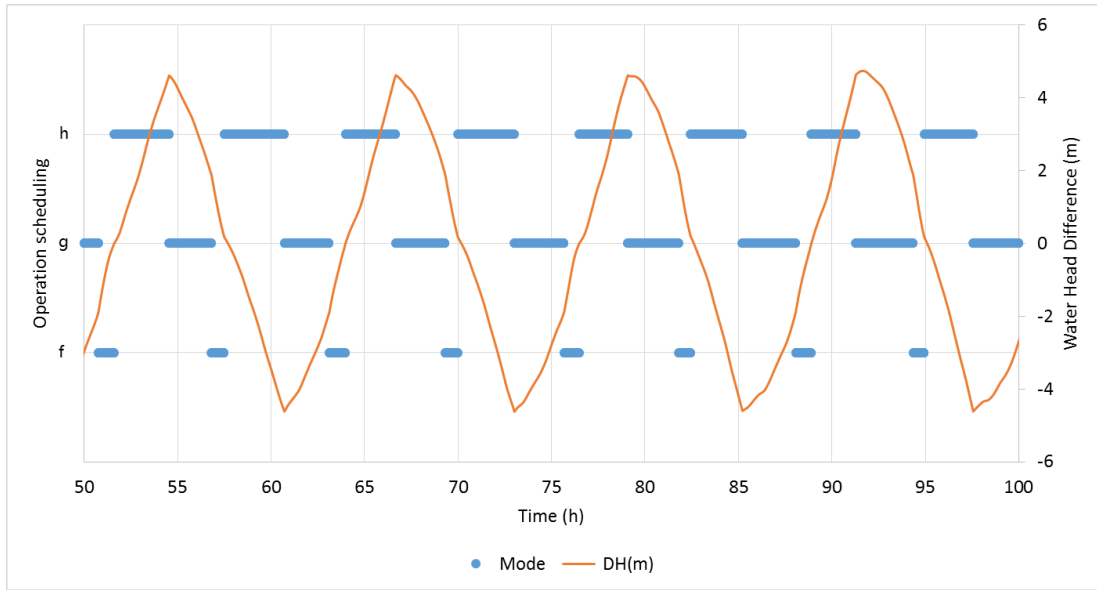


Fig 4. 6. Operation scheduling of the impoundment and water head difference for four neap tides in the 0-D model without pumping included, in which 'h', 'g' and 'f' denotes holding, generating and filling phases, respectively.

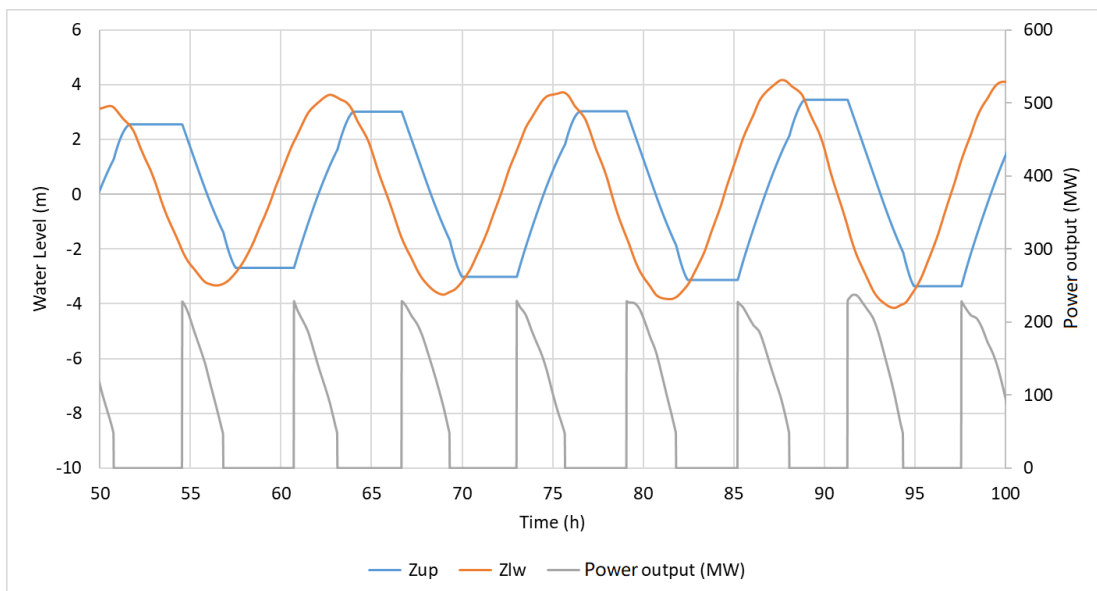


Fig 4. 7. Water levels inside the impoundment and power output for four neap tides in the 0-D model without pumping included.

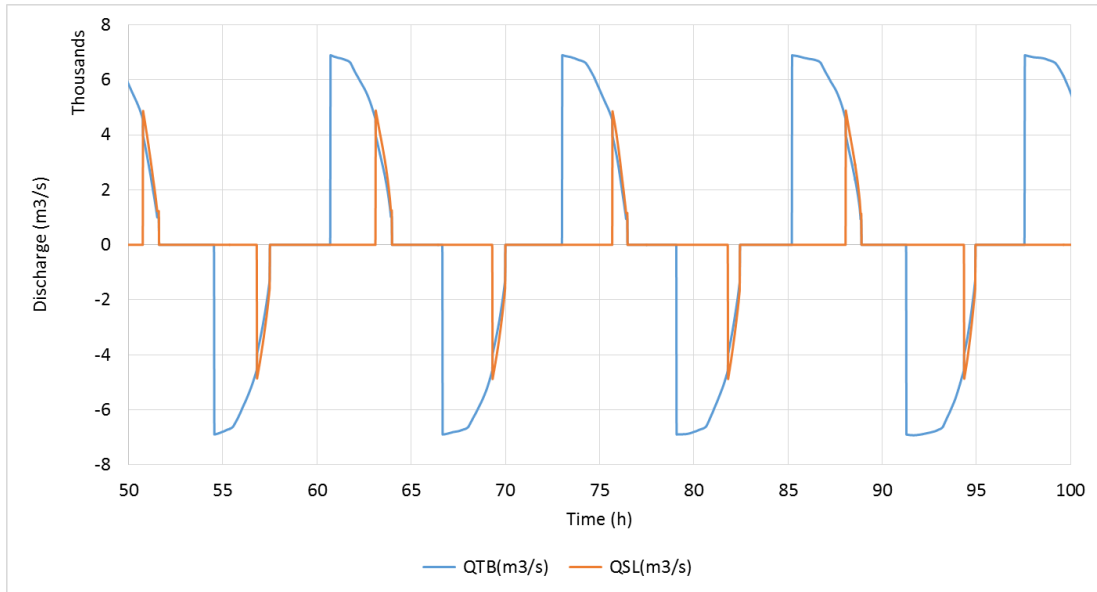


Fig 4. 8. Discharge through sluice gates and turbines comparisons for four neap tides in the 0-D model without pumping included.

4.2.1.3 Pumping

The model could include pumping in order to improve the generation and minimise loss of intertidal habitats. Range of pumping water elevations H_p from 0 m to 2 m and with 1 cm increments was considered. Results showed that the maximum electricity of 24.408 GWh could be obtained when the H_s of 4.8 m, H_e of 1.9 m and H_p of 2 m, which revealed an improvement of more than 10% compared with the scenario without pumping as reported in the previous section. The details of water levels and power output, discharge through turbines and sluice gates and water head differences and operation schedule are shown in Figures 4.9-4.11, respectively.

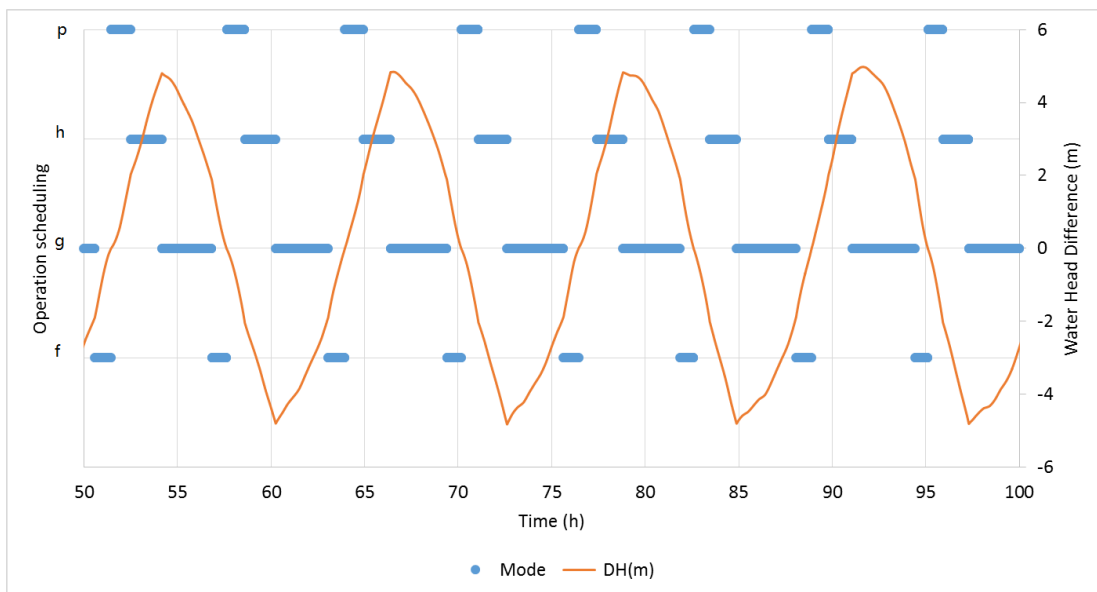


Fig 4. 9. Operation scheduling of the impoundment and water head difference for four neap tides in the 0-D model with pumping included, 'h', 'g', 'f' and 'p' denote holding, generating, filling, and pumping phases, respectively.

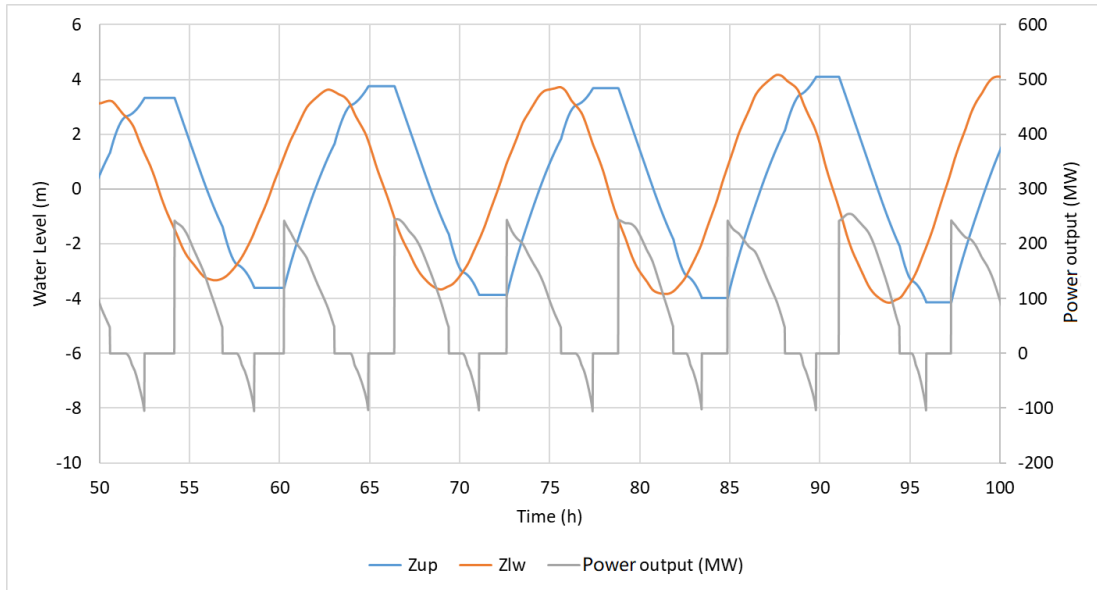
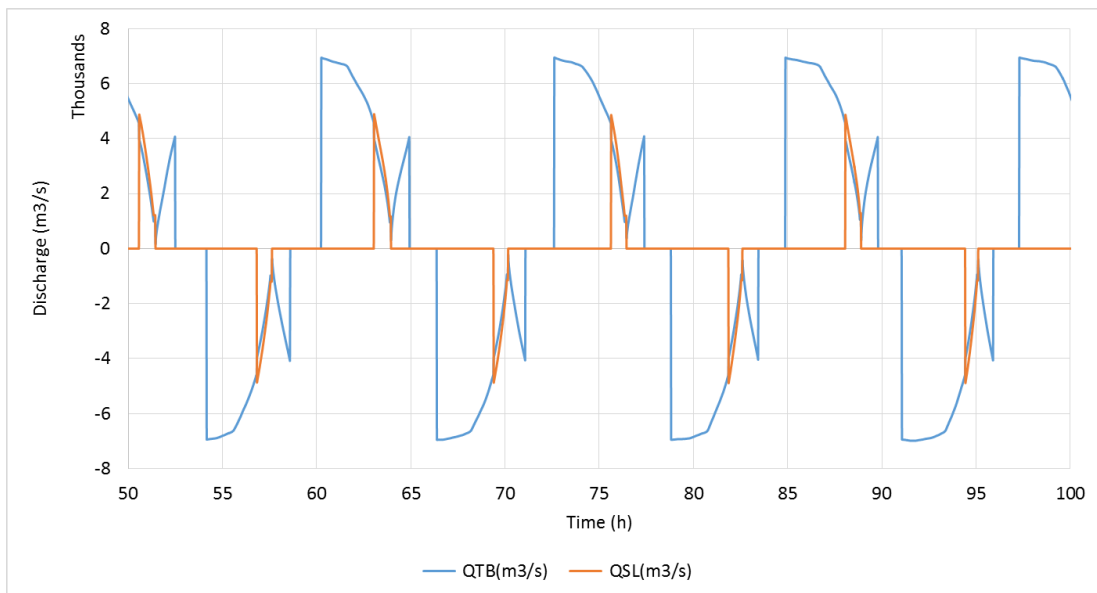


Fig 4. 10. Water levels inside the impoundment and power output for four neap tides in the 0-D model with pumping included.



(c)

Fig 4. 11. Discharge through sluice gates and turbines comparisons for four neap tides in the 0-D model without pumping included.

4.2.2 2-D modelling

4.2.2.1 Model Setup

The entire Bristol Chanel and Severn Estuary, which encompasses the lagoon area and covers an area of about 5,805 km², is modelled in this study to accurately simulate the tidal flow and energy prediction of SBL. The tidal elevation at seaward open boundary data were obtained from the National Oceanographic Centre [35] and the domain extended from the River Severn tidal limit closing to Gloucester, to the outer Bristol Channel [38]. This was set up based on sensitivity analysis of the domain considering the objective of this research using the past and existing studies [134], location of the boundary and computational cost. Average river inputs were included as point sources in the model. The bathymetry was provided by EDINA Digimap and was used to build the mesh in this study [126]. The lagoon representation, model bathymetry around the lagoon and validation points are shown in Figure 4.12, along with a satellite image as the background. It is necessary to validate the two-dimensional model before the inclusion of the TRSs to ensure that the results produced are reliable in further studies in this thesis.

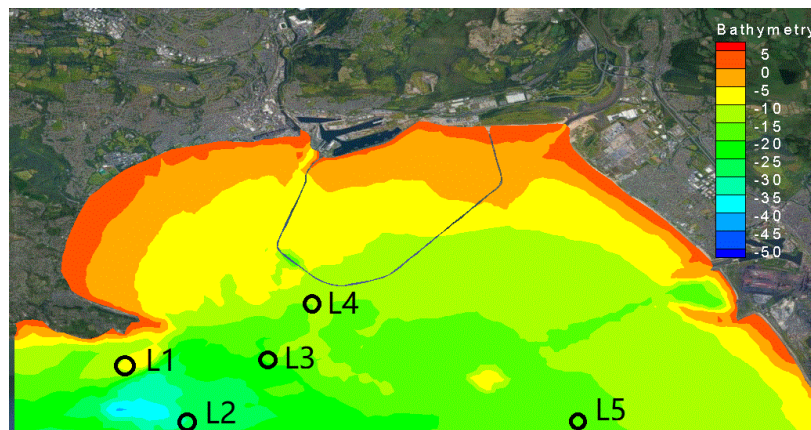


Fig 4. 12. Swansea Bay Lagoon region and bathymetry as included in the DIVAST 2-DU model.

Unstructured models including and excluding the lagoon were set up over the computational domain using different grid sizes. A mesh without SBL was refined to 50 m in the location of the lagoon to give a higher resolution around the lagoon site. The computational domain consisted of 117,377 nodes and 59,410 elements. The calculation of the discharges through the turbines and sluice gates were coupled with a ramp sinusoidal function of 10 minutes and a minimum duration of sluicing and pumping of 0.2 hours which will be further discussed in Chapter 6, to provide a smooth relationship between the operation regime modes [50].

The time step in this study was set to 1 second due to the insensitivity of the timestep to the electricity generation from this 2-D model, based on previous studies [51, 64]. The value of the bottom roughness, represented by the Manning's roughness coefficient, was selected to be 0.020 in the studied domain.

4.2.2.2 Model validation

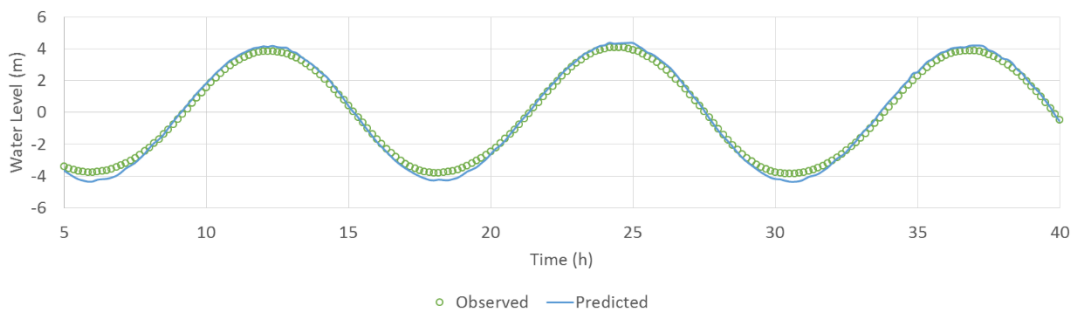
Validation of the models was carried out using available field measurements. In particular, the models were calibrated against water levels and velocity magnitudes and directions measured at five different offshore locations, shown in Figure 4.12. They were collected using seabed mounted Aquapro Acoustic Doppler Current Profilers (ADCPs) by Aberystwyth University as a part of the Smart Coast Project [129]. For brevity, 3 points representing the Western, Central and Eastern parts of the Bay, namely L2, L3 and L5, are shown here. Figures 4.13-4.15 show the comparisons between observed and predicted water levels, and depth average velocity magnitudes and directions, respectively. It can be seen that the 2-D model overestimated the water levels by roughly 0.2 m at high tide (HW) and 0.5 m at low tide (LW), compared with the observed ADCP data. The discrepancies between the measured and observed current speeds were limited, as shown in Figures 4.13(b)-4.15(b), and this is thought to be due to inaccuracies in the representation of the wind effects, recently changed bed elevations, and constant bed friction [71].

The root mean square error (RMSE) and the R-squared (R^2) between the predicted and measured water levels and current speeds at all validation sites were included in Table 4.2. The RMSE and R^2 values were calculated according to the formulations given in Eq. 4.2 and 4.3:

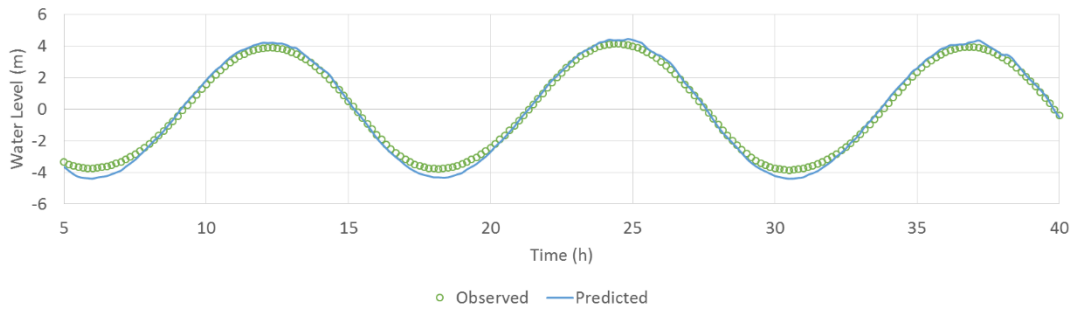
$$RMSE = \sqrt{\frac{\sum_{i=1}^n (P_i - O_i)^2}{n}} \quad (4.2)$$

$$R^2 = \left(\frac{n(\sum_{i=1}^n P_i O_i) - \sum_{i=1}^n P_i \sum_{i=1}^n O_i}{\sqrt{[n \sum_{i=1}^n P_i^2 - (\sum_{i=1}^n P_i)^2][n \sum_{i=1}^n O_i^2 - (\sum_{i=1}^n O_i)^2]}} \right)^2 \quad (4.3)$$

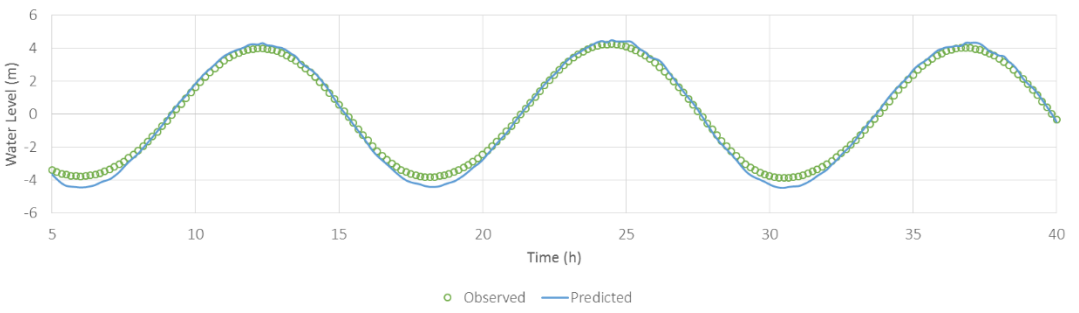
where n denotes the number of time steps during the simulation period, and P_i and O_i represent the predicted and observed terms at time step i , respectively. The relatively small RMSE and high R^2 values indicate a good correlation between the predicted and measured values with the errors in the predicted water levels being less than 0.15. Considering that the main purpose of this work is related to the 0-D modelling, 2-D model is only used as the input tool for water levels in the 0-D model and the validation tool in terms of the performance of the optimisation, the DIVAST 2-DU model can be regarded as a reliable tool in this study. However, the energy generation is very sensitive to the water level and there exists a difference in the prediction of water levels which impacts the energy generation prediction between different 2-D models. Consequently, in terms of the TRSs optimisation, a sensitivity analysis of the input water level from different 2-D models is worthy of being investigated in future work.



(a)

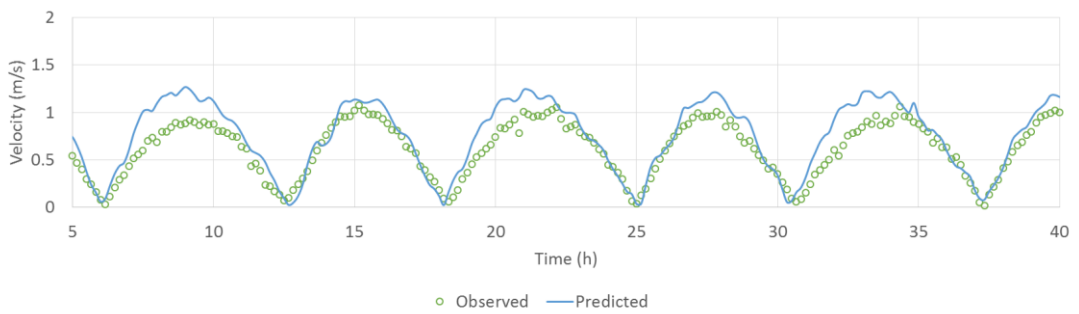


(b)

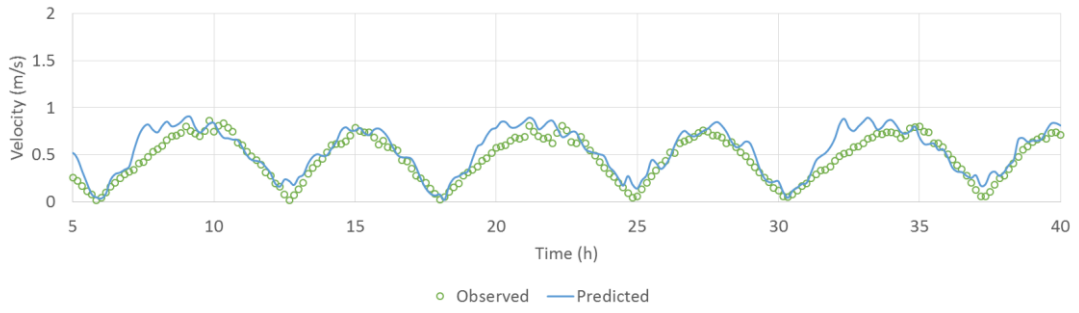


(c)

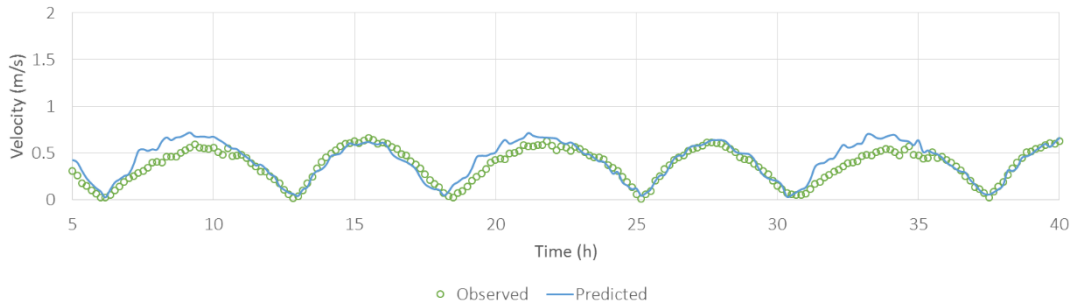
Fig 4. 13. Typical comparison of observed and predicted water levels at L2 (a), L3 (b) and L5 (c).



(a)

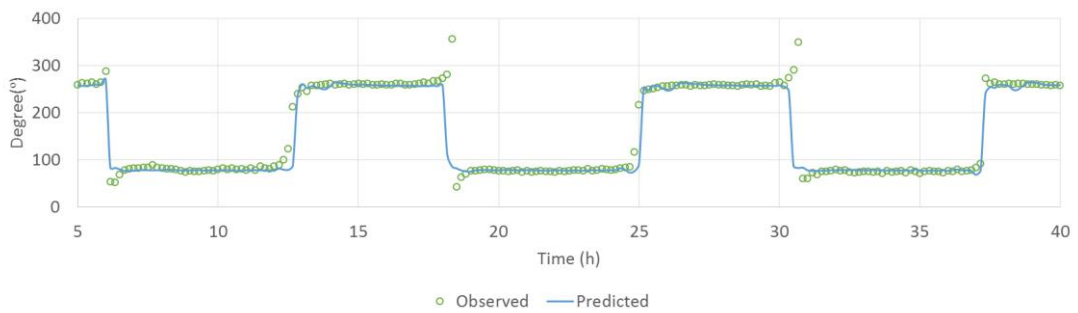


(b)

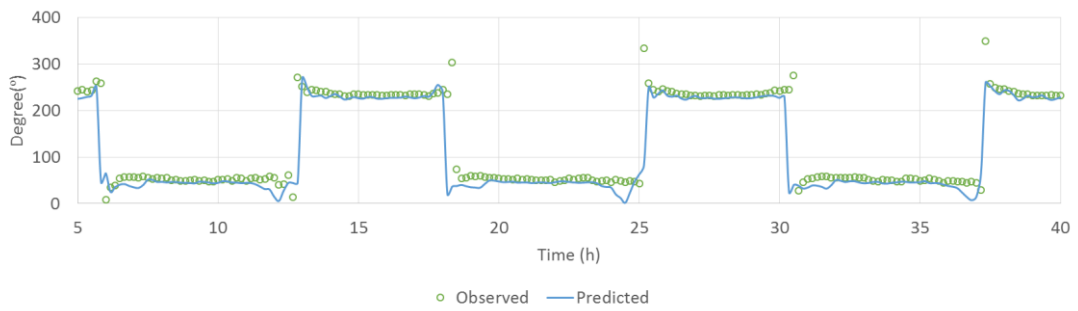


(c)

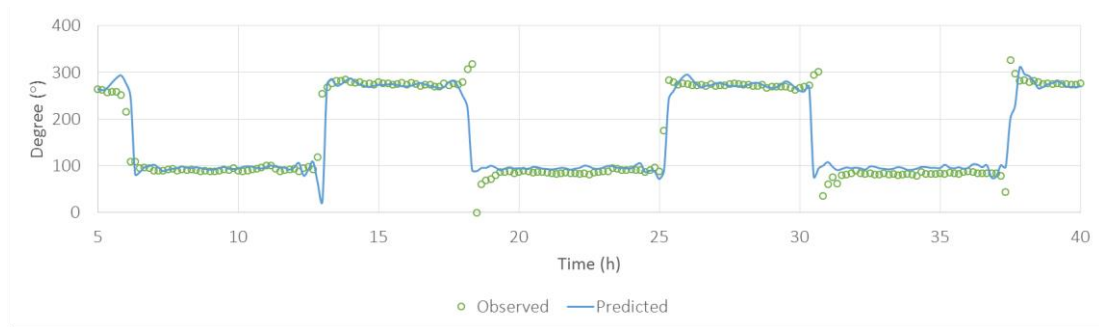
Fig 4. 14. Typical comparison of observed and predicted current speed at L2 (a), L3 (b) and L5 (c).



(a)



(b)



(c)

Fig 4. 15. Typical comparison of observed and predicted current direction from North at L2 (a), L3 (b) and L5 (c).

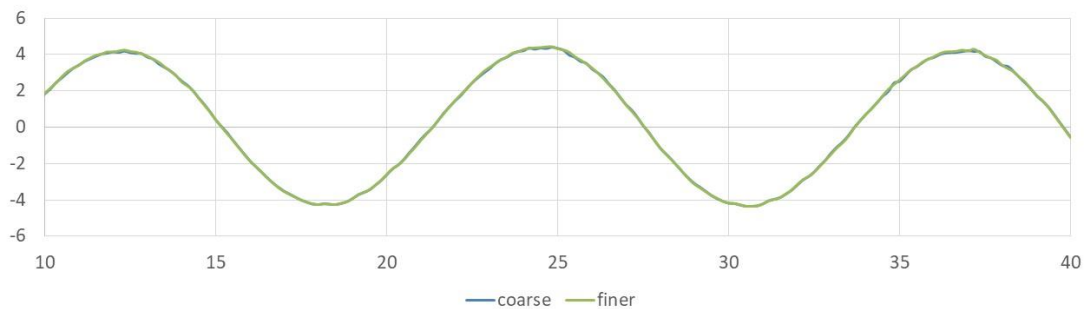
Table 4. 2. Analysis of measured and predicted data at L2, L3 and L5.

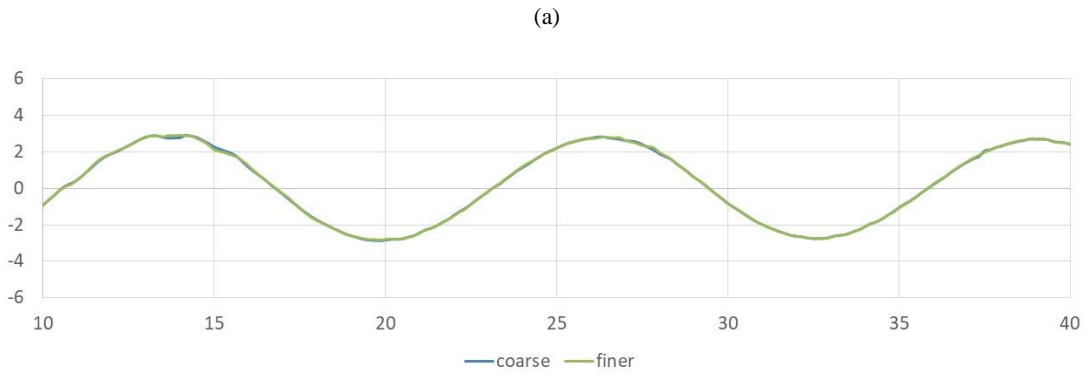
No	Location	Latitude	Longitude	Terms	RMSE	R ²
1	L2	51°31.78' N	003°58.96' W	Water Level (m)	0.111	0.997
				Velocity (m/s)	0.055	0.832
2	L3	51°33.56' N	003°56.32' W	Water Level (m)	0.136	0.997
				Velocity (m/s)	0.031	0.774
3	L5	51°31.82' N	003°51.25' W	Water Level (m)	0.147	0.997
				Velocity (m/s)	0.017	0.787

4.2.2.3 Model independency

A coarser mesh without SBL was set up, allowing the comparison with the previous mesh to check the model independency on the grid being used in the study. The current computation domain is divided into 22,074 unstructured triangular cells, equivalent to 11,404 nodes. One advantage of the coarser mesh was that the computational grid is limited to 200 m locally to give a cost of shorter simulation time although with a lower resolution around the lagoon site.

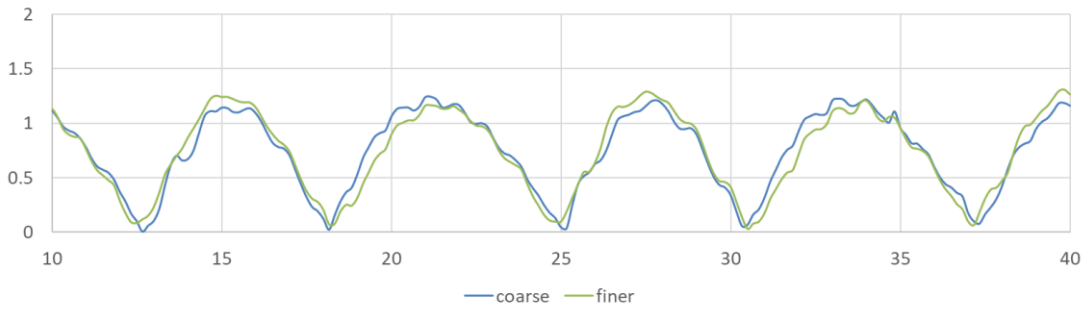
Comparisons between the coarse mesh and the finer mesh of tidal water levels, currents and directions are made at L2, L3 and L5 sites covering spring and neap tides. However, comparisons between the course and finer mesh only shown for L2 site here. Comparisons of water level, current speed direction for spring and neap tides are shown in Figures 4.16-4.18 respectively.



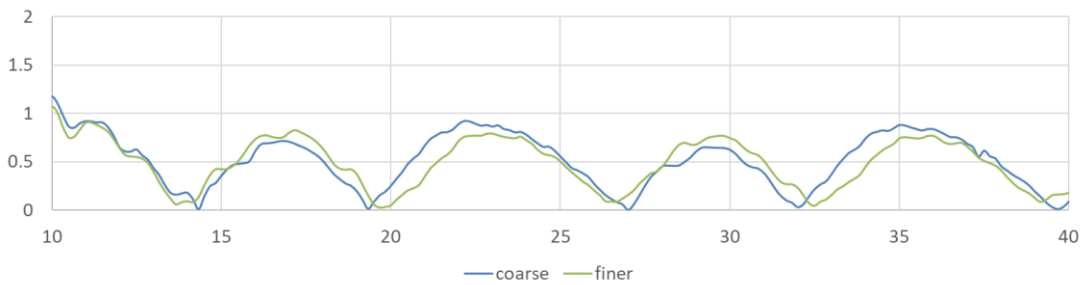


(b)

Fig 4. 16. Water Level of L2 for model independency in (a) spring and (b) neap tides.

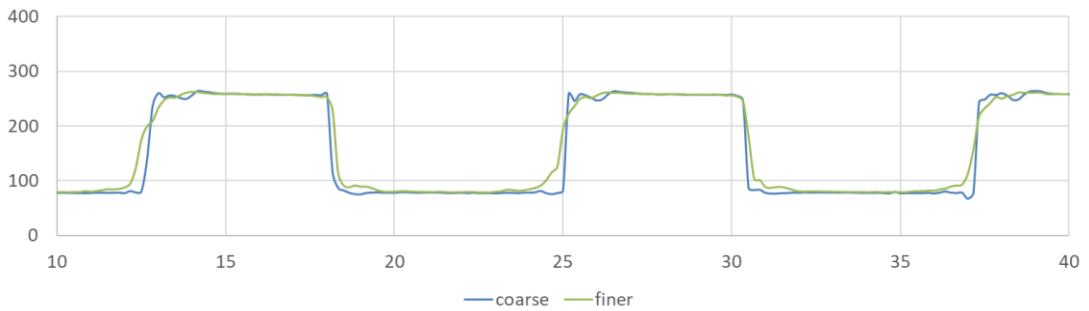


(a)

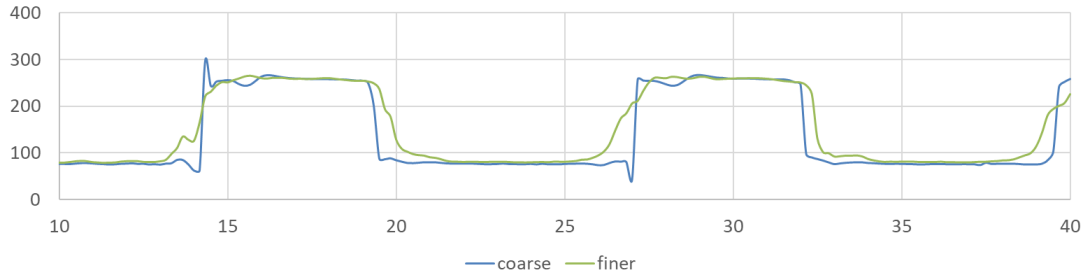


(b)

Fig 4. 17. Average velocity of L2 for model independency in (a) spring and (b) neap tides.



(a)



(b)

Fig 4. 18. Current direction of L2 for model independence in (a) spring and (b) neap tides.

There was only a slight difference in the water levels between the coarse and finer meshes. The main reason for these minor differences is thought to be due to the differences in the surface slope gradients, i.e. the term of $gH \frac{\partial \xi}{\partial x}$ in Eqs.3.5 and 3.6, as a result of differences in the bathymetry based on different grid sizes. Therefore, it was concluded that the models were not dependent on the grid size. Considering the running time for the computational model cost with the finer mesh, it is reasonable to apply courser mesh instead in this study.

4.2.2.4 SBL Modelling

Model decomposition was used to model the lagoon [26, 114] and the domains were linked using the hydraulic structures, i.e. the turbines and sluice gates [114]. The model only conserves mass through the turbines and sluice gates and no momentum transfer was considered in the DIVAST 2-DU model for the flow through the turbines and the sluice gates. This is mainly because the main purpose of this study has been focused on optimising the operation head to maximize the energy generation, with more detail being given in [117].

The coefficients for sluices (CoefQ_sluice) and turbines (CoefQ_Turb), and the coefficients of generator efficiency (CoefGT) were set to 1, 1 and 0.768, respectively, allowing the consistency with the 0-D model. Snapshots of water levels, currents and direction during ebb and flood generation across Swansea Bay are shown in Figures 4.19 and 4.20, respectively. These results are consistent with previous studies [52] and give further confidence in utilising the model for the purpose of energy generation prediction. The details of the water levels and power output, water head difference and electricity generation, discharge through the turbines and sluices gates in the 2-D can be found in Figures 4.21-4.23.

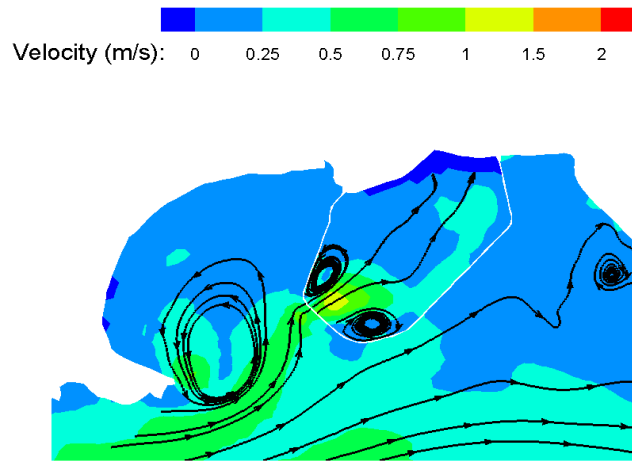
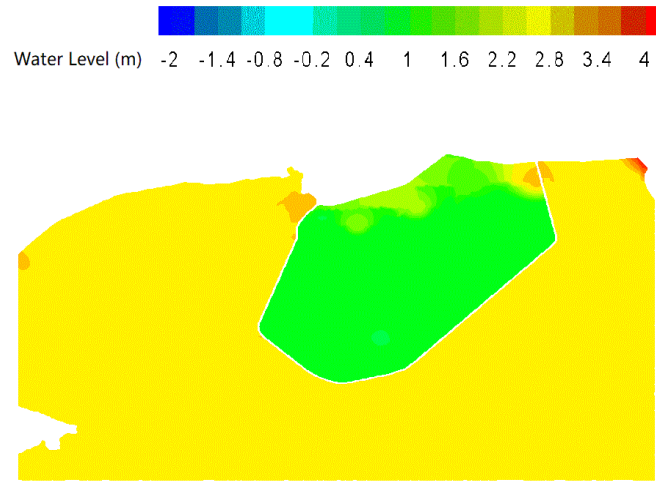
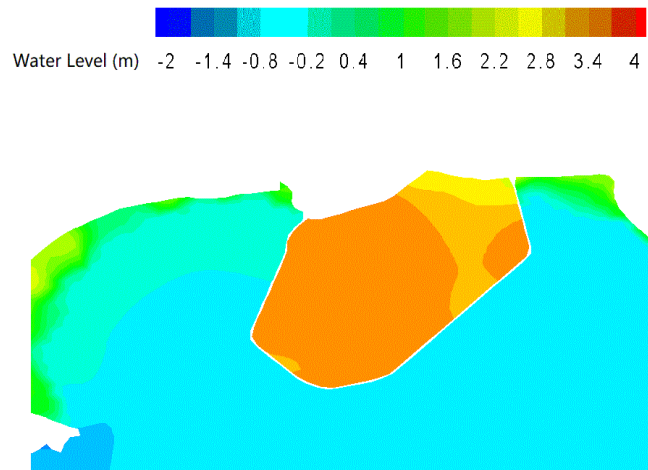


Fig 4. 19. Water level (a) and Current (b) streamlines during the flood generating mode in the 2-D model.



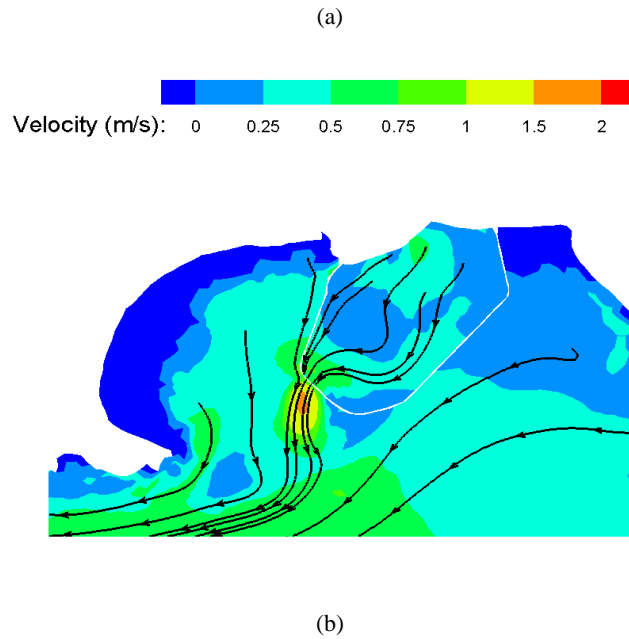


Fig 4. 20. Water level (a) and Current (b) streamlines during the ebb generating mode in the 2-D model.

4.2.3 0-D and 2-D comparison

In this section, in order to verify the 0-D model predictions, 0-D and 2-D model predictions were compared. The main reason for evaluating the differences between energy generation predicted by the 0-D and 2-D models is to ensure that 0-D optimised solutions are feasible hydrodynamically. The 2-D simulations were carried out using the optimised values derived from the 0-D model for constant operating heads. These values were H_s of 4.6 m and H_e of 1.9 m without pumping and H_s of 4.9 m, H_e of 1.9 m and H_p of 2.0 m with pumping, respectively. Simulations were conducted over the typical Spring Neap tidal cycles, i.e. the 2nd cycle as shown in Table 4.1. Figures 4.21- 4.26 demonstrated the water levels and power output, water head difference and electricity generation, discharge through the turbines and sluices gates in the 2-D and the 0-D models without and with pumping, respectively. The duration of generation per tide and electricity estimation in the typical cycle are summarised in Table 4.3.

There is good agreement between the 0-D and 2-D models. The electricity generation predicted using the 0-D model in this study overestimated the predictions relative to the 2-D model by approximately 7.5%, as shown in Table 4.3. These are consistent with the overestimation of about 7% reported for a similar 0-D prediction for an independent study [52]. If pumping involved, the difference could reach approximately 12%. This increase of electricity generation when pumping was considered is expected to be mainly due the differences in the calculated basin water levels in 0-D and 2-D models caused by the simplifications considered in the 0-D model. These simplifications and particularly assuming flat water levels inside the basin which is fundamental to the 0-D is expected to have higher impacts during the pumping phase. Generally, the 0-D model can be considered as a reliable tool for energy estimation

for the preliminary design stages and implementation during optimisation, which requires a large number of runs.

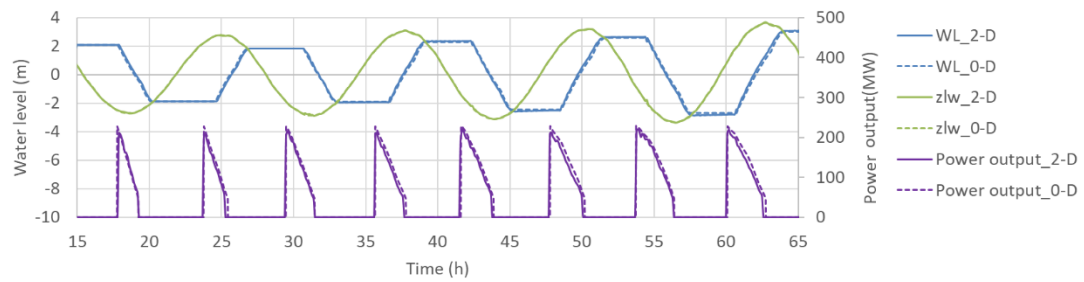


Fig 4. 21. 2-D and 0-D model comparisons between water level and power output.

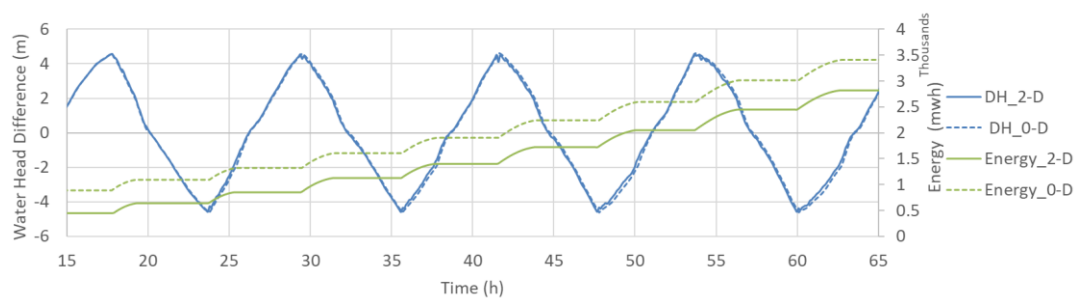


Fig 4. 22. 2-D and 0-D model comparisons between water head difference and energy generated.

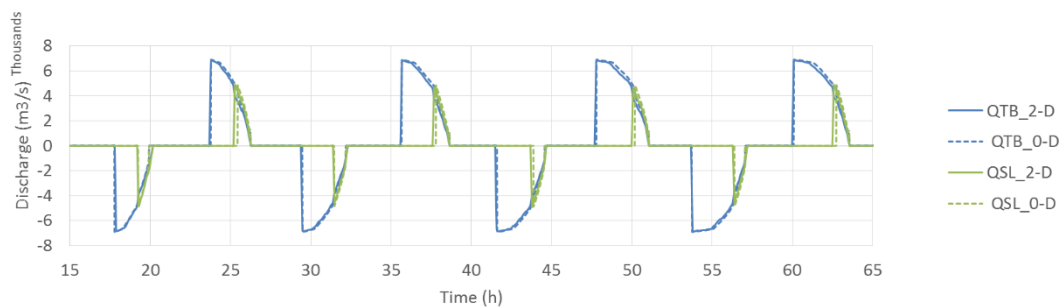


Fig 4. 23. 2-D and 0-D model comparisons between discharge through the sluice gates and turbines.

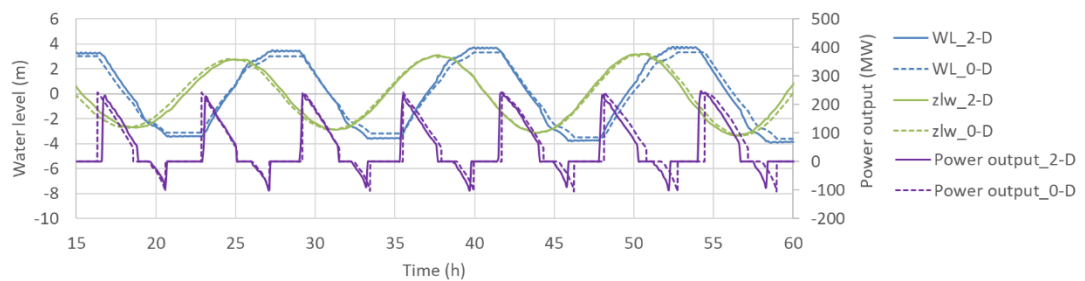


Fig 4. 24. 2-D and 0-D model comparisons with pumping between water level and power output.

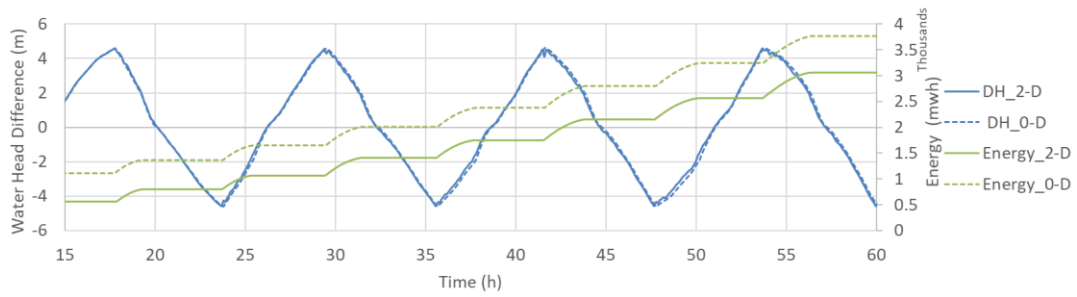
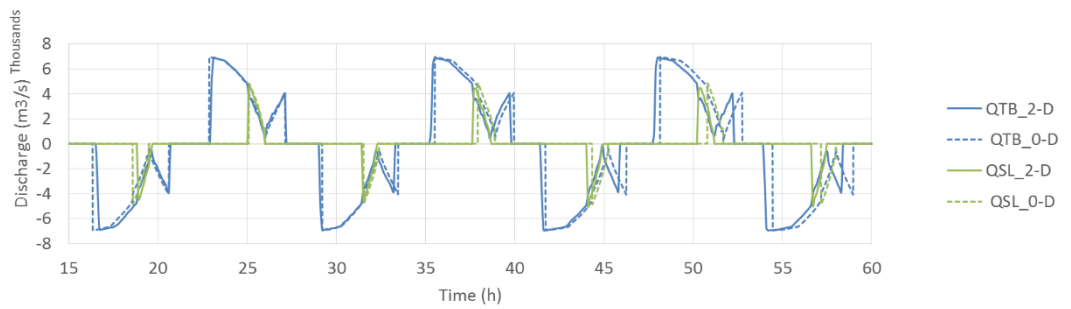


Fig 4. 25. 2-D and 0-D model comparisons with pumping between water head difference and energy generated.



(c)

Fig 4. 26. 2-D and 0-D model comparisons with pumping between discharge through the sluice gates and turbines.

Table 4. 3. Energy generation comparison between 0-D and 2-D models.

		Averaged duration of generating in every half tide of the typical cycle (hr)	Average energy generated in the typical cycle (GWh)
No pumping	0-D model	1.9	21.3
	2-D model	1.9	19.7
	change	0%	-7.5%
With pumping	0-D model	2.8	24.4
	2-D model	2.8	21.4
	change	0%	-12.3%

4.3 West Somerset Lagoon

One of the other TRSs proposed to be built in The Bristol Channel and Severn Estuary is the 14 km diameter of West Somerset Lagoon (WSL) promoted by Tidal Engineering and Environmental Services Ltd. (TEES) [130]. This company will manage the stage planning application process to ultimately acquire a Development Consent Order (DCO) and enter into the next stage of feasibility research, planning, and design [131]. As the project is a new project and no optimisation had been carried out previously as has been done for SBL, the design and parameters optimisation of the project is completely carried out in this study. This is reported in details in Chapter 6.

WSL has been proposed to be built with an about 22 km perimeter of wall encompassed covering approximately 80 km², from Culvercliff in Minehead to Blue Ben Point at West Quantoxhead [132, 133]. The life of the whole project is expected to be at least 125 years. The scheme will also act as a sea defence and combat coastal erosion and future flooding according to the developers Tidal Engineering and Environmental Services Ltd. (TEES) [130].

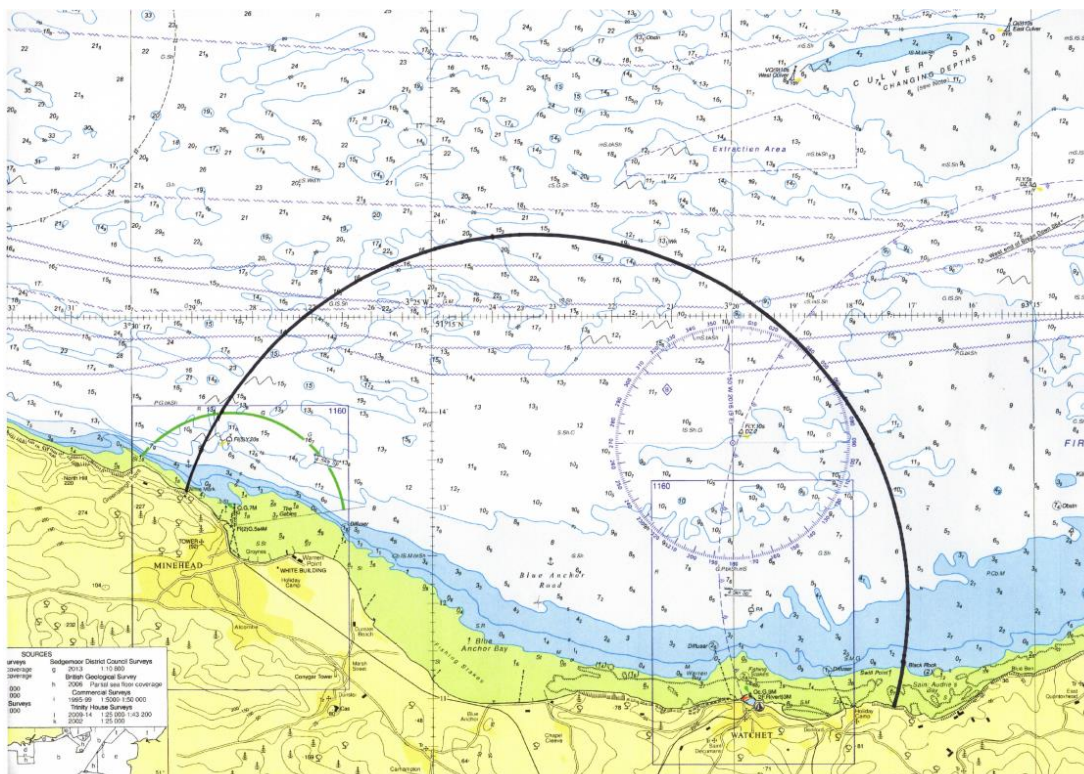


Fig 4. 27. Map of the West Somerset Lagoon.

4.3.1 WSL modelling

The bathymetry of the Bristol Channel and Severn Estuary including the area inside the lagoon is shown in Figure 4.28. The tidal elevation at seaward open boundary data were obtained from the National Oceanographic Centre [35]. Figure 4.29 illustrates the plan surface area of the WSL for

different impounded water levels which would be used in the 0-D modelling, as the term of $A(t)$ in Eq.3.3 for the calculation of $Z_{up,i+1}$.

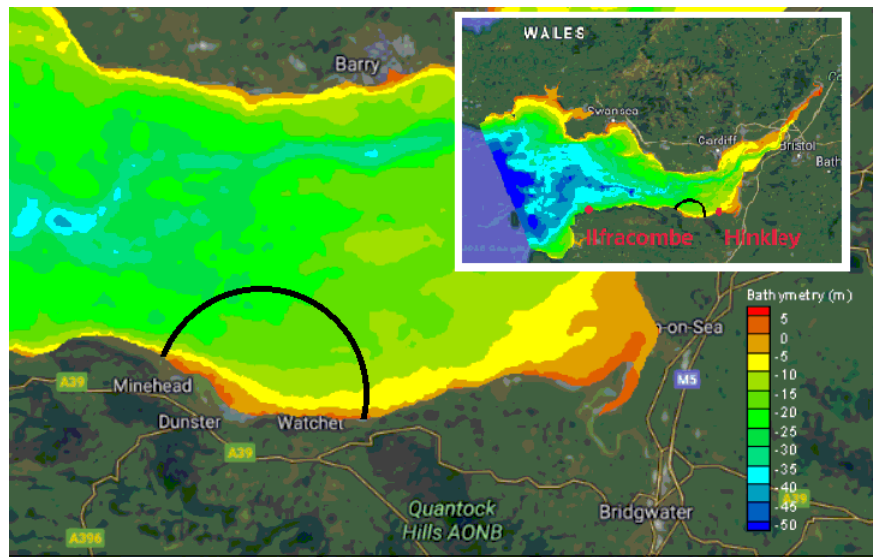


Fig 4. 28. Map of the Bristol Channel, known as the black line, showing the location of the West Somerset Lagoon along the south-west coast of England from Google Map [132]. The validation points of Hinkley and Ilfracombe in the 2-D model were marked as red dots.

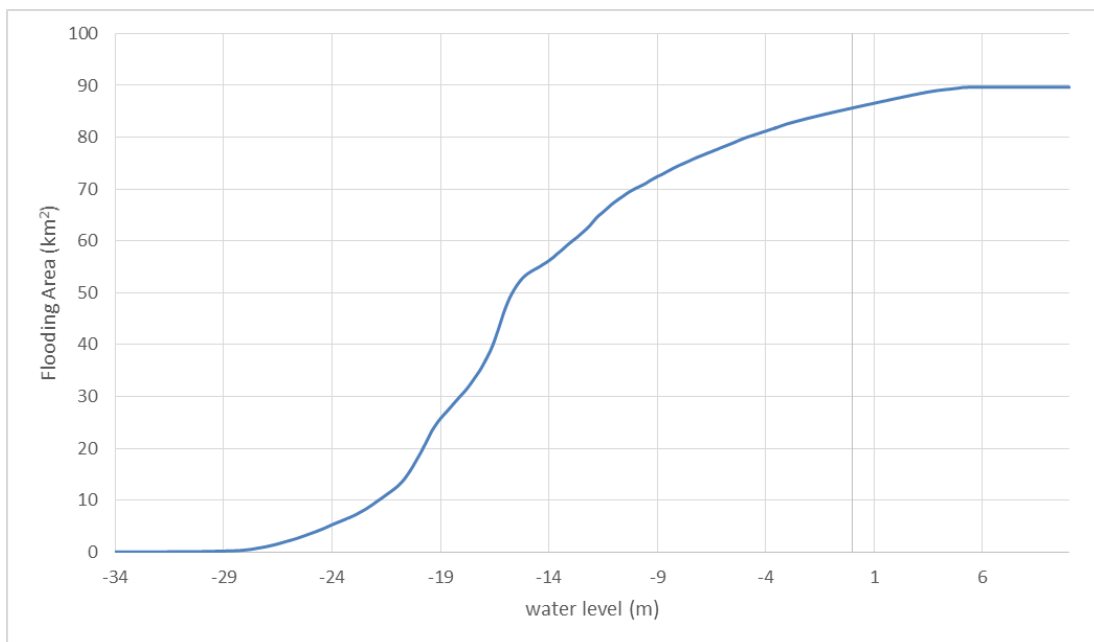


Fig 4. 29. Wetted area versus water level of West Somerset Lagoon.

As shown in Figure 4.30, in the preliminary stage, the options for bulb turbines numbers were 75,100 or 125, each of diameter 7.2 m and 20 MW of installed capacity with a single concentrated block. The parameter of Sluice To Power Capacity (STPC) was designed to be 0, 2 and 4, respectively, which indicated the sluice gate area (A_s) calculated as follows:

$$A_s = \text{NumTB} \times \text{IC} \times \text{STPC} \quad (4.4)$$

In this preliminary study, the water levels series of tides in the middle of the impounded wall was generated from the verified TELEMAC-2D before including any structures [134]. TELEMAC-2D was used to model NWTL and simultaneously modelling WSL and NWTL as shown in Guo [158]. TELEMAC-2D model was adopted here for consistency between the water levels used for WSL and NWTL. The input water levels located only in the middle of the impounded wall will be further improved in chapter 6. At the beginning of the design stages, the electricity production in the year of 2012 was shown in Figure 4.30 with the preliminary combination of NumTB and STPC when a non-flexible operation head scheme of 3.5 m H_s and 2.0 m H_e applied, referring to the settings for SBL. The peak output of 4.946 TWh/Year could be obtained when NumTB of 100 and STPC of 4, as shown in Figure 4.30.

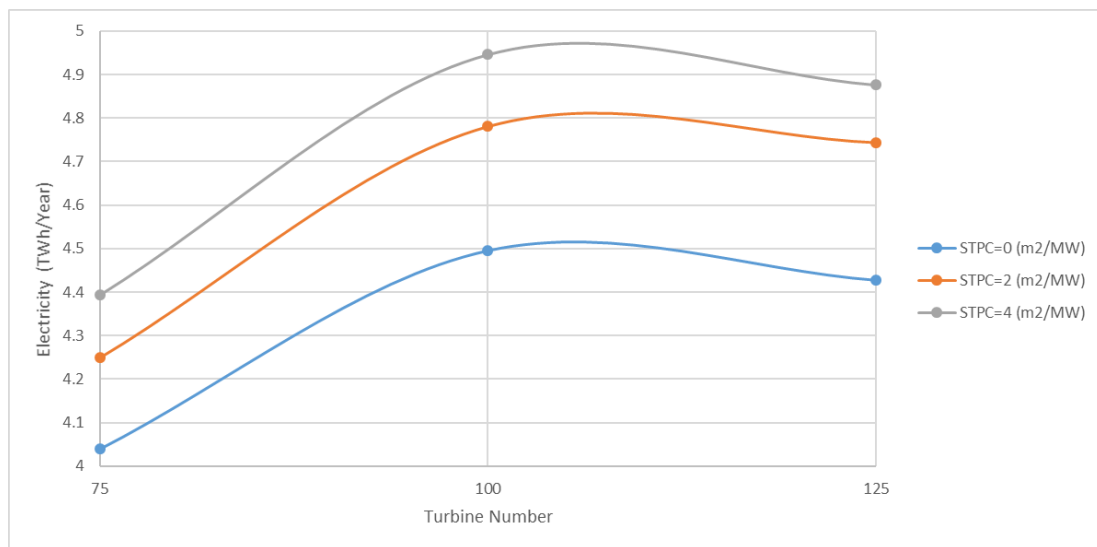


Fig 4. 30. Electricity generation with preliminary design parameters under non-flexible operation schemes.

Similar to SBL, a Spring Neap tidal cycle was adopted to represent the annual electricity generation in order to save computational time. As shown in Figure 4.31, the tides in 2012 were separated into 24 Spring Neap tidal cycles which were between the first neap tide of approximately 62 hours and the last neap tide of approximately 8570 hours, regarding the 01:00 on the date of 01/01/2012 as the 1st hour. An averaged electricity generation of approximately 200.84 GWh was simulated when NumTB of 100 and STPC of 4. It demonstrated the 16th cycle, from 5389.70 hours to 5737.70 hours with the electricity prediction of 201.28 GWh, was the nearest to the averaged and hence it could be selected as the typical cycle and the baseline scenario in this study. It needs to multiply a coefficient of about 24.6 if it converts to annual electricity generation of 4.946 TWh/Year.

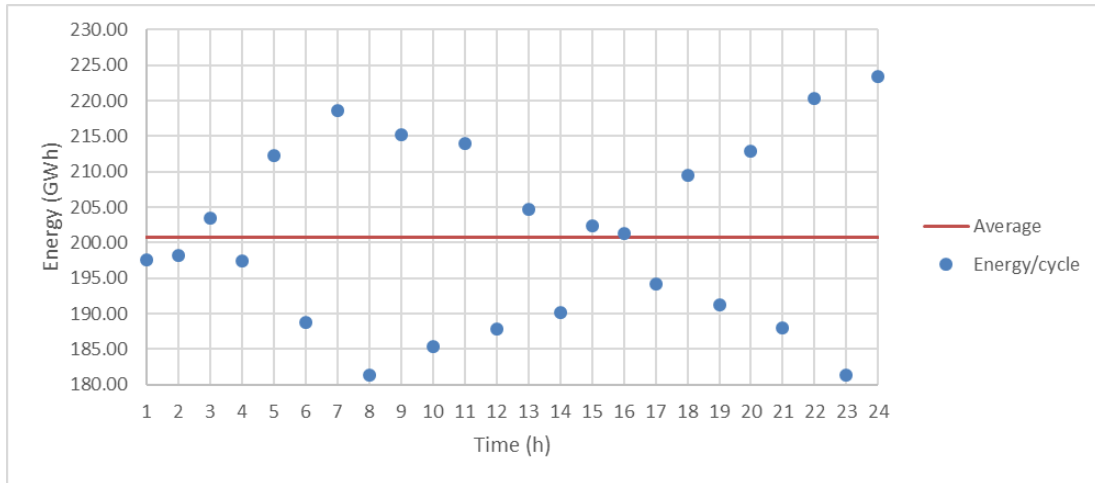
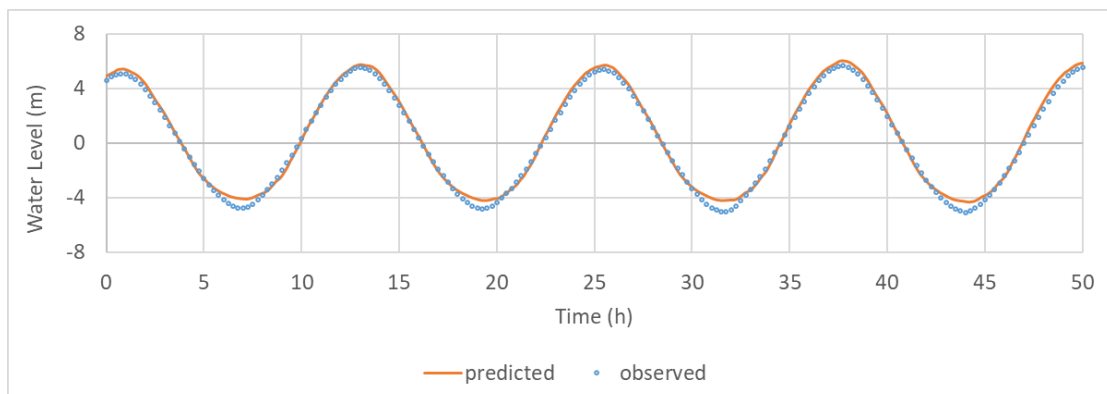


Fig 4. 31. Electricity generation per cycle for the 0-D model.

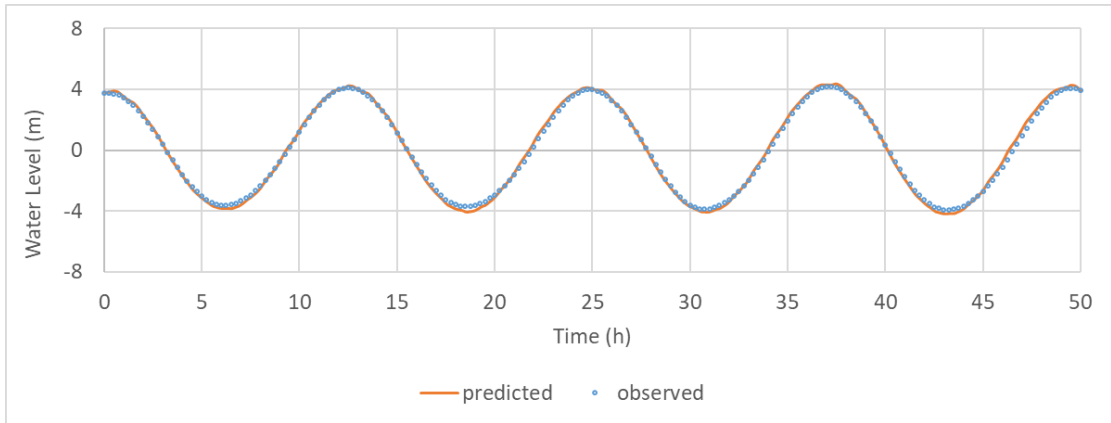
4.3.2 2-D Modelling

4.3.2.1 Model development

The DIVAST 2-DU model covering the Severn Estuary and Bristol Channel with an area of 5,805 km² was set up. The bathymetry data interpolated at the nodes from EDINA Digimap [126] and the seaward boundaries during the typical Spring Neap cycle were obtained from the National Oceanographic Centre [35]. The domain extended from the River Severn tidal limit closing to Gloucester, to the outer Bristol Channel joining with Irish Sea [38] ensuring a sufficient domain for the hydrodynamics study within an affordable computational cost. The model without the construction was verified at different sites by comparing with the observed data downloaded from the UK Tide Gauge Network of the BODC [128]. However, in Figures 4.32(a) and (b) for four spring tides, results were shown herein only at Hinkley and Ilfracombe marked in Figure 4.28, respectively. It can be seen that the numerical model predictions were in good agreement with the observed data.



(a)



(b)

Fig 4. 32. A typical comparison of observed and predicted water levels at (a) Hinkley and (b) Ilfracombe.

The model domain was divided into 72,760 nodes and 143,203 unstructured triangular cells. Figure 4.33 showed the distribution of grid cells in the boundary of the turbines and sluice gates at upstream and downstream. It can be seen that the computational grid was locally refined significantly to accurately simulate the hydrodynamics around the lagoon, with the minimum grid size being reduced to approximately 50 m. Two sub-domains represented the downstream and upstream of the lagoon, respectively, and with the length of about 1,200 m of sluice gates and about 1,800 m of turbines with about 200 m between them, as shown in Figure 4.33.

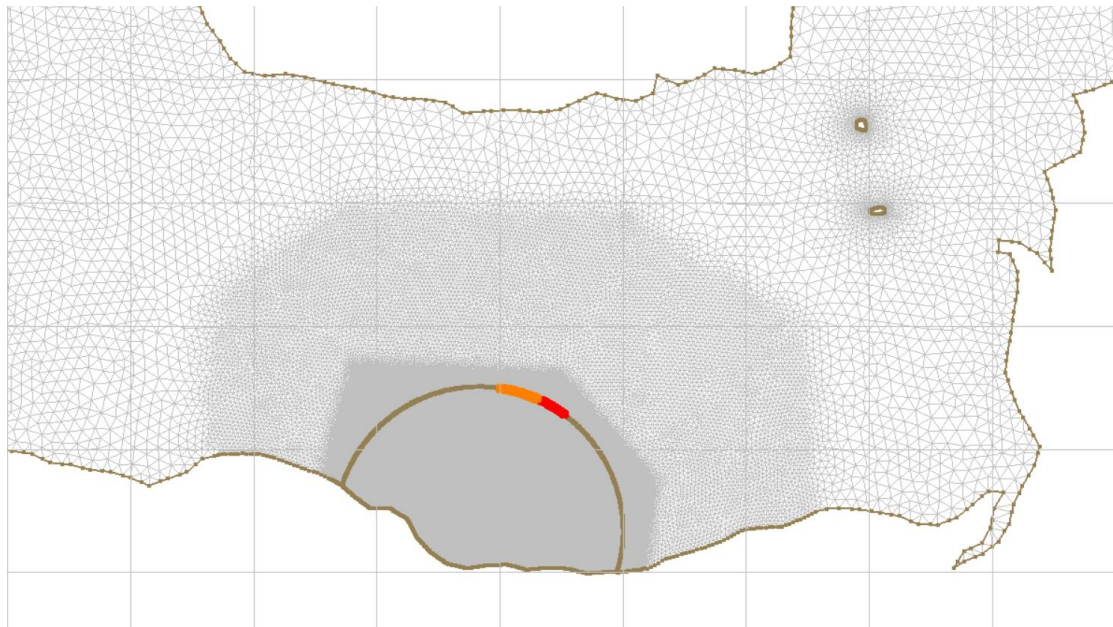
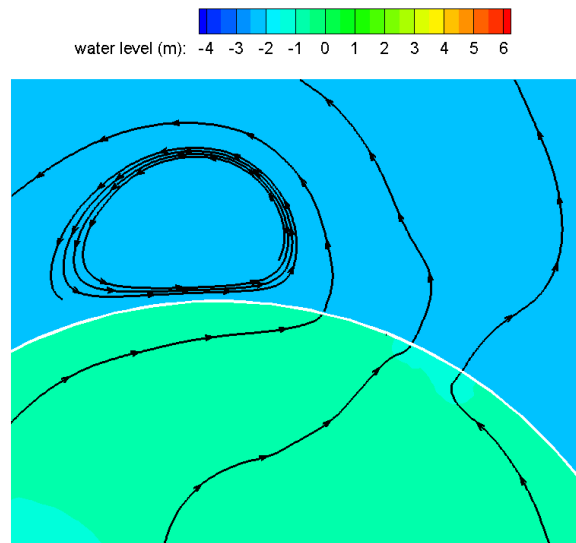


Fig 4. 33. Sketch of grid refinement and deployment of turbines and sluice gates (Brown line is the wall boundary in the mesh, with the Orange line showing the turbines and the Red line shows the sluice gates).

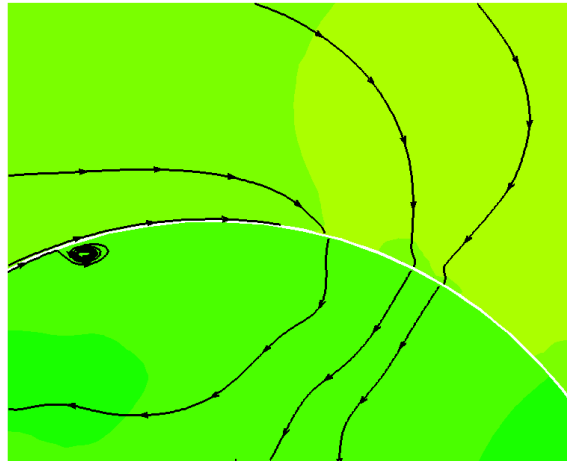
4.3.2.2 Hydrodynamics

After the construction of the lagoon, the water levels and currents distribution in the study domain was predicted which could contribute to a better understanding of navigating conditions around the WSL under the deployment of turbines and sluice gates. Figures 4.34 and 4.35 illustrated the complex velocity fields for ebb or flood tides during filling and generating modes under the baseline scenario, respectively. During the filling mode with the turbines and sluice gates opening, the velocity was usually less than 2.0 m/s at the downstream of sluice gates and 1.0 m/s at the downstream of turbines. During the generating mode, the water went through the turbines meanwhile all the sluice gates were closed. The velocity near turbines could reach 2.5 m/s with a lower magnitude of velocity existing around sluice gates. It emphasized that we should turn to optimise the turbines and sluice gates deployment, especially considering the safety of navigation and fish migration and other environmental factors including sediment transport. As a result, in the most updated map of WSL, 5 blocks of turbines and 8 blocks of sluice gates were distributed along the wall based on the findings in chapter 6, future work could be focused on the investigation of the hydrodynamics and environmental modelling with this new distribution.



(a)

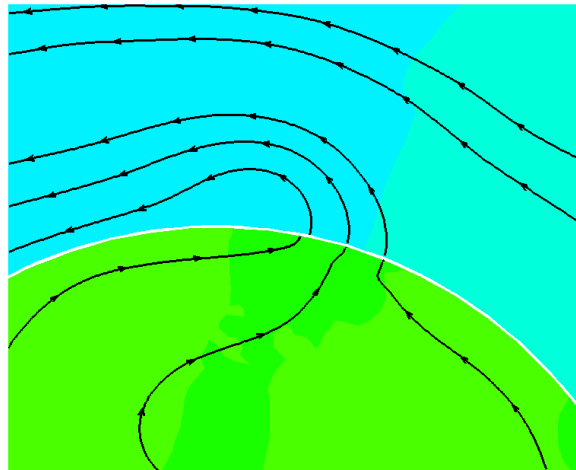
water level (m): -4 -3 -2 -1 0 1 2 3 4 5 6



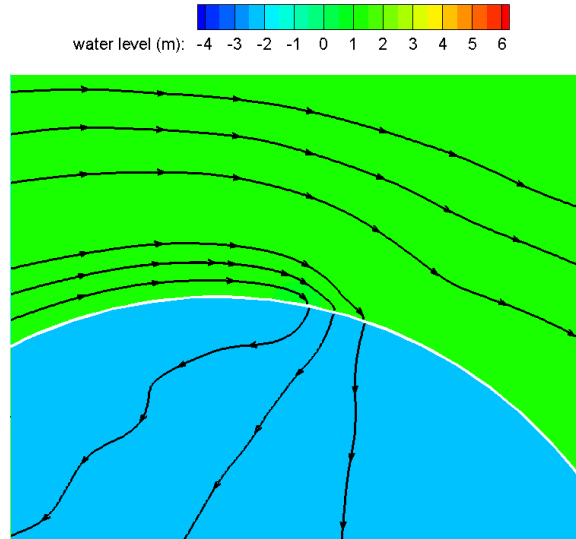
(b)

Fig 4. 34. Water level and Current streamlines in the 2-D model for (a) ebb and (b) flood filling mode, respectively.

water level (m): -4 -3 -2 -1 0 1 2 3 4 5 6



(a)



(b)

Fig 4. 35. Water level and Current streamlines in the 2-D model for (a) ebb and (b) flood generating mode, respectively.

4.3.3 0-D and 2-D comparison

In this phase, the DIVAST 2-DU model was modified and developed with the implementation of the optimum design and operational parameters described above. Similar to SBL, there is no extra momentum transfer added into the 2-D model, with more details can be given in [117]. In Figures 4.36-4.38, the comparison between 2-D and 0-D models was achieved towards the water levels upstream, downstream and power output, discharge through the turbines and sluices gates for 5 neap tides, as well as the accumulated electricity generation during the typical tidal cycle, respectively. It revealed a good agreement between the 0-D and 2-D models. It should be highlighted that for the WSL, the 0-D model overestimated the electricity generation by approximately 10%, which is consistent with the findings in [33, 52].

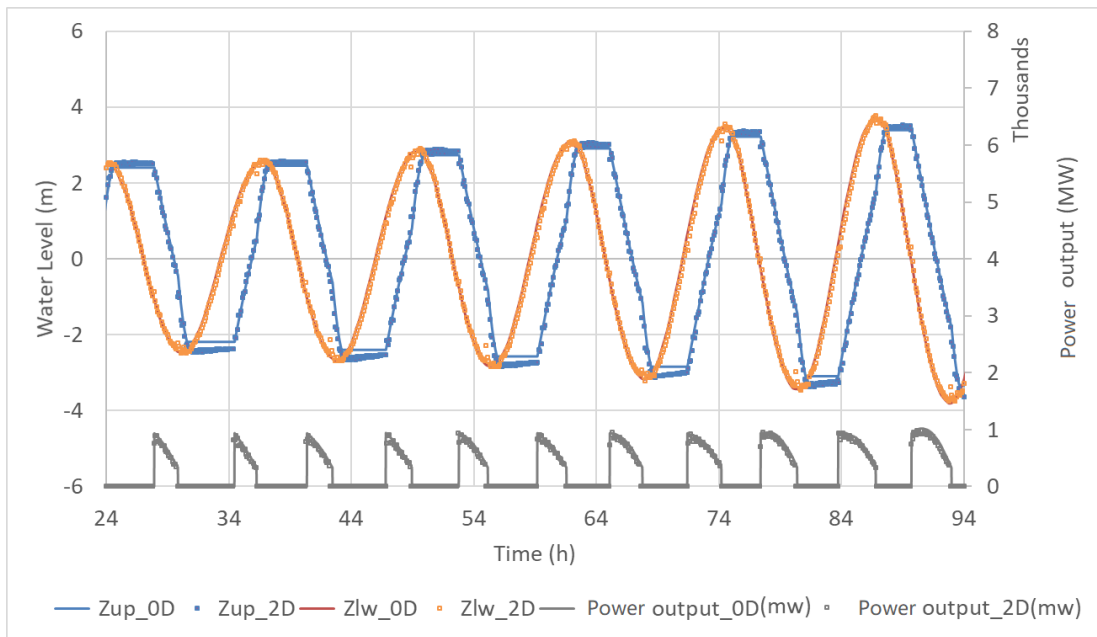


Fig 4. 36. 2-D and 0-D model comparisons between water level and power output during 5 neap tides, in which the ‘Zup’ and ‘Zlw’ represent the upstream and downstream water levels, respectively, ‘Power output’ denotes the power output.

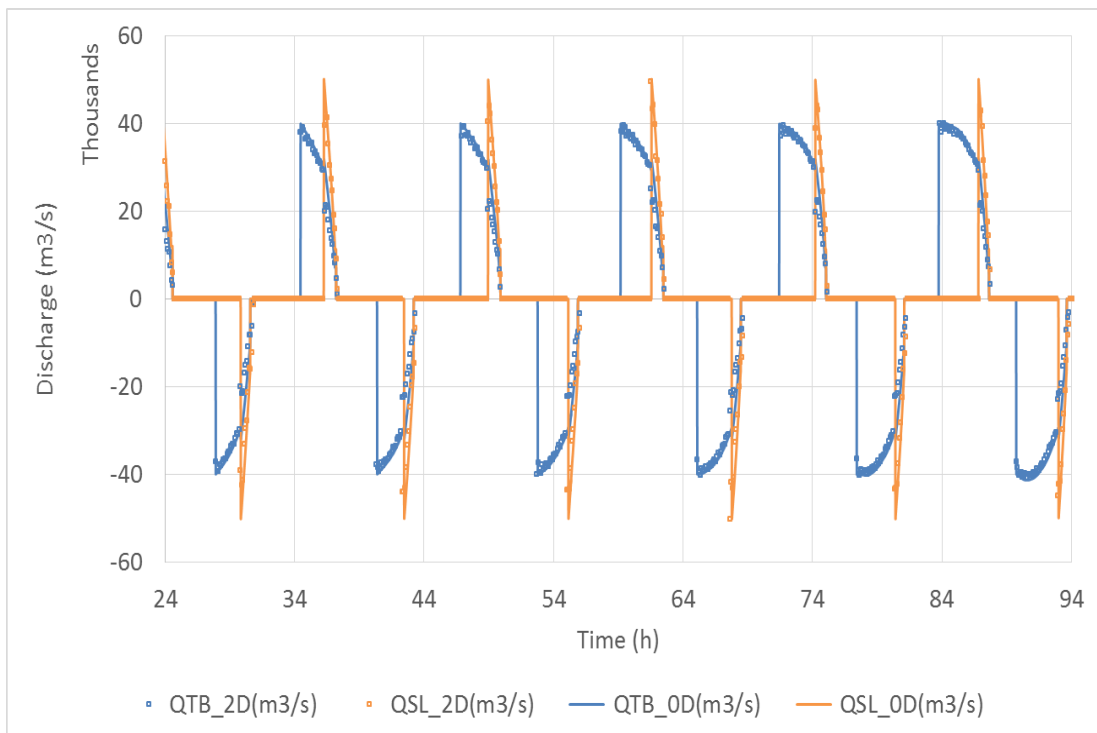


Fig 4. 37. 2-D and 0-D model comparisons between discharge through the sluice gates and turbines during 5 neap tides, in which the ‘QTB’ and ‘QSL’ denote the discharge through turbines and sluice gates, respectively.

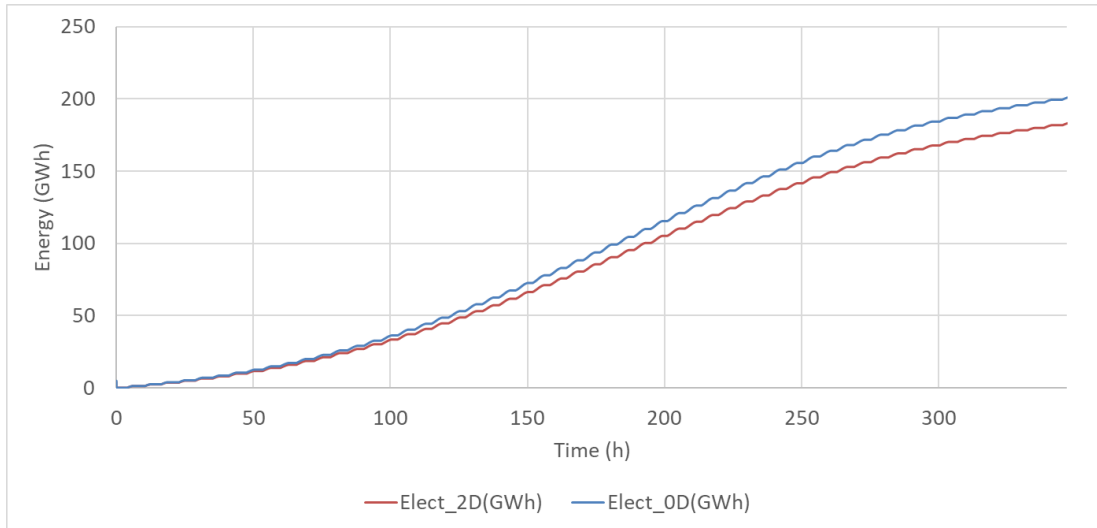


Fig 4. 38. 2-D and 0-D model comparisons between electricity generation throughout the typical Spring Neap cycle, in which the 'Elect' denotes the electricity generation.

4.4 North Wales Tidal Lagoon

North Wales Tidal Lagoon (NWTL) proposed by North Wales Tidal Energy & Coastal Protection (NWTE) to be built on the North Wales coast from Llandudno to Prestatyn [135]. It would comprise a 31km long impoundment wall enclosing an area of 157 km². Based on the initial assessment, the scheme would have an installed capacity of approximately 2.5 GW [136] by using about 125 20 MW bi-directional turbines and have sluice and lock gates within the impoundment wall as shown in Figure 4.39. It was anticipated that the project would generate sufficient electricity to power 1.1 million homes. It would reduce GHG emissions by 1.5 million tonnes annually, equivalent to 180 million tonnes over a 120-year project life [137].

The project aims to diversify the sources of renewable energy in the UK and take advantage of the tidal time differences in the North and South Wales. The chairman of the NWTE has pointed out that although other sources of renewables including wind and solar do a good job and are part of the energy solution, we need multi-schemes from TRSs to provide continuous power output as an important part of the UK's energy mix [138]. The opportunity provided by the tide difference between this scheme and schemes proposed in the Bristol Channel in the multi-scheme optimisation and potential for continuous electricity generation from TRSs led to the inclusion of this scheme in this work. The location of the scheme on the north wales coast is shown in Figure 4.39. The initial proposal included 10 sets of turbine housings and 8 sets of sluice gates distributed along the wall. The bathymetry of the area inside the lagoon is shown in Figure 4.40, and Figure 4.41 illustrates the wetted plan surface area of the NWTL for different impounded water levels.



Fig 4. 39. Location of North Wales Tidal Lagoon [135].

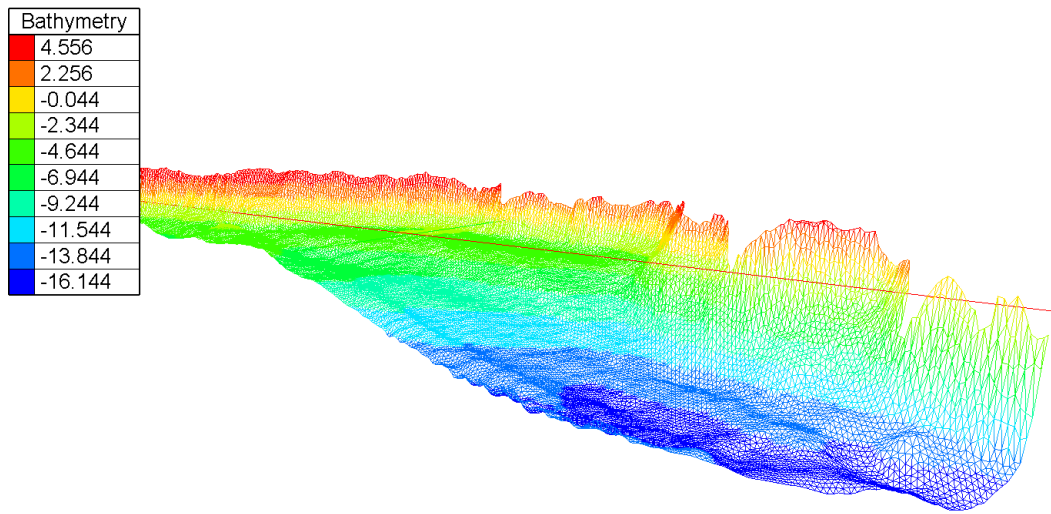


Fig 4. 40. North Wales Tidal Lagoon bathymetry.

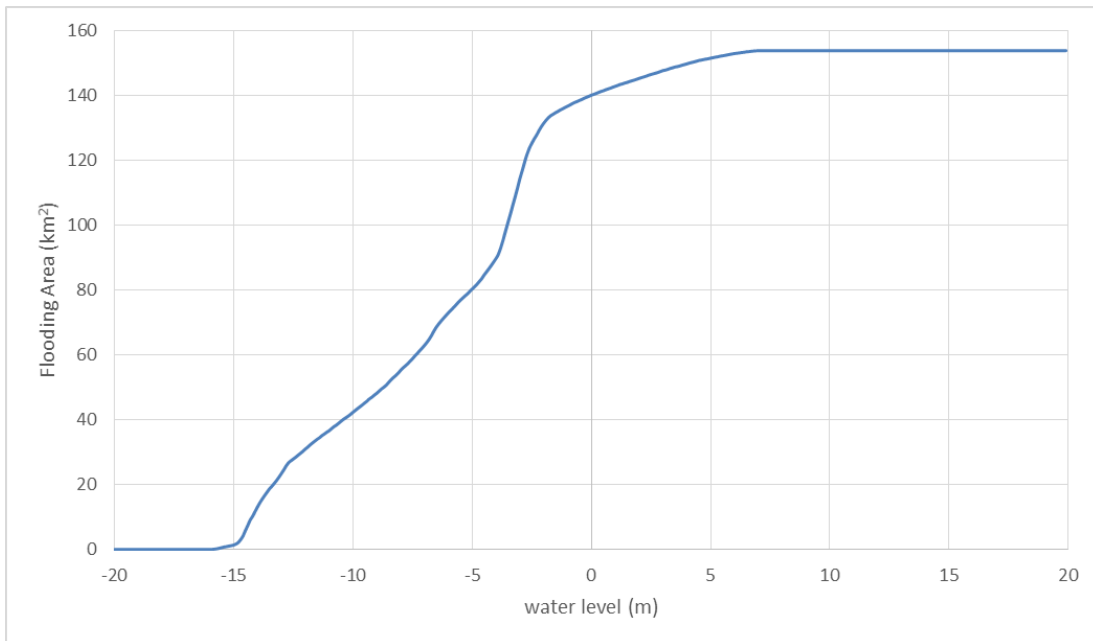


Fig 4. 41. Wetted area versus water level of North Wales Tidal Lagoon.

4.4.1 NWTL modelling

As illustrated in section 4.3.1, a typical cycle, e.g. Spring Neap tidal cycle, was adopted here to represent the annual electricity generation. It should be noted that the input water levels used in the 0-D model were obtained from the TELEMAC-2D model. As shown in Figure 4.31, the same time slot of the typical Spring Neap cycle used for WSL, from 12/08/2012 13:45:00 to 27/08/2012 01:45:00, was used for NWTL, ensuring a reliable joint optimisation to be done in Chapter 7.

According to the updated deployment of the blocks of turbines and sluice gates from Figure 4.42, there are 10 blocks of turbines and 8 blocks of sluice gates. The water levels at High Water (HW) and Low Water (LW) have been shown in Figures 4.43-4.44, which indicated that the water levels at point 6 was the nearest to the averaged water level and hence was selected as the representatives of the input water level point in the 0-D model. Figure 4.45 is the input water levels for the WSL and NWTL calculated from TELEMAC-2D during the typical Spring-Neap cycle, which will be used for Chapter 7 for the simulations of two TRSs at the same time.

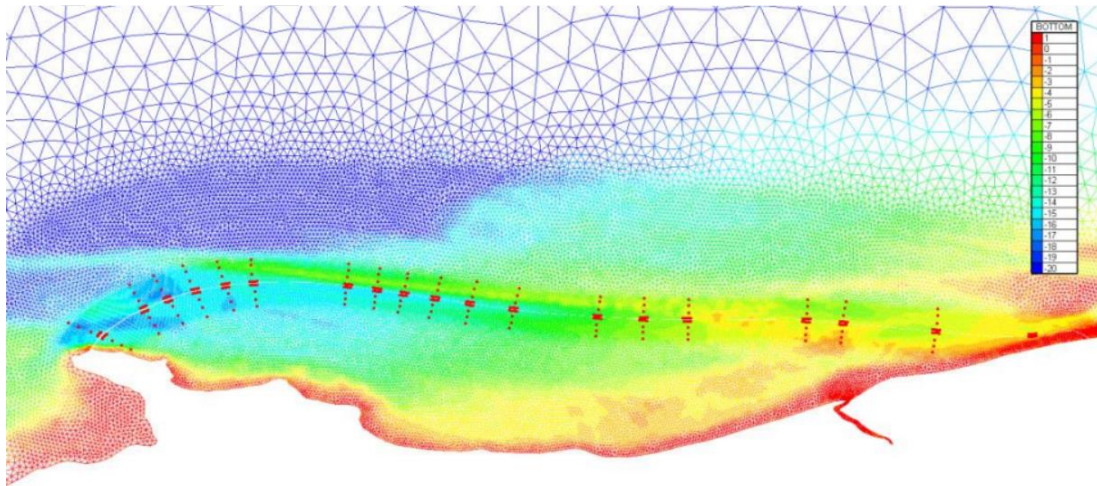


Fig 4. 42. Layout of the North Wales Tidal Lagoon constitutes including the blocks of turbines and sluice gates, in which the left 10 red rectangular represent the blocks of turbines and the rest 8 for sluice gates.

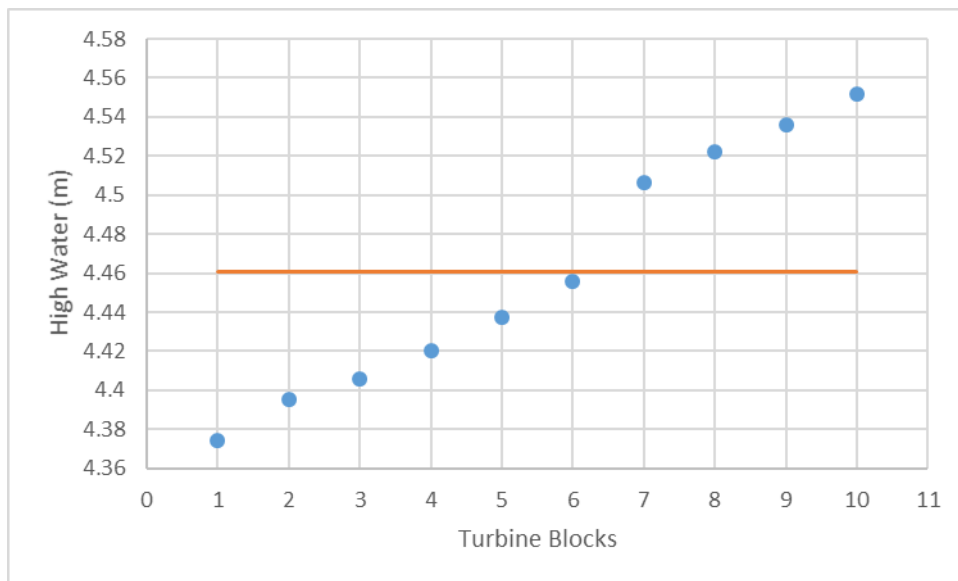


Fig 4. 43. High Water at the outside of each block of the North Wales Tidal Lagoon marked as blue dot with the averaged value shown as orange line.

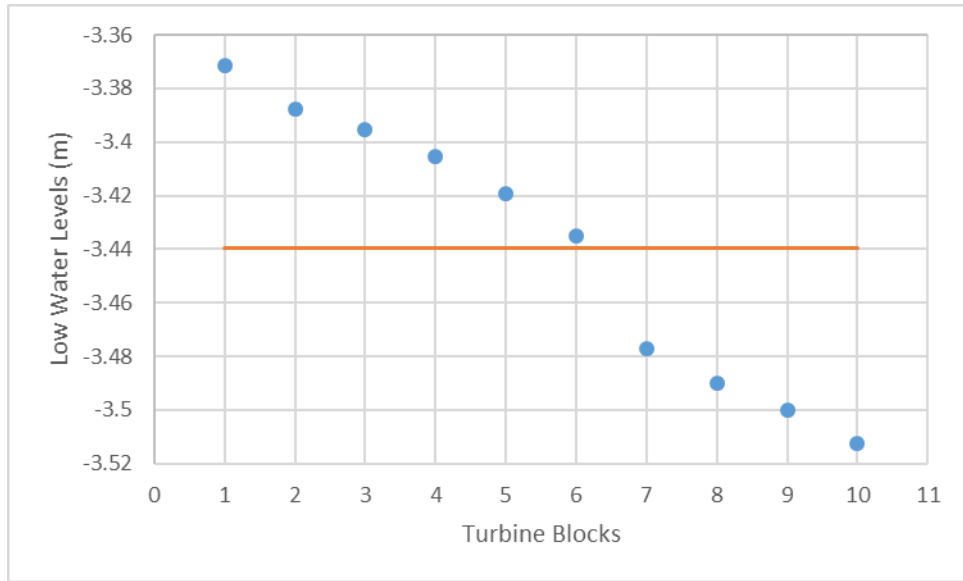


Fig 4. 44. Low Water at the outside of each block of the North Wales Tidal Lagoon marked as blue dot with the averaged value shown as orange line.

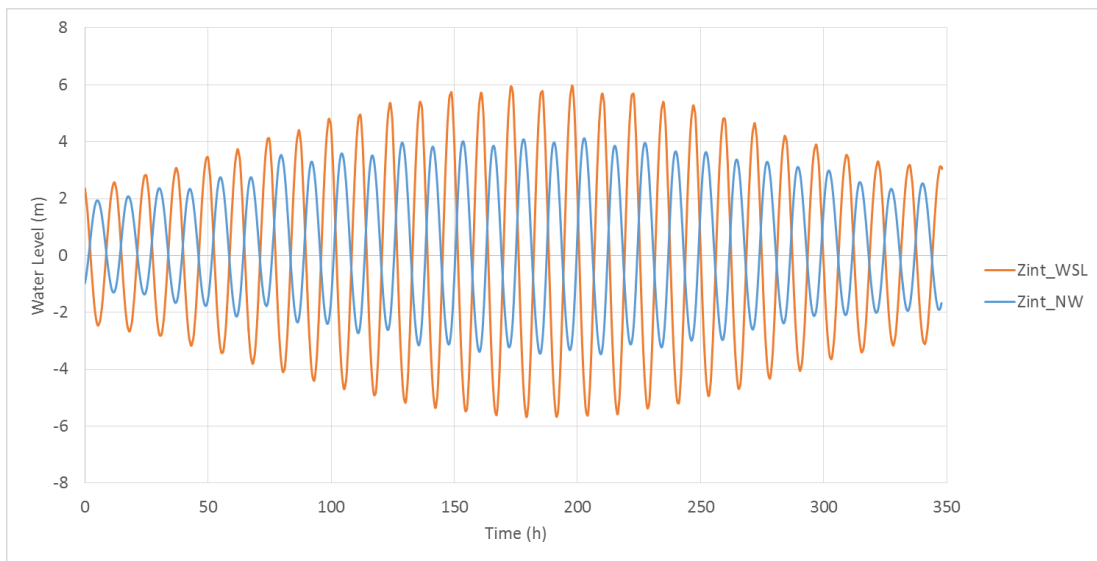


Fig 4. 45. Water levels in typical Spring Neap cycle for West Somerset Lagoon and North Wales Tidal Lagoon.

During the typical Spring Neap cycle, the electricity production under traditional non-flexible operation was shown in the Figure 4.46, a range of NumTB from 50 to 300 with 25 increase, STPC from 0 to 10 with 2 increase, H_s from 2.0 m to 8.0 m with 0.1 m increment and H_e from 0.5 m to 4.5 m with also 0.1 m increment. When the NumTB of 150 and STPC of 10 with the optimal operation heads of H_s of 3.7 m and H_e of 1.4 m, the maximum electricity generation of 159.71 GWh could be achieved during the typical cycle, equals to 3.84 TWh/Year with a coefficient of approximately 24.01 applied, as shown in Figure 4.46.

It should be noted that the water levels downloaded from BODC at Llandudno can also be considered as an alternative input source in the 0-D model with the RMSE of approximately 0.2 m. Following this, a maximum of 156.21 GWh electricity generation can be calculated with the same operation heads to it using the 2-D model, which corresponds to an around 2% difference. Similar to WSL, with the turbine numbers increases, the electricity estimated increases at the beginning and then decreases moderately with the peak value appeared when the NumTB around 150, and with the STPC increases, the production of electricity showed a growing trend. Furthermore, we can see that electricity estimation rises slightly when NumTB and STPC exceed approximately 150 and 8.

Under this scenario, the details of water levels inside the impoundment and power output; discharge through sluice gates and turbines; and water head difference for 5 neap tides and electricity generation during the typical cycle in the 0-D model have shown in Figures 4.47-4.50, respectively. It can be seen that although the non-flexible operation heads and design parameters have been optimised, there was still no power output for some neap tides because of the insufficient tidal range created. It re-emphasized the significance of exploring the optimally designed parameters combining with operation flexibly in NWTL project optimisation.

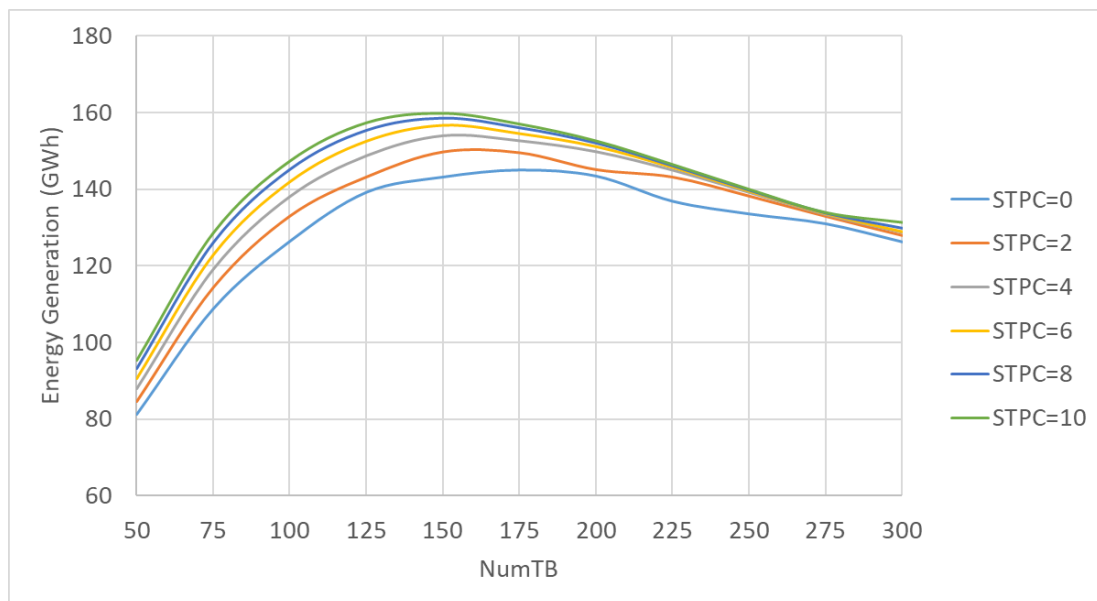


Fig 4. 46. Water levels and scheduling in the 2-D model with ‘time control’ method for operation.

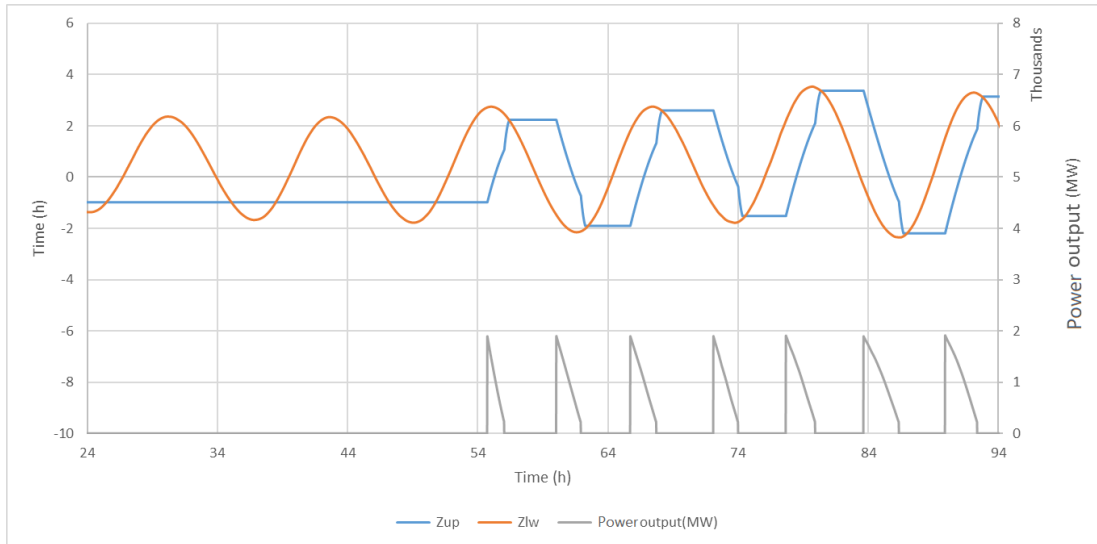


Fig 4. 47. Water levels inside the impoundment and power output for West Somerset Lagoon during 5 neap tides in the 0-D model.

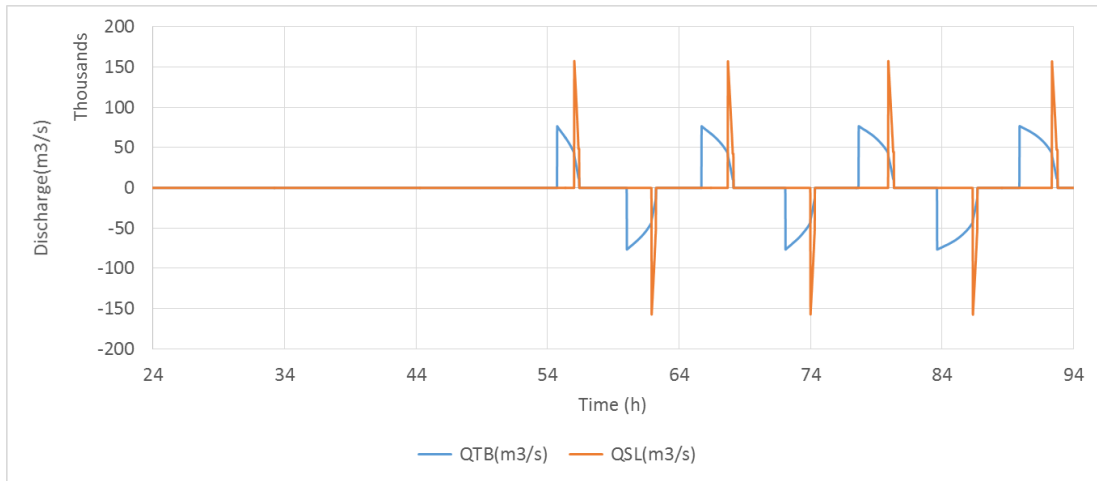


Fig 4. 48. Discharge through sluice gates and turbines for West Somerset Lagoon during 5 neap tides in the 0-D model.

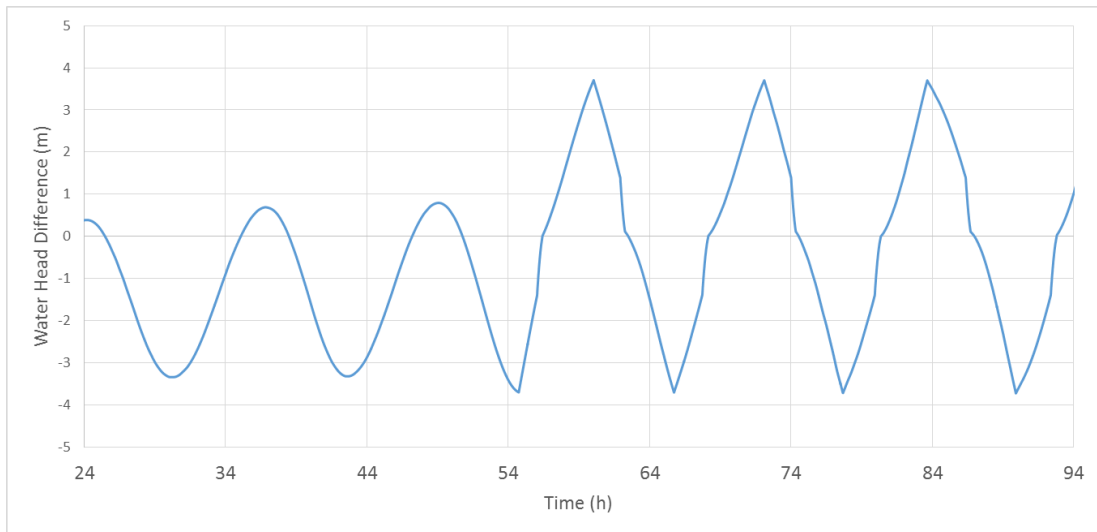
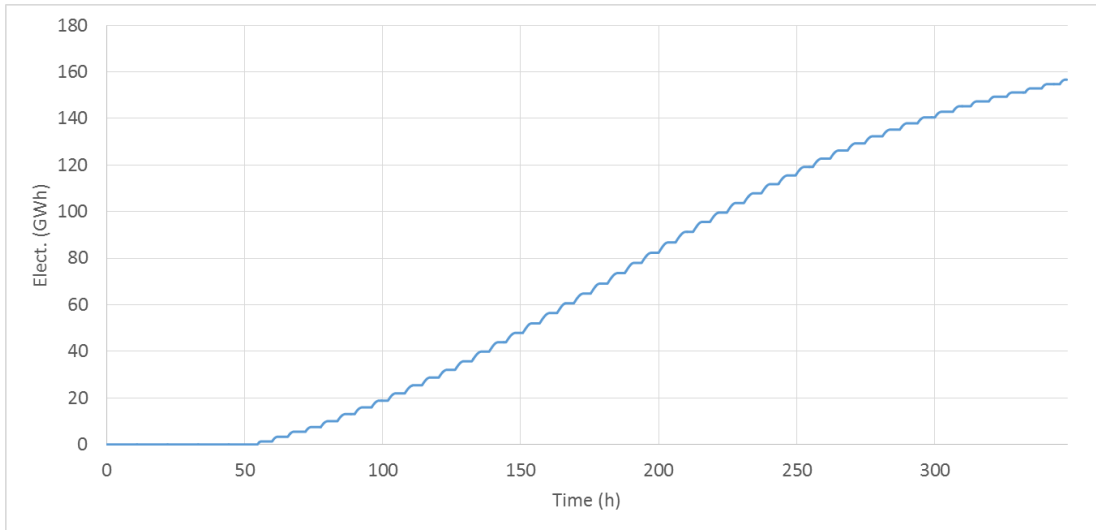


Fig 4. 49. Water head difference for West Somerset Lagoon during 5 neap tides in the 0-D model.



(d)

Fig 4. 50. Electricity generation for West Somerset Lagoon during the typical cycle in the 0-D model.

4.5 Chapter summary

This chapter outlined the three potential TRSs proposed to be built in the UK and used in this study, known as the Swansea Bay Lagoon (SBL), West Somerset Lagoon (WSL) and North Wales Tidal Lagoon (NWTL). Notably, one of the key objectives in this study was addressed, which was to set up and develop the 0-D model under a variety of fixed operation scenarios and will further be developed as part of the key contributions in this study. Then the verified DIVAST 2-DU model was set up to evaluate the 0-D simulation results, without and with pumping used, respectively. With the simulation of hydrodynamics in the 2-D model, more accurate electricity generation was estimated which makes it to be an ideal tool for the evaluation of optimisation performance developed from 0-D modelling. The electricity generation predicted using the 0-D model in this study overestimated the predictions relative to the 2-D model by approximately 10%. This revealed the availability of using the 0-D models in the prediction of electricity in TRSs optimisation.

In section 4.2 to 4.4, the design parameters of SBL, WSL and NWTL were illustrated, respectively. The 0-D models were set up and the details parameter setting in the 0-D model have been clarified. The input water level for the 0-D models were generated from the 2-D models, known as the 2-DU DIVAST model refers to SBL case study and TELEMAC-2D for WSL and NWTL. With using the variable wetting area instead of a constant value which has been traditionally used in 0-D modelling, the electricity estimations showed that only less than 5% compared with including the flooding and drying within the impoundment. It followed up by the optimisation of using a wide range of fixed operation heads for generating and sluicing during the typical Spring Neap cycle. Particularly, when optimised pumping head involved, a more than 10% improvement in electricity generation could be obtained.

Secondly, model independence has been demonstrated between the hydrodynamics comparison from finer and coarser meshes, with an example of SBL. It proved the reliability of using the 0-D model in the optimisation of further studies, especially in the flexible operation optimisation in Chapter 7 which required the prediction of generation duration with high accuracy to achieve multi-objective decision making. In conclusion, the 0-D model can be considered as a reliable tool for energy estimation for the preliminary design stages and implementation in terms of TRSs optimisation, which requires a large number of runs.

Importantly, it was founded that under fixed operation schemes, there might not have any power output during some neap tides due to insufficient tidal range, this emphasized the significance of using flexible operation schemes, which divided the tides into small components, e.g. every tide or half-tide and applied variable operation heads in each unit, to maximise the electricity generation in Chapter 5 and 6.

5. Tidal Range Schemes' Operational and Design Optimisation

5.1 Introduction

It has been shown that the electricity generation under the traditional non-flexible operation schemes during neap tides are limited and even zero [31, 55] due to the insufficient tidal range which was reconfirmed in Chapter 4. This highlights the significance of using flexible operation schemes to generate electricity even during neap tides. This chapter discusses the optimisation of flexible operation schemes using various Grid Search (GS) methods according to the tide splitting approach. SBL is selected to be an ideal case study in this chapter with couples of supports. Firstly, a certain number of studies for SBL have been put forward [65, 119]. Following that, the operational schemes optimisation could be further developed based on previous studies with confident design parameters. UK's Prime Minister Boris Johnson was urged to give the go-ahead for SBL recently [10], which highlights the importance of this study that optimising TRSs to generate maximum possible electricity and revenue while keeping the cost down.

In the GS models, the operation of TRSs is broken into small components, e.g. every tide or every half-tide, then using a widely used 0-D modelling methodology to evaluate the generation of electricity during each tidal cycle until the maximum electricity output obtained. Then the optimised operation schemes are used to simulate the lagoon operation by using the modified DIVAST 2-DU model and the differences between the GS and 2-D results are highlighted. Furthermore, the GS model was revised to alter the number of turbines being utilised during different cycles in order to ensure maximum generations. These flexibilities of the operations aimed to contribute to the improvement of electricity generation and once achieved, it could have a great impact on the feasibility of a TRS.

Section 5.2 demonstrates the methodology of various GS methods without and with pumping included. Then, the feasibility of the operation schemes designed by the GS method is verified using the DIVAST 2-DU model with the simulation of hydrodynamics. Section 5.3 is focused on the investigation of utilising flexible turbine numbers in the optimisation of TRSs. Accounting for the

changes of tidal range between spring and neap tides, the changes in water levels across the impoundment slow down by using fewer turbines.

5.2 Flexible operation heads

5.2.1 Methodology

In order to respond to the changes in the tidal range during the tidal cycle, the optimisation of starting and ending heads was carried out of smaller components of the simulation period as follows: Optimising the operation of every single tide, from high water to the next high water. This was denoted as Every Tidal cycle (ET) model in this study and illustrated in Figure 5.1 for 3 imaginary tides. The optimum operation was calculated separately for each tide A, B and C, as shown in Figure 5.1(a). This included running the 0-D model for the complete range of feasible starting heads for ebb tides, i.e. H_{se} , and flood tides, i.e. H_{sf} , from 2.0 m to 8.0 m with 1 cm increments and the ending heads for ebb tides, i.e. H_{ee} , and flood tides, i.e. H_{ef} , covering a range from 0.5 m to 4.5 m, also with an increment of 1 cm. In this method, different starting and ending heads were examined for Tide A, with the optimum starting and ending heads defined when the maximum energy for this cycle was achieved, as shown in Eq. 5.1. Similarly, the best and selected operations for Tide B and Tide C were calculated in isolation, as shown in Figure 5.1(a).

$$\text{maximise } P_{tb}(H_s, H_e), \text{ subject to } H_s \in [2.0, 8.0] \text{ and } H_e \in [0.5, 4.5] \quad (5.1)$$

where P_{tb} is the calculated power output for the designed turbines. H_s and H_e are the starting and ending heads.

However, the water level inside the lagoon for the start of Tide B was the water level calculated inside the lagoon at the end of Tide A, obtained using the selected operation for Tide A. The link between the operation of the tides led to the next approach to the optimisation of the operation. In the second method, the optimum operation for every cycle was decided in conjunction with the next cycle which was referred herein to Every Tidal cycle and Next (ETN). The 0-D model was used over the same range as for the ET method to simulate the optimum operation heads which gave the maximum power output for two successive tides; for instance, Tide A and B as shown in Figure 5.1(a). The optimum operation was used for the 1st tide of the two tides, namely Tide A in this example, and the process was repeated for the next two tides, Tide B and C. This method takes into account the fact that the inner water level for the consecutive tides, e.g., Tide B, was influenced by the inner water level at the beginning of this tide or the operation of the previous tide. In other words, the power output generated for each cycle would be affected directly by the previous cycle.

Alternatively, every tidal cycle could be seen as an ebb and a flood tide, as illustrated in Figure 5.1(b). Every Half tidal (EH) model was set up to simulate the most optimised operation head for every ebb and flood tide. In a similar manner to the ETN approach, the EH model could be used to consider the next ebb or flood half tide, which was referred to as Every Half tidal cycle and Next (EHN) model in this study. The rationalisation for using the next half tide in the EHN was the impact that the operation

at every half-tide would have on the next half-tide, similarly to the ETN approach. Briefly, the EH and EHN can be considered as the approaches between local and global optimisation methods.

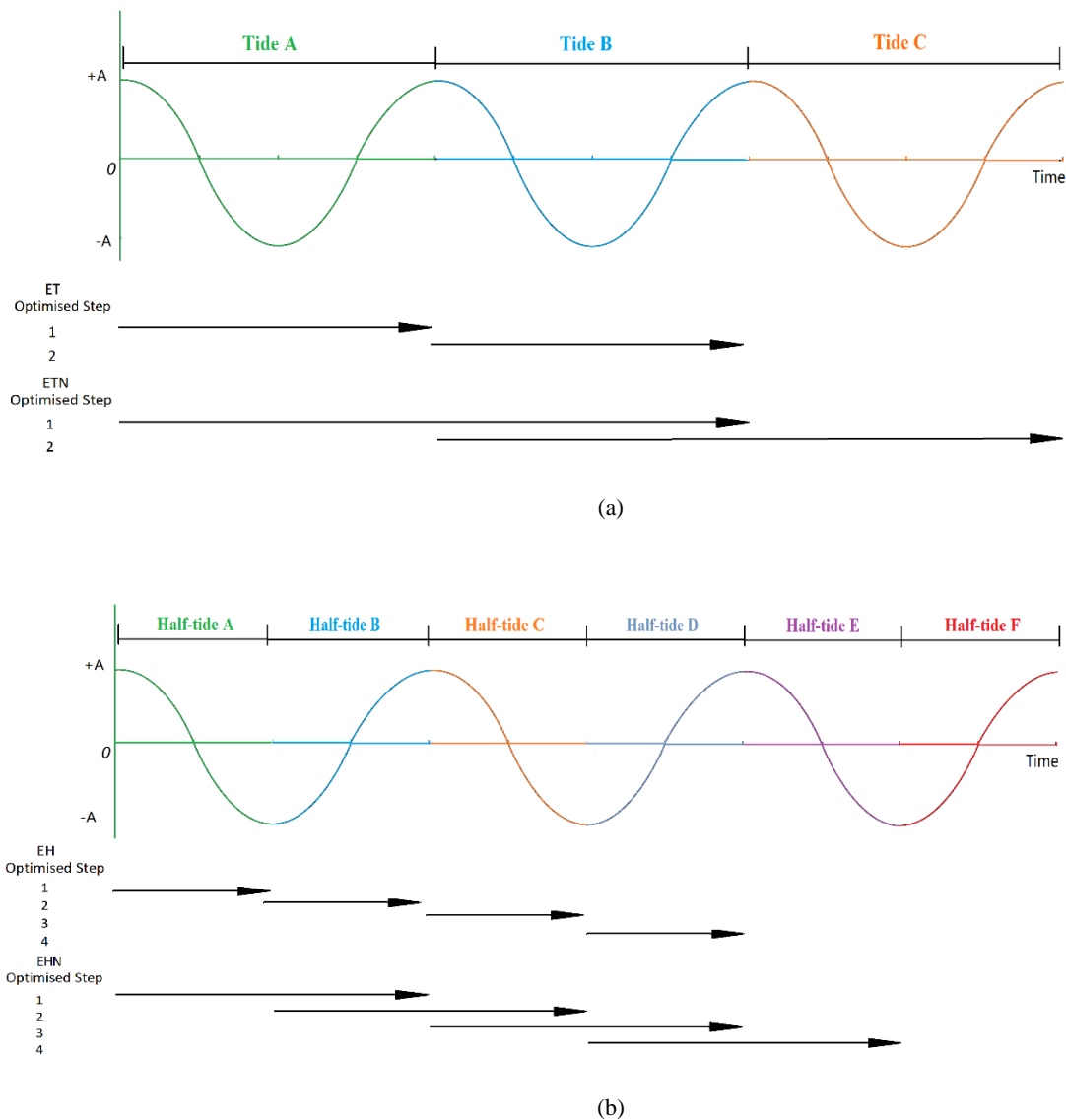


Fig 5. 1. 3 Schematic illustration of different optimisation methodologies: a) full tide optimisation illustrations: ET and ETN methods; and b) half-tide optimisation illustrations: EH and EHN methods.

Pumping was also considered in the flexible operation in a similar manner as discussed in Chapter 3. The letter 'P' has been added to the abbreviation for each model to show the inclusion of pumping. As a result, the models including pumping were: Every Tide cycle and Pump model (ETP Model with pumping), Every Tidal cycle and Next Pump model (ETNP Model with pumping), Every Half tidal cycle and Pump model (EHP Model with pumping) and Every Half tidal cycle and Next Pump model (EHN Model with pumping). The same range of starting head H_s , including H_{se} and H_{sf} , was chosen from 2.0 m to 8.0 m, with a 1 cm increment, and also the ending head H_e , including H_{ee} and H_{ef} , was from 0.5 m to 4.5 m, with a 1 cm increase. These models also included a wide range of flexible pumping

head H_p , including a pumping head during ebb tide, i.e. H_{pe} , from 0.0 m to 2.0 m, with a 1 cm increase; a pumping head during flood tide H_{pf} , from 0.0 m to 2.0 m, also with 1 cm increase, in order to capture all feasible scenarios.

5.2.2 Optimisation without pumping

A wide range of starting and ending heads was considered in this study to ensure that all the potential scenarios were captured. Figure 5.2 shows typical energy generation levels for different heads during 10 spring tides using the ET model. It can be seen that the electricity generated for the large and small operating heads was negligible. Similar results were found for other models and therefore, main energy generation graphs used in this study were focused on starting generation head of H_s from 0.5 m to 4.5 m and ending generation head of H_e from 2.0 m to 8.0 m for clarity. The maximum energy generation point, which corresponded to the best possible operation, is shown with a red cross in electricity output figures, highlighting the changes from tide to tide.

Figure 5.3 shows the water levels inside the lagoon and optimised operation heads of H_s and H_e from the ET model during the typical Spring Neap cycle. The 2nd order polynomial lines denote the trend of operation heads in terms of different tidal ranges. The optimum H_s ranged from 3.1 m to 5 m in which lower H_s were related to the neap tides and higher ones corresponded to the spring tides. When the optimum H_e varied between 1.3 m and 2 m, there was no significant difference observed for H_e values between spring and neap tides. Hence, It can be concluded that the H_s values were more sensitive to the tidal range changes in comparison with H_e .

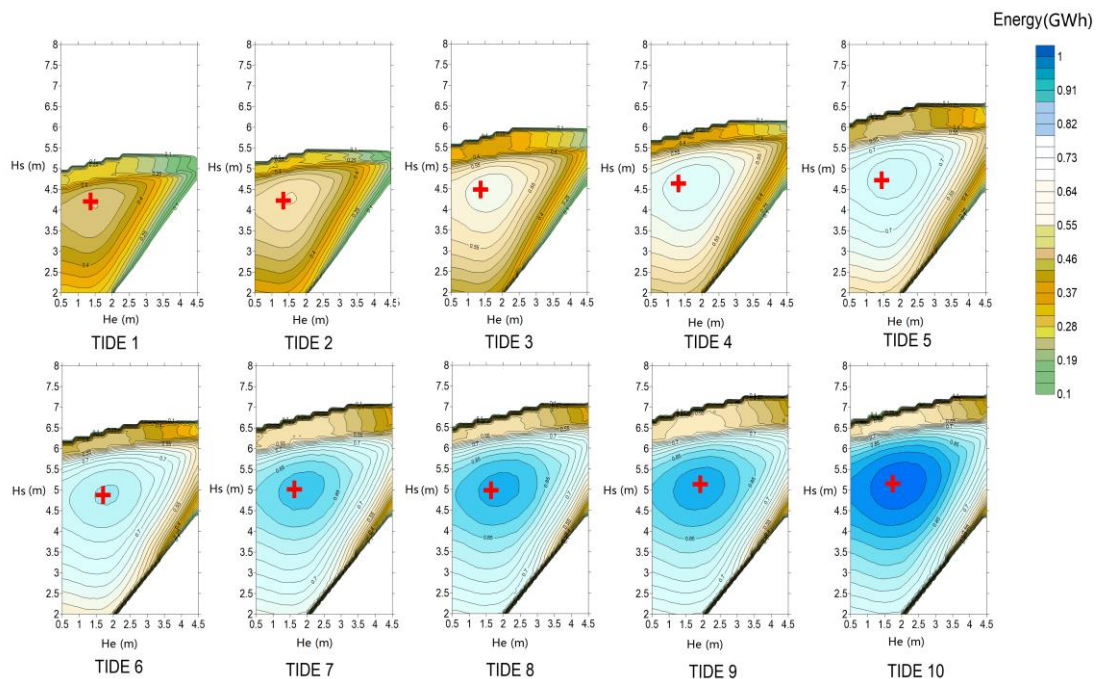


Fig 5. 2. ET model for 10 tides, with the maximum energy point, i.e. most optimised operation, is shown with a red cross.

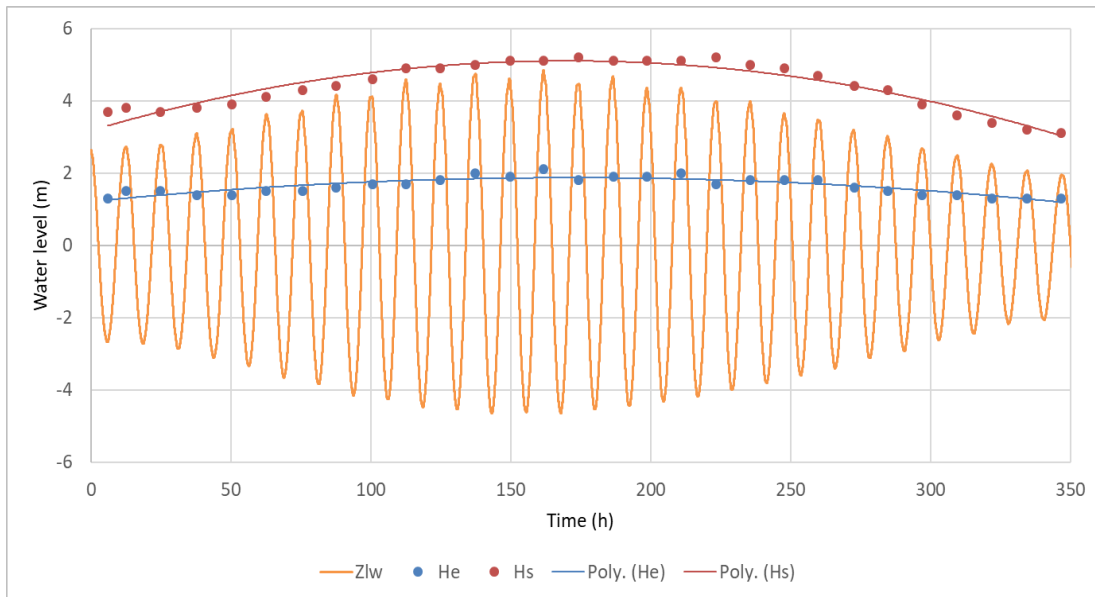


Fig 5. 3. Optimised operation schemes from the ET model during the typical Spring Neap tides.

The traditional fixed operation of the lagoon was optimised in Chapter 4, as the baseline in this study. The electricity generated for each method over the 2nd tidal cycle which represented the annual generation output is summarised in Table 5.1. The EHN model, i.e. Every Half tidal cycle and Next model, gave the best-optimised operation, resulting in the highest electricity generation [31]. The electricity estimated using the EHN model was approximately 12.5% higher than electricity generated for the fixed head operation. Using half tides as operational units, i.e. EH model, could improve the energy level generated by about 1.6% comparing to each tide based units, i.e. ET model. However, the inclusion of the next half tide, i.e. EHN model, only improved the outcome by about 0.6% comparing to excluded model, i.e. EH model.

Table 5. 1. Optimisation scenarios for 2nd tidal cycle.

Scenario	Energy (GWh)	Change to fixed head schedule
Fixed head schedule	21.3	-
Optimised		
ET model	23.5	10.5%
ETN model	23.6	10.6%
EH model	23.8	11.9%
EHN model	24.0	12.5%

The behaviour of impoundments operated based on different optimisation models, including fixed head operation models, are compared in order to highlight the differences. Figures 5.4-5.6 illustrate the operation scheduling of the impoundment, the water levels inside the impoundment and power output for four neap tides, based on different optimisation models, respectively. Comparisons of the models show that generation generally starts at a lower head difference for the fixed head models comparing to operation flexibly. This causes a lower peak generation and prolonged generating phases. Moreover, less reduction in the tidal range within the lagoon is observed with the flexible operation which is expected to have environmental benefits which require further detailed studies [51, 114]. Considering two successive tides or half-tides, i.e. the ETN and EHN models, showed a better capability of finding a balance point between each current tide and the next tide, thus allowing for the energy generated to be more consistent. It can also be concluded that the maximum power output obtained from each tide is usually less than the total installed capacity, even taking flexible operation schemes into consideration.

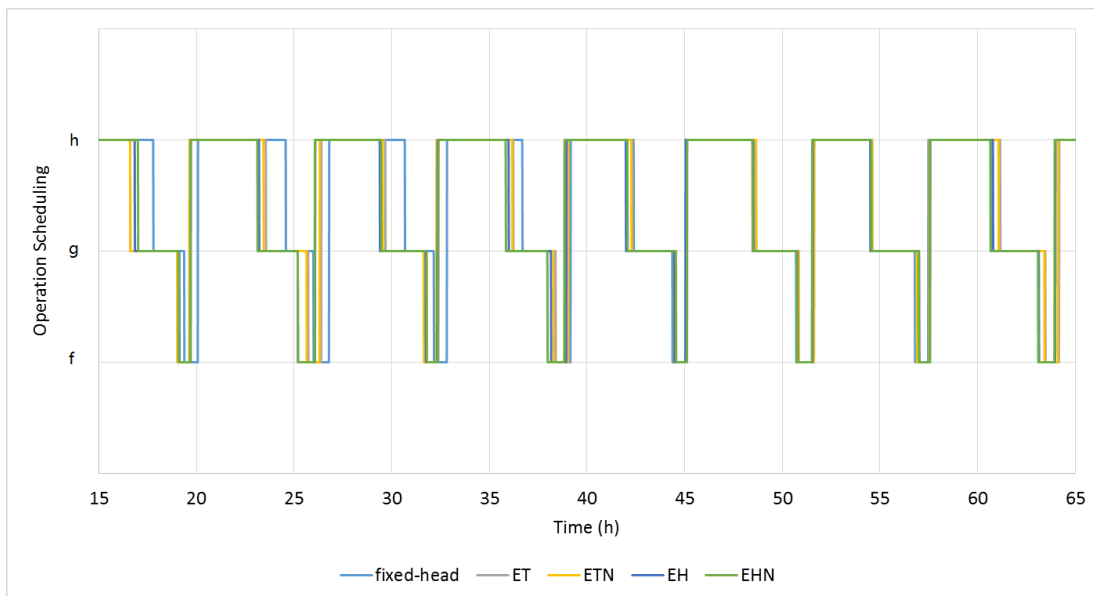


Fig 5. 4. Operation scheduling of the impoundment, in which ‘h’, ‘g’ and ‘f’ denotes holding, generating and filling phases, respectively, for 4 neap tidal cycles from the 15th hour during the Spring Neap cycle, equals to 13/08/2012 00:42 and based on ET, ETN, EH, EHN and fixed head models.

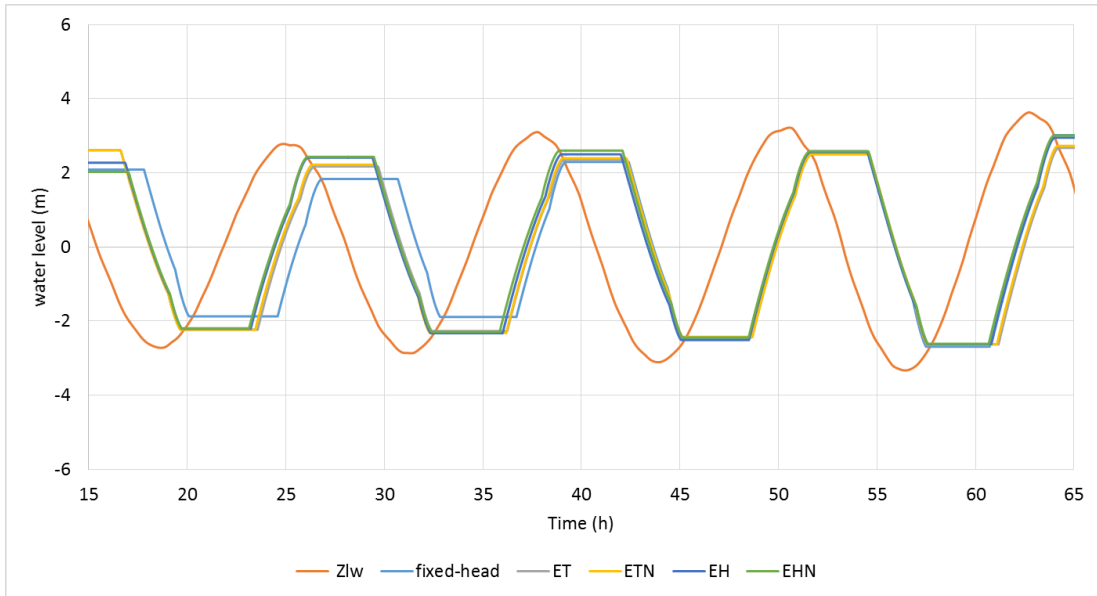


Fig 5. 5. water levels inside the impoundment for 4 neap tidal cycles from the 15th hour during the Spring Neap cycle, equals to 13/08/2012 00:42. and based on ET, ETN, EH, EHN and fixed head models.

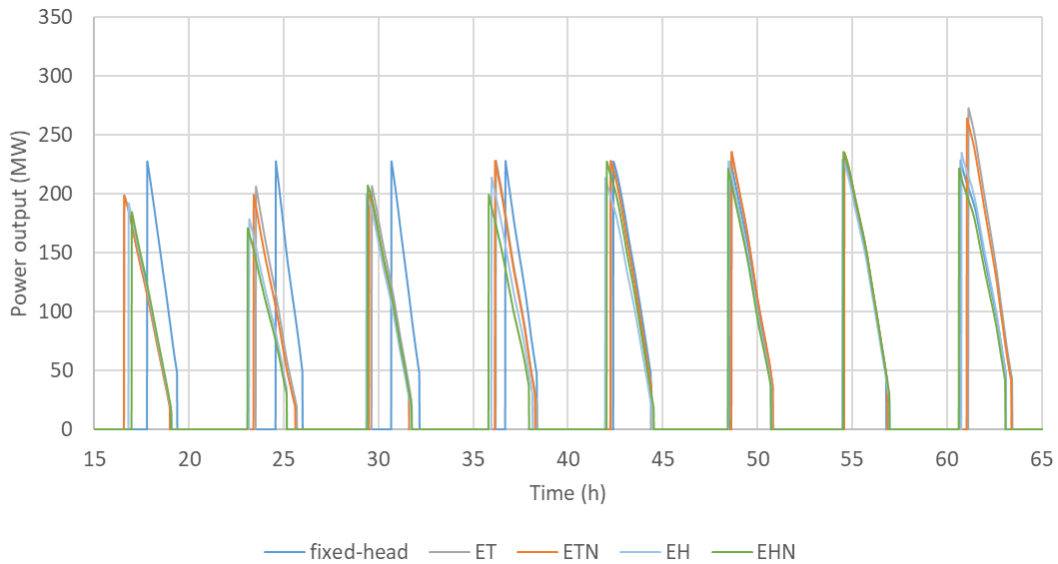


Fig 5. 6. Power output comparisons for four neap tides from the 15th hour during the Spring Neap cycle, equals to 13/08/2012 00:42. and based on ET, ETN, EH, EHN and fixed head models.

5.2.3 With pumping operation

The optimisation results of the flexible operation including flexible pumping are shown in Table 5.2. It can be seen that the EHNP model, which is Every Half tidal cycle and Next Pump model, produces the best optimised flexible operating schedule. This scenario, which includes flexible operation and pumping, resulted in approximately 27.2% more electricity in comparison to a fixed head operation without pumping. These results from the 0-D model suggested that the optimisation schemes including pumping can increase the potential of the lagoon for energy generation by at least 10% comparing to

pumping excluded schemes without any significant extra costs, e.g. construct more turbines or sluice gates.

Table 5. 2. Plus pumping optimisation scenarios for 2nd tidal cycle.

Scenario		Energy (GWh)	Change to fixed head schedule
Fixed head schedule		21.3	-
Optimised	ETP model	26.7	25.5%
	ETNP model	26.7	25.5%
	EHP model	27.0	26.7%
	EHNP model	27.1	27.2%

5.2.4 0-D and 2-D comparison

The DIVAST 2-DU model was modified to simulate the flexible operation including pumping which is derived from the optimisation models. Table 5.3 summarises the energy estimated using various flexible optimisation schemes in the 2-D and 0-D models and without and with pumping, respectively. Similar results are reported in Table 5.4 for optimisation including pumping. The electricity generation predicted using flexible 0-D models were in very good agreement and less than 5% with those predicted using the 2-D models under the same conditions. The differences between the 0-D and 2-D model predictions were lower for the flexible models compared to the fixed head model. This highlights that the optimised scheduling provided by the 0-D model including flexible operation and pumping were reliable and could be used at preliminary stages of the design which requires a large number of runs.

Table 5. 3. Comparison of optimisation scenarios without pumping.

Scenario	Energy(GWh)		Change to fixed head schedule 2-D (%)	Difference between 2-D and 0-D energy prediction (%)	
	2-D model	*0-D model			
Fixed head schedule	19.7	21.3	-	-7.5%	
Optimised	ET model	22.7	23.5	15.6%	-3.2%
	ETN model	22.8	23.6	15.7%	-3.2%
	EH model	22.8	23.8	15.8%	-4.3%
	EHN model	22.9	24.0	16.0%	-4.6%

*as shown in table 5.1.

Table 5. 4. Comparison of optimisation scenarios with pumping.

Scenario		Energy(GWh)		Change to fixed head schedule 2-D (%)	Difference between 2-D and 0-D energy prediction (%)
		2-D model	*0-D model		
Fixed head schedule		19.7	21.3	-	-7.5%
Optimised	ETP model	25.3	26.7	28.4%	-5.0%
	ETNP model	25.4	26.7	29.0%	-4.8%
	EHP model	25.4	27.0	29.0%	-5.9%
	EHNP model	25.5	27.1	29.6%	-5.8%

*as shown in table 5.2.

5.3 Flexible turbine numbers

Traditionally, the TRSs operate with all the turbines functioning during the generating phase. However, increasing the number of turbines does not always increase the generated electricity. Figure 5.7 illustrates the electricity generation with a range of turbine numbers utilised for SBL under non-flexible operation schemes. It can be seen that the number of turbines was able to seriously impact the electricity generated by the TRSs and the 16 turbines are the most optimised solution in this case. It is expected that very few turbines only allow very limited generation opportunities and hence limited electricity generation. Moreover, in this case, limited discharge goes in and out of the basin and hence sufficient water level difference across the scheme could not be created. In contrast, too many turbines could lead to very fast emptying of the basin which would result in short generation or generating at a low head difference with low-efficiency. Similar behaviour could happen during different tides considering the changes of tidal range. Consequently, to maximise the electricity generation, it might be reasonable to utilise the variable number of turbines to slow down the flow across the impoundment, e.g. shutting down a certain number of turbines, during neap tides.

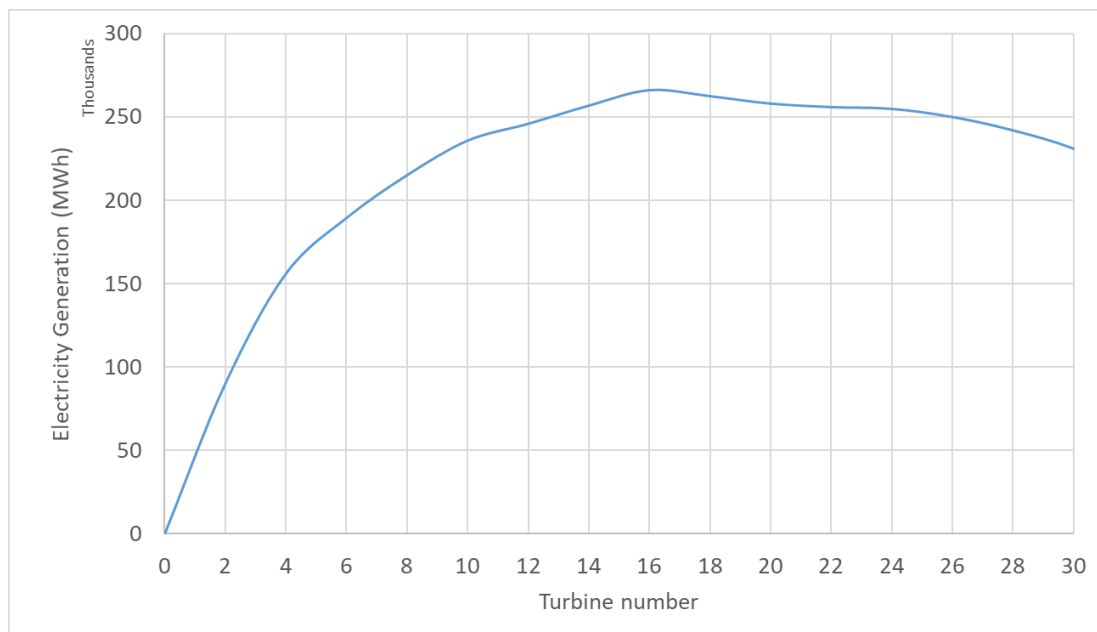


Fig 5. 7. Electricity generation with different turbine numbers within the typical Spring Neap cycle if the non-flexible operation adopted.

Such multi-parameter optimisation would be computationally expensive, for a Spring Neap tidal cycle, especially considering the flexible turbines combining with flexible operation heads. Consequently, to demonstrate such optimisation with affordable time, 8 neap tides at the downstream of SBL site in 2012, considered as typical neap tides for this optimisation in this chapter, were selected. These tides are shown in grey in Figure 5.8.

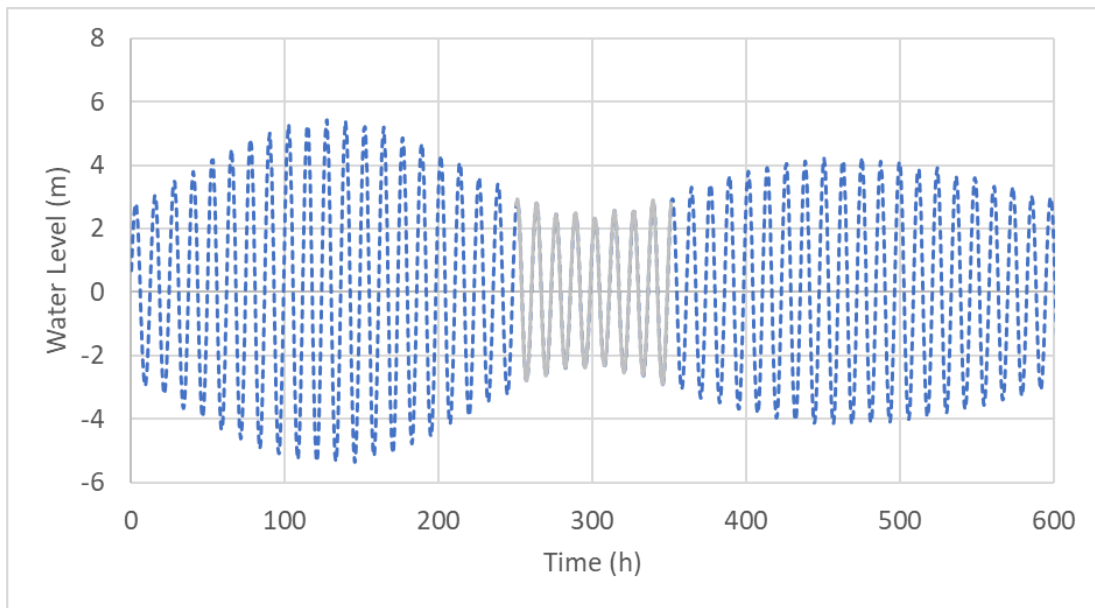


Fig 5. 8. Selected downstream water level during neap tides denotes as grey line.

5.3.1 Non-flexible operation schemes

5.3.1.1 No pumping operation

The fixed operation scheme with H_s of 2.5 m and H_e of 1.5 m, and the fixed turbines numbers ranging from 10 to 16 with the increment of 1 is considered first. The results are shown in Figures 5.9-5.14. It can be seen that with increasing the number of turbines, the upstream water level became higher during flood tides and lower during ebb tides. This is due to a more flow allowed through turbines during generating and sluicing phases. However, as the turbine number was increased, the impact on the discharge through sluice gates has become less significant. The water level difference was less during neap tides with the increased number of turbines, as shown in Figure 5.10. Although the more turbines opening during neap tides means the higher peak of power output, the electricity generation may not reach the maximum because of the shorter generation period. This can be seen in Figures 5.12-13 where the maximum electricity generation occurred when 14 turbines dispatched during these neap tides.

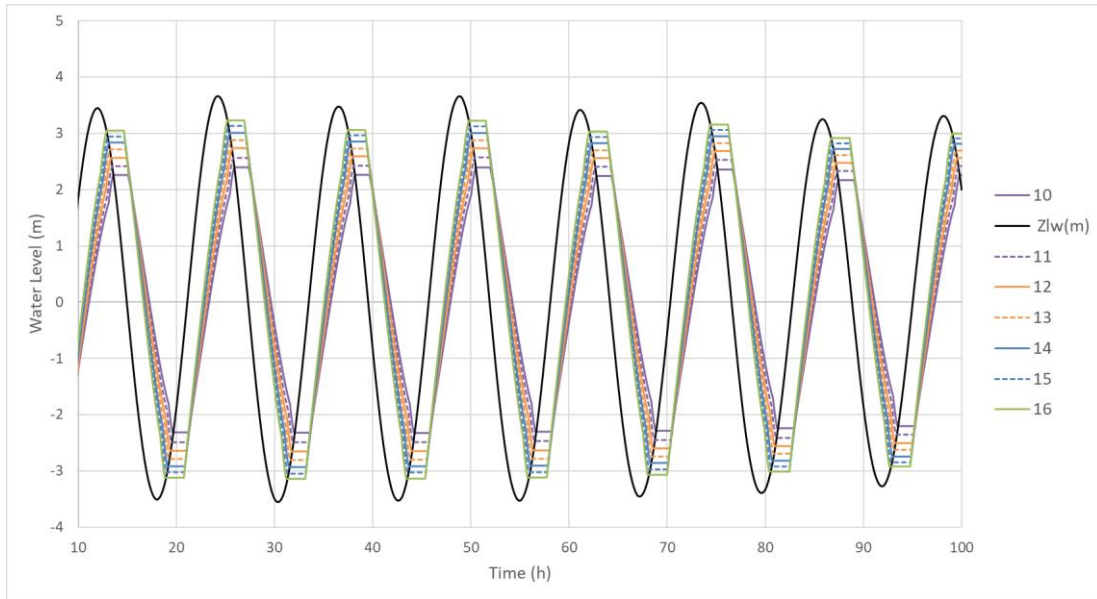


Fig 5. 9. Comparison of basin water levels with different turbine numbers (10-16) under constant head schemes during the neap tides from the typical Sprint Neap tidal cycle. 'Zlw' represents the downstream water levels.

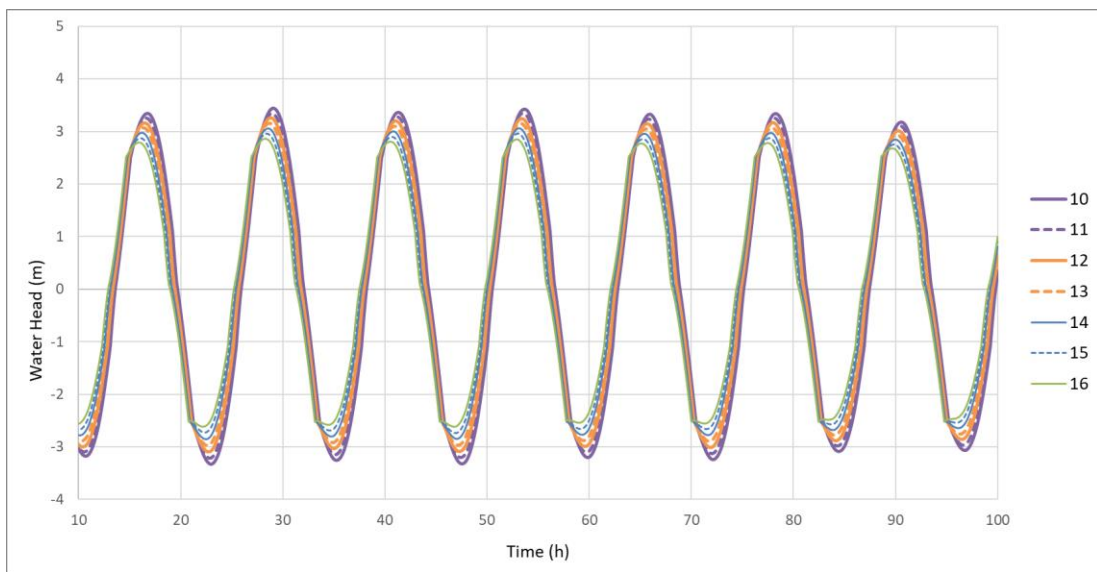


Fig 5. 10. Comparison of water head difference with different turbine numbers (10-16) under constant head schemes during the neap tides from the typical Sprint Neap tidal cycle.

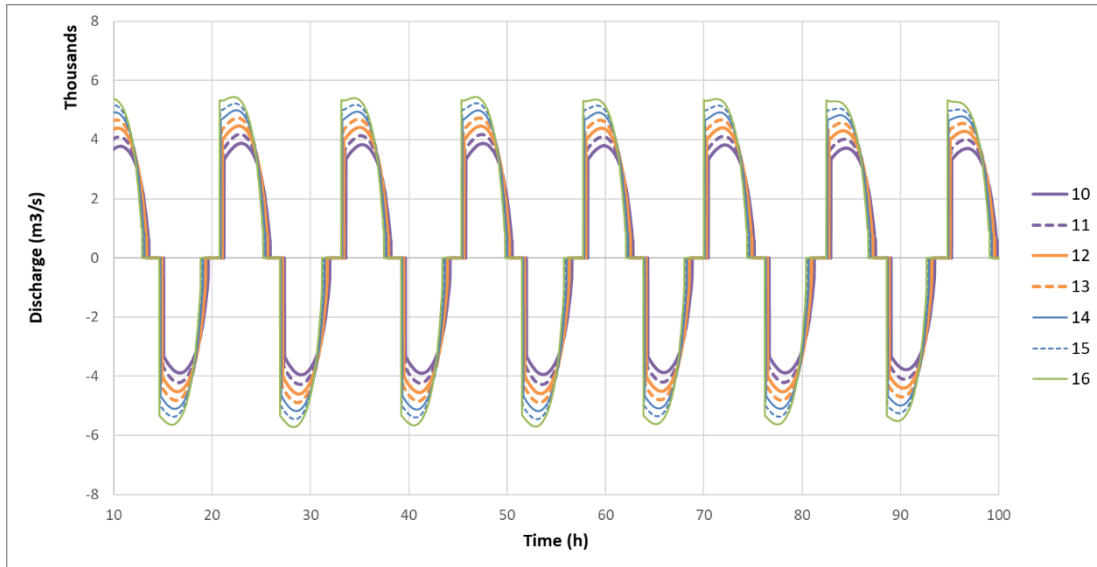


Fig 5. 11. Comparison of discharges through turbines with different turbine numbers (10-16) under constant head schemes during the neap tides from the typical Sprint Neap tidal cycle.

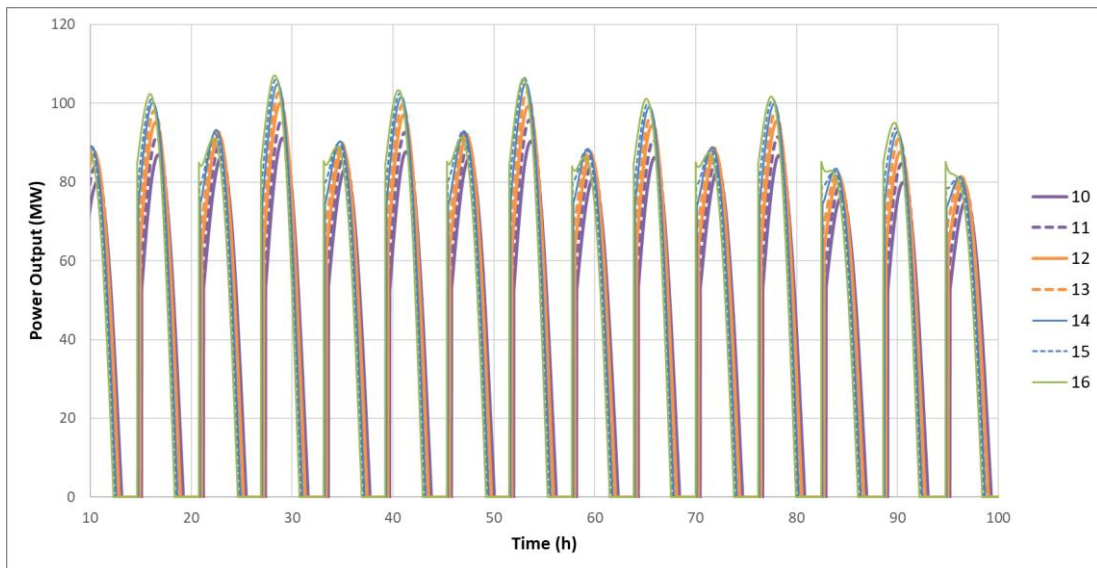


Fig 5. 12. Comparison of power output with different turbine numbers (10-16) under constant head schemes during the neap tides from the typical Sprint Neap tidal cycle.

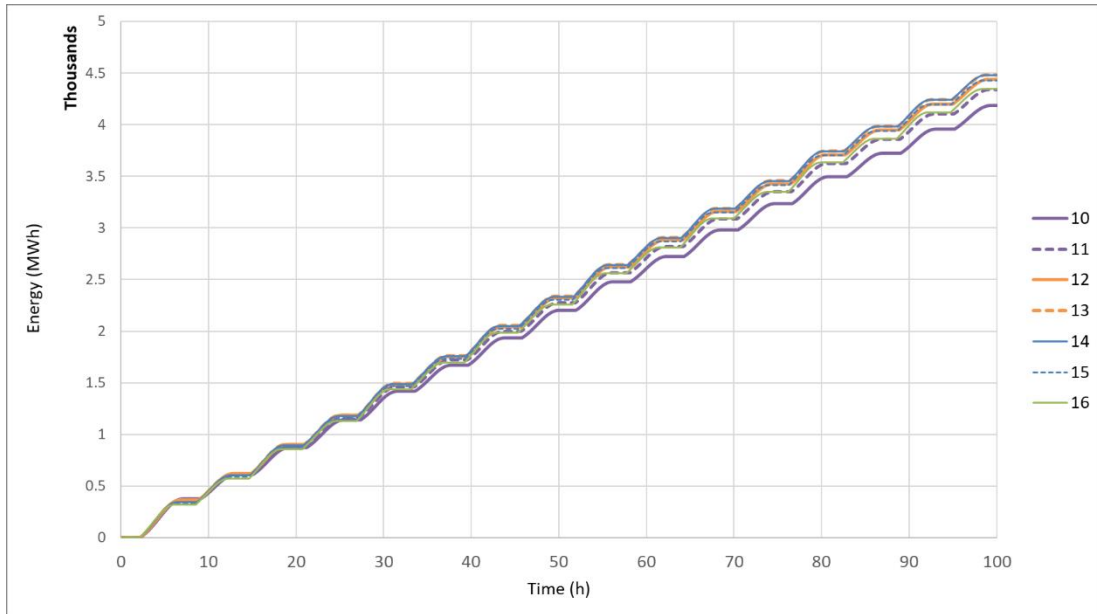


Fig 5. 13. Comparison of electricity generation with different turbine numbers (10-16) under constant head schemes during the neap tides from the typical Sprint Neap tidal cycle.

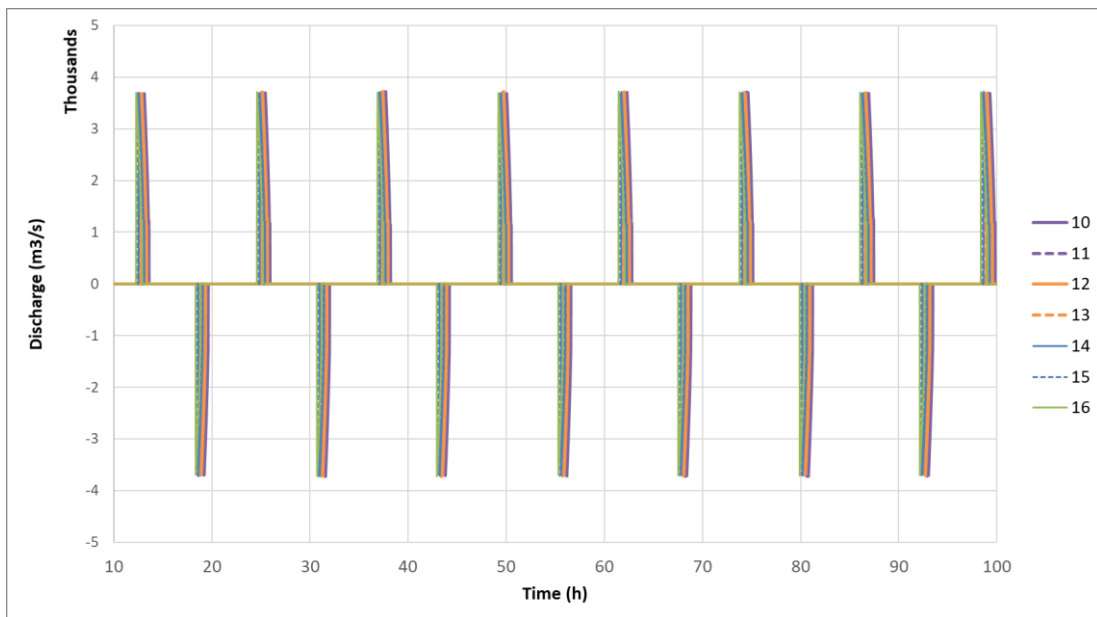


Fig 5. 14. Comparison of discharges through sluice gates with different turbine numbers (10-16) under constant head schemes during the neap tides from the typical Sprint Neap tidal cycle.

5.3.1.2 With pumping operation

Under fixed operation heads if pumping utilised, e.g. H_s of 2.5 m, H_e of 1.5 m and H_p of 1 m, the comparisons between the upstream water level, water head difference, turbine discharge, power output, electricity generation and sluice gates discharge can be seen in Figures 5.15-5.20, respectively.

Similar to the trends without pumping, as the number of turbines increased, higher and lower water levels were reached inside the basin during the high and low waters, respectively. This happened due to more discharge through turbines allowed as shown in Figure 5.17. In this case, it can be concluded that the maximum electricity generation can be obtained with 13 turbines, as shown in Figure 5.19.

Hence, it was reasonable to apply variable turbines during the operation under the non-flexible operation scheme and using fewer turbines during neap tides to increase the electricity generation during the selected tidal cycle.

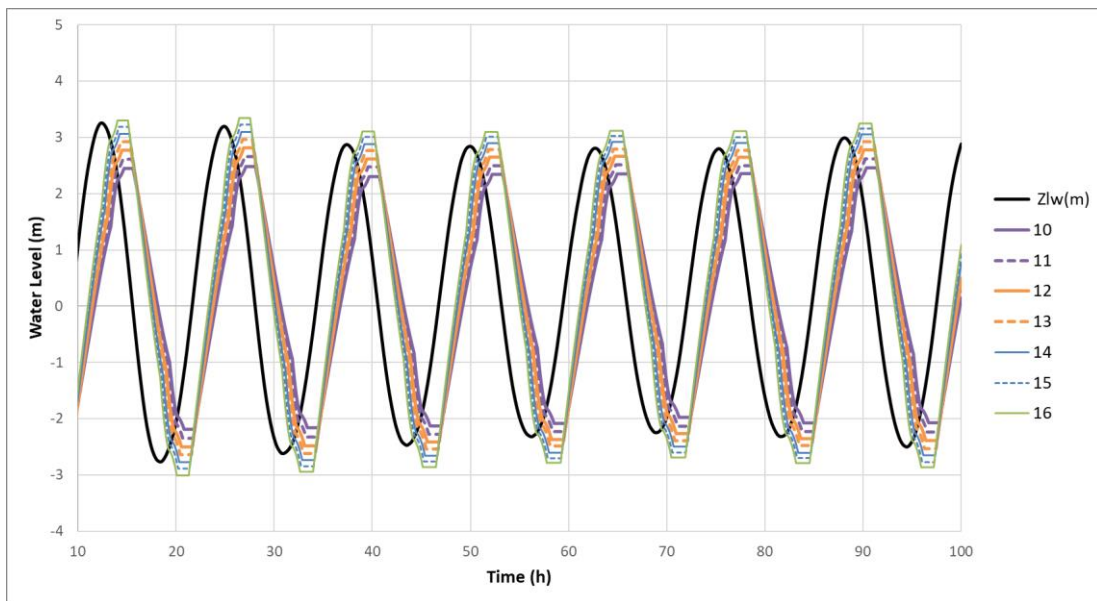


Fig 5. 15. Comparison of the basin water level with different turbine numbers (10-16) under constant head schemes plus-pumping during neap tides of the typical Spring Neap cycle. 'Zlw' represents the downstream water levels.

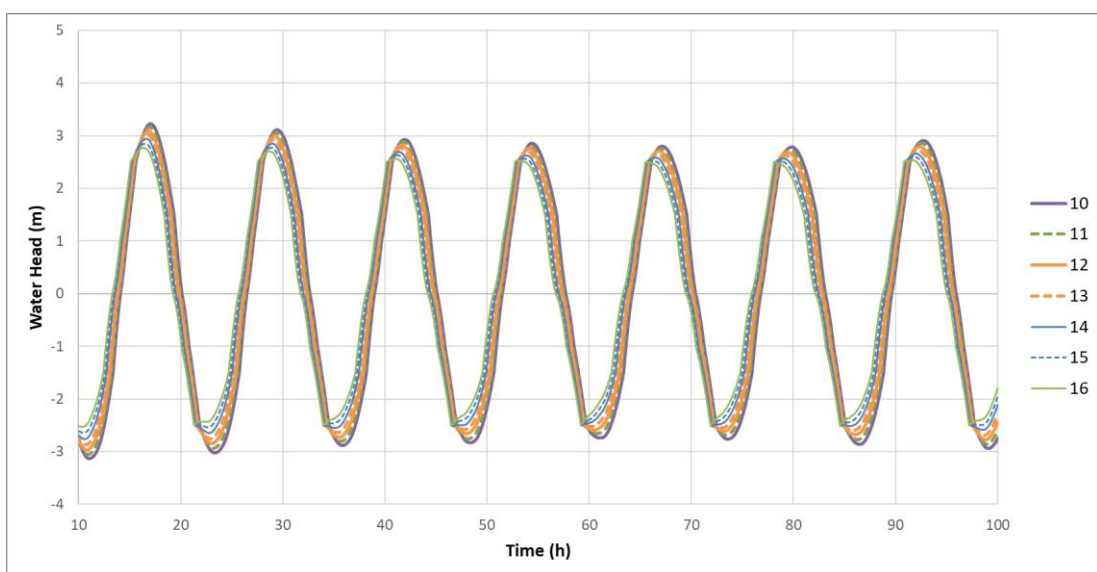


Fig 5. 16. Comparison of the water head difference with different turbine numbers (10-16) under constant head schemes plus-pumping during neap tides of the typical Spring Neap cycle.

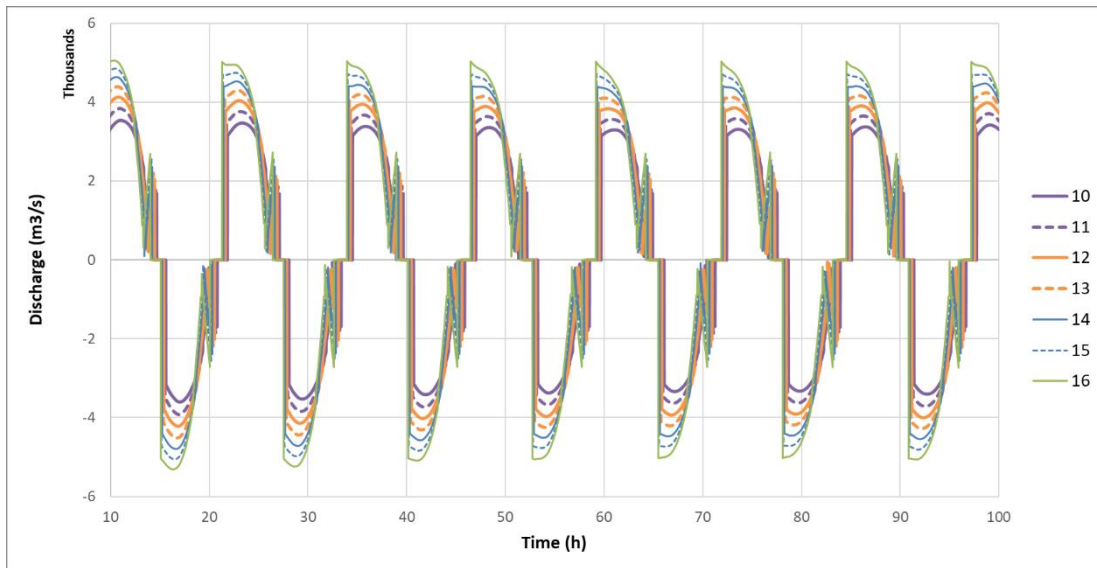


Fig 5. 17. Comparison of the discharges through turbines with different turbine numbers (10-16) under constant head schemes plus-pumping during neap tides of the typical Spring Neap cycle.

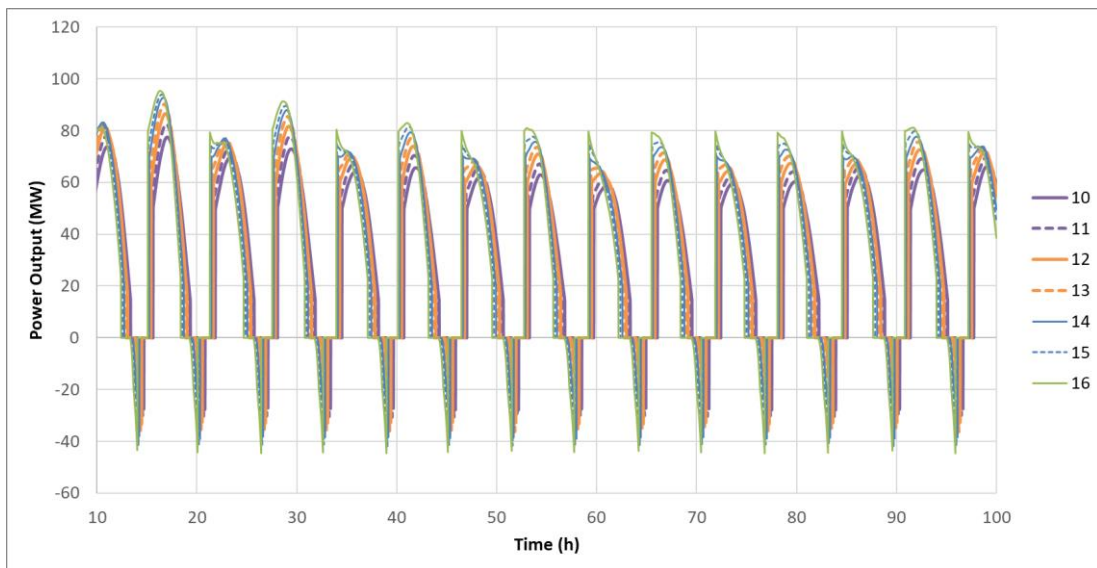


Fig 5. 18. Comparison of the power output with different turbine numbers (10-16) under constant head schemes plus-pumping during neap tides of the typical Spring Neap cycle.

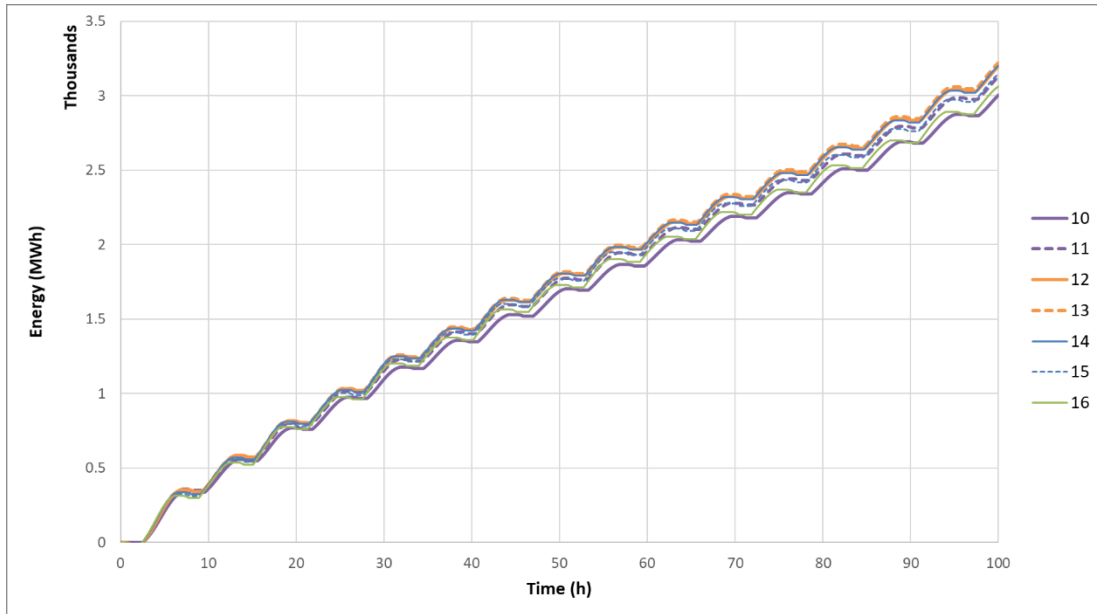


Fig 5. 19. Comparison of the electricity generation with different turbine numbers (10-16) under constant head schemes plus-pumping during neap tides of the typical Spring Neap cycle.

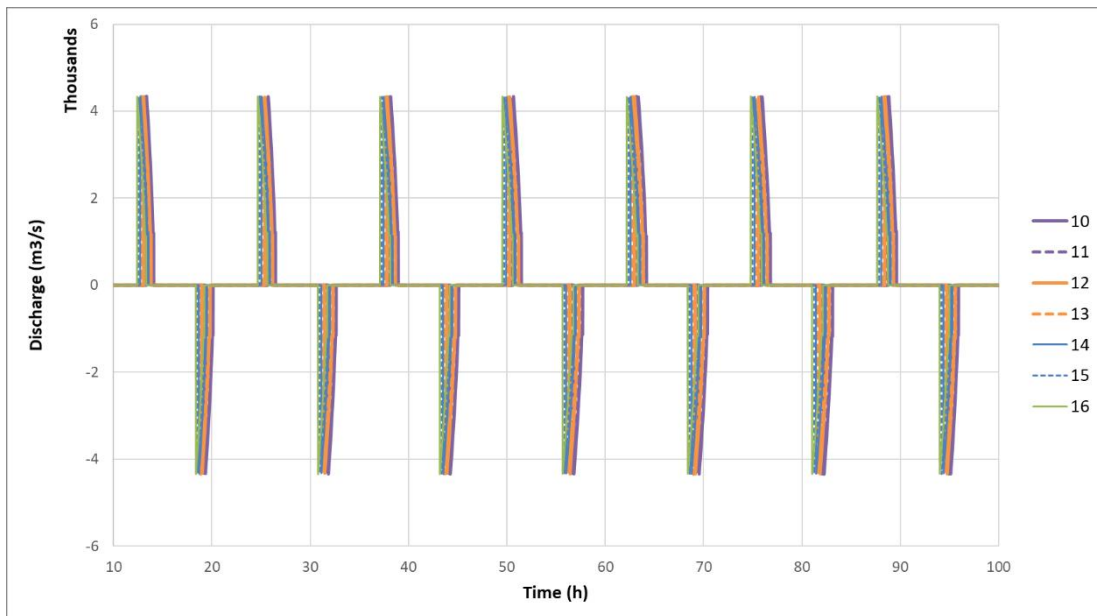


Fig 5. 20. Comparison of the discharges through sluice gates with different turbine numbers (10-16) under constant head schemes plus-pumping during neap tides of the typical Spring Neap cycle.

5.3.2 Flexible operation schemes

This study further added the flexible turbine numbers into flexible operation schemes, without and with pumping to investigate the potential of increasing electricity generation. Therefore, the potential of dispatching a different number of turbines in each generation component, e.g. every tide, for the flexible operation was considered. This required a lot of calculation due to a range of parameters being

optimised, including a wide range of starting heads, ending heads and turbine numbers and even pumping heads. This resulted in the computational time of approximately 20 hours for the optimisation simulation of 8 neap tides. However, for brevity, a neap tide, i.e., the 1st tide was presented here.

5.3.2.1 No pumping operation

The optimised operation heads and its electricity generation, and details for the 1st neap tides can be seen in Figures 5.21-5.22 and Table 5.5, respectively. The proximity of 16 turbines shows that the scheme can be run with one or two less turbine, due to maintenance, during neap tide with only less than 5% loss in electricity. The optimum number of turbines for the flexible operation was 16, as shown in Table 5.6.

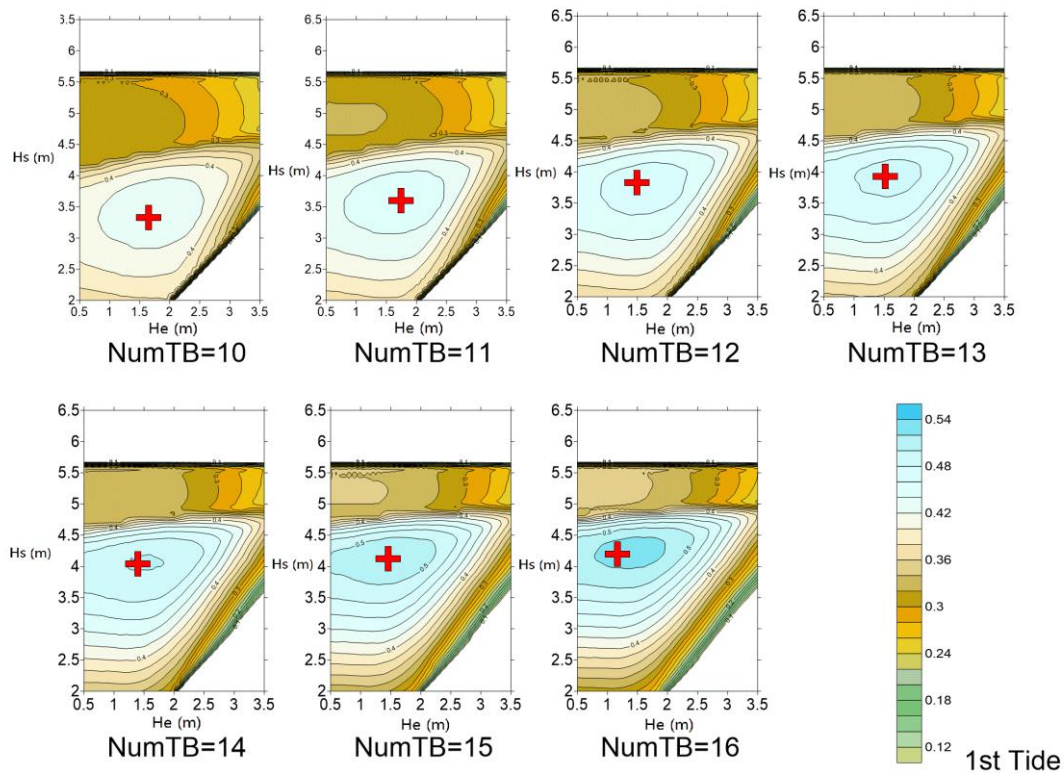


Fig 5. 21. Optimised operation head moving trend under different turbine numbers during selected 1st neap tide.

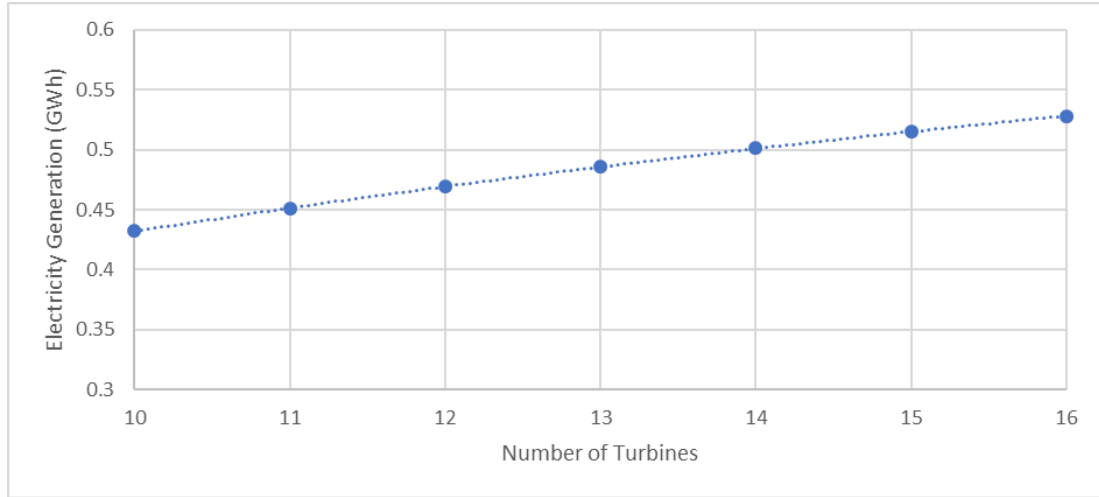


Fig 5. 22. Optimised electricity output under different turbine numbers during selected 1st neap tide.

Table 5. 5. Optimised operation heads under different turbine numbers during selected 1st neap tide.

NumTB	H _s	H _e	Elect.(GWh)
10	3.4	1.7	0.432
11	3.6	1.7	0.451
12	3.9	1.6	0.469
13	3.9	1.5	0.486
14	4.1	1.5	0.502
15	4.2	1.6	0.515
16	4.2	1.3	0.528

Table 5. 6. Optimised electricity output under different turbine numbers during selected neap tides.

NumTB	TIDE	H _s	H _e	Max_Elect.(GWh)
16	1	4.3	1.4	0.528
16	2	3.9	1.4	0.444
16	3	3.7	1.4	0.361
16	4	3.6	1.3	0.337
16	5	3.6	1.4	0.364
16	6	4.0	1.5	0.414
16	7	4.0	1.5	0.430

5.3.2.2 With pumping operation

The optimum number of turbines was 16 when pumping was considered alongside the flexible operation which is consistent with the flexible generation without pumping, as shown in Table 5.7. The electricity generation with optimised operation heads during each tide is summarised in Table 5.8. It should be mentioned that a comprehensive range of operation heads was considered with H_s varying from 2m to 8m, H_e from 0.5m to 4.5m and H_p from 0 m to 2 m with the increment of 0.1 m which is consistent with the simulations used in Chapter 4.

Table 5. 7. Optimised electricity output under different turbine numbers during selected neap tide with pumping.

NumTB	TIDE	Hs	He	Hp	Max_Elect.(GWh)
16	1	4.9	1.8	2	0.639
16	2	4.6	1.8	2	0.528
16	3	4.4	1.6	2	0.432
16	4	4.3	1.5	2	0.406
16	5	4.4	1.6	2	0.437
16	6	4.6	1.6	2	0.495
16	7	4.6	1.7	2	0.507

Table 5. 8. Summary of the flexible turbine numbers operated during selected neap tides.

Scenarios	NumTB	
Non-flexible	No pumping	14
	pumping	13
Flexible	No pumping	16
	pumping	16

5.4 Chapter summary

In Chapter 5, the simulation of TRSs under fixed operation schemes revealed that there may not generate any electricity during the neap tides due to the insufficient tidal range. This problem has been addressed in this chapter, by breaking the operation into small components and optimising the operation for each component. The electricity estimated using the GS method was at least 10% higher than using the traditional non-flexible operation, and this improvement can be at least 10% if pumping involved. Furthermore, the optimisation model was further developed to dispatch the flexible number of turbines for non-flexible and flexible operation schemes. Results showed that under non-flexible operation schemes, the electricity estimation could be potentially improved by closing a certain number of turbines. Furthermore, with the schemes operated flexibly, the proximity of 16 turbines show that the scheme can be run with one or two less turbine, due to maintenance, during neap tide with only less than 5% loss in electricity. However, this optimisation using the elaborated GS method resulted in the computational time of approximately 20 hours for only 8 neap tides which could be more if considering the typical Spring Neap tidal cycle into the optimisation. This highlights the significance of exploring more efficient algorithm into the TRSs optimisation, as studied in Chapter 6.

6. Tidal Range Schemes optimisation using a Genetic Algorithm

6.1 Introduction

Optimising the operation of the TRS is one of the challenging aspects of the design of any TRS in early stages due to the large variety of scenarios where various numbers of turbines and sluice gates, and different operation schemes are being considered. However, these are important as they directly impact the cost and revenue of the scheme and subsequently its feasibility. This hyperparameter optimisation could be done using GS introduced in Chapter 5 but it was proved to be very elaborate and time-consuming especially for the optimisation of operation flexibly along with the design parameters including turbine numbers and sluice gates. This chapter proposes a novel approach for optimisation of the design of TRSs by maximising their electricity generation using Genetic Algorithm (GA). The GA model developed here is applied to two case studies, i.e. West Somerset Lagoon (WSL) and North Wales Tidal Lagoon (NWTL), respectively.

In section 6.2, the GA model is set up using parallel programming to optimise the operation of TRSs. Importantly, two recombination method, namely Linear Recombination Method (LRM) and Ring Recombination Method (RRM) along with the Sequential Mutation Method (SMM) are simulated, separately, aim to improve the convergence speed of the GA model. The GA model is coupled with a 0-D model and consider flexible operation for the smallest unit of operation. The GA optimisation has been compared with the GS method, to validate the performance of the GA model.

In section 6.3, the GA model is further developed to include optimisation of the turbine numbers, sluicing areas as well as the operational scheme. The optimisation of electricity generation is simulated under non-flexible operation schemes and flexible operation schemes, without and with pumping. As for the large discharge rushing through the turbines and sluicing gates during sluicing phase under the concentrated deployment, 3 solutions put forward and demonstrated. Traditionally, the operation of hydraulic structures are considered to be synchronous, e.g. the same operation heads are applied to different blocks of turbines and sluice gates. However, the operation of the TRS can be further optimised

as the tidal range varies significantly along with the scheme and between various blocks of turbines and sluice gates. Hence multi-block optimisation is implemented for the case studies as well.

6.2 Operational heads optimisation

6.2.1 Model Setup

The pseudocode and flow chart of the GA model are listed in Table 6.1 and Figure 6.1, respectively. The steps in executing the GA model can be summarized as follows:

- I. Randomly create a certain number of solutions with flexible operational characteristics for every half-tide in the selected typical cycle.
- II. Iteratively perform the following sub-steps on every population until the termination criterion has been satisfied:
 - i. Copy survival individual solutions to the new solutions with their specific power outputs.
 - ii. Create new solutions from the copied solutions by randomly mutating the operational heads at each half-tide in every scheme.
 - iii. Create new solutions by genetically recombining sub-solutions which are randomly chosen from all solutions, including mutated solutions and non-mutated solutions.
 - iv. Evaluate the energy generation of the solutions over all the selected typical cycle, based on the principle of ‘survival of the fittest’.
- III. The best operational scheme with maximum electricity generation that appeared in any generation (i.e., the best so-far scheme) is designated as the optimised result of the GA for the run. This result may present a scheme (or an approximate scheme) to the operational characteristics optimisation.

Table 6. 1. Pseudocode of the Genetic Algorithm.

Algorithm The pseudocode of the GA

```
1: proc Set_up //Set up algorithm's parameters
2: Generate the initial operation schemes and evaluate their fitness;
3: While NOT Termination_criterion() do
4: Offspring <- Copy(Parents);
5: Offspring <- Mutation(Pm, Offspring);
6: Offspring <- Recombination(Pr, Offspring);
7: Evaluate_Fitness (Offspring); //Running Parallely using OpenMP in Table 3.2
8: Survivals <- Selection(Ps, Parents, Offspring); //Selection the individuals with higher
fitness
9: Parents <- Survivals;
10: End While
11: End Proc Set_up;
```

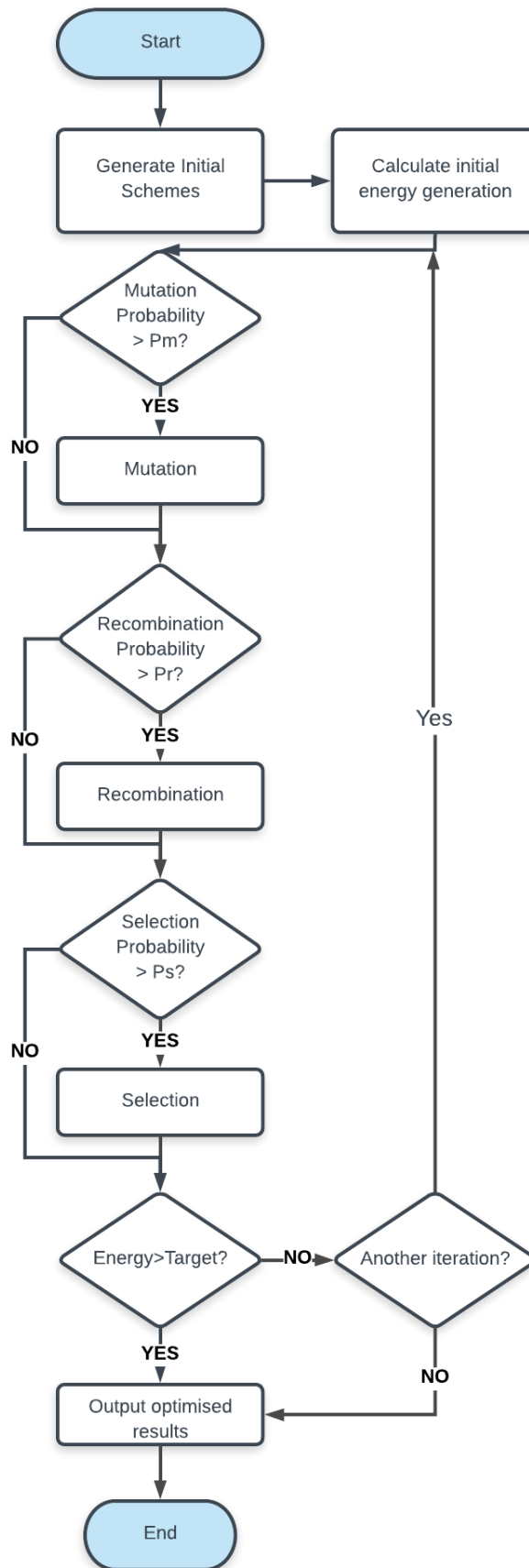


Fig 6. 1. Flow-chart of the GA model.

In the GA, an operation scheme including the starting and ending heads for every half-tide was considered as an individual with different genes. The GA method uses a population of solutions/individual which are updated iteratively. Each iteration of solutions was also referred to as a generation in the GA model and therefore the n^{th} iteration was referred to as the n^{th} generation. In every iteration, a new population was generated based on the most optimum solution of its previous population through copy, mutation, recombination and selection processes. The new populations were referred to as offspring in the GA while the previous population was referred to as the community of parents. To control the population size during each generation, the best genes were selected based on their performance using a fitness assessment, i.e. the electricity generation predicted over the simulation period, calculated using the 0-D model in Chapter 4; that is, the electricity generation of parents and offspring during each iteration was evaluated. Then the solutions with higher electricity generation were selected to survive and were considered as the parents for its following iteration. This process was referred to as selection, which was designed with the intention of imitating the process of natural selection and evolution.

The GA model was developed as a part of this study using the Sequential Mutation Method (SMM), Linear Recombination Methods (LRM) and Ring Recombination Methods (RRM). In SMM, only one half-tide, e.g. half-tide i within the successive half-tide n , could be selected for mutation and the selection of the half-tide follows a sequence with the generation increasing, that is, the half-tide $(i+1)$ would be selected for the mutation in the next generation, as shown in Figure 6.2. In the selected half-tide i , the operation heads of $[H_{s,i}]$ and $[H_{e,i}]$ could be mutated with the probability of P_m as mentioned in Chapter 2. The mutated operation head follows a normal distribution with an assumed variance of 0.1 herein and a mean of this distribution of the initial operation head during its generation. That is, the change of mutated operation head was according to the operation head before mutation. This representation gave insight into the nature of evolution that the genes' mutation of children kept a certain relationship with the genes from their parents, so that it is possible to find the optimum range of change within the search space that resulted in greatest improvement. If the number of the generation reaches half-tide n , in the $(n+1)$ generation, the mutation will be applied to the 1st half-tide and this process is continued. Although the SMM in the mutation process was supposed to improve the original algorithm efficiency, it still suffered from being slow especially when the size of the initial population was extremely large.

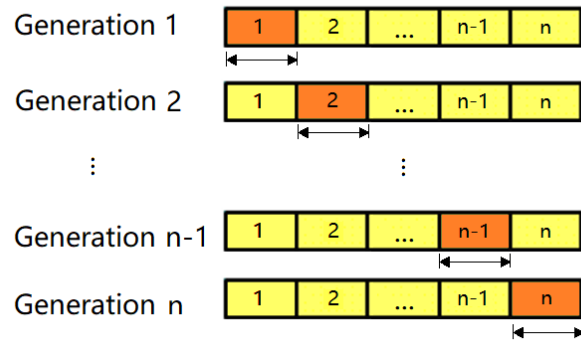
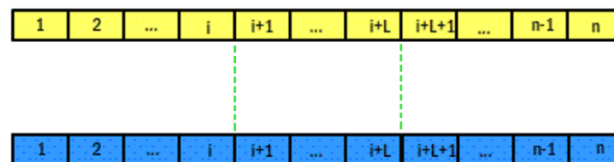


Fig 6. 2. Sequential Mutation Methods (SMM) illustration (the highlighted cell represents the place of applying the mutation in each generation).

Moreover, it is believed that recombination does enhance the performance of GAs [139]. In both of the yellow and blue bars representing the selected solutions in LRM as shown in Figure 6.3(a), the bits in the two points are swapped between the ‘parent organisms’ [139] as shown in Figure 6.3(b). This strategy can be generalised to n-point crossover from any positive integer i , picking L crossover points randomly. However, as illustrated in Chapter 2, the RRM was able to further develop the GA model by imaging operational heads in every scheme was a circle. Similarly to LRM, two solutions were selected for recombination in Figure 6.4(a), then the recombined solutions were generated after exchanging information as shown in Figure 6.4(b).

Parallelisation was one of the appealing features of this GA model, which was achieved by utilising the OpenMP (as illustrated in section 3.5) and 10 CPU with an HPC for approximately 1,640 minutes. As the cost time of energy calculation for each scheme was the same within a certain period, so the evaluations of a number of possible solutions could be represented at the same time and hence no consideration was needed to be given to the inevitable variation of cost time within every single generation.

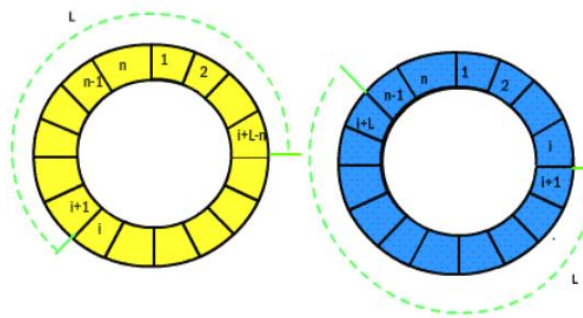


(a)

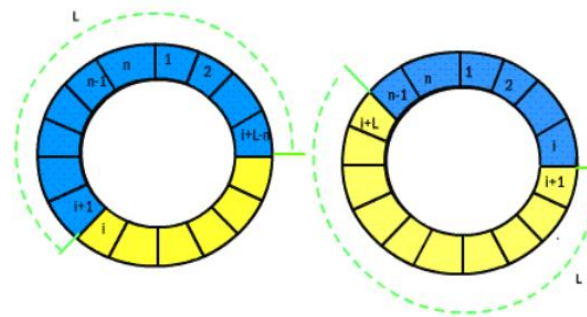


(b)

Fig 6. 3. Linear Recombination Methods (LRM) illustration: a) before LRM; and b) after LRM.



(a)



(b)

Fig 6. 4. Ring Recombination Methods (RRM) illustration: a) before RRM; and b) after RRM.

It has been shown that the efficiency of GAs highly depends on their probability parameters settings [140]. Furthermore, the optimisation could be completed faster with appropriate parameters [139]. In this study, P_m , P_r and P_s were assumed to be 0.5, 0.5 and 1, respectively, based on the literature [141]. This was assumed to be satisfactory for this research as the desired performance was achieved by the GA model. However, the impact of the choice of parameters used in the simulation and their influence on the performance of the GA model is worthy to be studied in future work.

In order to obtain optimised results while avoiding the endless running of this GA model, two termination criteria were defined herein, as illustrated in Figure 6.1. That is, if the energy production of

the most elite scheme for the generation reached the ideal generated energy which was given by users, or the maximum number of generations or iterations was reached, then the GA process was ended and the optimisation results were output. It should be noted that in this case, the ideal generated electricity was set to infinity as the more energy generation obtained the better. The number of iteration was set to 3000, ensuring a sufficient time to achieve convergence. As the most important factor affecting the running time of the GA model, the size of initial solutions was set to be 1000. Considering more initial solutions generated will lead to longer simulation time to calculate power output over a longer period. While a large solutions size provided more individuals for testing, it also diluted the fitness of the best scheme [139]. In this study, the GA model was operated in the selected 2nd cycle with a time step of 1 minute, the same as in Chapter 5, allowing the reliability of the comparison between the GA and EHN models which would be discussed further in this section.

6.2.2 Performance of GA model

From Figures 6.5-6.6, It can be seen that the GA model using RRM converged after approximately 1000 iterations while LRM converged after 1500 iterations and hence RRM was roughly 30% less computationally expensive comparing to LRM. Moreover, RRM, which is recognised as a more advanced approach in finding elite schemes, was able to yield approximately 24.0 GWh over the typical tidal cycle instead of a maximum of 22.8 GWh produced using LRM. Higher efficiency and superior performance of RRM have been consistent with the findings [142, 143] and therefore RRM will be used in the GA model for further studies in this thesis.

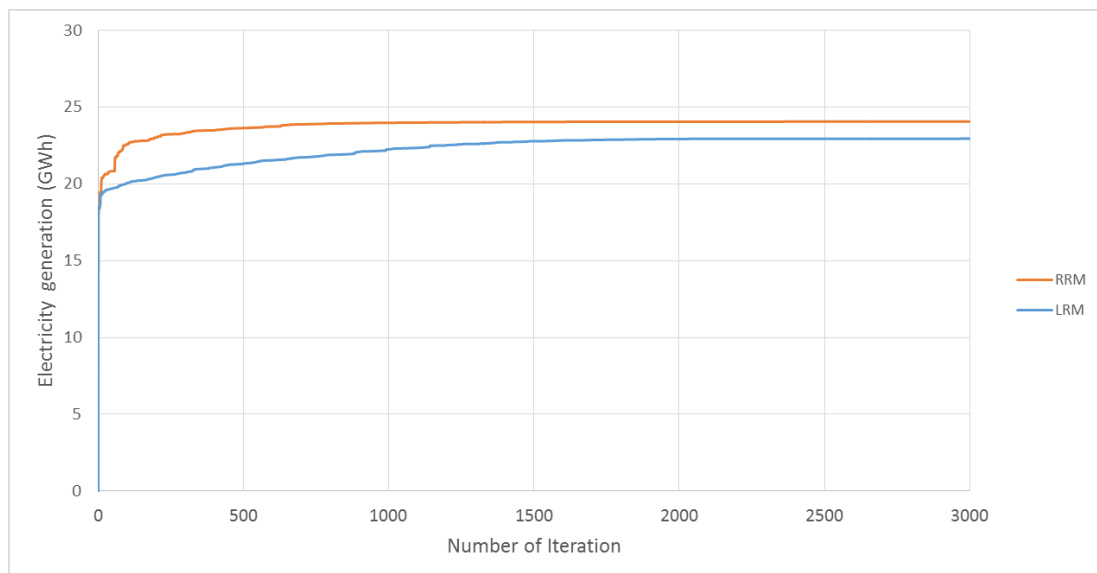
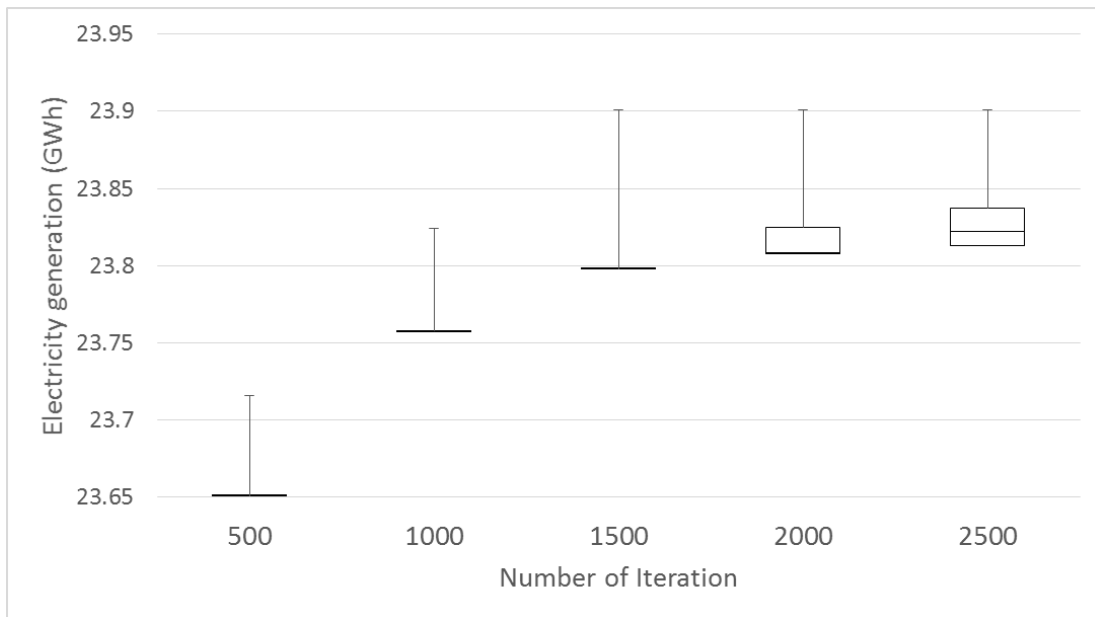
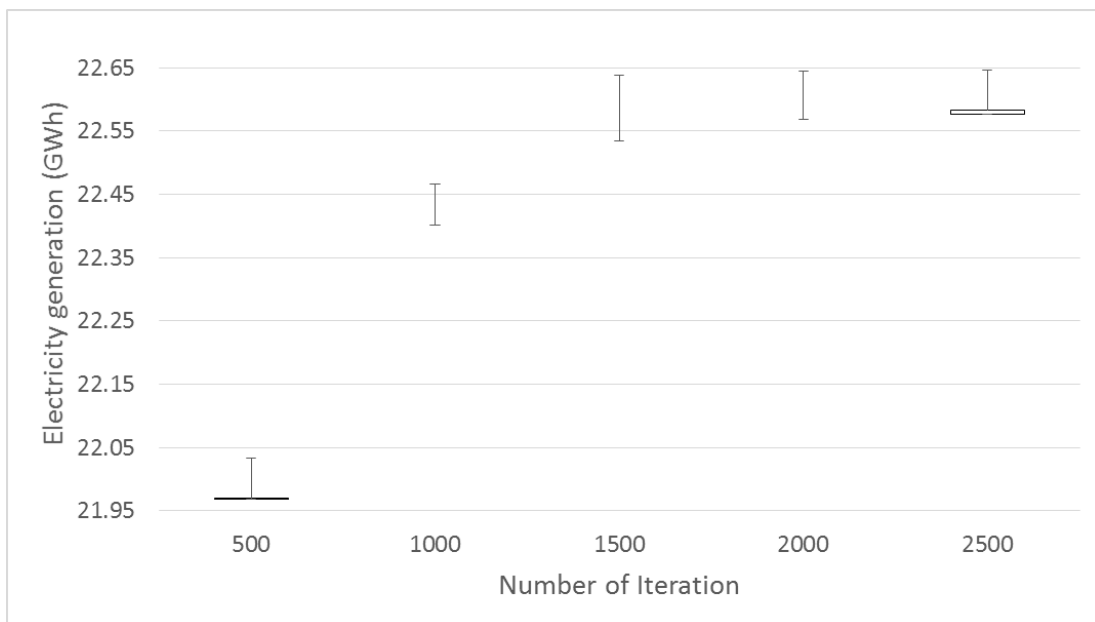


Fig 6. 5. Convergence speed comparison.



(a)



(b)

Fig 6. 6. Box plots of convergence speed using (a) RRM or (b) LRM.

The power output of operation schemes optimised by different methodologies has been summarised in Table 6.2. It shows that using the GA model, which used half-tides' starting and ending heads as genes, had improved power output by 16% compared to the GS method with fixed operation heads. In other words, the GA could reach the similar energy output with the most optimised GS method, known as EHN, under the flexible operation scheme, but with significantly improved efficiency.

Table 6. 2. Comparison of different approaches used to optimise the operation of TRSs.

Optimisation methodology	Electricity over 1 tidal cycle (GWh)		Change to electricity prediction using 2-D with the fixed head operation (%)
	0-D model	2-D model	
*GS fixed head	21.3	19.7	-
GA model	24.0	23.0	16.0%
*GS-EHN model	24.0	22.9	16.0%

*as shown in Table 5.1.

6.2.3 Validation of the GA model by comparing with EHN method

Figure 6.7 illustrates the comparison of the lagoon operation designed using GA and EHN models during 4 neap tides for a better understanding of the differences as a result of the utilisation of the two methods. Further details during 1 neap tide are shown in Figure 6.8. It can be seen that there were only negligible differences between the GA and EHN models, as shown in Table 6.2. The outcome of this comparison, which was consistent with the comparisons over other tides, validated the effectiveness of the GA model in optimising TRSs' operation with higher running efficiency of approximately 50% compared with the most optimised GS model, i.e. the EHN model. It should be noted that the cost of the GA model can be influenced by a variety of factors [86], such as the iteration time (of 3000 in this study), initial operation solutions (of 1000 in this study) as well as the performance of HPC, which is worthy to be further studied in the future work to contribute a higher efficiency of this optimisation using GA.

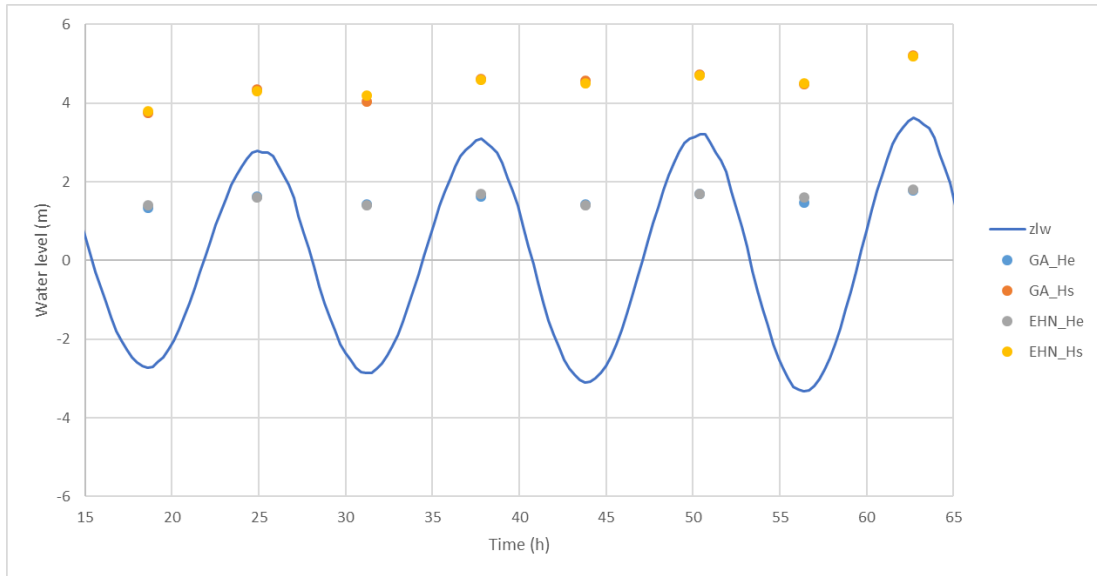


Fig 6. 7. Optimised operation heads comparison from GA and EHN models for 4 neap tides. Triangular and cycler represent the starting head (Hs) and ending head (He) using GA (Green) and EHN (Orange), respectively. Solid blue line denotes the water levels outside the basin.

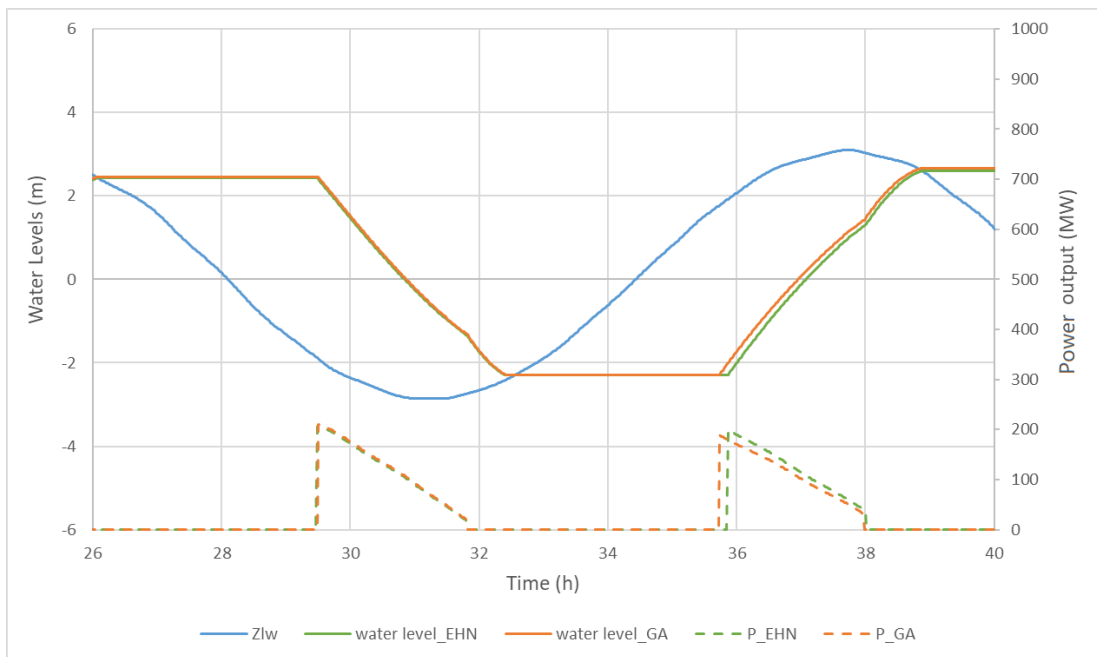


Fig 6. 8. Comparison of the lagoon operation optimised by GA and EHN models for a tidal cycle. Solid lines show water levels. Dashed lines show electricity generated. Green: GA model. Orange: EHN model. Blue: Water levels outside the basin. 'P' denotes the power output.

In order to validate the performance of the GA model which used a 0-D model as the fitness assessment, the DIVAST 2-DU model was implemented to simulate the SBL and then its electricity generation was evaluated using the solution obtained from the GA model. The comparison of output

predicted by 0-D and 2-D models is shown in Table 6.2. It can be seen that the difference between 2-D and 0-D models is lower than 5% when utilising flexible operations. It should be mentioned that the electricity prediction in 2-D could be influenced by various sources of uncertainties including storm surges although the effect was proved to be relatively limited [144].

6.2.4 Inclusion of Pumping in the GA model

At the next stage, pumping was added as one of the optimisation parameters of the GA model. Instead of a fixed maximum pumping head of 2 m utilised in the GS model, the pumping head in the GA model was limited to the maximum and minimum water levels in the impoundment without the lagoon (denoted as $H_{p_limited}$) for each half-tide. This means that the basin water level during flood pumping phase should not be lower than the LAT of about -4.63 m or higher than the HAT of about 4.84 m during ebbing tides in the typical Spring Neap cycle. This is mainly in order to utilise as much extra electricity as possible without imposing any extra cost of new flood defences or affecting. Hence, the $H_{p_limited}$ was higher in the neap tides than it in the spring tides. The power output of turbines is able to reach 320 MW with pumping which can be seen from Figure 6.10. Results have shown that the electricity could reach approximately 26.12 GWh in the selected typical cycle, around 3.6% lower than the most optimised grid search model of 27.1 GWh. This difference is partially caused by the implementation of $H_{p_limited}$. Typical operation of the scheme, water levels and power output and discharge through turbines and sluice gates are demonstrated in Figures 6.9-11.

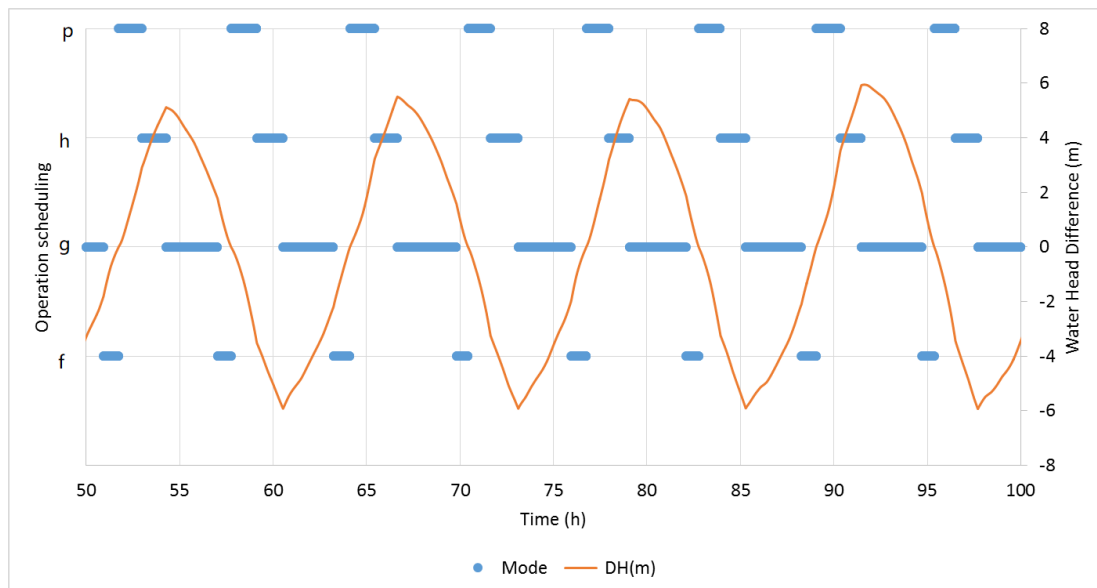


Fig 6. 9. Operation scheduling of the impoundment and water head difference (a), in which 'f', 'g', 'h', and 'p' denotes filling, generating, holding and pumping phases, respectively, for four neap tides in the 0-D model without pumping included.

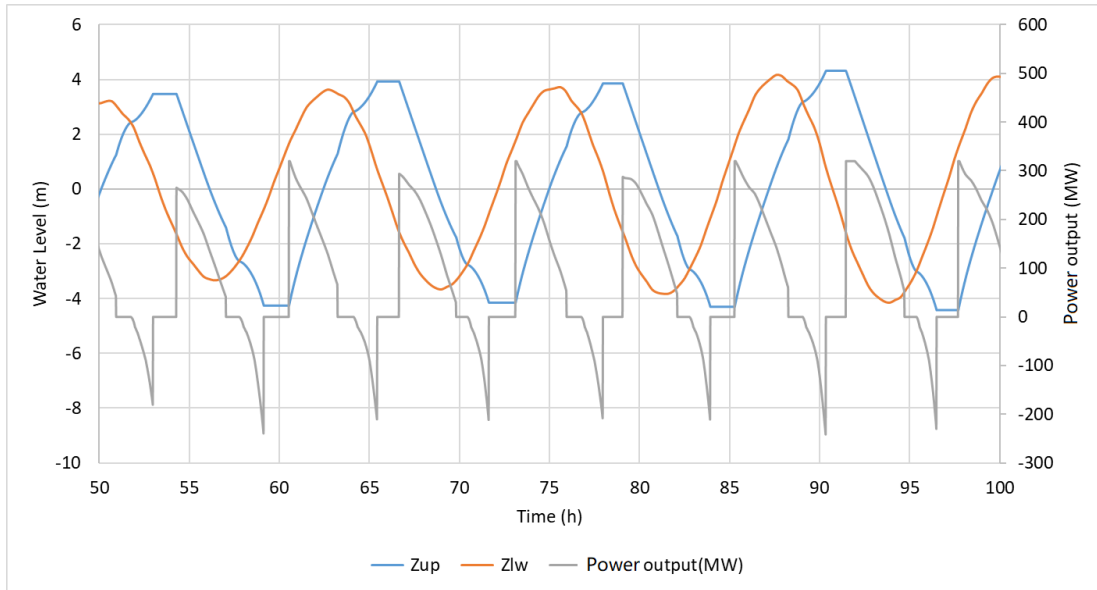


Fig 6. 10. water levels inside the impoundment and power output comparisons for four neap tides in the 0-D model without pumping included.

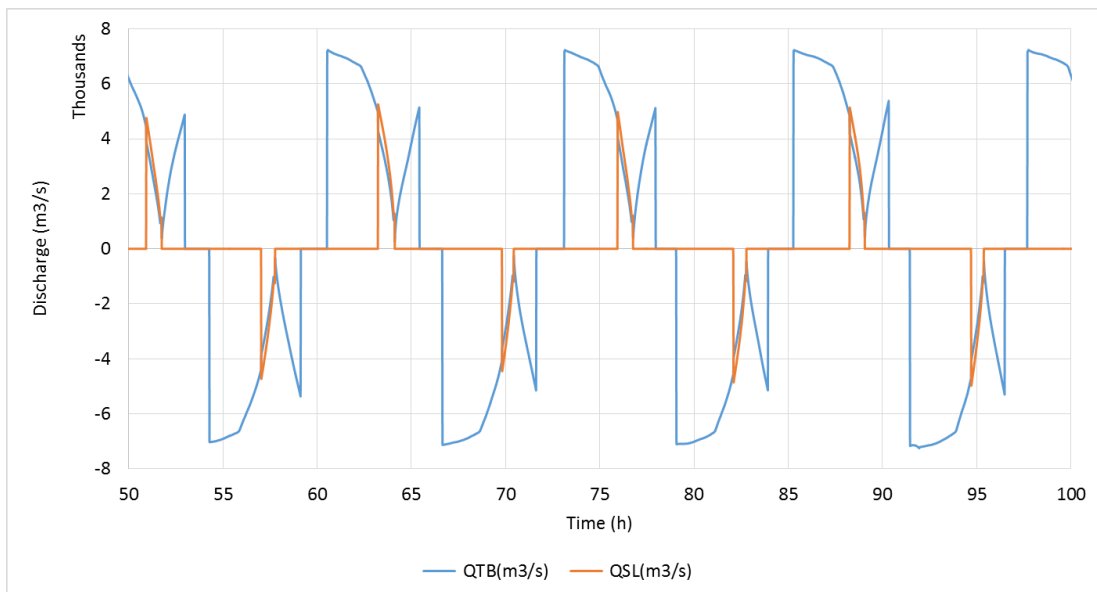


Fig 6. 11. Discharge through sluice gates and turbines, respectively, for four neap tides in the 0-D model without pumping included.

6.3 Design parameters optimisation

The design of TRSs could result in a very large number of scenarios including the various number of turbines, sluice gates and operation schemes being considered. Considering various scenarios is particularly important because it affects the electricity generation and cost and benefit of the scheme and hence impacts the financial feasibility of the scheme [55]. Most of the optimisations are only focused on single-parameter optimisation [109] while ignoring the combination of the design and operational parameters in TRSs optimisation. This is mainly because a comprehensive optimisation of TRSs requires a large number of simultaneous simulations. In particular, the efficiency of the multiple variables optimisation highly relies on the efficiency of calculating algorithms and therefore a more elaborate algorithm of GS and a more advanced algorithm of GA will be improved and compared in this section, to demonstrate the selection of the appropriate algorithm for the promotion the efficiency in such optimisation.

Since the design of SBL has been completed and considering the relatively small size of the scheme, it was decided to carry out such optimisation for larger schemes, such as WSL and NWTL, which are currently going through the feasibility study. The case studies considered here are part of the multi-scheme simulation in Chapter 7.

6.3.1 The Improved Model

6.3.1.1 The improved GA model

In the improved GA model, the design of the scheme was encoded by including two values for the number of turbines and sluice gates area, represented by NumTB and STPC, as well as two vectors for starting and heads, represented as $[H_{s,1}, H_{s,2}, \dots, H_{s,n}]$ and $[H_{e,1}, H_{e,2}, \dots, H_{e,n}]$, for n successive half-tides. For optimisation including pumping, another vector for pumping heads for all the half-tides, shown by $[H_{p,1}, H_{p,2}, \dots, H_{p,n}]$, were also considered. The number of turbines varied from 75 to 150 and STPC from 0 to 8, based on the developers' advice in order to allow a reasonable and effective cost of the device. The range of $H_{s,i}$ was between 2.0 m and 8.0 m, $H_{e,i}$ was between 0.5 m and 4.5 m and $H_{p,i}$ varies from 0 to $H_{p_limited}$ in which tide number i varies from 1 to n . It should be mentioned that the operation heads could be variables for each half-tide if flexible schemes adopted or constant values if non-flexible schemes applied. However, the NumTB and STPC were fixed in each scheme considering that the turbines and sluicing area cannot be changed once the project constructed.

The SMM and RRM were implemented in the GA model because of higher efficiency, as illustrated in section 6.2. In SMM, only one half-tide in each generation was selected from all half-tides in the selected typical cycle and mutation was applied on the operational and designed parameters including NumTB and STPC in this half-tide. The selection of half-tide was in sequential order for

generations. The mutated parameter followed a normal distribution with an assumed variance of 0.1, as same as it in section 6.2.

6.3.1.2 Validation of the GA model

Then the performance of GA model was validated by comparing with it using GS method. In the GS model, every operational scheme is encoded as two constant values, namely the NumTB and STPC, and two vectors, namely $[H_{s,n}]$ and $[H_{e,n}]$, representing the operation water heads for n successive tides. The range of starting heads was from 2.0 m to 8.0 m with 0.1 m increments, ending heads covers a range of 0.5 m to 4.5 m, also with an increment of 0.1 m. NumTB varied from 75 to 150, with increments of 5 and STPC varied from 0 to 8, with an increment of 1. The most optimised GS methods, i.e. Every Half tidal cycle and Next (EHN), was adopted for the methodology used for the GS method. The GS model was run with a time step of 1 minute. Figure 6.12 shows two synthetic tides to demonstrate EHN approach, in which tides are decomposed to the smallest operational unit, namely half-tide, and then the electricity generated was calculated using a complete range of feasible starting and ending heads, during two successive half-tides such as the half-tide A and B in Figure 6.12. As mentioned in Chapter 5, under fixed NumTB and STPC, there were 5,760 million scenarios for each pair of half-tides or about 8.1 billion scenarios for one year of operation to consider in this case. However, this number of scenarios will be 135 times more (15×9 where the 15 and 9 represent the scenarios of NumTB and STPC, respectively) during the design of the operation schemes, making it to be more elaborated and computationally expensive.

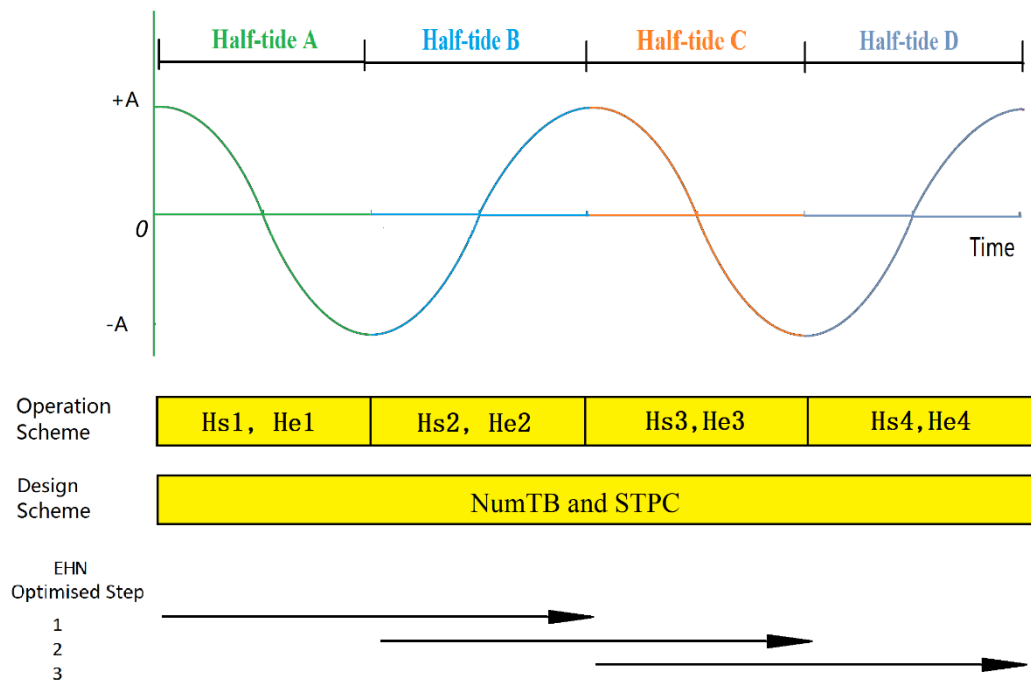


Fig 6. 12. Schematic illustration of the updated EHN optimisation methodology.

6.3.2 Case study of West Somerset Lagoon

6.3.2.1 Optimisation

6.3.2.1.1 Non-flexible operation schemes

The typical Spring Neap selection was illustrated in Chapter 2. The maximum electricity generated with different STPC using GA with non-flexible operation schemes are listed in Table 6.3 and the lines in Figure 6.14 were used to show trends of the maximum electricity generation that estimated with a range of NumTB and STPC over the typical Spring Neap cycle. The maximum electricity over the simulation period for a fixed-head operation schedule, known as the non-flexible operation schedule, was achieved with a starting head of 5.5 m and an ending head of 2 m, with the NumTB of 140 and a STPC of 8, indicating a more than 25% increase of electricity generation under this scenario. It can be concluded that with the turbine numbers increases, the electricity estimated first increases and then decreases moderately with the peak value appeared when the NumTB between 140 to 150, and with the STPC increases, the production of electricity showed a growing trend.

Furthermore, we can see that the production of electricity rises slightly when NumTB and STPC exceed approximately 125 and 7. When considering the optimisation of cost and benefits in the design stage of TRSs, this has significant reference value to the selection of optimum design parameters, e.g., turbine numbers and sluice gates. As a result, in the updated deployment of WSL in Figure 6.13, the optimum NumTB and STPC were selected to be 125 and 8, respectively. The updated deployment with 5 distributed blocks of turbines and 8 blocks of sluice gates was confirmed with the 125 turbines and a STPC of 8 which indicates a sluicing area of 20,000 m², as illustrated in Figure 6.13. In details, there were 5 blocks of turbines (T1 to T5) with 25 turbines in each block, spaced at 1,000 centres. 8 blocks of sluice gates (S1 to S8) were distributed and nested into the wall, in which S1-S5 have 14,300 m² sluicing area totally with 2,840 m² per block and S6-S8 have 5800 m² sluicing area totally with 1,900 m² per block.

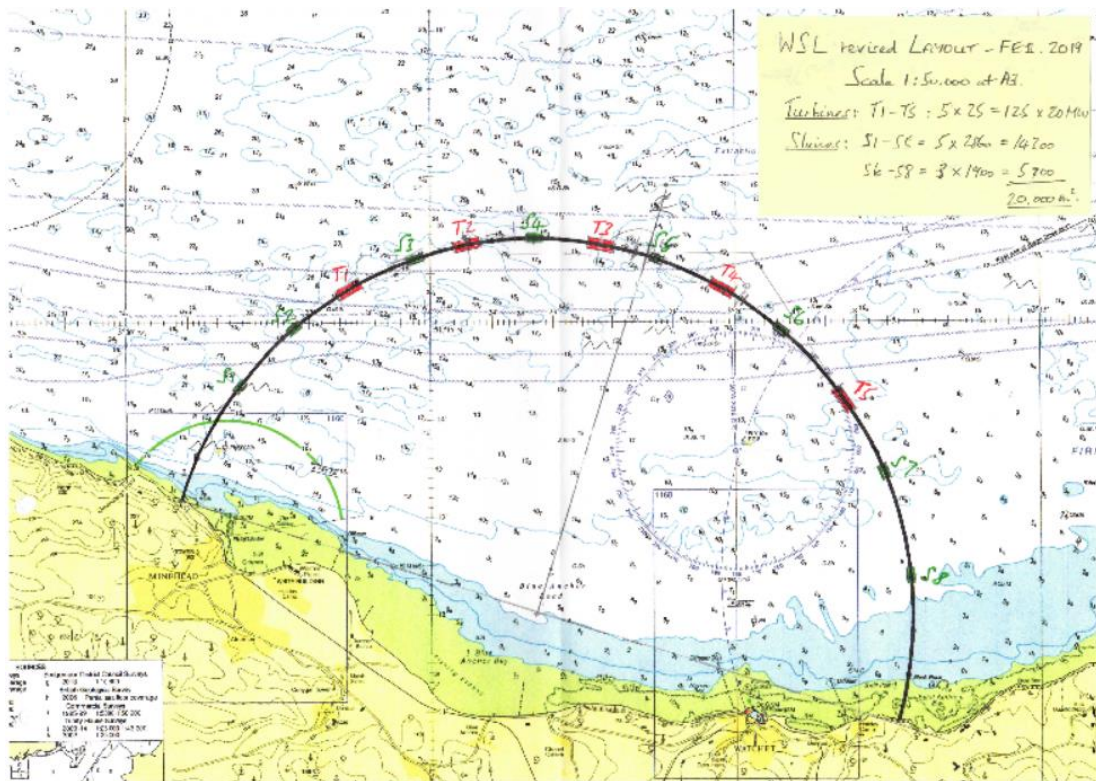


Fig 6. 13. Map of the updated West Somerset Lagoon.

Meanwhile, if the non-flexible operation schemes adopted in the GA model, the most optimised scenario can be obtained with an electricity production of 254.61 GWh when H_s of 5.3 m and H_e of 1.8 m with the NumTB of 149 and STPC of 8, which equals to a sluicing area of 23,840 m². The optimisation of multiple variables including the turbines numbers and sluice gates with non-flexible operation schedules yields an increase of more than 25% of electricity generation. It can be seen that the GA could reach a very similar electricity generation compared to the GS, which is in line with the finding in section 6.2.

Table 6. 3. Optimisation under fixed operation schemes using GA and GS

Scenario	Electricity Generation(GWh)						
	STPC	NumTB	A_s	H_s	H_e	Elect (GWh)	Increase (%)
baseline	4	100	8,000	3.5	2	201.282	-
GS	4	150	12,000	5.5	1.8	253.143	25.87
	5	145	14,500	5.5	1.9	254.682	26.87
	6	150	18,000	5.5	1.8	256.832	27.86
	7	145	20,300	5.5	2	257.803	28.36
	8	140	22,400	5.5	2	258.566	28.86
GA	8	149	23,840	5.3	1.8	254.61	26.87

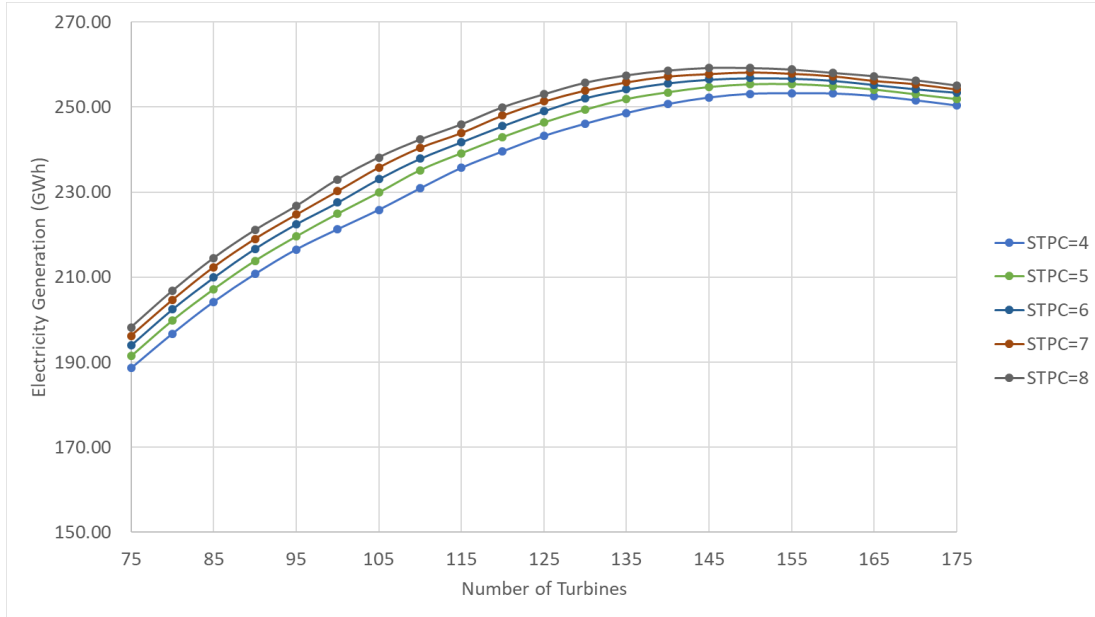


Fig 6. 14. Electricity generation with a range of turbines numbers and STPC, under the non-flexible schedules.

6.3.2.2.2 Flexible operation schemes

As a result, the electricity estimated can be further improved by at least 10% if the flexible operation adopted, which is in line with the findings by Xue et al. [33] and Angeloudis et al. [31]. The addition of pumping results in superior electricity yields of 282.11 GWh, corresponding to a further improvement of at least 10% compared to the scenarios without pumping. The range of $H_{p,i}$ ($i=1, n$) varies from 0 m to $H_{p_limited}$, considering the water level after pumping should be limited by the HAT of about 5.98 m or LAT of about -5.68 m in the selected cycle, respectively. It can be seen that the optimisation of design parameters generally confirmed the selection of STPC of 8 and NumTB of about 148. However, taking the cost-efficiency into consideration, a NumTB of 125 has been adopted in the most updated roadmap by developers TEES [130].

The detailed operation heads, water levels inside and outside the impoundment and power output during 5 neap tides could be found in Figures 6.15 and 6.16, without and with pumping, respectively. It can be seen that the optimum operation heads during half-tides were varying among the tides and in the magnitude of optimum operation heads, H_s is the greatest, which is followed by H_e , and H_p . It shows the applicability of the flexible operation schemes in the maximisation of electricity generation. It should be noted that due to the lower tidal range, the power output during neap tide is still lower than that during spring tide even with the flexible operation schemes.

As shown in Table 6.3, the electricity estimated can be further improved by at least 10% if the flexible operation adopted with the STPC of 8 and NumTB of 150 and the GA model could reach a very similar optimisation result [33]. However, one point worth emphasizing is that a computational time of approximately 430 hours has been cost under the flexible operation schedule using GS, it will

be longer if considering pumping. While a cost time of fewer than 23 hours was required using GA, equivalents to an approximately 95% of cost time saved in comparison with the GS method. This re-emphasizes the significance of reducing the running time and improving the efficiency by adopting more advanced algorithms, e.g. GA into the multiple variables optimisation in TRSs. It should be noted that the cost of the GA model in Table 2 can be influenced by a variety of factors [86] which is worthy to be further studied in the future work to contribute a higher efficiency of this optimisation using GA.

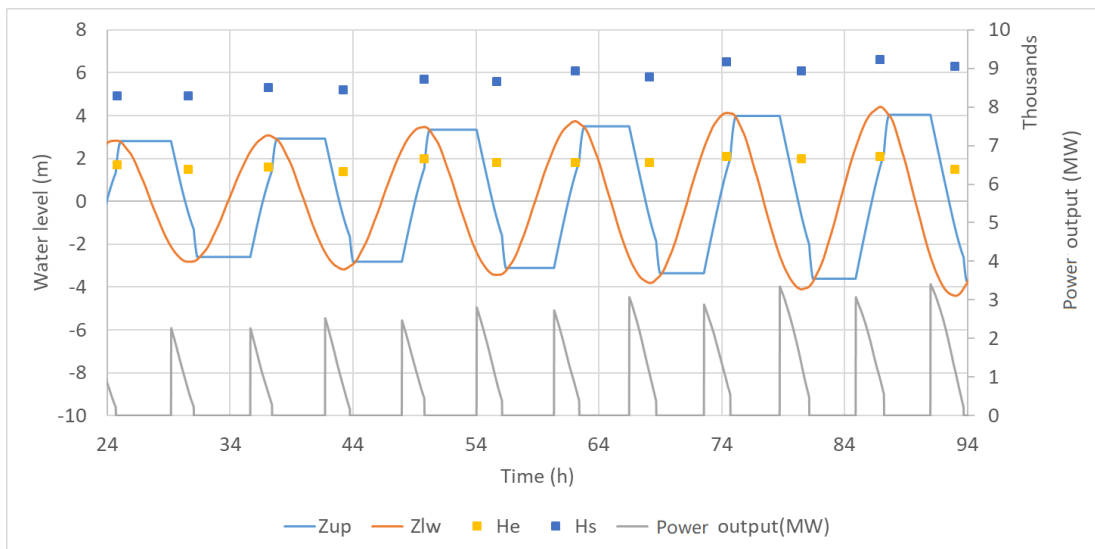


Fig 6. 15. Electricity generation under flexible operation schemes with no pumping optimised by the GA model.

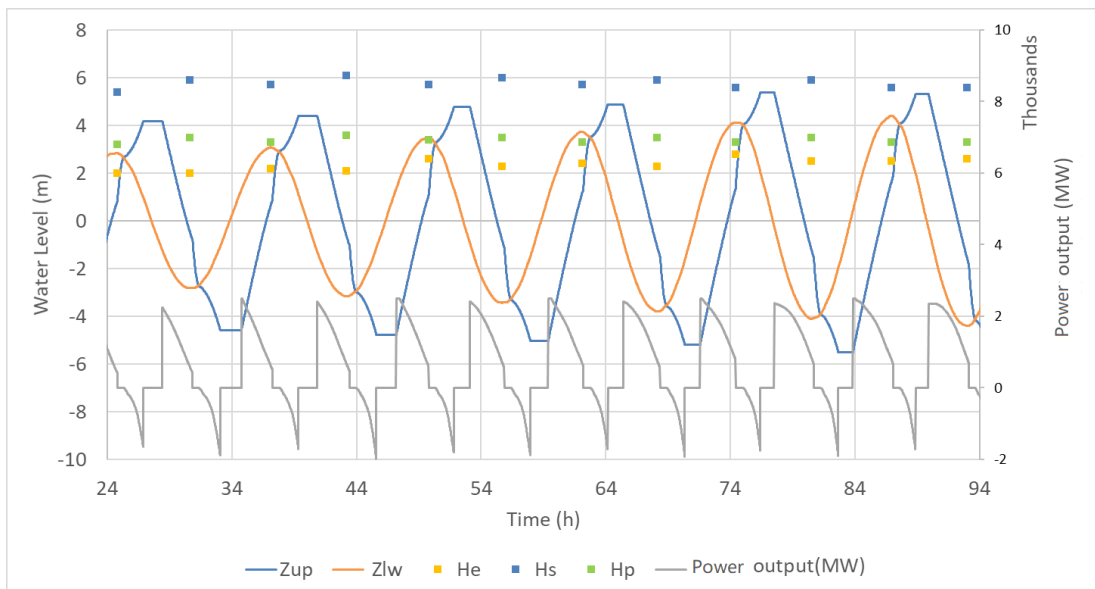


Fig 6. 16. Electricity generation under flexible operation schemes with pumping optimised by the GA model.

6.3.2.2 Validation of the optimised schemes

Table 6.4 summarised the cumulative electricity estimation during the typical tidal cycle between GA or 0-D models and 2-D models under various optimisation scenarios. It can be seen that the 2-D outcomes supported the GA performance very well. With no pumping involved, a more than 20% and 35% improvement if non-flexible and flexible scheme applied, respectively, compared to the baseline scenario. Furthermore, pumping can yield a more than 10% increase in electricity generation, which was consistent with the findings in [23, 31, 33]. Overall, the WSL could benefit significantly from the multi-parameters optimisation, including the design parameters of turbine numbers and sluice gates, as well as the operational parameters of starting generating heads, ending generating heads and also the pumping heads. More importantly, the GA model could perform as well as the best performing GS model, i.e. EHN model in terms of total electricity generation. However, the GA model simulation time has been 50% lower than the GS model in the optimisation of flexible operation as shown in section 6.2. The simulation time of modelling a full TRS, including turbine numbers, sluice gates and operation, was reduced to approximately 95% of the simulation time using GS model when the GA model developed to optimise full scheme simultaneously. This re-emphasizes the significance of reducing the running time and improving the efficiency by adopting more advanced algorithms, e.g. GA into the multiple variables' optimisation in TRSs.

In conclusion, developing GA into the TRSs optimisation shows great potential in terms of the various design variables of the scheme, including basin size, the number of turbines and sluice gates and its operation schedule which requires a large number of simulations, providing more certainty to cost-benefit analysis with exhaustive resources of the scheme to facilitate the development of TRSs.

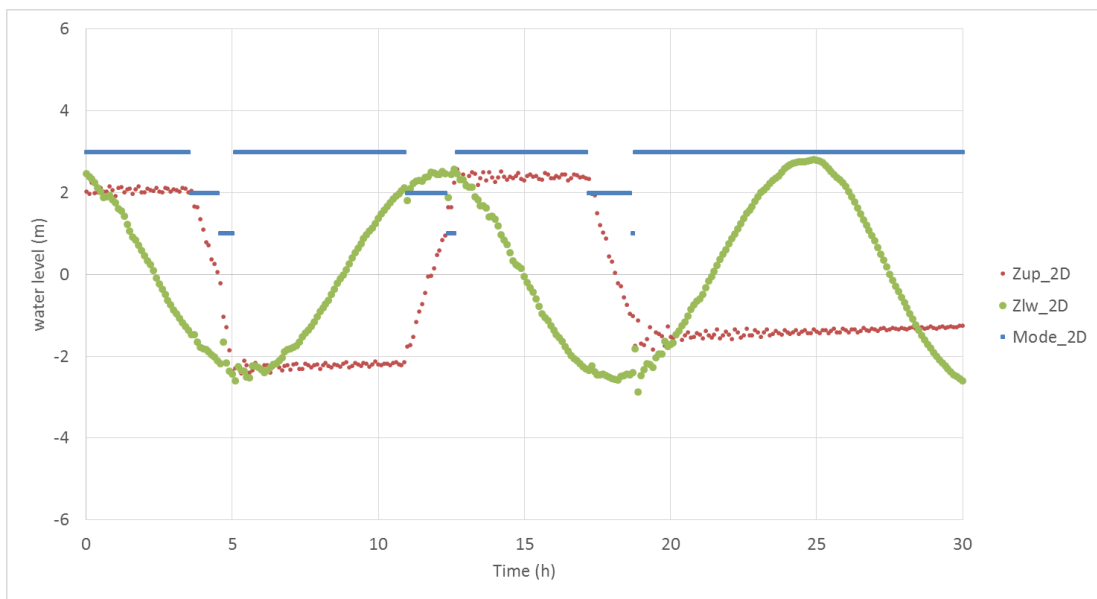
Table 6. 4. Comparison of optimisation scenarios using GA.

Scenario		Electricity Generation (GWh)				
		0-D or GA model	2-D model	0-D improvement (%)	2-D improvement (%)	Difference between 0-D and 2-D (%)
No pumping	baseline	201.28	183.47	-	-	-8.84
	GA-non-flexible	254.61	226.22	26.50	23.30	-11.15
	GA-flexible	286.70	258.96	42.44	41.15	-9.68
With pumping	GA-non-flexible	282.11	252.54	40.16	37.65	-10.48
	GA-flexible	307.44	278.86	52.74	52.54	-8.97

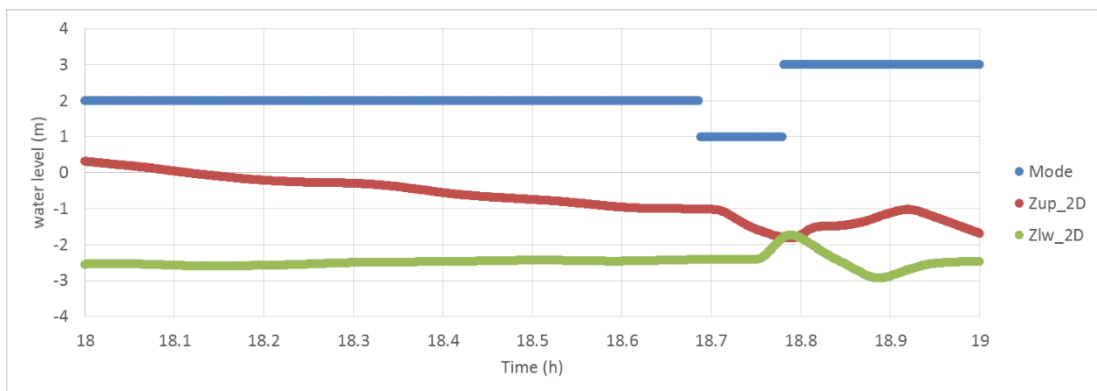
6.3.2.3 Control approaches in 2-D modelling

The operational schemes including H_s and H_e and even H_p were used to control the operation of TRSs, known as the approach of 'water head control'. Traditionally, the operation heads utilised in the 2-D was independent to the 0-D models under fixed operational schemes.

If the deployment of WSL (concentrated blocks of turbines and sluice gates) and the flexible operation schemes were adopted, results showed that the electricity generation from the 2-D model was significantly less than it from the 0-D model. The water levels and operation scheduling during the cycle without power output could be seen in Figure 6.17. It was clearly the sluicing phase only last for a very short time before holding phase starting, and this insufficient sluicing phase yielded an insufficient holding water level existing in the basin and hence insufficient generating heads for the next tides, and consequently no electricity generation for next generating phase. This is one of the reasons that were yielding a significant difference between 0-D and 2-D.



(a)

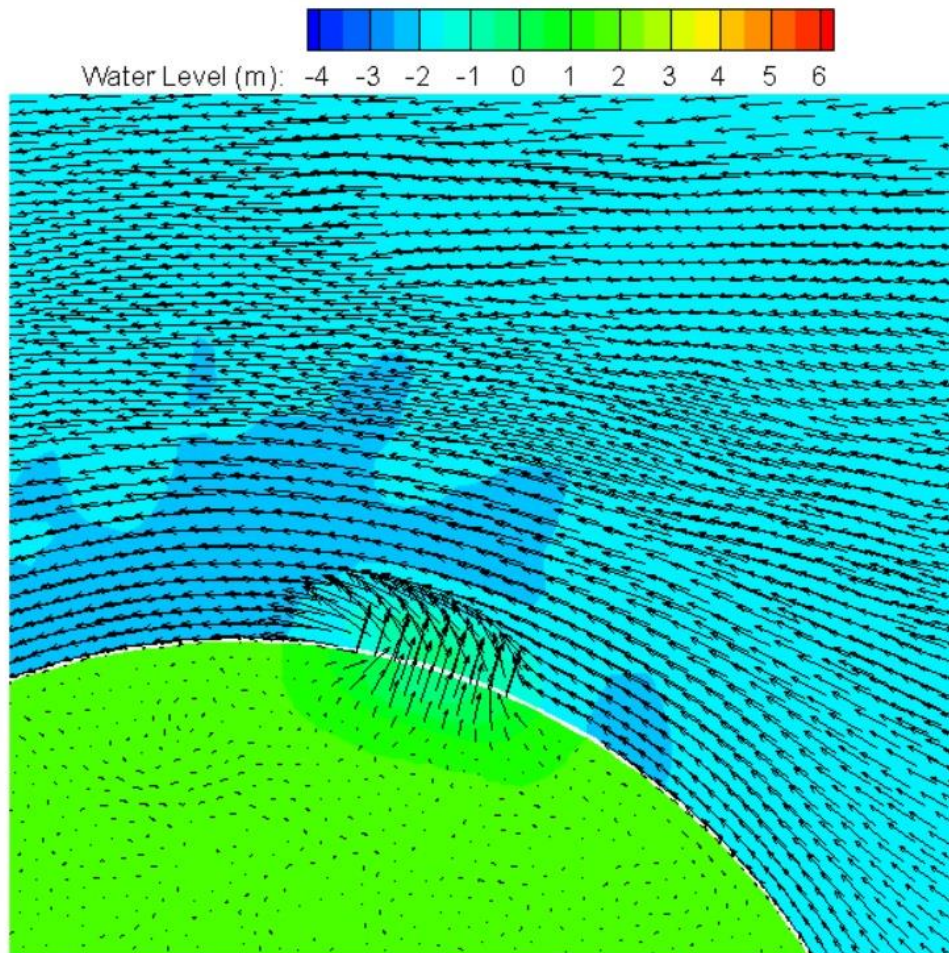


(b)

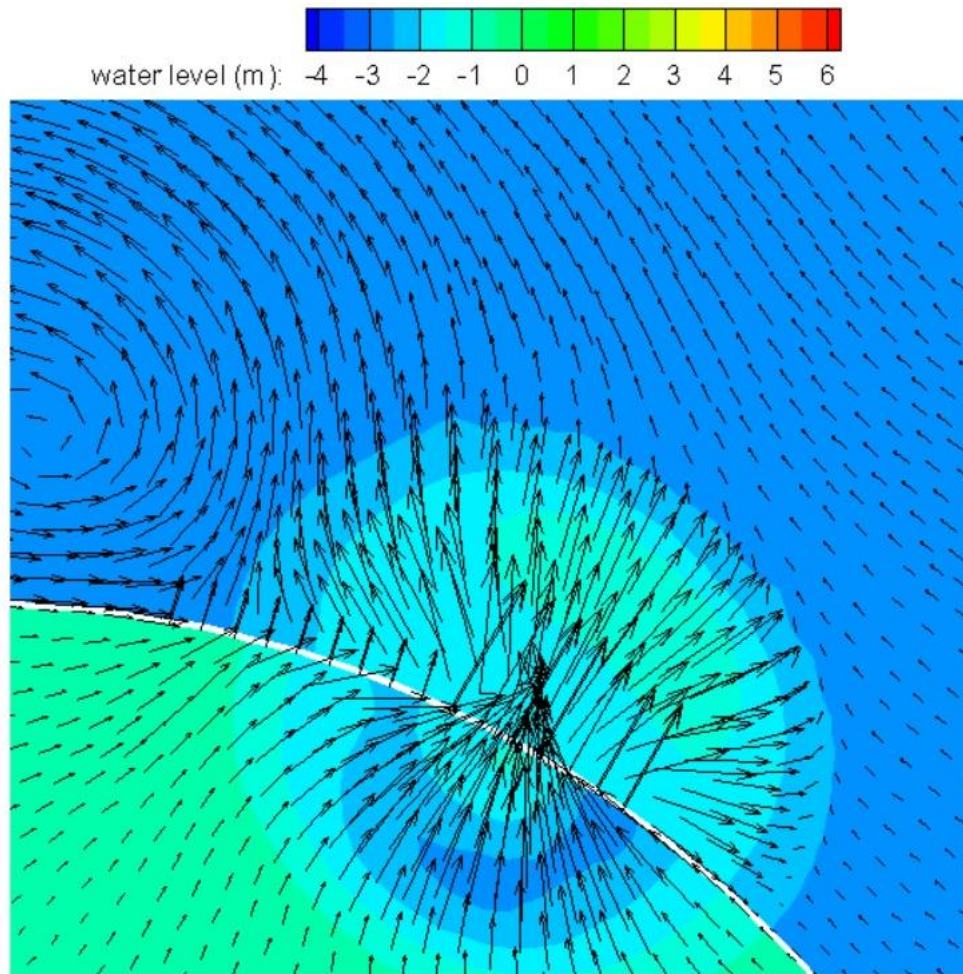
Fig 6. 17. Water levels and scheduling in 2-D model with traditional ‘head control’ method, in which the Mode denotes the operation phase with ‘1’ to ‘3’ represent filling, holding and generating, respectively; Zup denotes the basin water level; Zlw denotes the downstream water level.

As for the question of why the sluicing phase ended up so quickly? The hydrodynamics simulation could tell the answer. As shown in Figure 6.18, it can be seen that due to the opening of all the turbines

at the same time, a large discharge was formed going through the turbines. Then the water level at downstream and upstream was serious unsteadily although the cross-section used to control the operations between the impoundment was approximately 500 m away from the open boundary of the blocks. The jet of discharge through turbines or sluice gates took approximately 0.2 hrs to spread out and back to peace. Hence, it can be concluded that the difference of the electricity prediction between 0-D and 2-D was caused by the extremely big jet under the single block distribution of turbines and sluice gates.



(a)



(b)

Fig 6. 18. Hydrodynamics at the beginning of: (a) ebb generating; (b) ebb sluicing.

Three approaches have been put forward herein to address this problem:

1. Using a ‘time-control’ for the operation of TRSs.

In some studies [64, 134], the 0-D model outcomes were implemented in the 2-D based on the time from the start of the operation. However, in this approach, the operation is implemented in the 2-D model based on the head differences across the scheme derived by the 0-D model, allowing closer similarity between the 2-D model and the optimised 0-D results. For example, if the optimised time point for the first generating phase from the 0-D model was at 30.8 hr in the typical cycle, then in the 2-D model, the first generating phase was forced to start at exactly the same time point of 30.8 hr as well. Results showed that the electricity generation was 269.01 GWh during the typical Spring Neap cycle, equals to a difference was about 6.17% compared with 0-D electricity generation of 286.70 GWh, with details of water levels and operation scheduling for the first 2 tides shown in Figure 6.19. This approach for the operation of TRSs ignores the hydrodynamics impact to the operation of TRSs between

0-D and 2-D and makes the 2-D to be dependent on the 0-D model, which would bring more workload in the future studies.

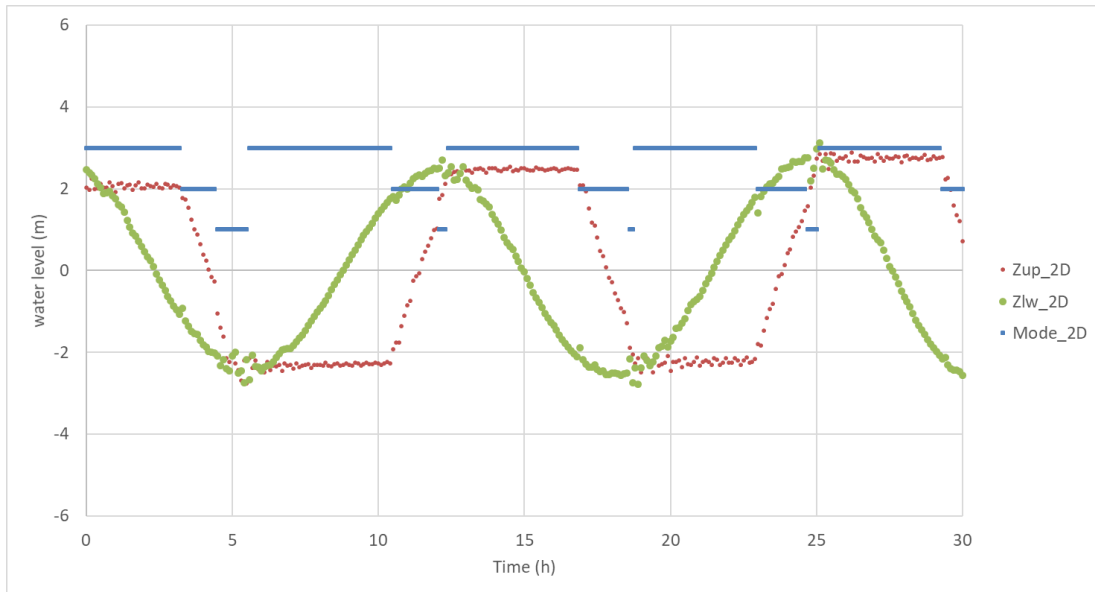


Fig 6. 19. Water levels and scheduling in 2-D model with 'time control' method for operation.

2. A duration of minimum sluicing phase

The approach of 'minimum duration control' was put forward and utilised in this thesis to avoid a short but fluctuant of discharge through sluice gates or turbines. That is, a minimum forced duration for sluice gates operating, e.g. 0.2 hrs, was allowed during sluicing phase. As a result, the 2-D could be independent of the 0-D model and avoid being affected by the jet discharge due to the opening of turbines or sluice gates suddenly. The electricity generation in these modes was about 258.96 Gwh with a difference of 9.76% as mentioned in Table 6.4.

3. Develop a new deployment which distributes the turbines and sluice gates.

It should be known that the problem was caused by a large discharge rushing out of the turbines or sluice gates due to the concentrated or single block distribution of turbines and sluice gates. Beyond that, it may also cause a problem to the ship navigation, fish migration and sediment transport, etc. Hence, it was necessary to develop a new deployment which distributed the turbines and sluice gates into several blocks and hence distributed the discharge through the operation. This solution was adopted in the updated deployment shown in Figure 6.13.

6.3.2.4 Multi-blocks Optimisation

Traditionally, the downstream water levels in the 0-D model were obtained at the middle point of turbines' sets. For example, the input water levels utilised for the simulation of WSL was obtained at the 3rd block in Figure 6.13. That is, there was only one location that providing the input water levels

and by the optimisation, the most optimised operation scheme (known as single-block operation scheme) only suited for the one location.

However, for a large project like WSL, there were 5 blocks of turbines in the updated deployment and the most optimised operation schemes for the middle block may not be the most optimum ones for the other blocks. In other words, the other blocks may not be activated using a single operation scheme. For example, firstly, the modified 0-D model was developed with 5 groups of water levels generated from TELEMAC-2D at the middle of the outlet of each turbines block. It should be noted that the water levels had a considerable difference between the 5 blocks. Then if the single-block operational scheme optimised from the GA model was implemented to this developed 0-D model, the electricity generation predicted was only approximately 171 GWh, significantly less than it of the original 0-D model. The details of water levels beside the impoundment, operation scheduling and power output were plotted in Figures 6.20-6.22, respectively. Apparently, due to the asynchronism of the operation between 5 blocks of turbines, during the first tide, the 3rd and 5th blocks entered the generating phase while the others still in holding phase due to insufficient H_s reached. At the meantime, the basin water level started to decrease and so the blocks of 1st, 2nd and 4th did not get a chance to operate anymore in this tide, which caused very limited electricity generated under this scenario.

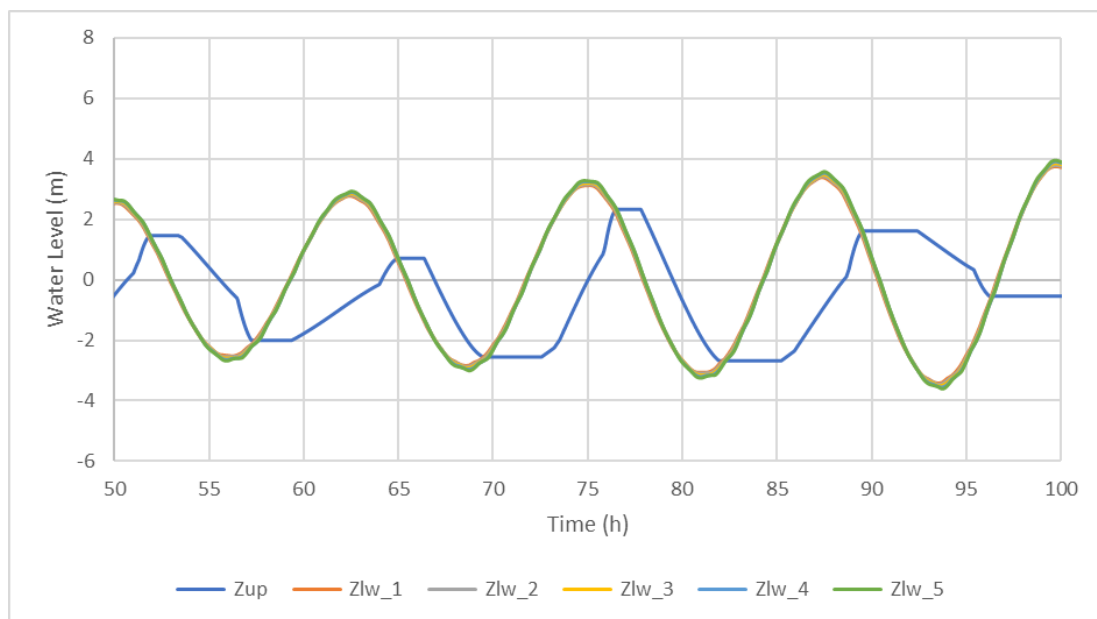


Fig 6. 20. Water levels in the modified 0-D model with 5 blocks of turbines under the single-block operation schemes, in which 'Zup' represents the basin water level; 'Zlw' denote the downstream water levels and '1'-'5' indicate the corresponding terms at 5 blocks of turbines.

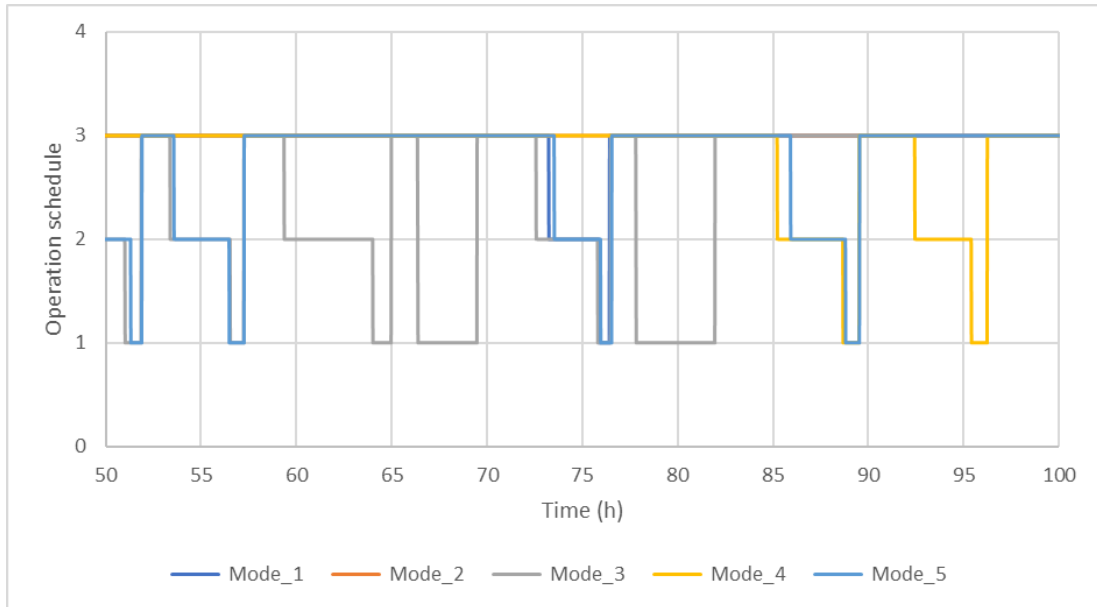
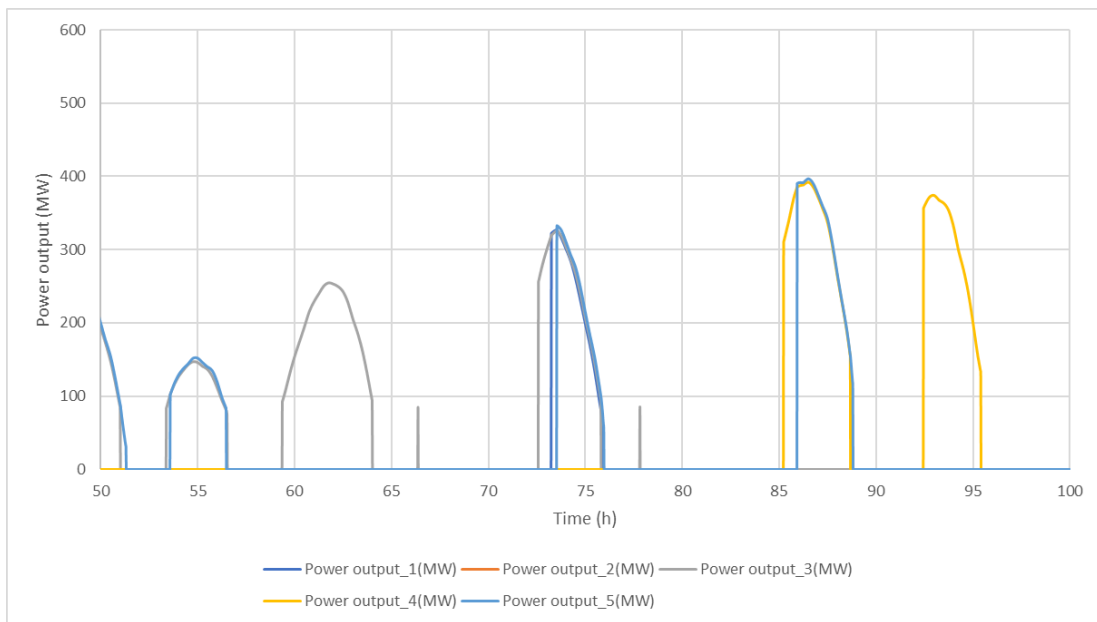


Fig 6. 21. Operation scheduling in the modified 0-D model with 5 blocks of turbines under the single-block operation schemes, in which ‘Mode’ stands for the operation scheduling and ‘1’-‘5’ indicate the corresponding terms at 5 blocks of turbines.



(c)

Fig 6. 22. Power output in the modified 0-D model with 5 blocks of turbines under the single-block operation schemes, in which ‘Power output’ represents the power output and ‘1’-‘5’ indicate the corresponding terms at 5 blocks of turbines.

6.3.2.4.1 Model development

As mentioned in this Chapter, 125 turbines and 20,000 m² of sluicing area were considered in the updated WSL proposal because of its satisfied electricity generation and cost of energy, as shown in Figure 6.13. It contains 5 arrays of turbines (T1-T5) with 25 turbines per array and 8 arrays of sluice

gates (S1-S8), which could benefit more to the ship navigation, sediment transport, etc., with distributed discharge through operation in comparison with the deployment with concentrated turbines and sluice gates.

The modified GA model, using the 0-D model as the evaluation tool for the electricity generation, was developed with 5 groups of water levels located at the middle of the outlet of each turbines block. The mean idea was to operate the turbines and sluice gates at 5 locations independently, and then at time step(i), the discharge of $Q(H, i)$ could be summed up for the calculation of $(Z_{up, i+1})$ at the time step of (i+1). Consequently, the new upstream water levels inside the impoundment $(Z_{up, i+1})$ at any point in time can be improved as follows, according to the Eq.3.3:

$$Z_{up, i+1} = Z_{up, i} - \frac{\sum_{T=1}^n Q(H) + Q_{in}(t)}{A(t)} \Delta t \quad (6. 1)$$

where T denotes the T^{th} block of turbines and in the case of WSL, the total array of turbines n was designed to be 5.

To keep the relative consistency of the operation between 5 blocks, a time adjustment, known as ‘mini_operation’ was set to 0.2 hours. That is, once the first block operated, the others should then be operated no later than the ‘mini_operation’. Results indicated that this limitation could improve the efficiency of the GA model due to narrowed searching space of the operation heads.

6.3.2.4.2 Operational optimisation

Results illustrated that the operation heads were different among the 5 blocks of turbines in this multi-blocks optimisation. As an example, the operation heads from T1 to T5 had slightly different because of the slight difference of the water levels at the outlet of T1 to T5, as shown in Table 6.5. As for the improvement of the operational optimisation at multi-blocks, it can be concluded from Table 6.6 that a very similar electricity generation could be produced in the multi-blocks optimisation although the different optimum operation heads were adopted at each block of turbines. Figures 6.23-27 showed the comparison between the multi-blocks using the optimum operation heads from the GA model, in terms of the water levels; water head difference; discharge through turbines; power output and discharge through sluice gates, respectively. Compared to Figures 6.20-6.22, the multi-blocks optimisation was proved to be able to address the asynchronism problem between the blocks and guarantee the optimum operation operated smoothly.

Table 6. 5. Optimum operation heads during the 1st tide in multi-blocks optimisation

No	T1	T2	T3	T4	T5
He	1.7	1.7	1.7	1.71	1.76
Hs	3.2	3.19	3.17	3.17	3.18

Table 6. 6. Comparison of optimisation scenarios with updated West Somerset Lagoon (NumTB =125 and STPC=8)

Scenarios		single block	5 blocks	5 blocks with multi-block optimisation
No pumping	Non-flexible	0.198	0.171	0.198
	Flexible	0.235	0.183	0.232
With pumping	Flexible	0.271	-	0.27

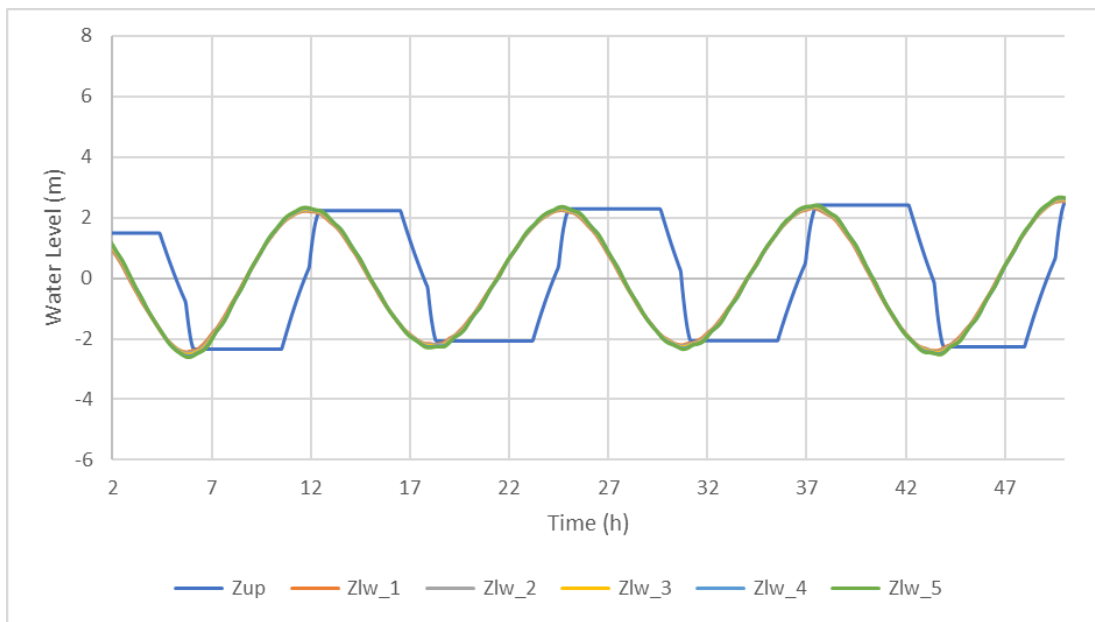


Fig 6. 23. Water levels comparisons for four neap tides in the modified 0-D model for multi-blocks optimisation, in which ‘Zup’, ‘Zlw’ represent the basin water level and downstream water level, respectively; ‘1’-‘5’ denote the number of turbines block, respectively.

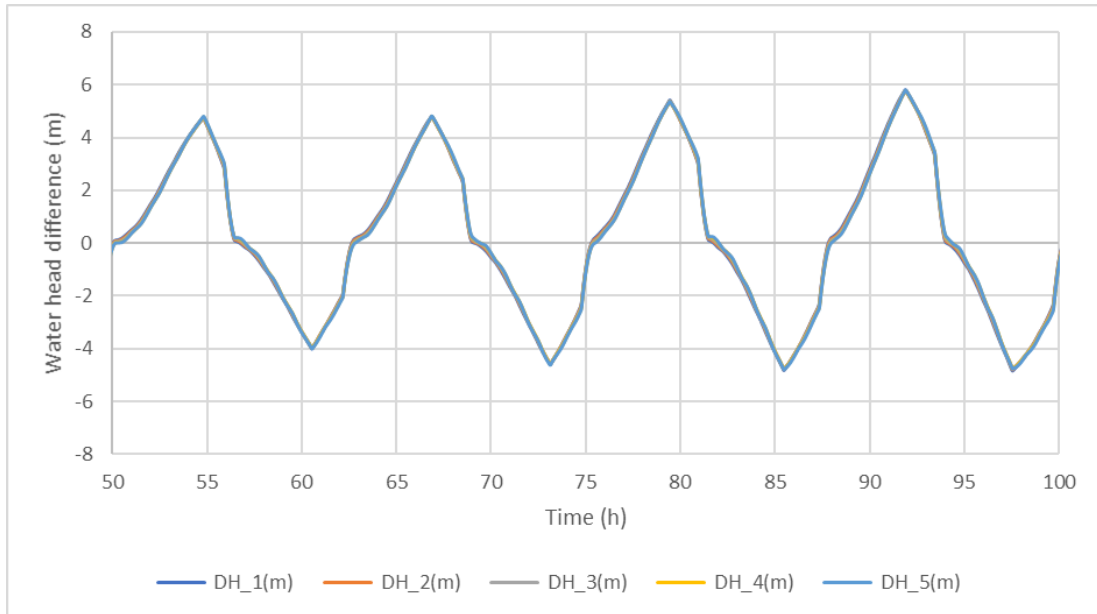


Fig 6. 24. water head difference comparisons for four neap tides in the modified 0-D model for multi-blocks optimisation, in which 'DH' represents the basin water level. '1'-'5' denote the number of turbines block, respectively.

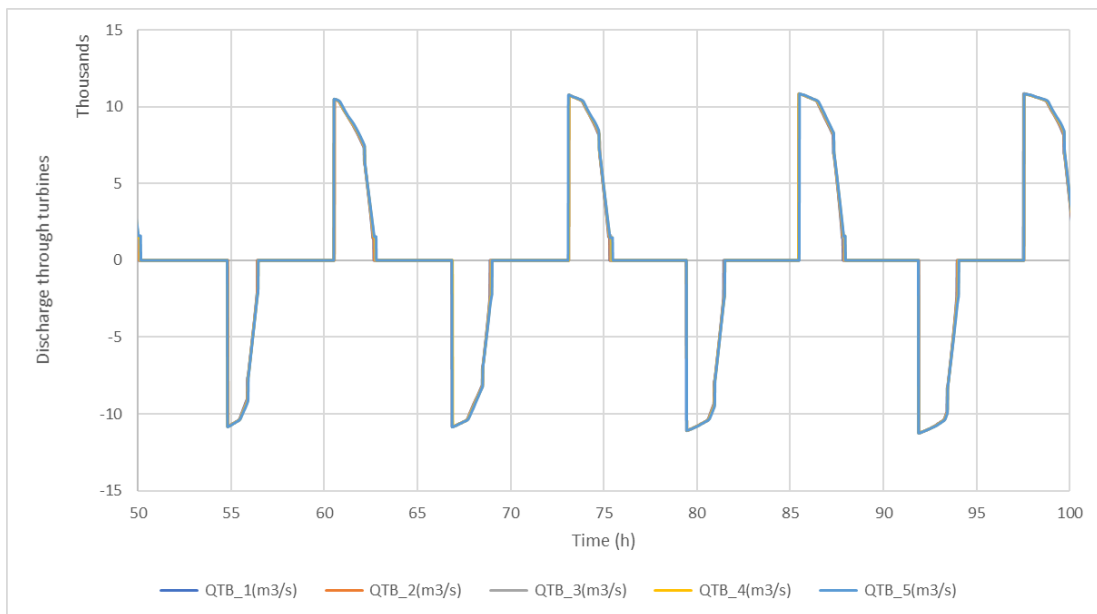


Fig 6. 25. Discharge through turbines, in which 'QTB' represents the discharge through turbines. '1'-'5' denote the number of turbines block, respectively.

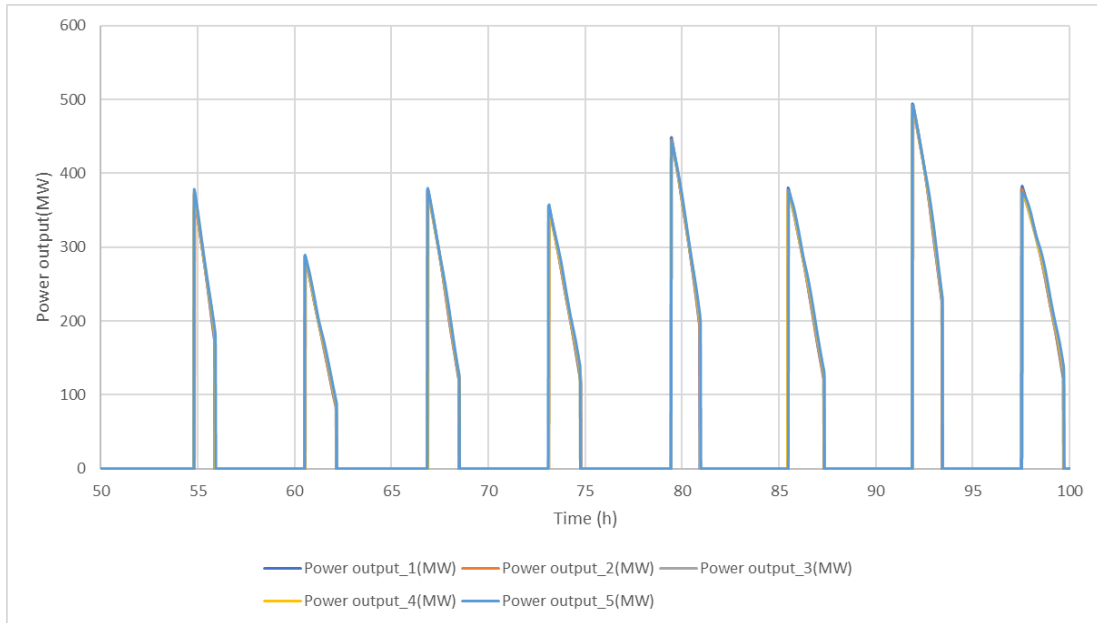


Fig 6. 26. Power output comparisons for four neap tides in the modified 0-D model for multi-blocks optimisation, in which ‘Power output’ represents the power output. ‘1’-‘5’ denote the number of turbines block, respectively.

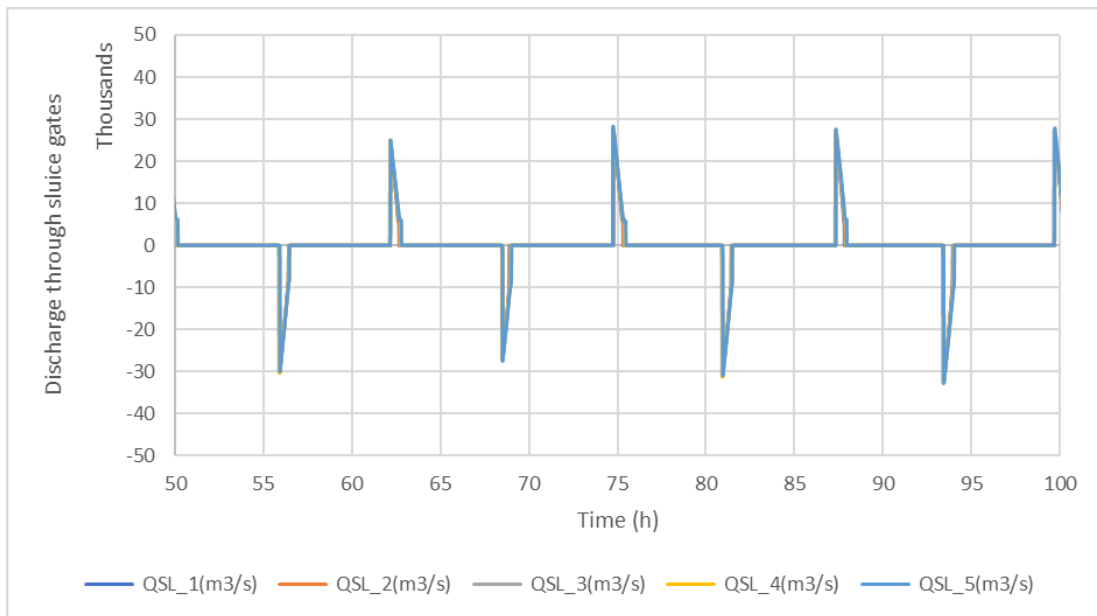


Fig 6. 27. Discharge through sluice gates comparisons for four neap tides in the modified 0-D model for multi-blocks optimisation, in which ‘QSL’ represents discharge through sluice gates. ‘1’-‘5’ denote the number of turbines block, respectively.

6.3.3 Case Study of North Wales Tidal Lagoon

6.3.3.1 Optimisation

As illustrated in Chapter 4, when the NumTB of 150 and STPC of 10 with H_s of 3.7 m and H_e of 1.4 m, the maximum electricity generation of 159.71 GWh could be achieved during the typical cycle, equals to 3.84 TWh/Year with a coefficient of approximately 24.01. According to the HW and LW at the outside of each block from Figures 4.43-4.44, the 10 blocks of turbines were divided into 5 groups for the multi-blocks optimisation. The 1st – 2nd, 3rd – 4th, 5th – 6th, 7th – 8th, 9th to 10th indicated the groups 1-5, respectively, and the electricity generation can be seen in Table 6.7.

Table 6. 7. Comparison of optimisation scenarios with North Wales Tidal Lagoon (NumTB =150 and STPC=10)

Scenarios		single block	5 blocks with multi-block optimisation
No pumping	Non-flexible	159.71	-
	Flexible	200.29	197.56
With pumping	Flexible	228.72	228.27

If the flexible operation schemes were utilised, an electricity generation of 200.29 GWh which equivalent to 4.81 TWh/Year, could be produced. The water levels inside the impoundment and power output; discharge through sluice gates and turbines; and water head difference for 5 neap tides and electricity generation during the typical cycle in the 0-D model have shown in Figures 6.28-32, respectively. A more than 10% electricity could be obtained if pumping included.

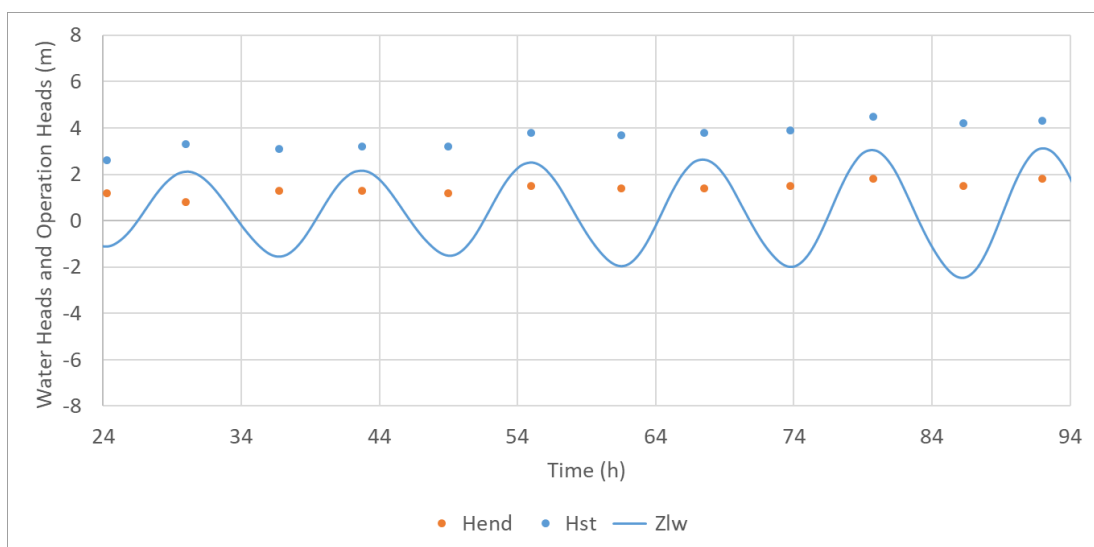


Fig 6. 28. Flexible operation schemes without pumping optimised by the GA model.

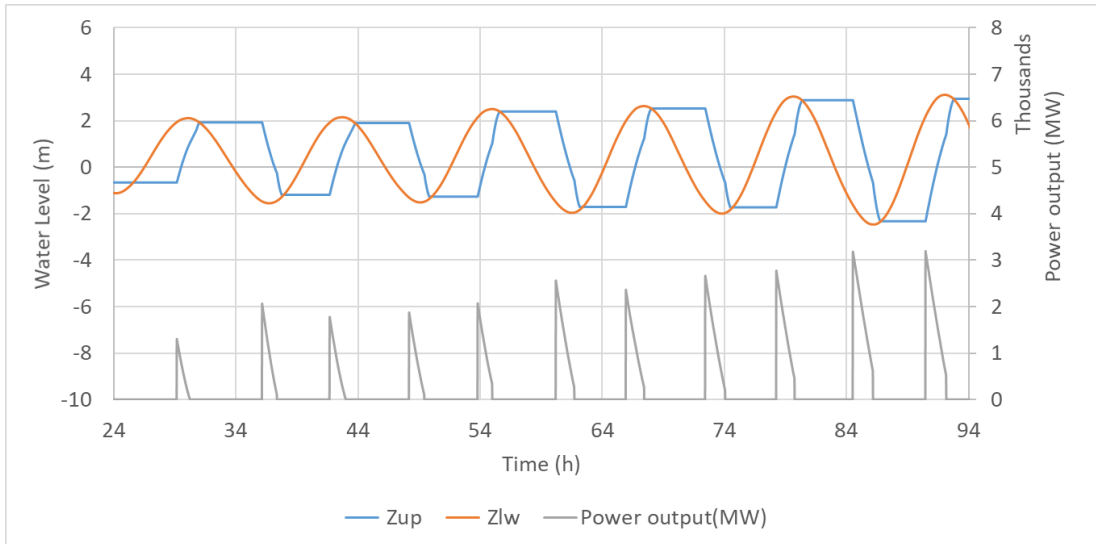


Fig 6. 29. Water levels inside the impoundment and energy for 5 neap tides for North Wales Tidal Lagoon.

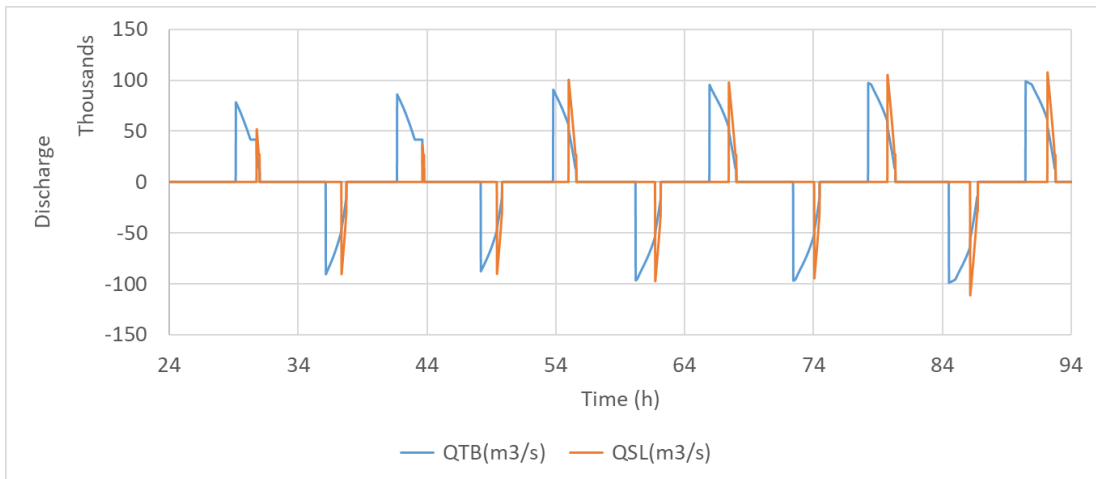


Fig 6. 30. Discharge through sluice gates and turbines for 5 neap tides for North Wales Tidal Lagoon.

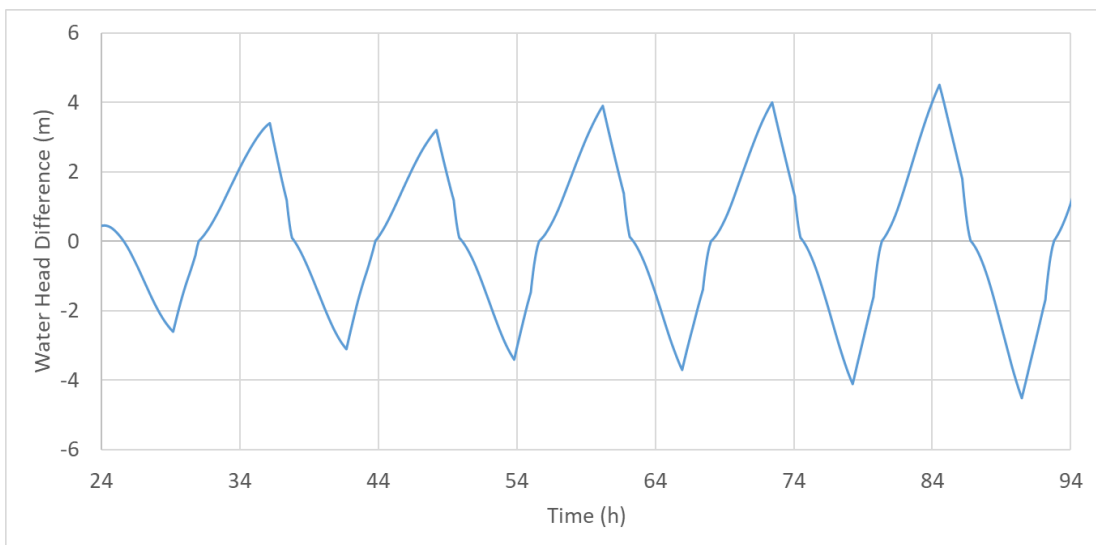


Fig 6. 31. Water head difference for 5 neap tides for North Wales Tidal Lagoon.

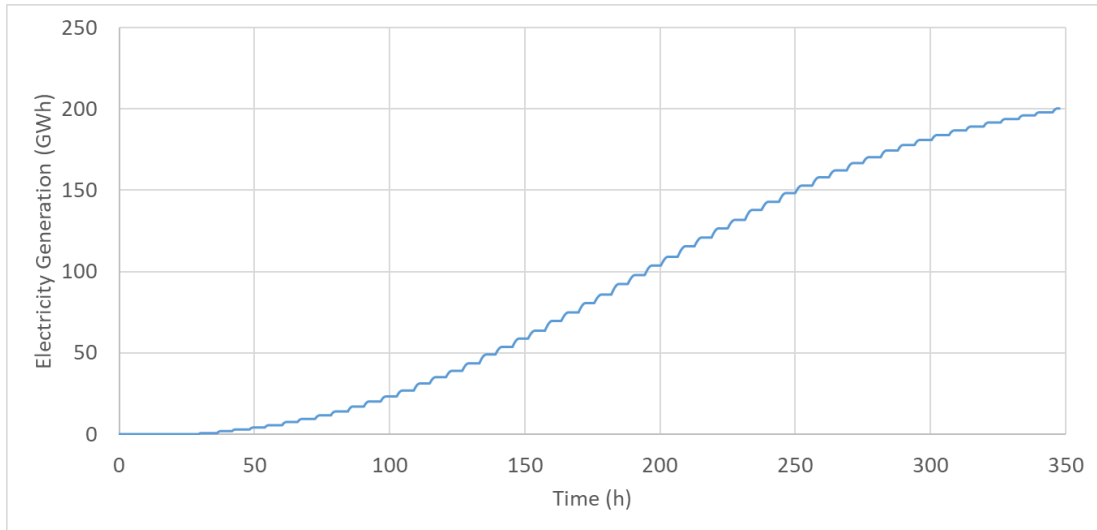


Fig 6. 32. Electricity generation during the typical cycle for North Wales Tidal Lagoon.

6.4 Chapter summary

In this chapter, on the one hand, an efficient approach was investigated in the optimisation of the design of the operation of TRSs by maximising their electricity generation, namely Genetic Algorithm (GA) model. A comparison between the GA and GS methods were achieved. Results indicated that both GA and GS models could deliver more than 10% increase in electricity generation comparing to non-flexible operation, i.e. using fixed heads for all tides, just by optimising the operation. The GA model could perform as well as the best performing GS model, i.e. EHN model, while GA model simulation time has been 50% lower than the GS model in the optimisation of operation flexibly. This re-emphasizes the significance of reducing the running time and improving the efficiency by adopting more advanced algorithms, e.g. GA into the multiple variables' optimisation in TRSs. The feasibility of the elite operational schemes was validated through a developed 2-D model.

On the other hand, the optimisation using GA was developed to deliver the complete design of new TRSs, including the number of turbines, sluicing areas and maximum amount of electricity for the scheme through identifying the most optimised operation schemes including pumping, for particular sites. The maximum electricity for different scenarios was evaluated by optimising the operation schemes flexibly for each block of turbines. Results showed that the GA model was capable of achieving largely the same number of turbines and sluice area with identical electricity and reducing the computational time by approximately 95% comparing to traditional GS methods. It should be noted that the cost of the GA model can be influenced by a variety of factors [86], such as the iteration time, initial operation as well as the performance of HPC, which is worthy to be further studied in the future work to contribute a higher efficiency of this optimisation using GA. The performance of the model was validated using a more sophisticated 2-D hydro-environmental model which supported the GA model predictions very well. It could be concluded that the WSL and NWTL are able to achieve the electricity generation of 5.57 TWh/Year and 4.81 TWh/Year if the optimum turbines of 125 and 150 with the STPC of 8 and 10 were applied, respectively. An approximately 10% electricity can be further obtained if pumping utilised.

7. Flexible operation optimisation

7.1 Introduction

It has been pointed out that the optimisation of the tidal lagoon can focus on the electricity generation maximisation by optimising operation schemes and design parameters, and hence decrease the cost per unit power generated [32]. However, the overall economic design of lagoon to minimise the cost of energy is another important aspect which might be more attractive to industry [145]. That is, lagoons must of course be able to export power to the grid, and so proximity to a suitable grid connection is a key constraint [146]. However, the electricity grid is a complex system in which power supply and demand must be equal at any given moment. Constant adjustments to the supply are needed for predictable changes in demand, such as the daily patterns of human activity, as well as unexpected changes from equipment overloads and storms. Flexible power output plays an important role in this balancing act and helps to create a more flexible and reliable grid system. For example, when there is a heavy storm and other renewable energy resources including solar and wind cannot work properly, the potential energy from tides can be used as a battery which ensuring the operation for some significant facilities. Also, when demand mismatches the supply, the power output from TRSs can be operated flexibly to the grid, making up the insufficient or surplus electricity. Following this, the energy output can in line with the need of demand principles and contribute to the revenue optimisation by generating more power output during the duration with higher electricity price. In conclusion, it is of importance to make flexible operation optimisation becomes more economically attractive through electricity arbitrage and providing additional system support [147].

In this way, it is worthy of investigating how to export flexible power to the grid by a single lagoon, or multiple tidal schemes working with other renewable energies including wind and solar [138]. A potential advantage of having multiple projects rather than a single project is that tidal power will be fed to the grid at several locations rather than being concentrated at one particular point [22], which will contribute to more efficient electricity distribution, and could perhaps alleviate cumulative hydrodynamic impacts [21]. However, it has been pointed out that providing flexible, especially a continuous tidal range power to the system remains a challenge especially during neap tides [57].

Hence, this chapter proposed a framework of flexible operation optimisation where using the GA to optimise the operation schemes over the typical Spring Neap tidal cycle. The combined operation of

multiple prospective tidal lagoon projects, i.e. WSL and NWTL, are used as case studies to demonstrate the potential of the flexible operation optimisation of TRSs [31].

In section 7.2, the methodology of the flexible operation optimisation with joint multi-schemes, e.g. WSL and NWTL, are illustrated. In section 7.3, the improved GA model is set up and several criteria are implemented to shape the power output distribution with users' requirements. In section 7.4, the outcomes of the flexible operation optimisation are presented and compared for various scenarios with different parameters setting, highlighting the recommended parameters to meet the needs of different developers, e.g., the maximisation of energy output, a continuous or flat energy output, or a compromised objectives between them.

7.2 Methodology

The joint performance of multiple lagoons could be achieved by treating the operation of the WSL and NWTL as a system that has the flexibility to adapt to the continuous power output [148, 149]. To achieve this, the GA model as described in Chapter 6 was further developed to simulate multi-tidal schemes, e.g. WSL and NWTL, which will be explained in comprehensively in this section.

To achieve flexible operation optimisation, the fitness function in the GA model updated to a combination of three parameters with different weight. In detail, the electricity generation was still a key control parameter to be maximised [31, 32] which is reflected by the averaged power output (Av), as shown in Eq.7.1. Furthermore, some other control parameters should be concerned for a flexible power output [150, 151]. The ‘standard deviation’ (St) in Eq. 7.2 was used to express the variability of the power output distribution by implemented it as one of the control parameters for the decision of optimal solutions. The solutions with the lesser standard deviations could represent the flatter power output. Apart from that, an accumulated duration when power output is zero, known as ‘total Duration with No Energy output’ (DNE) in Eq.7.3, was used to find the most continuous operation scheme. The solution with the lesser DNE represented the optimal solutions which were able to generate the longest continuous power output.

$$Av[i] = \text{Elect}[i] / N_{\text{step}} \quad (7.1)$$

$$St[i] = \sqrt{\frac{1}{N_{\text{step}}-1} \sum_{j=1}^{N_{\text{step}}} (\text{Energy}[i, j] - Av[i])^2} \quad (7.2)$$

$$DNE[i] = N \times Ts / 3600 \quad (7.3)$$

where Av[i], St[i] and DNE[i] are the Av, St and DNE for operation scheme i. Elect[i] represents the electricity generation for scheme i and Energy[i, j] denotes the power output at time step j when using the scheme i. Nstep and Ts represent the total time steps and simulation time in second during the typical cycle, respectively. N is the accumulated number of time steps when the Energy[i, j] = 0.

To achieve this, three weight factors, known as the positive coefficient of co_av, negative coefficient of co_st and negative coefficient of co_dne for Av, St and DNE, respectively, were used in statistical evaluation for selecting the optimal solutions for multi-objective decision making according to users’ different requirements, as shown in Table 7.1.

7.3 Model development

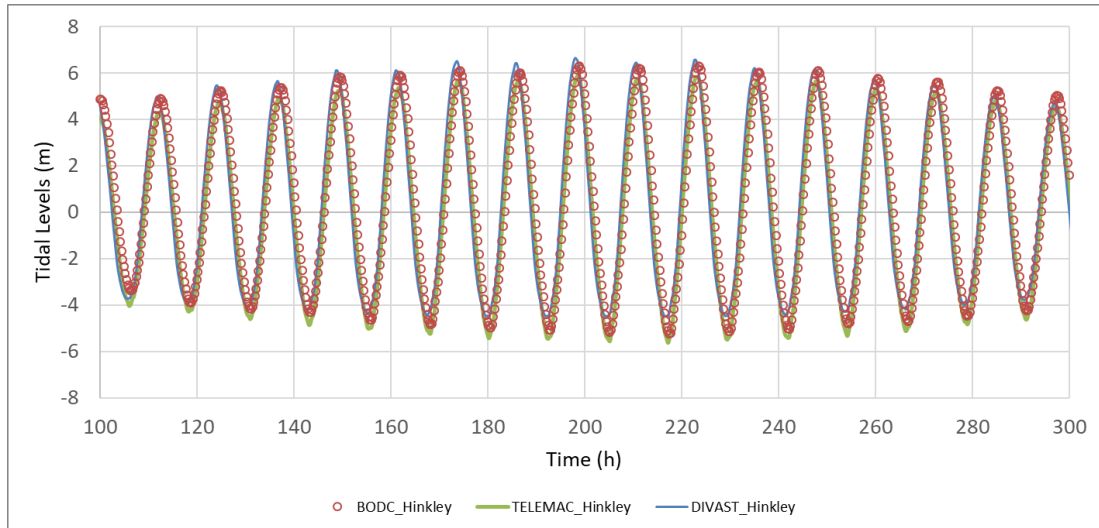
7.3.1 Input tidal levels

Literally, the continuous power output is regarded as one of the key objectives for this flexible operation optimisation, which will be achieved by taking advantage of the combined effect between multi-scheme to make up the gap duration with no power output for a single scheme. Hence the accuracy of input water level is very significant when dealing with joining multi-schemes. The main purpose of this chapter is to show the model applicability in terms of flexible operation optimisation and so the more accurate prediction of tides is able to yield more reliable results.

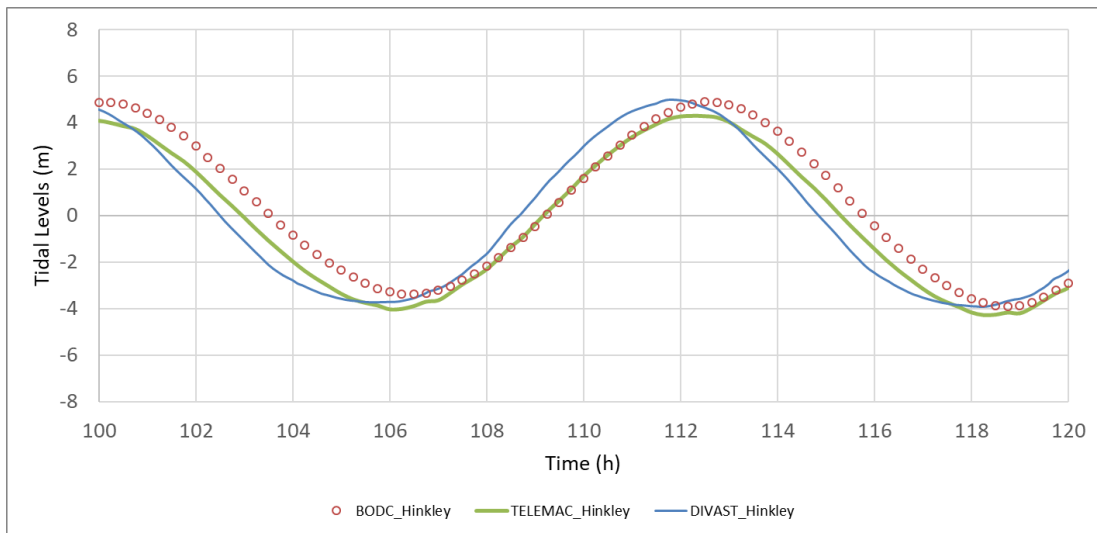
The input water levels for NWTL was obtained from the BODC at Llandudno. The input tidal levels for WSL can be obtained either from DIVAST 2-DU or TELEMAC model in the middle of turbines block (T3) as shown in Figure 6.13. Figure 7.1 illustrates the water level comparison at the gauge station of Hinkley obtained from TELEMAC-2D, DIVAST 2-DU and BODC website, respectively, to confirm a reliable tidal level utilised for WSL in the flexible operation optimisation. Figure 7.1(a) shows that the tidal levels generally agree well between the two models.

From Figure 7.1(b) which highlighted the difference of tidal levels from DIVAST 2-DU, TELEMAC-2D and the observed data during one tide, it can be seen that the DIVAST model did not predict well the difference at various stages of the tides between NWTL and Hinkley Point. This can be reflected with the term of tidal difference which is the averaged time lag of high tide or low tide between multi-scheme. A tidal difference using DIVAST 2-DU is approximately 1.16 hr while it is of about 1.50 hr from the observation data. However, TELEMAC-2D showed a better prediction capability in the accuracy of the tidal difference of 1.43 hr which is much closer to the observation data than DIVAST 2-DU. Hence, the tidal levels from TELEMAC-2D were selected for the flexible operation optimisation due to its higher accuracy in the prediction of tides.

It should be noted that this study mainly focuses on the flexible operation optimisation which directly linked to the tidal difference between NWTL and WSL, the further researches regarding the difference between DIVAST 2-DU and TELEMAC-2D will not be studied here.



(a)



(b)

Fig 7. 1. Tidal level comparison between TELEMAC, DIVAST and BODC at Hinkley.

According to the conclusion from Chapter 6, the multi-block optimisation could reach very similar generated electricity with a single-block scenario. Hence the single-block scenario was adopted in the flexible operation optimisation in the interest of computational cost.

7.3.2 Improved Genetic Algorithm model

The GA model was considering the maximisation of A_v as the only criteria of optimal schemes selection in Chapter 6. However, for this flexible operation optimisation, the developed fitness function was a combined effect of the A_v , St and DNE .

How to achieve the combination of these parameters using GA? As introduced in [159], the weighted sum method combines all the multi-objective functions into one scalar, composite objective function using the weighted sum. Hence, the multi-objective optimisation can be achieved through a weighted

sum of the individual optimisation functions. As described in chapter 6, the size of offspring is a user-defined value of `pop_size` which is the same for parents in each generation. Parents and offspring will be evaluated based on their fitness and half of them will be eliminated which ensure that the size of parents in each generation keeps unchanged. This elimination mechanism to control the population size in the selection is achieved via the limitation of $co_av + co_st + co_dne = 1$. The pseudocode below highlighted the process of selection in GA and how this limitation helps.

Table 7. 1. Pseudocode of the Genetic Algorithm with developed part highlighted based on Table 6.1.

Algorithm	The pseudocode of the GA
------------------	--------------------------

```

1:  proc Set_up           //Set up parameters. For example: 1000 initial operation schemes, co_av,
co_st, co_dne are assumed to be 0.5,0.3 and 0.2, respectively
2:  Generate the 1000 initial operation schemes and evaluate their fitness; // Fitness includes the
Av, St and DNE
3:  While NOT Termination_criterion() do
4:      Offspring <- Copy(Parents); //the size of offspring is 1000
5:      Offspring <- Mutation(Pm, Offspring);
6:      Offspring <- Recombination(Pr, Offspring);
7:      Evaluate_Fitness (Offspring)
8:      Survivals <- Selection(Ps, Parents, Offspring); //Fitness Function
8.1: P1 <- sort (Parents, Offspring)[500:2000] by Av // eliminate 500 (=1000* co_av) solutions
with lower Av
8.2: P2 <- sort (P1)[1:1200] by St // eliminate 300 (=1000* co_st) solutions with higher St
8.3: P3 <- sort (P2)[1:1000] by DNE // eliminate 200 (=1000* co_dne) solutions with higher
DNE
8.4: Survivals <- P3 //the size of survivals controlled to 1000 successfully
9:      Parents <- Survivals;
10: End While
11: End Proc Set_up;

```

Note: P1, P2 and P3 indicate the intermediate solutions after each process of eliminations.

7.4 Optimisation

7.4.1 No pumping utilised

The coefficients of co_av , co_st and co_dne for the multi-objective decision making were listed in Table 7.1 with outcomes can be seen in Table 7.2. The weight of co_av and co_dne ranges from 0 to 1, referring to the different objectives, e.g., the maximisation of energy output and a continuous energy output, or between them. The weight of co_st in this study only selected to be 0.1 or 0.2 due to the limited time for this study, so future work could further explore the co_st to achieve a flat energy output.

The range of Av varies from about 10.07 to 17.85 MW and DNE from about 27.67 to 203.73 hours according to different coefficients given to the parameters, as shown in Table 7.2. Each scenario is referring to specific objective decision making. For example, scenario 2 mainly focuses on a continuous power output distribution by the weight of 0.9 given to the DNE. The water levels and power output for this scenario are illustrated in Figures 7.2(a) and (b), respectively. As a result, the DNE in this scenario is approximately 27.67 hours, equals to a more than 85% reduction of DNE but 40% reduction in the electricity generation, in comparison with scenario 1 which is the maximisation of energy generation. In scenario 2, although a continuous power output cannot be 100% achieved during some neap tides even with operation flexibly, it could cover about 92% of the simulation period. This better emphasizes the potential of flexible operation not only for the aims of maximising electricity generation as illustrated in chapter 5 and 6, but also the flexible operation optimisation in this chapter. 3rd scenario mainly highlights that due to a larger weight given to Av , the energy output has been improved to 13MW, comparing to 10 MW for the 2nd scenario. What's more, the Av , DNE and St are proved to significantly rely on the coefficients according to user's requirements, which can be easily adjusted to achieve a wide range of purposes in multi-objective decision making.

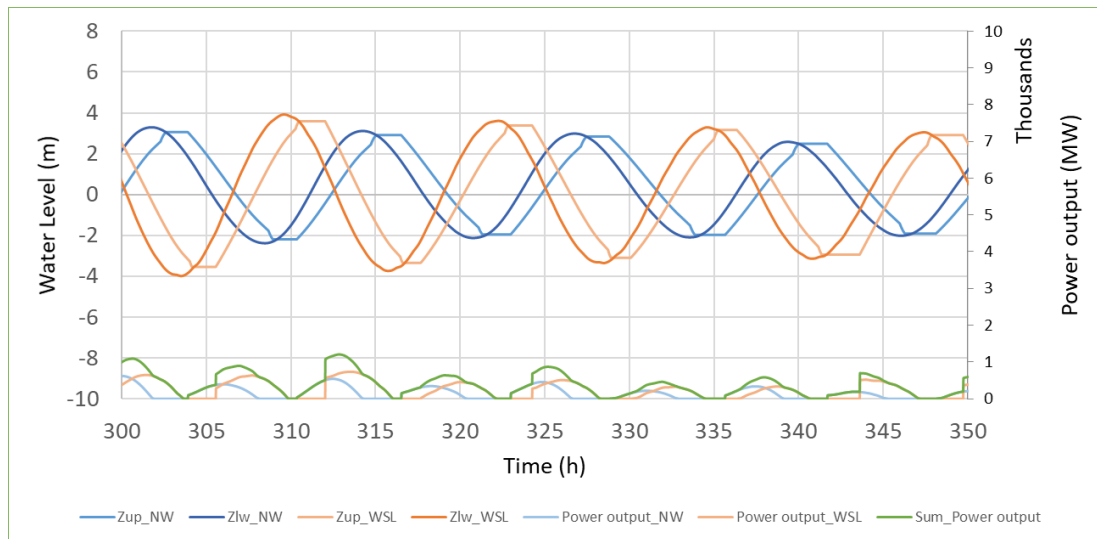
Table 7. 2. Parameters setting in scenarios for flexible operation optimisation.

Scenarios	co_av	co_st	co_dne
1	1	0	0
2	0	0.1	0.9
3	0.4	0.2	0.4
4	0.65	0.1	0.25
5	0.25	0.1	0.65

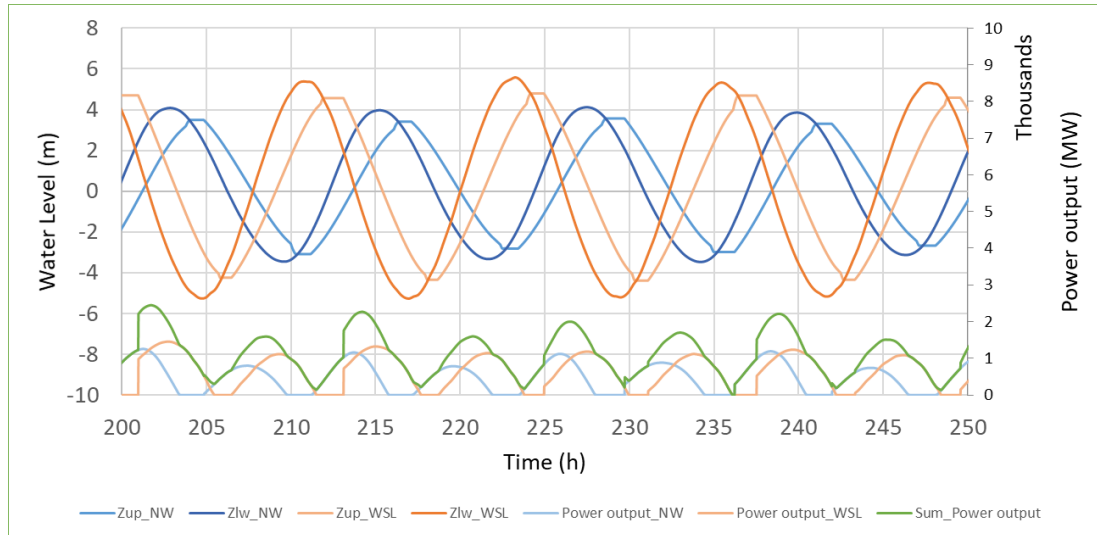
Table 7. 3. Summary of scenarios of flexible operation optimisation.

Scenarios	Elect.total (GWh)	WSL	NW	Av (MW)	St	DNE (hr)
1	0.388	0.222	0.166	17.846	1701.915	203.733
2	0.22	0.132	0.088	10.07	600.966	27.667
3	0.291	0.187	0.104	13.457	1007.723	169.667
4	0.331	0.193	0.138	14.46	1136.987	188.083
5	0.303	0.174	0.129	11.358	1206.045	45.433

* A coefficient of approximately 24.6 could be used if the electricity generation during the typical Spring Neap cycle required to convert to annual.



(a)



(b)

Fig 7. 2. Water level and power output with optimisation of revenue under scenario 2, during (a): neap tides and (b): spring tides, in which ‘Zup’, ‘Zlw’ and ‘Power output’ denoted the basin water levels, downstream water levels and power output at each time step for West Somerset Lagoon and North Wales Tidal Lagoon, respectively.

7.4.2 pumping utilised

The flexible operation scenario with pumping includes a wide range of searching spaces for operating heads, including the H_s varying from 2 m to 6 m, H_e varying from 0.5 m to 4.5 m, and H_p varying from 0 m to $H_{p_limited}$ similarly to Chapter 6. The coefficients of co_av , co_st and co_dne for the multi-objective decision making were listed in Table 7.3 with outcomes can be seen in Table 7.4.

The range of Av varies from about 12.47 to 22.70 MW and DNE from about 18.63 to 69.98 hours according to different coefficients given to the parameters, as shown in Table 7.4. In scenario 7 which mainly focuses on the continuous power output, more than 30% reduction in DNE was achieved because of pumping and covers about 95% of the simulation period, in comparison to the scenario 2. It should be noted that this decrease in DNE includes the duration that the net electricity generation is negative or the scheme is only using electricity for pumping. This should be further investigated in future studies.

In conclusion, the performance from the flexible operations scenario depends on the selection of coefficients in the GA model. However, it is able to bring significant benefit to the flexible operation optimisation for multi-objective decision making and it is proved to be able to provide a continuous power output covering the majority of the simulation period. The flexible operation schemes with pumping could contribute to a more promising continuous power output with lesser DNE, in comparison with the scenario without pumping. The results from a wide range of scenarios confirm a DNE varying from 0.0 to 2.0 hours in every tide if more focus is put on the continuous power output which comes with the sacrifice of a certain amount of electricity generation. In addition, it is supported that this gap should be potentially filled by using hydro-power plants [59, 152] and gas-based power [153, 154].

Table 7. 4. Parameters setting in scenarios for flexible operation optimisation with pumping.

Scenarios	co_av	co_st	co_dne
6	1	0	0
7	0	0.1	0.9
8	0.4	0.2	0.4
9	0.65	0.1	0.25
10	0.25	0.1	0.65

Table 7. 5. Summary of scenarios of flexible operation optimisation with pumping.

Scenarios	Elect.total (GWh)	WSL	NW	Av (MW)	St	DNE (hr)
6	0.411	0.235	0.176	22.702	752.542	69.983
7	0.221	0.131	0.09	12.468	912.068	18.633
8	0.331	0.187	0.144	15.719	1043.02	56
9	0.382	0.234	0.148	16.723	1105.853	64.917
10	0.313	0.174	0.139	15.7	1446.185	23.65

* A coefficient of approximately 24.6 could be used if the electricity generation during the typical Spring Neap cycle required to convert to annual.

7.5 Chapter summary

TRSS can be optimised to operate flexibly to achieve a multi-objective decision making by considering a combined operation of multiple prospective tidal lagoon projects, i.e. WSL and NWTL. The results showed that two TRSSs ran in a synchronised way would generate electricity over approximately 95% of the simulation period with the flexible operation if more focus was put on the continuous output although this will be at the cost of about 40% reduction in the total electricity generation in comparison to the optimisation in terms of maximisation of electricity generation.

In section 7.2 and 7.3, the flexible operation optimisation using a developed GA was introduced and achieved. Three parameters, including A_v , St and DNE , were used to evaluate the Averaged power output, Standard Deviation of time series of power output distribution and Duration with no energy output for each scenario. The weight of each parameter, namely co_av , co_st and co_dne , was used to indicate different priorities or give greater or fewer weights to different factors which can influence the selection of optimal solutions. In section 7.4, the outcomes under a variety of scenarios for the flexible operation optimisation have been discussed. The range of A_v varies from about 10.07 to 22.70 MW and DNE from about 18.63 to 203.73 hours according to different operation schemes with different weightings.

In conclusion, the flexible operation optimisation was proved to facilitate better utilisation of renewable energy through the development of TRSSs by making multi-objective decisions to the needs of different researches.

8. Conclusion and future work

8.1 Conclusions and limitations

The work presented in this thesis was mainly focused on the operation and design optimisation of TRSs. By using two typical hyperparameter optimisation approaches, namely the Grid Search methods (GS) and a Genetic Algorithm (GA), the benefits can be maximised, such as maximising the electricity generation or achieving the flexible operation optimisation for multi-objective decision making.

There is a much better understanding of the impact of GHG on climate change and there is further social and political pressure to reduce GHG [1]. To achieve this, the development of renewable energy is more than necessary to meet current energy demand on a global scale [155]. Tidal lagoons are designed to partially block estuaries or rivers and are considered to be more environmentally friendly structures than other tidal structures including barrages, particularly due to smaller impact on fish migration [14]. In the design and preliminary stage which significantly influences the feasibility of a TRS, the electricity prediction using 0-D modelling methodology was widely utilised as an ideal tool for the optimisation of the processes [17] due to its reduced computational time by ignoring the hydrodynamics impact. The 0-D modelling technology can be used to analyse the influence of the operational parameters, e.g. starting head, ending head and pumping heads, or the active number of turbines during operation. These parameters can also be employed to optimise the design parameters, e.g. turbines number and sluice gates, by using an appropriate algorithm. This optimisation could make TRSs become more economically attractive through electricity arbitrage and provide corresponding system support to domestic electricity consumption. Followed by the optimisation using 0-D modelling, the more sophisticated and expensive 2-D or 3-D models could be developed with the simulation of hydrodynamics, water quality, etc., to evaluate the performance of the scenarios optimised from 0-D models. Therefore, this collaboration between 0-D and multi-dimensional models could contribute to main targets of the TRSs optimisation which leads to the maximisation of electricity generation as well as the minimisation of environmental impact.

The first objective of this study was to identify the reliability of using the 0-D model for the electricity generation, in comparison with the multi-dimensional model. It was achieved by setting up the 0-D model and developing it under a variety of non-flexible operation scenarios, with the case study of Swansea Bay Lagoon (SBL). The verified DIVAST 2-DU model was then set up to evaluate the 0-D simulation results. It has been identified that with the simulation of hydrodynamics in the 2-D model, more accurate electricity generation can be estimated. This has made the 2-D model to be an ideal tool to evaluate the optimisation performance developed from 0-D modelling.

In addition, the wetting area parameter was set to be a variable compared to the fixed value traditionally used in 0-D modelling. The electricity estimations only have less than 5% difference compared with that including the flooding and drying within the impoundment. More importantly, the representative tidal cycle was chosen in order to exemplify an average tidal cycle that represents the annual results, allowing an affordable cost of time can be paid on the following optimisation which may require a large number of simulations. Particularly, when optimised pumping head was involved, a more than 10% improvement in electricity generation could be obtained. Besides, it was proved that the verified 2-D model does not depend on the size of the grid significantly. Finally, the electricity predicted using the 0-D model in this study overestimated the predictions relative to the 2-D model by approximately 7.5% which was consistent with the overestimation of about 7% reported for a similar 0-D prediction for an independent study [52], and this could be approximately 12% if pumping was employed. There was very small or even no difference in the average duration of generating phases between 0-D and 2-D models. In conclusion, the 0-D model can be considered as a reliable tool for energy estimation for the preliminary design and implementation stages in terms of TRSs optimisation, which requires a large number of runs.

The second research objective of this study was to address the optimisation of flexible operation schemes in terms of the maximisation of energy generation by using various GS methods with the case study of SBL. It was founded that under the traditional non-flexible operation schemes, there may not have any power output during some neap tides due to insufficient tidal range. This emphasized the significance of using flexible operation schemes, which divided the tides into small components, e.g., every tide or half-tide and applied variable operation heads in each small unit, to maximise the electricity generation. The GS models used a common 0-D modelling methodology to evaluate the generation of electricity during each tidal cycle until the maximum electricity output obtained. On the one hand, the optimised operation schemes were implemented into the modified DIVAST 2-DU model to evaluate the performance of optimisation. On the other hand, the GS model was further developed by implementing flexible turbine numbers into the non-flexible and flexible operation schemes, respectively. These flexibilities of the operations aimed to contribute to the improvement of electricity generation which has a great impact on the feasibility of a TRS.

Results concluded that the optimisation schemes using flexible operation schemes could yield a more than 10% increase to the electricity generated, rather than using the traditional non-flexible head operation. This increase had an extra of more than 10% when pumping was included. Notably, the electricity generation predicted using GS models were in very good agreement with those predicted using the 2-D models under the same conditions, with the difference being around 5% for the flexible models. Hence, it has been supported from the GS and 2-D model that if the operation flexibility could be adopted, the electricity generation from a TRS was able to be improved significantly and it could contribute more if pumping utilised. Besides, with an increasing number of turbines utilised, the higher peak of basin water levels could be reached due to more discharge allowed going through activate

turbines, and thus higher peak of power output could be reached at the same time although the duration of generating might be shortened. As a result, under non-flexible operation, shutting down a certain number of turbines at some neap tides could help to increase the electricity generation, compared with that of all 16 turbines being switched on for the SBL case study. If the flexible operation adopted, the results illustrated that 16 was the most optimal turbine numbers in both with and without pumping scenarios, respectively. The proximity of 16 turbines shows that the scheme can be run with one or two less turbine, due to maintenance, during neap tide with only less than 5% loss in electricity.

The third research objective of this study was to optimise the design parameters, e.g. the turbine numbers (NumTB) and sluice gates which were denoted by a coefficient known as Sluice To Power Capacity (STPC), with operation flexibly by employing advanced optimisation methods. This approach has been applied to two new case studies, namely the West Somerset Lagoon (WSL) and North Wales Tidal Lagoon (NWTL) which are currently under the preliminary design stage. To achieve this, the GA was firstly implemented in the operational optimisation for SBL, to highlight the higher efficiency of the GA by comparing with GS methods. As a result, the GA model performed as well as the best performing GS model, i.e. EHN model. Nevertheless, the computational time of the GA model can be saved about 50% in the optimisation of operation flexibly, and approximately 95% in the optimisation of multiple variables, e.g. the number of turbines and sluice area combining with operation flexibly, in comparison with the more elaborated GS method. It should be noted that the cost of the GA model can be influenced by a variety of factors [86], such as the iteration time, initial operation as well as the performance of HPC, which is worth to be further studied in the future work to contribute a higher efficiency of this optimisation using GA. The DIVAST 2-DU model supported the GA model predictions very well. It can be concluded that about 25% increase of electricity generation can be obtained by optimising the device numbers under non-flexible schemes, i.e. using fixed heads for all tides, compared with a baseline scenario in this study. The increase of energy generation would be at least 10% more if flexible operation schedule adopted, and a further about 10% increase can be reached by utilising pumping into the optimisation. This re-emphasizes the significance of reducing the running time and improving efficiency by adopting more advanced algorithms, e.g., GA, into the multiple variables' optimisation in TRSs. As a result, it can be concluded that the WSL and NWTL are able to achieve the electricity generation of 5.57 TWh/Year and 4.81 TWh/Year if the optimum turbines of 125 and 150 with the STPC of 8 and 10 were applied, respectively.

In details, in the GA model, two recombination method, namely Linear Recombination Method (LRM) and Ring Recombination Method (RRM) along with the Sequential Mutation Method (SMM) have been achieved, respectively. These methods can help to improve the convergence speed of the GA model. Results indicated that RRM was roughly 30% less computationally expensive than the LRM. As for the large discharge rushing through the turbines and sluicing gates during sluicing phase under the concentrated deployment, 3 solutions put forward to address the unsteady of water levels during the operation. Additionally, the operation of WSL was further optimised for the multi-block optimisation

using GA, which treated the blocks of turbines operated independently with their specific flexible operation schemes. It has been confirmed that a very similar of electricity generation could be produced in the multi-blocks optimisation although the optimum operation heads were slightly different at each block of turbines.

The fourth and final research objective of this study was to achieve the flexible operation optimisation by simulating two tidal lagoon projects, e.g., WSL and NWTL, to match the trends of power output defined by users, including a relatively continuous power output. TRSs can be operated flexibly for multi-objective decision making, such as maximising electricity generation, or also importantly, storing potential energy and generating electricity at certain times which are known as the flexible operation optimisation. A potential advantage of having multiple projects rather than a single project is that tidal power will be fed to the grid at several locations rather than being concentrated at one particular point [22], which will contribute to more efficient electricity distribution, and could perhaps alleviate cumulative hydrodynamic impacts [21]. A continuous power output, as one of the flexible power output scenarios, can be generally achieved over approximately 95% of the simulation period with flexible operation using the GA although this will be at the cost of about 40% reduction in the total electricity generation in comparison to the maximisation of electricity generation scenario.

In order to achieve this research objective, NWTL and WSL have been joined together under a variety of scenarios under flexible operation schemes with or without pumping involved, respectively. Three parameters, including A_v , St and DNE , were used to evaluate the Averaged power output, Standard Deviation of time series of power output distribution and Duration with no energy output under each scenario. The weight of each parameter, namely co_{av} , co_{st} and co_{due} , was used to indicate different priorities or give greater/lesser weight to different factors which can influence the selection of optimal solutions. The range of A_v varies from about 10.07 to 22.70 MW and DNE from about 18.63 to 203.73 hours according to different operation schemes with different weightings. In conclusion, the flexible operation optimisation was proved to facilitate better utilisation of renewable energy through the development of TRSs by making multi-objective decisions to the needs of different researches.

To conclude, the outcomes of this thesis are summarised as follows:

- The electricity predicted using the 0-D model in this study overestimated the predictions relative to the 2-D model by approximately 7.5%.
- Using the improved variable wetting area instead of a constant value which has been traditionally used in 0-D modelling, the electricity estimations showed a difference of only less than 5%.
- The GS model could bring a more than 10% increase to the electricity generated, rather than using the traditional non-flexible head operation. This increase was improved at least 10% when pumping was included. Hence, if the operation flexibility could be adopted, the

electricity generation from a TRS was able to be improved significantly and it could contribute more if pumping utilised.

- As for the optimisation of the flexible active number of turbines, the proximity of 16 turbines showed that the scheme could be ran with one or two fewer turbines, due to maintenance, during neap tide with only less than 5% loss in electricity.
- In the GA model, it is indicated that RRM of recombination method was roughly 30% less computationally expensive comparing to LRM. GA model was able to achieve very similar electricity generation but with approximately 50% reduction of the cost-time in the operational optimisation. This could reach approximately 95% if the design optimisation added with, in comparison with the GS methods.
- The WSL and NWTL were able to achieve the electricity generation of 5.57 TWh/Year and 4.81 TWh/Year if the optimum turbines of 125 and 150 with the STPC of 8 and 10 were applied, respectively.
- The multi-block optimisation using the developed GA has shown that each block of turbines should be operated with its own flexible operation scheme although it does not contribute to a significant increase of the electricity generation in total, compared to a unified operation scheme for all blocks.
- The flexible operation optimisation which simulates the joint performance of multiple schemes, e.g. WSL and NWTL, was proved to be able to deliver a continuous power output covering approximately 95% of the simulation period. It was proved to facilitate better utilisation of renewable energy through the development of TRSs by making multi-objective decisions to the needs of different researches.

8.2 Recommendations for future work

Even though a wide range of optimisation on TRSs has been addressed in this research, some areas of interest were left unexplored due to data, time and computational constraints.

- With regard to the optimum design and operational characteristics of tidal lagoons, more research should turn to the study of the far-field hydrodynamic impact. The combined effects of other proposed tidal lagoons and barrages can be considered, with a studied domain of the northwest European shelf area and including the entirety of the British Isles and French north coast. Additional studies of particular interest could focus on the method of implementing these schemes as the operational characteristics may vary during the whole tide.
- It has been shown that storm surges could affect the instantaneous power output, although the two-way generation mode of operation utilised in this study has been shown to be least influenced by storm surges [144]. Further studies could evaluate the impact of storm surges and improve on the simplified 0-D modelling approach used in this study to predict the total energy generated for a Spring Neap or annual cycle.
- Similar to the flexible operation optimisation, the transferable technology of GA could be developed for the revenue optimisation. Referred to the previous research, very attractive income can be potentially achieved in the flexible operation optimisation with the simulation of a single scheme [32]. In this way, provided by multiple TRSs, the total energy output could be further investigated. For example, a creditable attempt can be made to deliver more energy output during the time periods with higher electricity demand or electricity price by taking advantage of the flexibility of TRSs operation.
- Bayesian Optimization (BO) is a sequential design strategy for global optimization of black-box functions. Considering that the TRSs optimisation using GA still suffer from the relatively high computational cost, meanwhile, BO-based algorithm shows better performance with higher efficiency than GAs in the optimisation problems [156]. Following this, BO combining with metamodel approaches, as another hyperparameter optimisation tool to achieve global optimisation, may have great potential in finding the maximum of the expensive cost function [157], e.g., the electricity generation using 0-D modelling in TRSs. The main motivation of developing the BO optimisation is to explore a better performance to address more sophisticated hyperparameter optimisation in the TRSs, compared to it using GA, due to a variety of efficiency terms from BO could help direct the sampling and trade-off exploration and exploitation of the searching space.

Reference

- [1] Y. Wang et al., "A global map of emission clumps for future monitoring of fossil fuel CO₂ emissions from space," *Earth System Science Data* 2018;11(2);1-25.
- [2] Department of Energy & Climate Change, "Annual report and accounts 2012-13" 2012. <https://assets.publishing.service.gov.uk/government/uploads/system/uploads/attachment_data/file/209325/9589-TSO-DECC_AR-2012-13_Accessible.pdf>
- [3] E. Thicknesse, "Renewables set to make up half of the UK's electricity production by 2025" 2019.< <https://www.cityam.com/renewables-set-to-make-up-half-of-the-uks-electricity-production-by-2025/#:~:text=Renewables%20are%20expected%20to%20contribute,a%20new%20report%20from%20Moody's.>>
- [4] HM Government, "The carbon plan: delivering our low carbon future," 2011.< https://assets.publishing.service.gov.uk/government/uploads/system/uploads/attachment_data/file/47613/3702-the-carbon-plan-delivering-our-low-carbon-future.pdf>
- [5] M. Shepherd."UK net zero target," 2020.< <https://www.instituteforgovernment.org.uk/explainers/net-zero-target>>
- [6] World Energy Council, "World energy resources marine energy," 2016.< <https://www.marineenergywales.co.uk/wp-content/uploads/2016/01/World-Energy-Council-Marine-Energy-Resources-2016.pdf>>
- [7] National Statistics, "Energy trends: UK renewables," 2019.< https://assets.publishing.service.gov.uk/government/uploads/system/uploads/attachment_data/file/811974/Renewables_June_2019.pdf>
- [8] Department for Business, Energy & Industrial Strategy, "Wave and tidal energy: part of the UK's energy mix," 2013.< <https://www.gov.uk/guidance/wave-and-tidal-energy-part-of-the-uks-energy-mix>>
- [9] Support The Guardian, "Government rejects plan for £1.3bn tidal lagoon in Swansea," 2018.<<https://www.theguardian.com/business/2018/jun/25/government-rejects-plan-for-tidal-lagoon-in-swansea>>
- [10] Tidal Lagoon Power, "Press release 22nd June 2020," 2020. <<http://www.tidallagoonpower.com/news/2020/06/22/press-release-22nd-june-2020/>>
- [11] F. O'Rourke, F. Boyle, and A. Reynolds, "Tidal energy update 2009," *Applied Energy* 2010;87(2);398-409.
- [12] M. Mueller and R. Wallace, "Enabling science and technology for marine renewable energy," *Energy Policy* 2008;36(12);4376-4382.
- [13] A.Cornett, J.Cousineau, and I.Nistor, "Assessment of hydrodynamic impacts from tidal power lagoons in the Bay of Fundy," *Energy* 2013;1;33-54.
- [14] BBC Wales, "Swansea tidal lagoon: the environmental arguments," 2016.< <https://www.bbc.co.uk/news/uk-wales-37863807>>
- [15] J. Zhou, R. A. Falconer, and B. Lin, "Refinements to the EFDC model for predicting the hydro-environmental impacts of a barrage across the Severn Estuary," *Renewable Energy* 2014;62;490-505.
- [16] G. Gao, R. A. Falconer, and B. Lin, "Modelling the fate and transport of faecal bacteria in estuarine and coastal waters," *Mar Pollut Bull* 2015;100(1);162-168.
- [17] A. Angeloudis, R. Ahmadian, R. A. Falconer, and B. Bockelmann-Evans, "Numerical model simulations for optimisation of tidal lagoon schemes," *Applied Energy* 2016;165;522-536.
- [18] G. A. Aggidis and D. S. Benzon, "Operational optimisation of a tidal barrage across the Mersey estuary using 0-D modelling," *Ocean Engineering* 2013;66;69-81.
- [19] D. Prandle, "Simple theory for designing tidal power schemes," *Water Resources* 1984;7;21-27.

- [20] D. Prandle, "Design of tidal barrage power schemes," *Proceedings of the Institution of Civil Engineers - Maritime Engineering* 2009;162(4);147-153.
- [21] A. Angeloudis and R. A. Falconer, "Sensitivity of tidal lagoon and barrage hydrodynamic impacts and energy outputs to operational characteristics," *Renewable Energy* 2017;114(A);337-351.
- [22] N. C. Yates, I. Walkington, R. Burrows, and J. Wolf, "Appraising the extractable tidal energy resource of the UK's western coastal waters," *Philosophical Transactions of the Royal Society A Mathematical Physical and Engineering Sciences* 2013;371.
- [23] N. C. Yates, I. Walkington, R. Burrows, and J. Wolf, "The energy gains realisable through pumping for tidal range energy schemes," *Renewable Energy* 2013;58;79-84.
- [24] R. Ahmadian, R. A. Falconer, and B. Lin, "Hydro-environmental modelling of proposed Severn barrage, UK," *Proceedings of the Institution of Civil Engineers - Energy* 2010;163(3);107-117.
- [25] J. Xia, R. A. Falconer, and B. Lin, "Impact of different tidal renewable energy projects on the hydrodynamic processes in the Severn Estuary, UK," *Ocean Modelling* 2010;32(1-2);86-104.
- [26] J. Xia, R. A. Falconer, and B. Lin, "Impact of different operating modes for a Severn Barrage on the tidal power and flood inundation in the Severn Estuary, UK," *Applied Energy* 2010;87(7);2374-2391.
- [27] J. Xia, R. A. Falconer, and B. Lin, "Hydrodynamic impact of a tidal barrage in the Severn Estuary, UK," *Renewable Energy* 2010;35(7);1455-1468.
- [28] J. Zhou, S. Pan, and R. A. Falconer, "Effects of open boundary location on the far-field hydrodynamics of a Severn Barrage," *Ocean Modelling* 2014;73;19-29.
- [29] R. Burrows, I. A. Walkington, N. C. Yates, T. S. Hedges, J. Wolf, and J. Holt, "The tidal range energy potential of the West Coast of the United Kingdom," *Applied Ocean Research* 2009;31(4);229-238.
- [30] R. Burrows et al., "Tidal energy potential in UK waters," *Proceedings of The Institution of Civil Engineers - Maritime Engineering* 2009;162(4);155-164.
- [31] A. Angeloudis, S. C. Kramer, A. Avdis, and M. D. Piggott, "Optimising tidal range power plant operation," *Applied Energy* 2018;212;680-690.
- [32] F. Harcourt, A. Angeloudis, and M. D. Piggott, "Utilising the flexible generation potential of tidal range power plants to optimise economic value," *Applied Energy* 2019;237;873-884.
- [33] J. Xue, R. Ahmadian, and R. A. Falconer, "Optimising the operation of tidal range schemes," *Energies* 2019;12(15);2870.
- [34] R. Burrows, I. Walkington, J. Holt, and J. Wolf, "Environmental impacts of tidal power schemes," *Proceedings of The Institution of Civil Engineers - Maritime Engineering*, 2009;162;165-177.
- [35] R. Ahmadian, J. Xue, R. A. Falconer, and N. Hanousek, "Optimisation of tidal range schemes," *The 12th European Wave and Tidal Energy Conference* 2017;2309-1983;1059.
- [36] G. Aggidis and O. Feather, "Tidal range turbines and generation on the Solway Firth," *Renewable Energy* 2012;43;9-17.
- [37] S. Waters and G. Aggidis, "Tidal range technologies and state of the art in review," *Renewable and Sustainable Energy Reviews* 2016;59;514-529.
- [38] R. Ahmadian and R. A. Falconer, "Assessment of array shape of tidal stream turbines on hydro-environmental impacts and power output," *Renewable Energy* 2012;44;318-327.
- [39] P. Breeze, "Chapter 6 - Small hydropower," *Hydropower* 2018;53-62.
- [40] A. Merlin, P. Sandrin, J. M. Grès, and M. Hilairat, "The New Operation Model For the La Rance Tidal Power Plant," 1982, pp. PAS-101:290-4: *IEEE Trans Power Apparatus Syst.*
- [41] J. Constans, "Chapter 5 - Tidal energy conversion," *Marine Sources of Energy* 1979;121-133.
- [42] V. Khare, C. Khare, S. Nema, and P. Baredar, "Chapter 2 - Introduction of tidal energy," *Tidal Energy Systems* 2019;41-114.
- [43] P. Breeze, "Chapter 9 - Tidal barrage power plants," *Power Generation Technologies* 2014;181-194.
- [44] C. Baker, "Chapter 7 - Tidal Energy," *Renewable Energy* 1993;107-112.
- [45] S. Waters and G. Aggidis, "A world first: Swansea Bay Tidal Lagoon in review," *Renewable and Sustainable Energy Reviews* 2016;56;916-921.

- [46] Wikipedia, "Sluice," <<https://en.wikipedia.org/wiki/Sluice>>
- [47] D. Lee et al., "Experimental investigation on the relationship between sluice caisson shape of tidal power plant and the water discharge capability," *Renewable Energy* 2010;35;2243-2256.
- [48] Tidal Lagoon Power, "Sluice house section-Swansea Bay Tidal Lagoon," 2016.<
<http://www.tidallagoonpower.com/projects/swansea-bay/>>
- [49] A. S. Bahaj and L. E. Myers, "Fundamentals applicable to the utilisation of marine current turbines for energy production," *Renewable Energy* 2003;28(14);2205-2211.
- [50] J. Xia, R. A. Falconer, B. Lin, and G. Tan, "Estimation of annual energy output from a tidal barrage using two different methods," *Applied Energy* 2012;93;327-336.
- [51] R. Ahmadian, R. A. Falconer, and B. Bockelmann-Evans, "Comparison of hydro-environmental impacts for ebb-only and two-way generation for a Severn Barrage," *Computers & Geosciences* 2014;71;11-19.
- [52] A. Angeloudis, R. A. Falconer, S. Bray, and R. Ahmadian, "Representation and operation of tidal energy impoundments in a coastal hydrodynamic model," *Renewable Energy* 2016;99;1103-1115.
- [53] F. Vieira and H. Ramos, "Hybrid solution and pump-storage optimization in water supply system efficiency: a case study," *Energy Policy* 2008;36;7.
- [54] International Renewable Energy Agency, "Flexibility in conventional power plants: innovation landscape brief," 2019.<
https://www.irena.org/-/media/Files/IRENA/Agency/Publication/2019/Sep/IRENA_Flexibility_in_CPPs_2019.pdf?la=en&hash=AF60106EA083E492638D8FA9ADF7FD099259F5A1>
- [55] J. Xue, R. Ahmadian, and O. Jones, "Genetic algorithm in tidal range schemes' optimisation," *Energy* 2020;200.
- [56] S. P. Neill, M. R. Hashemi, and M. J. Lewis, "Tidal energy leasing and tidal phasing," *Renewable Energy* 2016;85;580-587.
- [57] S. P. Neill et al., "Tidal range energy resource and optimization – past perspectives and future challenges," *Renewable Energy* 2018;127;763-778.
- [58] L. Mackie, F. Harcourt, A. Angeloudis, and M. Piggott, "Income optimisation of a fleet of tidal lagoons," *European Wave and Tidal Energy Conference* 2019.
- [59] K. D. Strang, "Feasibility of a hidden renewable energy hydro power storage battery," *Journal of Energy Storage* 2017;13;164-175.
- [60] L. E. Schaffer and T. R. Næss, "A profit maximisation model for operation of a tidal lagoon power plant," *Master Desertation, Department of Industrial Economics and Technology Management, Norwegian University of Science and Technology* 2016.
- [61] L. Mackie, D. Coles, M. Piggott, and A. Angeloudis, "The potential for tidal range energy systems to provide continuous power: a UK case study," *Journal of Marine Science and Engineering* 2020;8(10);780.
- [62] A. Angeloudis, S. Kramer, N. Hawkins, and M. Piggott, "On the potential of linked-basin tidal power plants: An operational and coastal modelling assessment," *Renewable Energy* 2020;155; 876-888.
- [63] P. B. Leite Neto, O. R. Saavedra, and L. A. Souza Ribeiro, "Optimization of electricity generation of a tidal power plant with reservoir constraints," *Renewable Energy* 2015;81;11-20.
- [64] A. Angeloudis, M. Piggott, S. Kramer, A. Avdis, D. Coles, and M. Christou, *Comparison of 0-D, 1-D and 2-D model capabilities for tidal range energy resource assessments*. 2017.
- [65] S. Petley and G. Aggidis, "Swansea Bay Tidal Lagoon annual energy estimation," *Ocean Engineering* 2016;111;348-357.
- [66] C. Baker, "Tidal power - energy engineering," *Energy policy* 1991;8.
- [67] N. C. Yates and B. Tatlock, "Optimising tidal lagoons," *The European Wave and Tidal Energy Conference* 2017.
- [68] T. H. Douglas, "Pumped Storage," *Proceedings of the Conference Organized by the Institution of Civil Engineers at Imperial College of Science* 1990.
- [69] S. Wilhelm, G. Balarac, O. Métais, and C. Ségoufin, "Analysis of head losses in a turbine draft tube by means of 3D unsteady simulations," *Flow, Turbulence and Combustion*, 2016;97;1255-1280.

- [70] N. Čož, R. Ahmadian, and R. A. Falconer, "Implementation of a full momentum conservative approach in modelling flow through tidal structures," *Water* 2019;11(9);1917.
- [71] M. Namin, B. Lin, and R. A. Falconer, "Modelling estuarine and coastal flows using an unstructured triangular finite volume algorithm," *Advances in Water Resources* 2004;27(12);1179-1197.
- [72] J. Brammer, R. A. Falconer, C. Ellis, and R. Ahmadian, "Physical and numerical modelling of the Severn Barrage," *Science China Technological Sciences* 2014;57(8);1471-1481.
- [73] R. Ahmadian, C. Morris, and R. A. Falconer, "Hydro-environmental modelling of off-shore and coastally attached impoundments off the North Wales Coast," *Proceedings of the 1st European IAHR Congress 2010*.
- [74] J. Xia, R. A. Falconer, and B. Lin, "Numerical model assessment of tidal stream energy resources in the Severn Estuary, UK," *Proceedings of the Institution of Mechanical Engineers, Part A: Journal of Power and Energy* 2010;224(7);969-983.
- [75] J. Zhou, S. Pan, and R. A. Falconer, "Optimization modelling of the impacts of a Severn Barrage for a two-way generation scheme using a continental shelf model," *Renewable Energy* 2014;72;415-427.
- [76] Li, H. Liu, Mei, Shao, Wang, and Y. Yan, "Comparative analysis of building representations in TELEMAC-2D for flood inundation in idealized urban districts," *Water* 2019;11;1840.
- [77] A. Seenath, M. Wilson, and K. Miller, "Hydrodynamic versus GIS modelling for coastal flood vulnerability assessment: which is better for guiding coastal management?" *Ocean & Coastal Management* 2016;120;99-109.
- [78] C. Briere, S. Abadie, P. Bretel, and P. Lang, "Assessment of TELEMAC system performances, a hydrodynamic case study of Anglet, France," *Coastal Engineering* 2007;54;345-356.
- [79] A. Forster, J. Costi, W. Marques, A. Wormsbecher, and A. Bendô, "Application of the TELEMAC-2D Model in the fluvial hydrodynamics simulation and reproduction of flood patterns," *Defect and Diffusion Forum* 2019;396;187-196.
- [80] S. Smolders, A. Leroy, M. Teles, T. Maximova, and J. Vanlede, "Culverts modelling in TELEMAC-2D and TELEMAC-3D," *Telemac-Mascaret User Conference 2016*;23.
- [81] L. Blunden and A. Bahaj, "Initial evaluation of tidal stream energy resources at Portland Bill, UK," *Renewable Energy* 2004;3(2);121-132.
- [82] P. K. Stansby, N. Chini, and P. Lloyd, "Oscillatory flows around a headland by 3D modelling with hydrostatic pressure and implicit bed shear stress comparing with experiment and depth-averaged modelling," *Coastal Engineering* 2016;116;1-14.
- [83] A. Abdul Rahman and V. Venugopal, "Inter-comparison of 3D tidal flow models applied to Orkney Islands and Pentland Firth," *11th European Wave and Tidal Energy Conference 2015*.
- [84] J. Lin, J. Sun, L. Liu, Y. Chen, and B. Lin, "Refined representation of turbines using a 3D SWE model for predicting distributions of velocity deficit and tidal energy density," *International Journal of Energy Research* 2015;39.
- [85] W. Wang *et al.*, "A systematic review of machine learning models for predicting outcomes of stroke with structured data," *PLOS ONE*, vol. 15, p. e0234722, 06/12 2020.
- [86] P. Liashchynskyi and P. Liashchynskyi, "Grid search, random search, genetic algorithm: a big comparison for NAS," *Mathematics, Computer Science* 2019.<
<https://arxiv.org/pdf/1912.06059.pdf>>
- [87] B. Panda, "Hyperparameter tuning," *Department of Computer Science* 2019.
- [88] D. Charlotte and R. Alexander, "Hyperparameter optimization," *Tutorium in Wissensaustausch Workshop Machine Learning Conference 2019*.
- [89] M. R. Karahroudi, S. A. Mousavi Shirazi, and K. Sepanloo, "Optimization of designing the core fuel loading pattern in a VVER-1000 nuclear power reactor using the genetic algorithm," *Annals of Nuclear Energy* 2013;57;142-150.
- [90] T. Ueno, T.D. Rhone, Z. Hou, T. Mizoguchi, and K. Tsuda, "An efficient Bayesian Optimization library for materials science," *Materials Discovery* 2020;4;18.
- [91] K. Bestuzheva, "Global optimisation for energy system," *Thesis(PhD) The Australian National University* 2018.

- [92] O. Sener and V. Koltun, "Multi-task learning as multi-objective optimisation," *Advances in Neural Information Processing Systems* 2018.
- [93] R. Cipolla, Y. Gal, and A. Kendall, "Multi-task learning using uncertainty to weigh losses for scene geometry and semantics," *Proceedings of the IEEE Computer Society Conference on Computer Vision and Pattern Recognition* 2018;7482-7491.
- [94] J. Bergstra and Y. Bengio, "Random search for hyper-parameter optimization," *Journal of Machine Learning Research* 2012;13;281-305.
- [95] H. Dinh and M. Baan, "A grid-search approach for 4D pressure-saturation discrimination," *Geophysics* 2019;84;1-65.
- [96] K. Ensor and P. Glynn, "Stochastic optimization via grid search," 1997.<
<http://citeseerx.ist.psu.edu/viewdoc/download;jsessionid=612B42B896412F51FC07414D061390D5?doi=10.1.1.57.3528&rep=rep1&type=pdf>>
- [97] F. Liu, C. Ye, and E. Zhu, "Accurate grid-based clustering algorithm with diagonal grid searching and merging," *IOP Conference Series: Materials Science and Engineering* 2017;242.<<https://iopscience.iop.org/article/10.1088/1757-899X/242/1/012123/pdf>>
- [98] A. Slowik and H. Kwasnicka, "Evolutionary algorithms and their applications to engineering problems," *Neural Computing and Applications* 2020;32;12363–12379.
- [99] A. P. Alves da Silva and P. J. Abrao, "Applications of evolutionary computation in electric power systems," *Proceedings of the 2002 Congress on Evolutionary Computation* 2002;2;1057-1062.
- [100] B. Pavez-Lazo and J. Soto-Cartes, "A deterministic annular crossover genetic algorithm optimisation for the unit commitment problem," *Expert Systems with Applications* 2011;38(6);6523-6529.
- [101] J. Johnson and V. Rahmat-Samii, "Genetic algorithms in engineering electromagnetics," *Antennas and Propagation Magazine, IEEE* 1997;39;7-21.<<https://pdfs.semanticscholar.org/4b8c/870140a70aba606e320fd0be7ebc4abaa9.pdf>>
- [102] X. Yan, H. Liu, Z. Zhu, and Q. Wu, "Hybrid genetic algorithm for engineering design problems," *Cluster Computing* 2017;20;1-13.
- [103] P. G. Remya, R. Kumar, and S. Basu, "Forecasting tidal currents from tidal levels using genetic algorithm," *Ocean Engineering* 2012;40;62-68.
- [104] B. Cañellas, S. Balle, J. Tintoré, and A. Orfila, "Wave height prediction in the Western Mediterranean using genetic algorithms," *Ocean Engineering* 2010;37(8);742-748.
- [105] S. Ratheesh, R. Sharma, and S. Basu, "Prediction of sea level anomaly in the Arabian Sea using genetic algorithm," *International Journal of Ocean and Climate Systems* 2011;2;55-63.
- [106] P. Sullivan and P. McCombie, "Optimisation of tidal power arrays using a genetic algorithm," *Proceedings of the Institution of Civil Engineers - Energy* 2013;166;19-28.
- [107] B. F. M. Child and V. Venugopal, "Optimal configurations of wave energy device arrays," *Ocean Engineering* 2010;37(16);1402-1417.
- [108] E. Kontoleonos and S. Weissenberger, "Annual energy production maximization for tidal power plants with evolutionary algorithms," *International Journal of Fluid Machinery and Systems* 2017;10(3);264-273.
- [109] R. Baños, F. Manzano-Agugliaro, F. G. Montoya, C. Gil, A. Alcayde, and J. Gómez, "Optimization methods applied to renewable and sustainable energy: a review," *Renewable and Sustainable Energy Reviews* 2011;15(4);1753-1766.
- [110] R. Subramanian, "Continuity Equation," *Department of Chemical and Biomolecular Engineering Clarkson University* 2019.<
<https://web2.clarkson.edu/projects/subramanian/ch490/notes/Continuity%20Equation.pdf> >
- [111] I. Fairley, R. Ahmadian, R. A. Falconer, M. R. Willis, and I. Masters, "The effects of a Severn Barrage on wave conditions in the Bristol Channel," *Renewable Energy* 2014;68;428-442.
- [112] F. Y. Teo, "Study of the hydrodynamic processes of rivers and floodplains with obstructions," *Thesis(PhD), Cardiff University*, 2010.
- [113] J. Wu, "Wind-stress coefficients over sea surface from breeze to hurricane," *Journal of Geophysical Research: Oceans* 1982;87(C12);9704-9706.

- [114] S. Bray, R. Ahmadian, and R. A. Falconer, "Impact of representation of hydraulic structures in modelling a Severn Barrage," *Computers & Geosciences* 2016;89;96-106.
- [115] A. Quarteroni, "Chapter 9 - The finite volume method," *Numerical Model for Different Problem* 2017;213-223.
- [116] R. A. Falconer, J. Xia, B. Lin, and R. Ahmadian, "The Severn Barrage and other tidal energy options: hydrodynamic and power output modeling," *Science in China Series E: Technological Sciences* 2009;52(11);3413-3424.
- [117] R. Ahmadian, R. A. Falconer, and B. Bockelmann-Evans, "Far-field modelling of the hydro-environmental impact of tidal stream turbines," *Renewable Energy* 2012;38(1);107-116.
- [118] A. Bogdanov, K. Sone, and K. Zaya, "Performance of the OpenMP and MPI implementations on ultrasparc system," *Computer Research and Modeling* 2015;7;485-491.
- [119] G. Rajgor, "Time for tidal lagoons?" *Renewable Energy Focus* 2016;17(5);202-204.
- [120] *Renewable Energy Focus*, "Green light for world's first tidal lagoon," 2015.<<http://www.renewableenergyfocus.com/view/42607/green-light-for-worlds-first-tidal-lagoon/>>
- [121] C. Hendry, "The role of tidal lagoons," 2016.<<https://hendryreview.files.wordpress.com/2016/08/hendry-review-final-report-english-version.pdf>>
- [122] BBC, "David Cameron's enthusiasm for Swansea tidal lagoon 'reducing'," 2016.<<https://www.bbc.co.uk/news/uk-wales-politics-35306084>>
- [123] BBC, "£1.3bn Swansea Bay tidal lagoon project thrown out," 2018.<<https://www.bbc.co.uk/news/uk-wales-south-west-wales-44589083>>
- [124] Tidal Lagoon Power, "Environmental statement chapter 4: project description," 2017<<http://www.tidallagoonpower.com/wp-content/uploads/2017/05/DCO-Application-ES-4.0-project-description.pdf>>
- [125] Tidal Lagoon Power, "Swansea Bay Tidal Lagoon,"<<http://www.tidallagoonpower.com/projects/swansea-bay/>>
- [126] "DiGSBS250K [SHAPE geospatial data], Scale 1:250000, Tiles: GB, Updated: 6 September 2011, BGS, Using: EDINA Geology Digimap Service 2017.<<http://digimap.edina.ac.uk>>
- [127] C. Baker, "Tidal lagoon power generation scheme in Swansea Bay," 2006.
- [128] British Oceanographic Data Centre, "Download UK Tide Gauge Network data from BODC,".<https://www.bodc.ac.uk/data/hosted_data_systems/sea_level/uk_tide_gauge_network/>
- [129] Tidal Lagoon Power, "Hydrodynamic model update and validation report," 2013;3.<<http://www.tidallagoonpower.com/wp-content/uploads/2018/02/App-7.1-Hydrodynamic-Model-Update-and-Validation-Report.pdf>>
- [130] C. Binnie, "A Review of tidal power," BHA Hydro Network 2019 <<http://www.british-hydro.org/wp-content/uploads/2019/07/1.3-Binnie-C.pdf>>.
- [131] Water Briefing, "New plans announced for 2.8GW West Somerset Tidal Lagoon," 2015.<<https://www.waterbriefing.org/home/technology-focus/item/10233-new-plans-announced-for-28gw-west-somerset-tidal-lagoon>>
- [132] S. Salter, "Now look at West Somerset Lagoon, MP tells ministers," 2018.<<https://www.somersetcountygazette.co.uk/news/16317922.now-look-at-west-somerset-lagoon-mp-tells-ministers/>>
- [133] Offshore Energy, "West Somerset Tidal Lagoon details submitted to planning inspectorate," 2015.<<https://www.offshore-energy.biz/west-somerset-tidal-lagoon-details-submitted-to-planning-inspectorate/>>
- [134] B. Guo, R. Ahmadian, and R. A. Falconer, "Improved hydro-environmental study of tidal lagoons: West Somerset Lagoon case study," *Applied Energy* (Under Review), 2020.
- [135] North Wales Tidal Energy, "North Wales presents a world-class site for a tidal lagoon,".<<https://www.northwalestidalenergy.com/concept>>
- [136] Wales Online, "The massive £7 billion tidal lagoon project for North Wales that promises to create 20,000 jobs," 2018.<<https://www.walesonline.co.uk/business/business-news/massive-7-billion-tidal-lagoon-14836557>>

- [137] Construction Enquirer, "Plan for £600m North Wales tidal energy lagoon," 2020.<
<https://www.constructionenquirer.com/2020/07/07/plan-for-600m-north-wales-tidal-energy-lagoon/>>
- [138] North Wales Live, "The North Wales tidal potential that could plug some of the power gap left by Wylfa Newydd freeze," 2019.<<https://www.dailypost.co.uk/business/business-news/north-wales-tidal-potential-could-15717457>>
- [139] S. R. Ladd, "Genetic Algorithms in C++," 1995;384.
- [140] D. Whitley, "Genetic algorithm and neural network," 1995.
- [141] K. Zhu and Z. Liu, "Population diversity in permutation based genetic algorithm," European Conference on Machine Learning 2004;537-547.
- [142] S. B. A. Bukhari, A. Ahmad, S. Raza, and N. Siddique, "A ring crossover genetic algorithm for unit commitment problem," Turkish Journal of Electrical Engineering and Computer Sciences 2016;24;3862-3876.
- [143] J. Game, K. Sitney, V. E. Cook, and R. K. Mortimer, "Use of a ring chromosome and pulsed-field gels to study interhomolog recombination, double-strand DNA breaks and sister-chromatid exchange in Yeast," Genetics 1990;123;695-713.
- [144] M. J. Lewis, A. Angeloudis, P. E. Robins, P. S. Evans, and S. P. Neill, "Influence of storm surge on tidal range energy," Energy 2017;122;25-36.
- [145] S. P. Neill et al., "Tidal range energy resource and optimization – past perspectives and future challenges," Renewable Energy, 2018;127;763-778.
- [146] S. P. Neill, M. R. Hashemi, and M. J. Lewis, "Optimal phasing of the European tidal stream resource using the greedy algorithm with penalty function," Energy 2014;73;997-1006.
- [147] I. Staffell and R. Green, "Is there still merit in the merit order stack? the impact of dynamic constraints on optimal plant mix," IEEE Transactions on Power Systems 2016;31(1);43-53.
- [148] J. D. Jenkins et al., "The benefits of nuclear flexibility in power system operations with renewable energy," Applied Energy 2018;222;872-884.
- [149] P. U. Sunil, J. Barve, and P. S. V. Nataraj, "A robust heat recovery steam generator drum level control for wide range operation flexibility considering renewable energy integration," Energy 2018;163;873-893
- [150] Y. Dong, X. Jiang, Z. Liang, and J. Yuan, "Coal power flexibility, energy efficiency and pollutant emissions implications in China: a plant-level analysis based on case units," Resources, Conservation and Recycling 2018;134;184-195.
- [151] H. E. Garcia, A. Mohanty, W.-C. Lin, and R. S. Cherry, "Dynamic analysis of hybrid energy systems under flexible operation and variable renewable generation – Part I: dynamic performance analysis," Energy 2013;52;1-16.
- [152] Renewable Energy Association, "Energy storage in the UK: an overview," 2015.<https://www.r-e-a.net/upload/rea_uk_energy_storage_report_november_2015_-_final.pdf>
- [153] T. Feehall et al., "Battery energy storage systems for the electricity grid: UK research facilities," 8th IET International Conference on Power Electronics, Machines and Drives 2016.<https://www.research.manchester.ac.uk/portal/files/49528491/Green_access_ESS.pdf>
- [154] "Energy storage use cases," DNV GL2016, Available:
https://assets.publishing.service.gov.uk/government/uploads/system/uploads/attachment_data/file/554467/Energy_Storage_Use_Cases.pdf.
- [155] M. Lewis et al., "Power variability of tidal-stream energy and implications for electricity supply," Energy 2019;183;1061-1074.
- [156] L. Sun, L. Lin, Y. Wang, M. Gen, and H. Kawakami, "A bayesian optimisation-based evolutionary algorithm for flexible job shop scheduling," Procedia Computer Science 2015;61;521-526.
- [157] S. Warder, A. Angeloudis, S. C. Kramer, C. Cotter, and M. D. Piggott, "A comparison of Bayesian inference and gradient-based approaches for friction parameter estimation (Preprint)," 2020.
- [158] B. Guo, "Refined hydro-environmental impacts assessment of tidal lagoon," Thesis(PhD), Cardiff University, 2020.

[159] X. Yang, "Nature-inspired optimization algorithms," 2014;14:197-211.